MODELLING THE GREENLAND ICESHEET

A DISSERTATION
SUBMITTED TO THE UNIVERSITY OF EDINBURGH
IN PARTIAL FULFILLMENT OF THE
REQUIREMENTS FOR THE DEGREE OF
DOCTOR OF PHILOSOPHY

By
Nicholas R J Hulton
September 1990

Declaration

I hereby declare that this thesis was composed by me and the work is my own research.

Nicholas R. J. Hulton.

Contents

List of Tables

List of Figures

Modelling the Greenland Ice Sheet

Nicholas R. J. Hulton 1990

ABSTRACT

A dynamic, vertically integrated, three-dimensional, mass continuity computer model of the Greenland ice sheet is used to predict the ice sheet's response to climatic perturbation. The ice flow is gravity driven according to glaciological physics, whereby ice flow is calculated as the sum of deformation and sliding components averaged over the ice thickness where longitudinal stresses are considered negligible. The model has inputs of the present-day ice surface and basal topography, and is forced by changes in sea level and surface mass balance, which are modelled by separately described and forced accumulation and ablation parts. The mass balance and the forcing terms are parametrized against present-day values and the present-day ice sheet is initially used as the starting condition for model experiments. By repeating model experiments from the same starting point and varying only one model parameter at a time the model's sensitivity to individual parameters is assessed. Characteristic behaviour patterns, reaction times and significant parameters are identified. The model is seen to produce a realistic simulation of present-day conditions. The ice dynamics model is robust compared to the changes that can be introduced by small variations in sea-level. The relationship between forcing temperatures and ablation rates exerts most control on the model. Confidence in the model allows a series of predictive runs to be undertaken to simulate three types of glacier fluctuation: Short term change, behaviour under maximum ice conditions and deglaciation trends. Whilst climatic forcing is important in driving the model overall, topographic effects and the influences of calving are crucial to understanding maximum state conditions and

retreat behaviour. In each of the three cases, the model results corroborate well with what is known about the real world. These matches and the closeness with which the present-day conditions are simulated are mutually supportive to the conclusion that the model is effective and realistic in the way long term ice sheet change in Greenland is represented. The theoretical processes and the model results are considered to describe real processes and events. Modelling, in conjunction with field techniques, is seen as an powerful means of understanding nature.

Acknowedgements

I would like to thank the Natrual Environment Research Council for funding my studenship which enabled me to undertake this research, and for funding two field seasons in Greenland. I would also like to thank U. Radok and the World Data Centre-A for Glaciology, Colorado for providing digital data on the the Greenland Ice Sheet.

In addition, I would like to thank the following people:

David Sugden for his guidance, counsel and friendship and above all his endless, infectious enthusiasm;

David Mitchell for devoting many hours in helping to type-set and print this thesis and for discussion concerning the finer points of computing;

Steve Dowers for showing me how survive the VAX and for fixing anything remotely digital;

Andrew Dugmore for acting as an oak-shod sounding board for new ideas and recurrent problems at all hours of the day, the night and in-between;

Tony Payne and Richard Hindmarsh for guidance on modelling problems;

Charles Warren and Samantha Reynolds for being with me in Greenland;

Susan Mclaughlan, Margaret Milner and Sheena Smith for entering and editing text.

Mum and Dad for teaching me the value of knowledge;

and Hilary for being lover, fiancee and wife and bearing the brunt of 'thesis stress'.

Chapter 1

INTRODUCTION

1.1 Aims

The thesis of this research is that an enhanced understanding of the behaviour of the Greenland Ice sheet during the Holocene can be gained through the application of a numerical model. The main aims were to construct a suitable computer based model, to predict scenarios of behaviour for simulated Holocene conditions, and to assess these model results in the light of what we already know about the Quaternary geomorphology and geology of Greenland. Each of these aims is tackled in chapters two to five respectively. This chapter outlines the rationale behind the work; it aims to indicate why this kind of approach is important in understanding glaciological mechanisms and events in large continental ice sheets like Greenland.

1.2 Background : The Greenland ice sheet

The Greenland Ice Sheet is anomolous. It remains the only continental ice sheet in the Northern Hemisphere while its ice age cousins in similar latitudes in N. America and Scandanavia have long since disappeared. It extends from latitude $61°N$ to $80°N$, from an essentially maritime sub-arctic zone in the south to a continental, high arctic zone in the North. Figure 1 shows the location of the present-day ice sheet in Greenland and place names referenced in the text. Its different parts experience corresponding glaciological variety in mass balance and dynamic behaviour but it is nevertheless a single volumetric and mechanical entity. In contrast to the Antarctic, the majority of its margins terminate on land, even though it retains a number of calving ice streams. As such, it is the only contemporary parallel of the large Northern

Hemisphere ice masses of glacial periods. It provides a unique opportunity to examine the response this kind of ice mass has to environmental change. Like the major ice sheets it has its own deglacial history from which we can seek explanations, but the present-day ice sheet, with its range of glaciological regimes also provides a better suite of information than can be derived for former ice sheets. It should be easier to understand what took place to cause an ice sheet to shrink from a maximum to a known smaller size than from a maximum to nothing.

Although the geographical setting is particularly favourable for glaciogical studies, there are many things about the behaviour of the Greenland Ice Sheet which remain unknown or poorly understood. There are significant areas of the subglacial topography yet unsurveyed and a brief resumé of gross mass balance estimates in Table 1 demonstrates differences of ±20% from eq brium (Loewe 1936, 1964, Bauer 1955, 1967, Bader 1961, Benson 1962, Radok and others 1982). Other authors have suggested similarly varying figures for more local studies (Ambach 1985a, Bull 1961, Diamond 1961, Reeh and others 1978, Weidick 1975, Braithwaite and Olesen 1989, Mock 1967, Zwally 1989). Clearly, such wide differences could have fairly dramatic consequences for the short and longer term balance state of the ice sheet. It would be extremely useful to come up with a means of testing out the likehood of these measurements and suggesting what their glaciological consequences might be. Other glaciological inferences about ice dynamics have tended to be limited to the locality of ice cores from which they were measured. The opportunity to try to link together some of this information for the ice sheet as a whole is appealing. This could enable the measurements at the ice cores to be incorporated into a wider understanding of the ice sheet. Much information has been obtained as a result of coring at Camp Century and Dye3. A lot of this information, however, has more significance for global or Northern Hemisphere trends in Carbon dioxide levels, Oxygen isotopes and recent pollution trends than it it has to the glaciology of Greenland. Nonetheless, measurements on borehole tilt have yielded good data on vertical flow profiles which have been extended to explain the relationship between basal and surface undulations and the age of the ice (Dansgaard and others 1982, Whillans and others 1984, Dahl-Jensen 1985).

Recorded evidence for the postglacial history of the ice sheet is sporadic on the east coast but better documented in the West. In both areas it is open to some contention in interpretation even where good chronologies have been established (Weidick 1975, Kelly 1985, Funder 1990). For instance, it can be demonstrated that parts of

	Total accumulation km3/a	Total ablation km3/a	Calving flux km3/a needed for balance
Loewe			
1936	425	295	130
1964	500	280	220
Bauer			
1955	446	315	131
1967	500	330	170
Bader			
1961	630	120-270	510-360
Benson			
1962	500	272	228
Radok and others 1982:			
Outer Benson line			
	576	69	507
Inner Benson line			
	486	139	347
No ablation			
	614	0	614
This study			
Approx values for balance.	670	490	180

Table 1: Total accumulation and ablation estimates for Greenland from a variety of published sources. Estimates for this study refer to the Initial Standard Run.

the western ice front experienced sporadic standstills or readvances during the overall deglaciation. (Weidick 1968, 1972, Ten Brink 1974, 1975). These have variously been interpreted as direct indicators of climatic reversals during an overall warming (Weidick) or as results of topographic configuration which tend to favour a stepped form of retreat with a relatively stable margin at certain locations (Warren and Hulton 1989). In order to unravel these kinds of disparity, and for a more complete understanding in general, it is desirable to consider the complexity of the glacial history by looking at how the ice sheet reacts to its many inputs as an organic and dynamic whole.

In short, despite the fact that our knowledge about glaciology and glacial geomorphology has continued to advance for the last 150 years, there are still many fundamental aspects of the glacial system in Greenland and its global role which we have yet to comprehend. This may be so for a long time yet. Despite the clamour for 'more data' , in Greenland, as elsewhere, there will always be finite limits to how much can be measured. It will also always be the case that monitoring will never cover more than a fraction of the relevant time span needed to understand processes of ice sheet growth and decay during a glacial cycle. There are temporal and spatial limits to data gathering exercises. As the information base expands, so we need to be more rigorous in the way in which we construct 'knowledge' from it, both to make the most use of our data gathering efforts and to outline the most needful areas for future attention.

By applying some simplified glacial physics to the behaviour of the Greenland Ice Sheet through time and space, this work aims to elucidate some of the characteristic features of the Greenland ice sheet and how it interrelates with the atmosphere, lithosphere and oceans. Given what we already know about Greenland, it seeks to identify the behaviour of the ice sheet during a deglacial cycle and to relate the behaviour to the most probable climatic and environmental factors involved.

To summarise this section: The Greenland Ice Sheet still exists as a significant part of the global earth-ocean-atmosphere system. It has much to tell us about the behaviour of large ice masses in reponse to environmental forcing, particularly as a parallel to the Northern Hemisphere ice sheets. Our limited knowledge of it can be enhanced by careful theory construction.

1.3 A Critical Rationalist modelling approach

This thesis employs a modelling approach to the study of the past behaviour of the Greenland ice sheet. It is different from the alternative geomorphological approach concerned with reconstruction of past behaviour from landform evidence. Geomorphological evidence, by virtue of the way in which it is obtained, tends to concentrate on discrete localities for which it is possible to infer glaciological events. An understanding of regional or continental trends is often synthesised by comparison between more localised studies. Just as the initial interpretation may support a number of explanations, so, at each stage in such a synthesis do the possibilities of interpretation multiply, or become confused, because relating directly by chronology or mechanism the story at one location with that at another may similarly be done in a number of ways. A modelling approach turns this methodology on its head from the outset by laying primary emphasis on the overall rather than on the specific, and on the interrelating mechanisms rather than their geomorphological effects.

By adopting a numerical approach, this thesis concentrates on a subset of theoretical architecture. The knowledge it produces can only be sustained within the confines of this methodology, even if used to contribute to wider spheres.

1.4 Theories and models

The term 'model' is used to imply a construction of causally linked theories, and the word 'numerical' simply describes how the causal links are enumerated. Enumeration tackles 'how high', 'how long', 'how fast' and 'how much of this process does it take to cause this effect' questions. Because the model operates over space and time, its basic constructs vary not only in type but also with space and time. Basic constructs could be a time specific ice surface altitude of a single grid location or, for instance, an average ice velocity at that location. Rules govern not only how velocity relates to altitude but also how altitude at one location relates to altitude at another and to previous and future altitudes and their associated velocities. Rules like these collectively make up the model. The way they are defined affects the relationship of the model to reality, and therefore how it can be used as a sophisticated tool for theory construction in the further explanation of reality. In models, reality is abstracted not only into notional building blocks but also into a hypothetical relationship between building blocks. All that happens when we run a model is that we pass information

between the building blocks according to defined rules. If we are to explain reality then we have in some way to explore the results in the context of these rules in order to assess their truth.

A broadly critical rationalist methodology has been adopted. Certain model runs, that is certain groups of theories about the ice sheet behaviour bear a better relationship than others to the field evidence. They are therefore more coherent explanations of reality and the theories of which these models are constructed are more likely to explain reality.

Although the approach has clear advantages, it is important to stress the limitations. In reality the real world ice velocity is a complex continuous three dimensional phenomenon involving aspects of internal shear, fracturing, and basal sliding of different degrees and types. In the model, the representation of velocity is simplified to have only two components, one representing shear and one representing sliding which are both driven by ice thickness and surface slope. This is a highly generalized representation, but it still aims to demonstrate circumstances in which a sliding process would be more dominant than a shearing one and vice versa. The acceptance of a 'good fit' of a model result to the geomorphic record therefore implies an acceptance of the individual theories within the model as effective representations of reality. The value of this approach depends on the characterisation of the model at the outset. We can never characterise everything; we cannot replicate reality so we can only produce partial explanations and insights.

1.4.1 The choice of model type

The formulation and use of ice sheet models is now the focus of a significant proportion of the science of glaciology. In part this reflects the power of mathematics as an explanatory tool. Although harder to demonstrate, a second historiographic explanation is that, unlike many phenomena in the natural world, ice bodies are fairly clearly bounded, moderately homogeneous, structurally discrete entities subject to the laws of Newtonian physics. The major keystone was provided by Glen's (1955) laboratory experiments on polycrystalline ice that demonstrated the basis of its mechanical properties, namely its deformation rate when subject to applied forces. This demonstration of ice behaving as a non-Newtonian but predictable fluid paved the way for formulations about hypothetical and real glaciers.

The early models were concerned largely with the gross morphology of the steady

state profile, solved as a force-balance problem, assuming the conservation of momentum and negligible ice acceleration. Examples of this kind of model resolved in one, two or more dimensions are numerous, but among the most seminal are Nye's (1952[a], 1952[b], 1957). From a wider perspective, the disadvantage of this category of model is that it cannot by definition, describe the evolution of an ice sheet. Some fixed boundary condition of height or length scale must be assumed initially in order to define the model at any point in time.

The second category of models all derive from the inclusion of the principle of conservation of mass. Though in common use in many sciences previously, the concept of using mass conservation or continuity equations were first applied to ice sheet modelling by Mahaffy (1976). Most significantly, it allows the definition of evolutionary, dynamic models that can demonstrate how ice mass will distribute itself within the glacier over time. It becomes a powerful tool for explaining glacier change when combined with some form of surface mass balance model.

The third step in the development of ice sheet models was to include the principle of conservation of energy. Equations describing this process define the heat status of the ice sheet as energy from the earth's mantle, from the latent heat of incorporated snow, from heat lost to the atmosphere in melting and radiation and from frictional shearing within the ice. Not only does this define the overall energy state of the ice sheet, but it also defines the temperature fields which directly affect the immediate mechanical behaviour of the ice as governed by Glen's flow law.

In the most precise models of ice sheets, the coexisiting stress and temperature fields are solved simultaneously over time in order to calculate the redistribution of mass and energy that will result from those fields. The major difficulty with these more sophisticated formulations is in their solution. The increasing number of degrees of freedom requires solution by complex and computationally intensive numerical analysis. This is the realm of continuum mechanics and much is still done to find precise solutions to these kinds of formulations, namely Hutter (1983), Hutter and Alts (1985) and Mo rland (1984).

In addition to these basic categories of formulation governing ice flow, many authors have developed subsets of theory and built them into models to describe more exactly parts of the glacier system. Examples of this would be Weertman's sliding law (Weertman 1957) and other works specifically on sliding (Kamb 1970, Mo rland and others 1984, Shreve 1984), ice shelf and land based glacier transitions (Muszynski and Birchfield 1987) and ice shelves (MacAyeal and Thomas 1982).

At whatever level of sophistication, the initial formulation of an ice sheet model usually results in the specification of a number of differential or partial differential equations. Whilst the former are usually soluble by simple analytical means, more complex examples are usually tackled by some form of explicit numerical solution, typically finite difference (Oerlemans 1985, Budd and others 1984)) or finite element methods (Hodge 1985, Hooke 1979, Fastook and Schmidt 1982). These equations have to be solved within some spatial system but are commonly simplified into one or two dimensional plan or profile systems in order that the equations are tractable.

1.5 A modelling approach for Greenland

For this research a model was developed to investigate specific aspects of the Holocene behaviour of the Greenland Ice Sheet. The focus is on the relationship between climatic and sea-level driving forces and the glacial response over time. This reflects not only the dynamic behaviour of the ice sheet but also the specific effects of the topography of Greenland and its juxtaposition to climatic regimes. The model was developed in order to predict which behavioural features of the ice sheet system in Greenland have been of key significance. In good Popperian tradition, the gaps which exist presently in our understanding of these dominant controls point to the types of ice sheet model which might be employed in order to narrow them. Testable theories can be enshrined usefully in such models.

Consequently, the nature of the model was directed by some broad aims.

1. It needed to contain a representation of ice sheet flow which would be accurate at the spatial and temporal scales being considered.

2. The ice flow model needed to be driven by some representation of climatic forcing via mass balance and 'eustatic' sea level changes.

3. The mass balance and ice flow models had to be expressed as dynamic functions of altitude, geographic position and locational characteristics of the bed surface and the overlying ice mass. This needed to include isostatic adjustments to ice loading.

These conditions ensured and provided external signals to the evolving ice sheet. In addition the approach was governed by the requirement that the model had to be

soluble over large areas and at a reasonable spatial resolution. The detailed specification of the model elements is given in Chapter 2.

For pragmatic reasons, the ice flow part of the model followed strongly work by Mahaffy (1976), Budd and Smith (1982), Oerlemans (1981,1982) and Payne (1988). The major characteristic of these models is that they are based on a continuity equation for ice mass, expressed as a function of time, solved for grid locations which represent columns. Growth or decline of these columns through time is found as the sum of the mass balance at the system boundary, usually the surface, and ice flux to other surrounding points. Mass flux, driven by gravity, is calculated as the product of the thickness and the vertically integrated velocity. These changes are solved iteratively over discrete time periods whereby all the individual column thicknesses are redefined in one time step. Thus modelled ice distribution and shape evolves through simulated time. Where these models differ is in the topology of the grid, the specification of mass balance, the consideration of ice shelf and ice stream flow, the inclusion or lack of coupled lithospheric and heat balance models, and in the derivation of a velocity, especially sliding equations. The most refined example to date is Huybrecht's (1989) thermomechanical model of the Antarctic Ice Sheet which additionally resolves the ice mass into ten horizontal layers thereby giving a more sophisticated representation of ice flow variations with depth and thickness. These models are invariably solved numerically using finite difference (Oerlemans 1982, Budd and Smith 1982, Budd and others 1984, Payne 1988) or alternating direction implicit methods (Huybrecht 1989). Their major similarities are a dependence on local surface slope and ice thickness as the main driving mechanisms, and therefore their strong dependence on surface altitudes as a feedback mechanism in their evolution (Oerlemans 1984).

Simplifications are involved in the vertical integration of ice flow, the lack of consideration of logitudinal stresses, poor physical representation of ice sliding and ice shelf-ice stream boundaries, and the breakdown of the validity of assumptions towards the ice margin.

It is arguable, from previous work that these errors in flow simulation are small when considering the gross change and response of the ice sheet over long time periods. Good representations of ice sheet evolution as a response to climatic signals have already been produced with the method used here. However, an important caveat to this argument is that it is possibile that non-linear amplifications of small signals may exist in critical areas such as tidewater ice streams or ice fronts retreating into their own ablation areas. The question of whether such a non-linear response can

be realistically produced with relatively simple model assumptions is tackled by this reasearch.

The poor representation of ice sheet flow at certain points could be tackled by incorporating less simplified physical laws, solving them for high resolutions, for instance, by using finite element analysis. Whilst these techniques may produce more accurate simulations of the distribution of mass and energy, they are far more computationally intensive. It is equally questionable whether the detail gained over ice sheet scales and long time intervals is justified when crucial input such as surface mass balance is poorly understood.

The application of this finite difference modelling approach requires as boundary conditions a good climatic model specific to Greenland, and the relevant topography. The existing ice sheet provides one set of boundary conditions in which a known topography and its relationship to mass balance are relatively well known. However, the ice sheet simultaneously obscures the subglacial topography which is imperfectly known. A finite difference scheme was employed because it is relatively easily encoded, adapted and controlled. However, inherent in this method are limitations on time and distance scales, in this case about two years and 20km. (see equation 44, Chapter2).

1.6 Other Greenland Models

Nye (1951) developed the first modern mathematical model of ice sheet dynamics applied specifically to Greenland. He demonstrated the relationship between the surface profile predicted by the model, and the bedrock depression from a steady-state, force-balance analysis. He derived other physical quantities such as basal shear stress, and mass flux. Despite significant programmes of field research in the fifties, sixties and seventies (eg. Battle 1951, La Chapelle 1955, Bader 1961, Benson 1962, Friese-Greene and Pert 1965, Bauer and others 1968), the next theoretical modelling work applied directly to Greenland did not appear until the early eighties with the work of Radok and others (1982) and Reeh (1982, 1984).

That by Radok is by far the most comprehensive numerical study of the ice sheet to appear. It deals almost entirely with the present ice mass for which it derives thermal and mechanical characteristics for an assumed equilibrium. Resolved over a grid these include velocity, mass flux, basal shear, surface and basal temperature gradients and total heat budgets. No dynamic treatment of mass redistribution is

tackled and consequently it does not predict past or future changes and their associated regimes. Reeh's approach (1982, 1984) applies perfect plasticity theory along calculated flowlines using the ice sheet perimeter as the necessary boundary condition. This was developed in 1984 to examine paleo-conditions from maximum glacial extents inferred from geological evidence, particularly for N. Greenland. These reconstructive approaches are extremely useful in examining the shape and basic mechanics of putative profiles. But, short of comparing parts of the reconstructed profile with a number of known margin sites they are essentially untestable. The ice sheet analysis is limited. There is nothing to suggest that even the most obvious geologically infered maximum limits were necessarily synchronous.

Using these models, it is difficult to view the ice sheet as a whole and to study its response to climatic forcing. Further it is impossible to judge the magnitude of perturbation required to cause ice sheet growth and decay. The model by Grigoryan and others (1985) is based on a continuity expression and seeks to predict ice sheet changes produced by climatic perturbation. They predict the ice sheet evolution for seven simulation scenarios for 13000 years forward from the present. The attractive aspect of the model is its full thermomechanical specification even though the the thermal regime is simplified in parts. They use a reasonably fine resolution of 32km. However ther are a number of limitatons. The topographic boundary conditions based on a review by Weidick (1975) are rather limited. Whilst the mass balance terms were based on reasonable assumptions from Bader (1961), no dynamic ice sheet coupling was introduced. The ice sheet was forced in the different scenarios by gross changes in temperature and mass balance. In addition, no terms were included to represent basal sliding, calving, isostatic readjustment or sea-level change. Their thrust seems more to be more towards prediction of the effects of human climatic temperature disturbance than at understanding past simulations. It is difficult to evaluate their own assessment of the geological evidence because the mapped results do not reflect the modelled grid resolution.

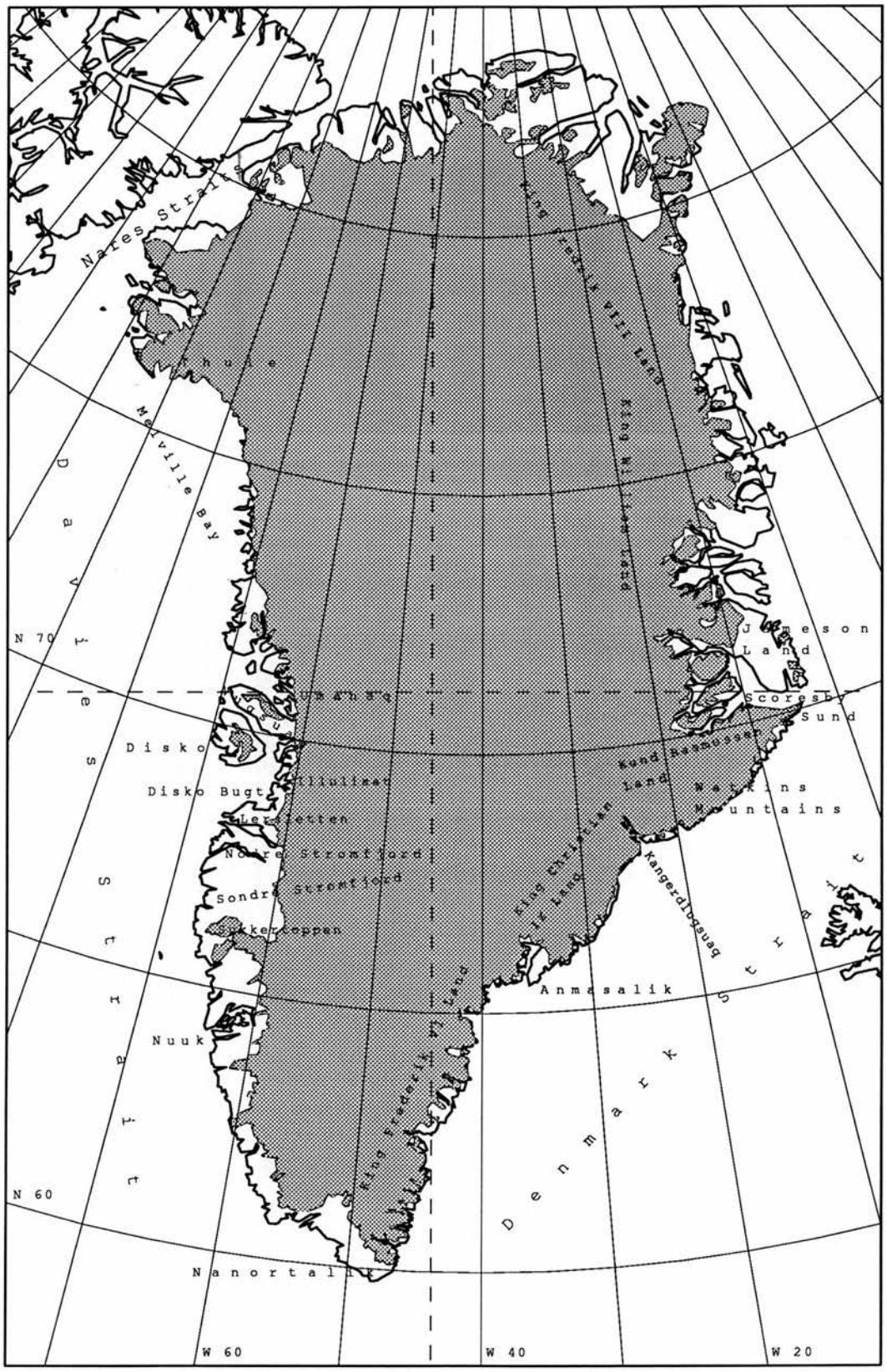

Figure 1: Greenland, the ice sheet (shaded) and the places named in the thesis. The box bounds the model area and the north-south east-west quadrants denote the sector limits used in the volume calculations. Produced from digital data used to extract the model data, projected into an Albers equal area conic projection with standard parallels at $68°N$ and $76°N$.

Chapter 2

IMPLEMENTING THE ICE SHEET MODEL

2.1 The architecture of the system

The ice sheet model, the input information needed to drive it, and the various different forms of output are structured into a linked system of programs and data files. A conceptual view of the system architecture showing its main parts and linkages is given in Figure 2. The diagonal boxes represent processing steps and the rectangular boxes represent data. Key features of this system are its modularity and the storage and transfer of control information between its separate units. This means that individual parts of the model could be analysed more easily, and substituted where necessary. The control information, such as forcing temperatures and sea-level, which defines a particular run is passed from unit to unit as necessary. It needs only to be specified once for a particular run and is held in separate computer files which can act as reference sources during subsequent analysis.

The geographically located information is initially stored and co-located using the ARC-INFO software, chosen because of the ease with which it will capture and manipulate geographical data. This facility is important in the case of Greenland because the different data sets come from a variety of different sources in different projection systems. It is necessary to ensure that they are projected into a common system in order to run the model.

The disadvantage of this kind of proprietary software, at present, is that it does not support internal data structures which allow external computer models to be executed efficiently on them. ARC-INFO stores data as a complex of vectors and

vector attributes in a suite of files held under one directory for each set of information, whereas the model runs on a raster grid and benefits in speed and intermediate storage from using this format for input and output. Consequently, binary grid files were produced from ARC-INFO as input into the Fortran program that actually ran the model. Further programs had to be written to check the data quality. The output files were of the same physical format as the input files and so could be used as new input.

The aim of this chapter is to describe and explain the various parts of the overall modelling procedure. It concentrates in particular on the formulation of the ice sheet model, both its ice dynamic and climatic parts, the topographic data sources and the manipulation of topographic data, practical computing considerations and the production of output.

2.2 The Ice Sheet Model : Theory

The equations which describe the ice and isostatic dynamics form systems of partial differential equations which define the flow of ice and lithospheric mass from one part of the system to another. These equations are solved numerically using conventional finite difference techniques (eg. Smith 1985). The method of solution and the simplifications used, whilst in essence a separate problem, are included in the overall description of the model to maintain the flow of explanation from the initial equations to the actual algorithms used.

2.2.1 Mass Continuity

The model applies directly the work of Mahaffy (1976), Budd and Smith (1982), Budd and others (1984), Oerlemans (1981, 1982) and Payne (1988). It is driven by a vertically integrated ice mass continuity equation. This relates the principal of mass conservation to the ice sheet. Mass cannot be destroyed, and so ice flow into a point must equal ice flow out of the point.

Conceptually, the model can be thought of as a grid of individual ice columns between which ice is allowed to flow. This is shown schematically in Figure 3. The rate at which ice flows between the columns can be calculated from the slope and thickness. Added to this ice flows in and out of the column by surface mass balance exchange and calving. If more ice flows out of a column in a particular time step than

flows into it, then the column thickness reduces and the surface height drops. Once all the new column heights and thicknesses have been assigned the procedure is repeated for the new set of column heights and thicknesses. The system can evolve because the rate of ice flow is a function of the thickness and surface slope and because the surface mass balance rate is a function of surface altitude which also varies with ice thickness. This basic idea is now expressed more formally and exactly.

An ice column for any point on the ice sheet of thickness Z is defined. Through time, the net gain or loss in the volume of the ice column must be equal to the sum of the mass balance external to the system and the net difference in ice flux into and out of the same column. Therefore, the change in ice thickness over time is expressed by the differential mass continuity equation :

$$\frac{\delta Z}{\delta t} = b - \nabla \left(\overline{U} \cdot Z \right) \tag{1}$$

where the rate of change of column thickness Z, over time, t is equal to the sum of the external mass balance rate, b and the mass flux rate to other parts of the system, $\nabla \left(\overline{U} \cdot Z \right)$, the vector product of the ice thickness Z and the vertical average of the column velocity $\overline{U}$. The grid operator ∇ operating on the point flux $Z \cdot \overline{U}$ defines the relative mass flux loss through the column, as being equal to the rate of change in mass flux $\overline{U} \cdot Z$ across the column, in other words, the differential of the two dimensional flux gradient. At any point, this can be resolved in x and y so the rate of change in thickness, z, equals the sum of the mass balance rate and the flux gradients in x and y, where these are conventionally expressed as negative from low to high potential. The flux balance equation becomes :

$$\frac{\partial Z}{\partial t} = b - \frac{\partial q_x}{\partial x} - \frac{\partial q_y}{\partial y} \tag{2}$$

where q_x and q_y are the flux rates resolved in x and y.

The model solves this partial differential equation explicitly using spatial and temporal finite differences solved over a uniform square grid (Smith 1985). This grid relates directly to the same grid of conceptual ice columns described first. More exactly, the time differential continuity equation can be expressed in difference form for a single time step at any grid location by the following equation :

$$Z_{(t+1)} = Z_t + \Delta t \left(b - \frac{\partial q_x}{\partial x} - \frac{\partial q_y}{\partial y} \right) \tag{3}$$

where the subscripts t and t+1 indicate incremental time steps where Δt is the length of the time step. This allows the evolution over time to be approximated but the differential form of the flux gradients over space remains.

These can be solved numerically over the regular grid by turning them into the spatial finite difference form based on the grid cell separation. So in one dimension the change in flux over the grid can be approximated :

$$\frac{\partial q_x}{\partial x} \simeq \frac{q_{x_{i+\frac{1}{2}}} - q_{x_{i-\frac{1}{2}}}}{\delta x} \tag{4}$$

where $q_{x_{i+\frac{1}{2}}}$ and $q_{x_{i-\frac{1}{2}}}$ are the flux rates at the half distances $x_{i+\frac{1}{2}}$ and $x_{i-\frac{1}{2}}$ between grid cells of separation δx (fig 3). The subscripts i, i-1/2 , and i+1/2 refer to the grid position being calculated and the backward and forward positions half the distance to the points x_{i+1} and x_{i-1}, the x-adjacent points in the grid. The flux rate at the half-distances can be approximated as the product of the average ice thickness and ice velocity at the upstream and downstream points x_{i+1} and x_{i-1} thus :

$$q_{i+\frac{1}{2}} = \left(\frac{u_{i+1} + u_i}{2}\right) \times \left(\frac{Z_{i+1} + Z_i}{2}\right) \tag{5}$$

where $\overline{U}$ is vertically averaged velocity and Z ice thickness. This calculation is repeated in the opposite direction for $q_{i+\frac{1}{2}}$. The calculation of ice flux applies similarly to the y dimension.

Given that the ice flux rates have been specified at any given point the next steps are to calculate the thickness, the external mass balance and the vertically integrated velocity, at each point. The model calculates ice velocity by applying physical laws which describe the stress-strain characteristics of ice. Existing reviews describe the ways in which the complex physics of ice can be described mathematically (eg, Colbeck 1980, Paterson 1981, Hutter 1983). The ice dynamics equations used here are therefore not derived from first principals but are presented in order to show how the ice physics is simplified and described by mathematics in the model. Two characteristic types of flow are modelled, that of grounded ice and that of floating ice shelves.

2.3 The calculation of velocity

2.3.1 Grounded ice velocity

Ice velocity is assumed to be the sum of internal deformation and basal sliding movement. The model adopts assumptions commonly used by researchers modelling ice flow. Mahaffy (1976) following Nye (1952, 1959) makes the following simplyfying assumptions in order to permit the vertical averaging or integration of ice velocity :

1. That shear stress variation in the x-y plane is minimal.

   This assumption can break down when shear occurs because of a horizontal velocity gradient. This can happen if two ice flows of differing velocity impinge on one another or if ice flows past a stationary wall. Such situations tend to occur most often at glacier outlets where ice flow is channelled into streams between relatively high bedrock walls.

2. That all normal stresses are equal to the hydrostatic pressure.

3. That the increase of hydrostatic pressure with depth is large compared to the variation of vertical shear stress with horizontal distance.

The last two assumptions can break down when normal stress variation is large in comparison to shear stress variation such as near the ice divide and at the margin. Overall these assumptions mean that the prediction of flow is likely to be poorest near the margin and in areas when bedrock gradients are steep or the topographic amplitude is large compared to the ice thickness. In general, these assumptions were accepted as part of the simplifying procedures and no attempt was made to compensate for them in the modelling procedure. However, they need to be borne in mind when assessing the flow predictions.

The flow law for ice is used as the base for calculating ice flow (Glen 1955, Nye 1957).

$$\dot{\varepsilon}_{xz} = A\tau^{n-1}\tau_{xZ} \tag{6}$$

Where $\dot{\varepsilon}$ is the shear strain in the xz and xy planes, τ is the effective shear stress and A and n are flow constants.

Shear strain can be used to describe ice velocity using conventional continuum analysis : (eg. Chadwick 1976,Harris 1977)

$$\dot{\varepsilon}_x Z = \frac{1}{2}\left(\frac{\partial U_y}{\partial Z} + \frac{\partial U_\varepsilon}{\partial y}\right) \tag{7}$$

Manipulation of these two equations produces a vertically averaged expression for deformation velocity $\overline{U}_d$. The deformation velocity, $\overline{U}_d$ is dependent on the n^{th} power of slope, and the $(n+1)^{th}$ power of thickness as follows :

$$U_{dx} = 2A\,(n+2)^{-1}\,(\rho g)^n\, Z^{n+1} |\alpha|^{n-1} \alpha_x \tag{8}$$

when the slope is considered to have average $|\alpha|$ and resolved α_x parts. This equation is derived by Mahaffy (1976) and Colbeck (1980). It is applied similarly to the y dimension. The Arrhenius constant, A and the power law exponent, n are held invariate for a given model run. The value of A is the average value over the column, weighted in favour of the lower layers where strain is greatest. In reality these terms are derived from empirical equations. The value of n=3 was used throughout, and A was set initially to be $5.0 \times 10^{-25} kg^3 km^3 a^{-6}$. Values for n and A were taken from previous theory (Paterson 1982). A discussion of the justification of these values is given in Chapter 3. The apparent surface slope in one dimension, α_x is approximated as:

$$\alpha_x \simeq \left(\frac{E_{i+1} - E_{i-1}}{2\delta x}\right) \tag{9}$$

similarly in y, where E = surface elevation.

The slope $|a|$ averaged in x and y, is given as :

$$|\alpha| = \sqrt{\left(\alpha_x^2 + \alpha_y^2\right)} \tag{10}$$

Equation 8 is a derivation of the flow law for ice. It assumes negligible normal strain rates compared to shear strains, and small surface and bed slopes. These assumptions tend to break down in the centre of the ice sheet, toward the edges and in any area where sliding velocities become large.

2.3.2 Sliding velocity

The physics of sliding is poorly understood and complex relative to ice deformation. Many attempts have been made to describe the process mathematically. Weertman (1973) and Morland and Smith (1984) have both stressed the importance of regelation and enhanced plastic flow. The significance of water and bed normal load has been

discussed by Weertman (1964) and Lliboutry (1968). Shreve (1984) demonstrates the importance of normal stress on the sliding behaviour at subfreezing temperatures. Some authors have tried to integrate the importance of some of these different effects and how they affect flow in glaciers overall (eg. Kamb 1970, Balise and Raymond 1985). Many of these approaches are difficult to incorporate in this kind of model. On the one hand their fundamental complexity means that they do not lend themselves to simple solution, two dimensional analysis. On the other hand they require predictions of the basal melting regime which cannot be done unless the basal thermal field is also solved. The use of an isothermal model prevents this.

Because of this overall physical complexity, other research has been directed towards generating empirical equations to describe ice flow. Morland and others (1984) have used empirical data to parametize theoretical work. Other approaches do not aim to describe explicitly the processes involved in sliding but rather highlight the key elements which influence sliding velocities. Budd's work is of this type and has been adopted for use in the model (Budd 1979, Budd and others 1984, 1985). Based on work in Antarctica this work produces predictive equations to describe sliding. Specifically, Budd and others (1984) relate the basal shear stress to sliding velocity in the following way :

$$U_s = \frac{k\gamma_b}{Z_*^2} \tag{11}$$

Where γ_b the basal shear stress is defined as :

$$\gamma_b = \rho g Z \alpha \tag{12}$$

and Z_* is a quantity referred to as the effective thickness :

$$Z_* = Z - \frac{\rho_w B}{\rho_I} \tag{13}$$

where,

$$\frac{\rho_w}{\rho_i} B = 0 \tag{14}$$

if the ice is grounded and ρ_i and ρ_w are the ice and water densities respectively, and B is the basal elevation.

The thickness, Z gives a measure of normal stress, thus incorporating one of the important influences on sliding into the prediction. The quantity Z_* in effect describes a buoyancy effect whereby the normal stresses are allowed to diminish with

increased floatation. Equation 14 simply states that no flotation takes place if the ice is grounded above sea-level. The incorporation of γ into the equation is important because as with deformation velocity it is shear stress which drives the ice movement. The constant k (eq 11) was given by Budd as a best fit to the real data and is given the value $2.0 \times 10^4 m^3 bar^{-1} a^{-1}$. This was the value used at first in the model.

2.3.3 Ice shelves

Flow on ice shelves is unconstrained and is dominated by normal stresses in the absence of shearing. In general, the strain rate of unconfined ice depends on ice thickness. McInnes and Budd (1984) approximate ice shelf deformation as a constant strain rate of 0.005 a^{-1}. This model uses the same approach. Floating ice velocity is therefore estimated as :

$$\overline{U}_x = \overline{U}_{x0} + \Delta x \varepsilon_s \tag{15}$$

where $\overline{U}_{x0}$ is the velocity of ice flowing into a particular cell, and ε_s is the constant strain rate. The same applies in the y direction. The term $\overline{U}_{x0}$ links grounded ice flow to ice shelf flow but causes a sharp transition at the grounding line. In reality there is gradual transition from very fast sliding velocities to the normal shear of ice shelves (McIntyre 1985). Some authors predict that longitudinal stresses on the ice shelf can accelerate grounded ice into the ice stream if the ice shelf is unconstrained by sidewalls or islands (Hughes 1987). But because longitudinal stresses are omitted from the model this effect cannot be replicated. The likely retarding of ice flow into ice shelves when they are constrained by obstacles (eg Fastook 1985) is also not simulated because backward stress gradients are similarly missing. However if the ice shelf builds up sufficiently, it reduces ice gradients back onto the grounded ice and can reduce flow in this manner. Similarly, if ice is evacuated quickly by calving at the margin the overall altitude of the ice shelf falls, and this steepens gradients back towards the grounding line which increases flow rates.

2.4 Basal elevations and isostatic readjustment

In order to calculate the surface gradients used in equation 8, basal elevations need to be known. Theory suggests that ice sheet stabilities are influenced if their beds rise or fall as an isostatic response to changes in ice overburden. Such a relationship

is simulated in the model using an equation which relates the second order mass flux rate in the asthenosphere to a diffusivity constant and function described by the relaxed asthenosphere surface, the present asthenosphere surface, and the additional water and ice loads (Oerlemans and van der Veen 1984). The change in the bedrock elevation over time is described as a diffusion of mass to other areas depending on the mass difference between the present and relaxed bed and the additional overlying water and ice loads. Areas of the lithosphere which are 'heavy' push bed mass towards areas which are 'light'. This relationship is given by the following diffusion equation :

$$\frac{\partial B}{\partial t} = D_a \nabla^2 \cdot (B' - B + L) \tag{16}$$

Where D is the diffusity constant and the additional load L, is :

$$L = L_i + L_w \tag{17}$$

where the subscripts i and w indicate ice and water loads respectively, and:

$$L_i = Z \frac{\rho_i}{\rho_w} \tag{18}$$

if the ice is grounded above sea-level, and :

$$L_i = Z_* \frac{\rho_i}{\rho_w} \tag{19}$$

if the ice is grounded below sea-level, and :

$$L_i = 0 \tag{20}$$

if the ice floats or is absent, and :

$$L_w = \frac{\rho_w}{\rho_m} (B_0 - B) \tag{21}$$

if the current or relaxed bedrock is below sea-level, and :

$$L_w = 0 \tag{22}$$

if both are below sea-level and B' is the relaxed bed elevation, B is the present bed elevation and B_0 is sea-level. The B terms here equate lithosperic mass weightings directly with altitude and so assume constant lithospheric density, $\rho_m = 3300 kgm^{-3}$. The bedrock therefore responds at a lagged rate to changes in the overlying ice and water masses. Rock is literally squeezed out from under growing ice sheets. Global

falls in sea-level tend to push asthenospheric mass to seaward and so counteract the fall in absolute sea-levels.

This partial differential was solved using finite differences over the same grid system as for the ice flux calculations. For one time step at one grid cell this becomes :

$$\frac{\partial^2 (B' - B + L)}{\partial x^2} + \frac{\partial^2 (B' - B + L)}{\partial y^2} \tag{23}$$

where,

$$\frac{\partial^2 (B' - B + L)}{\partial x^2} \simeq \frac{\left[(B' - B + L)_{i+1} - 2(B' - B + L)_i + (B' - B + L)_{i-1}\right]}{\delta x^2} \tag{24}$$

Intuitively, the above represents an 'extremely sticky bathwater' model in which the lithosphere, oceans and ice sheets are allowed to float on an extremely viscous but liquid asthenosphere, that has no inherent strength. The asthenospheric mass flux responds to disturbance from a relaxed state, trying to redistribute mass to achieve an archimedian equilibrium. As a consequence, there is no single time lag, only a response to additional change in loadings which constantly 'remembers' previous loadings by reference to an assumed relaxed state and present basal elevations, which are themselves a function of previous trends. In reality, the cooler rocks near the surface are not very viscous and tend to form a more rigid and elastic 'skin' on top of the underlying more fluid asthenosphere. The model therefore cannot replicate results from flexural effects as a semi-rigid lithosphere is loaded and unloaded through time. This would involve the solution of another time and location-dependent equation to describe the strength and elasticity of the upper layers of the lithosphere.

The 'relaxed' bedrock surface is calculated at the outset of the model simply by removing the asthenospheric mass equivalent of present ice cover :

$$L = z\frac{\rho_i}{\rho_m} \tag{25}$$

Consequently, if the model starts from present the modelled isostasy is by definition in equilibrium. So the assumption is made that this is the case in reality too. Starting the model with other ice conditions means this 'relaxed' surface has to be introduced separately, because the modelled asthenosphere would not necessarily be in equilibrium.

2.5 Mass balance and external forcing

The mass balance rate is simply expressed as :

$$b = V_p + V_a + V_c \tag{26}$$

Where V_p, V_a , and V_c are the accumulation, surface ablation and calving fluxes respectively. Additional ablation from basal melt, wind blowing of snow and ice shelf bottom melt was assumed to be of minimal influence and not included in the estimation of mass balance.

However problematic the ice flow assumptions may be, to some extent that part of the model acts purely as a 'machine' for processing ice mass whose input is snow accumulation and whose output is surface ablation and calving. Realistic modelling depends crucially on accurate modelling of these individual mass balance terms. To allow the model to evolve over time they need preferably to be derived from a 'global' temperature signal which can act as a proxy for Milankovitch forcing, and which can be estimated from the deep sea or ice core records as a real signal. A second driving function is 'global' sea-level, which again acts as a proxy to reduced ocean volume during glaciation. Sea-level also directly affects the isostatic and ice sliding relationships above.

There are a number of things to consider here. Whereas the ice dynamics equations may be regarded largely as temporally and geographically aspecific, accumulation and surface ablation rates depend strongly on local topography and positioning relative to climatic variables such as atmospheric temperature fields and air mass circulations. Mass balance is then a function both of 'global' climatic variables and the topography of the ice sheet surface which is itself dynamic. This allows the modelling of an important feedback loop in ice sheet development. In other words, ice sheets self-influence their own climatic regimes.

Secondly, the Greenland Ice Sheet exists presently. This can aid the understanding of climatic variability but can also present modelling hazards. Certain of the factors which are typical of the way the climate alters under the presence of an ice sheet can be surmised whereas without an ice sheet, analogous conditions are difficult to infer. The problem is that a mass balance model could end up being a statistical or empirical artifact of the present whose behaviour in other situations is erroneous and erratic and has little bearing on physical process.

So there were two clear objectives here. Firstly, to attempt to develop a model with

some underlying physical rationale which would be topographically and temperature dependent. Secondly, to use what is known about the present ice sheet climate to quantify the magnitude of the modelled relationships and critically assess the accuracy and response of the models under the present topography. Some circularity exists here because for a given model, certain parameters are likely to be derived from a present-day 'best fit'. However, it is possible to critically eliminate models which do not give good simulations and rely on the fact that the basic model assumptions are made before obtaining parameters.

2.6 Surface ablation

Surface ablation is more easily understood and successfully modelled than accumulation. Physically it is a relatively simple process involving the absorption of heat into the ice to provide latent heat for melting or sublimation. This itself is dependent on insolation, albedo and surface and air temperatures. On real ice sheets these quantities differ diurnally and with changing surface characteristics. Theoretically, it would be possible to produce a model containing some of these factors and drive it using solar radiation, seasonal cloud cover, and daily temperature regimes whilst making assumptions about albedo as a function of seasonal duration and surface ablation rates. However, reconstructing these variables from a single, global temperature signal presents problems. The dominant controls are nonetheless all strongly correlated with temperature. It seems reasonable to attempt to produce a model using this alone as a first order approximation.

The surface ablation model used follows work by Budd and Smith (1981). This uses data derived from Canada and Scandinavia to predict surface ablation as a function of altitude and latitude (Fig 4). Surface ablation is expressed as :

$$\log_{10} V_a = \frac{1}{2000} (E_0 - E) \tag{27}$$

Where V_a is surface ablation, E is surface elevation and E_0 the altitude of the 1m/year surface ablation. A maximum of 15m/a was imposed on the model but in practice this value was rarely reached. This figure is the maximum value typically recorded for Greenland (Braithwaite and Olesen 1989). Budd and Smith derive the elevation of E_0 for the Northern Hemisphere from present-day glaciers in Norway and Canada. In the model an quadratic equation is generated to predict E_0 at a given latitude of the form :

$$E_0 = a + b\Theta + c\Theta^2 \tag{28}$$

The values of the parameters are obtained by regression on four fixed E_0 points taken from Budd and Smith's data, fixed initially at 60, 70, 80 and 90 degrees North, where :

- E_0 at $60°N = 1700$
- E_0 at $70°N = 1040$
- E_0 at $80°N = 570$
- E_0 at $90°N = 170$

The variation of surface ablation with altitude and latitude for present-day conditions is shown by the centre panels of figure 8. Unlike accumulation, it does not vary with continentality (see below on accumulation).

The surface ablation model is forced by moving the fixed points of E_0 to new latitudes. So, for a fixed E_0 altitude, the new latitude becomes;

$$\Theta_0' = \Theta_0 + F\delta T \tag{29}$$

where F is an ablation forcing parameter which describes by how many degrees of latitude the fixed E_0 points need to be moved for a change in the global temperature value, δT. New parameters are found for the quadratic equation (30) which defines the entire E_0 line. A new, forced, ablation value can then be calculated for each cell. The problematic area is how to relate this artificial movement of the E_0 line to new latitudes with the global temperature parameter. This means obtaining a value for the ablation forcing parameter F. As a guide to evaluating this parameter it is possible to look at the present-day relationship between temperature and ablation.

Figure 4 shows a graph of E_0 altitudes against latitude, the E_0 line, for present-day(solid) and a forced(dashed) case. At fixed latitudes there is a change, δE, in E_0 altitudes for the forced case and corresponding to the change $\delta\Theta$ for fixed altitudes. It is first necessary to consider what is happ ening to temperatures along the E_0 line. The are two components affecting temperatures along the E_0 line. Toward the south, temperatures rise with latitude, but there is a compensating fall in temperature associated with the rise in altitude of E_0. If temperatures along the E_0 line were

constant, the latitudinal temperature lapse rate would need to be matched by the altitudinal lapse rate component.

It is possible to evaluate these two components. The latitudinal lapse rate can be approximated linearly as $dT/d\Theta = 0.973°C/°\Theta$. The altitudinal gradient along E_0 is non-constant but can be linearly averaged between $60°N$ and $90°N$. This evaluates as $(1700 - 170)/30 = 51m/°\Theta$. The temperature equivalence of this altitude gradient can be found by applying an altitude-temperature lapse rate. This has a linear value of about $0.8°C/100m$ for Greenland, or $0.008°C/m$. This value is derived below (eq 38). Thus the temperature gradient equivalent to the altitudinal gradient along E_0 is $0.008 \times 51 \simeq 0.4°C/°\Theta$. This demonstrates that temperatures are not constant along E_0. In fact they are falling at a rate of approximately $0.973 - 0.4 \simeq 0.573°C/°\Theta$, even though, by definition, the ablation rate is constant along the E_0 line.

The separaration of the latitudinal and altitudinal components affecting temperature along E_0 set two putative boundaries on possible values of the ablation forcing function F. If the assumption is made that ablation rates vary directly with temperature over latitude, then this prompts the use of the latitudinal lapse value of $0.973/°C$ to describe a minimum shift in the E_0 line latitudinally for a given temperature perturbation:

$$F = dL/dT \tag{30}$$

or $dT/d\Theta = 1/F$. If the linear approximation to dT/Θ is about $0.973°C/°\Theta$, then $F = 1/0.973 = 1.02°\Theta/°C$.

Alternatively, the value of $0.4°C/°\Theta$ for the altitudinal equivalent temperature gradient can be used as a maximum putative boundary on how much to shift the E_0 line with temperature forcing.

$$F = (dL/dE)(dE/dT) \tag{31}$$

so $1/F = 0.4°C/°\Theta$ and $F = 2.5°\Theta/°C$.

Further analysis indicates which of these two values is more likely correct. If we reconsider that temperatures change along E_0, then, at constant altitudes, changes in ablation rates with latitude are associated with smaller temperature changes than are the same changes in ablation rates at constant latitudes and changing altitudes. It seems that, with the assumptions made, equivalent ablation can occur at lower temperatures further south. There is an additional effect enhancing ablation rates

relatively at lower latitudes and reducing them at higher latitudes which is not directly attributable to temperature differences.

Energy balance studies bear this out. Ambach (1985) uses the following expression to describe the energy balance of ice at the glacier surface.

$$NB + HS + HL + HC + HM = 0 \tag{32}$$

if each term can have negative or positive value. The overall radiation energy sum, consisting of longwave and shortwave elements is the value NB; HS is sensible heat, HL is latent heat and HC is conducted heat. The amount available for melt HM is the remainder of the other terms. Radiation balance is governed by the Stephan-Boltzman law which determines that radiation emission varies as the fourth power of temperature thus :

$$\eta = \sigma T^4 \tag{33}$$

where η is energy and T the absolute temperature and σ the Stephan Boltzman constant. Net radiation is the balance of longwave emission from the ice surface and long and shortwave incoming radiation. At temperatures close to zero, additional heat transfer for progressive changes in temperature is about 1.1 times greater than the change in absolute temperature. Heat conduction terms are governed by diffusion equations which are dependent on relative temperature gradients. The sensible heat capacity of the surface depends on the ice density there.

It is clear from this analysis that direct correlation between ice surface temperatures and surface ablation rates does not exist. Furthermore, the prediction of surface ablation rates using full energy balance models requires fairly complex specification. In the first instance individual balance terms need to be calculated separately. Melt rates are governed by the amount of excess heat at the ice surface for a given period. Therefore, the way in which heating is concentrated into days and seasons is important. This model averages seasonal mass balance and so an energy balance approach would need to be weighted to take into account differing seasonal and day length. Some of the best predictive models for Greenland by Braithwaite and Olesen(1989) bear this out. They generate regression equations between measured surface ablation and temperatures above freezing summed for days in which the temperature is above freezing. This makes annual surface ablation a function both of temperature and season length. Braithwaite and Olesen find that regressing surface ablation against

mean summer temperatures produces poorer correlations. Averaging with annual temperatures would degrade the process further. In addition, they find that even on glaciers with similar dry surfaces different locations give different energy balance relationships. With even more variability in surface characteristics over larger areas poorer generalisations result. Differences in the seasonal concentration of energy budgets act so that higher surface ablation rates can occur with lower mean temperatures. It is the large excesses of heat in the summer time which are significant for surface ablation and these are greatest in the south. The differences in surface ablation rates between latitudes is greater than their corresponding mean temperatures for this reason. Modelling this correctly is a major problem in itself and so the adoption of an explicit energy balance model was avoided because of the complexities it could have introduced.

Nonetheless, energy balance considerations show that the divergence between the equivalent temperature gradient of E_0 and the latitudinal temperature gradient are unsurprising. Furthermore, whilst the process involved in creating more energy positive situations to exist further south for a given temperature is not explicitly derived, the magnitude of the effect is suggested by the divergence of surface ablation and temperature gradients. It is this fact which can be used to suggest a good value with which to relate temperature forcing and surface ablation forcing. Consequently, the assumption was made that the $2.5°\Theta/°C$ value was the rate at which the fixed E_0 points needed to be moved in order to force surface ablation. This assumes that the energy balance differences which presently allow the same surface ablation rates to occur at different mean temperatures are directly transferable to temperatures of the perturbed model. For a $+1°C$ warming, for instance, it predicts that, at a given latitude and altitude, surface ablation rates can occur at cooler temperatures than they did before. An E_0 point inherits the energy balance characteristics of places where under normal conditions, the temperature difference in altitude between the points would be $+1°C$. That location under present conditions can produce the same surface ablation rates at lower physical temperatures.

It is worth considering briefly how realistic this assumption is. The problem relates to the permanency of the energy balance patterns. Some changes can be expected because changes in solar insolation are phased with temperature change. However the relationship between insolation variation and temperature is not constant (Oerlemans 1985). Increase in longwave return could be anticipated with increased cloudiness,

which in these latitudes would most likely occur with warming. Likewise, more extensive ice cover produces higher albedo surfaces for longer periods, and reduces the effectiveness of the season length. Overall, the surface ablation temperature gradient is less steep than the physical temperature gradient. Whilst this lessened surface ablation temperature gradient can in part be related to fairly fixed solar input, it can also be expected to maintain a similar gradient over time because the majority of the effects which cause it are not locationally specific. The time permanency of the surface ablation temperature gradient is not testable in itself. It was therefore of interest to test different values of the surface ablation forcing constant, F. Experiments showed that it was difficult to force the model sufficiently using high values of the surface ablation forcing constant. Only runs with the two extreme values of $F = 1.02°\Theta/°C$ and $F = 2.5°\Theta/°C$ are presented in the results but other values were explored, particularly when trying to get the model to grow to maximum. In the end, only the $2.5°\Theta/°C$ value suggested by the present-day gradient of the E_0 line proved sufficiently small to force growth to full maximum.

2.7 Temperature

An expression was derived separately for surface temperatures. The surface temperature T_s is obtained by applying a lapse rate dT/dE to a sea-level temperature, T_0.

$$T_s = T_0 + \frac{dT}{dE}(E - E_0) \tag{34}$$

where E is the surface elevation in metres above sea-level. Values for T_0 and dT/dE are obtained below.

The surface temperature model provided the means for driving the accumulation model (below) and also gave a temperature-latitude relationship to force the surface ablation model.

The Sea-level Temperature model

Forcing surface temperatures by a global temperature signal needed to be done with reference to a standard base so the first step was to derive a sea-level temperature model. This was done with reference to assumed equivalent sea-level temperatures for the present-day which were obtained by working back from the real world surface

temperature distribution using a lapse rate.

Equivalent sea-level temperatures are known to be a function of variations in radiation with latitude and the distribution of land and sea areas. A model of sea-level temperatures was therefore derived in terms of in terms of latitude and the continentality factor. This was done by regressing the derived sea-level temperatures against latitude, the square of latitude and the continentality factor. This was then used with a lapse rate to obtain surface temperatures (above) and thence accumulation values (see below). The following equation defines sea-level temperatures, T_0 :

$$T_0 = -83.4 + \left(3.53\Theta \times 10^{-2}\right) - \left(0.3104\Theta \times 10^{-2}\right)^2 - 9.787C \qquad (35)$$

Where Θ is latitude in degrees North, and C a continentality factor which has values $\geq 1, < 2$. The value C, follows a scheme used by Oerlemans (1984) and is calculated by considering a circle of diameter Dc centred on the location for calculation. C is defined as :

C = (Area of circle over land/ Area of circle over sea) + 1

Therefore, if the circle encompasses entirely land based areas, C=2, and if it encompasses entirely sea areas, C=1. The value of Dc used in the calculation of C for parametization was 350km, the approximate east/west mean half-width of Greenland.

2.7.1 Surface temperatures and lapse rates

Radok and others (1982) obtain an expression for an altitudinal environmental lapse rate by dividing geographic temperature gradients by surface slope. Several experiments with this method showed that it is not possible to define unique point values for a lapse rate; they vary depending on the distance over which they are defined. A lapse rate applicable over all distances is needed, which can be obtained by regressing surface elevation against surface temperature. Even though a low r-squared value is returned the surface elevation accounts for a certain proportion of the variance, and its coefficient indicates the strength of the relationship, namely :

$$T = T_0 - 7.46 \times 10^{-3} E \qquad (36)$$

where T is surface temperature, T_0 is temperature at the base elevation, E is elevation from base. A quadratic form of this relationship was also determined

$$T = T_0 - 3.67 \times 10^{-3}E - 8.32 \times 10^{-7}E^2 \tag{37}$$

Lapse rates can be obtained in each case by differentiation :

$$\frac{dT}{dE} = -7.468 \times 10^{-3}E°C/m \tag{38}$$

$$\frac{dT}{dE} = -3.67 \times 10^{-3} - 1.67 \times 10^{-6}\ E°C/m \tag{39}$$

Integration of dT/dE, allows the lapse rate to be applied to surface temperature to obtain sea-level temperatures in each case. The quadratic form of the lapse rate was used in predicting surface temperatures for predicting accumulation because it provided less unexplained variance in the overall accumulation model. This provides some sort of sea-level temperature map which can be used in deriving a sea-level temperature model (above). The same lapse rate can be used subsequently to reconstruct a surface temperature model. Since the lapse rate explicitly defines the altitude:temperature relationship, and its value is already derived, it was easier to use the derived surface temperatures in the accumulation model rather than search for a new parameter describing altitude/temperature relationships.

2.7.2 Evaluating modelled temperatures

Because no real data on sea-level temperature exist, assessment against real data could not be done directly. However, by applying the original lapse rate to the modelled values, modelled surface temperatures could be obtained, for which real world equivalents do exist. A comparison of the real and modelled surface temperature values can thus give a measure of the model 'fit' even though a direct comparison of real and modelled sea-level temperatures cannot be made. The aim here was to reduce the model error as much as possible where the total error is given as :

$$r_m^2 = \frac{\sum(Res^2)}{\sum\left(\overline{T} - T\right)^2} \tag{40}$$

and individual residuals as :

$$Res = T_{model} - T_{real} \tag{41}$$

where T_{real} and T_{model} are the real and modelled surface temperature values respectively. The resultant residuals from the model are therefore that part of present

surface temperatures which cannot be accounted for either by elevation or sea-level temperature model relation. In practice, this sequence of procedures was conducted as a series of experiments in order to find models with less error.

2.8 Accumulation

Accumulation is daunting to model. A data set describing present-day mass balance rates was obtained from the WDC-A for Glaciology. Stemming mainly from snow pit studies in the 1960's (especially Benson 1961) it is unfortunately rather sparse and covers a limited time period. To do the accumulation analysis, some assumed surface ablation value had to be added to the interpolated mass balance values to arrive at some estimate of accumulation. A Budd calculation for present-day surface ablation was applied with a 1.5m ceiling on the surface ablation rates. The Budd figures relate to total potential surface ablation which can be far above any realistic accumulation value for an individual year which these pit studies represent.

A predictive equation was formed by a two stage parametrization of theoretical relationships against the real world mass balance data. The means for processing the input data are described below. One stage of the parametrization produced the accumulation equation as follows :

$$V_a = -2.721 - 9.24 \times 10^{-3} T_s + 8.84 \times 10^{-5} T_s^2 \tag{42}$$

Where V_a, is the predicted accumulation rate in m/year and T_s is the modelled surface temperature in Kelvin. (This allows for the incorporation of the quadratic form). A minimum value, initially of 5cm/a, was put on this evaluation, indicated by the smallest observed values over Greenland and Antarctica. This is because in some circumstances the model can produce very low or negative values. The surface temperature T_s is obtained as above (eq 34).

Comparative maps of the input accumulation data, the modelled values for present-day conditions and absolute model error residual are shown in the figure 6. Similar maps are given for the temperature model in figure 7. It is worth noting that the real surface temperature and accumulation maps are also subject to errors. The real maps are interpolated from a sparse number of data points compiled by Radok and others (1982), relating to numerous expeditions this century. They are therefore not time-coincident. Accumulation rates have largely been calculated from net mass-balance rates derived from snow-pit studies. The source information for the real accumulation

pattern does not therefore differ from Radok and others (1982) but the interpolation scheme is different. Radok's work only refers to net balance rates whereas here, modelled surface ablation rates have been applied to the net mass balance values to obtain a measure of actual accumulation. This is necessary to relate real accumulation values to the separately calculated modelled values.

Modelled accumulation values for the latitude-altitude and continentality envelope of Greenland for present-day conditions are shown in figure 8. This shows the effect of all three variables in the temperature equation which governs the accumulation. Accumulation decreases non-linearly with both altitude and latitude. Roughly speaking, the available altitude variability over Greenland accounts for the same order of accumulation difference as does the available latitude variability. Less continental areas (C=1.0) are warmer and wetter than the most continental ones (C=2.0). Increasing continentality therefore depresses the latitudinal and altitudinal accumulation and temperature gradients.

2.8.1 The derivation of the accumulation model

There were two important criteria for the accumulation model. Firstly that it should relate in some manner to physical process, and secondly that it should be able to be forced by the same 'global' temperature signal as for the surface ablation model. Ideally, some form of atmospheric circulation model or moisture diffusion model would have been used to represent the physical complexities of moving moisture-laden air masses.

This kind of model has been used by Oerlemans (1984). He develops a dynamic mass continuity equation to describe the water vapour content in the atmosphere as a function of advection of water by horizontal winds, horizontal mixing, input in the form of evaporation and output in the form of precipitation which has a constant and orographic part. As an example, he solves this equation numerically to a converged steady state over present-day Europe and produces a credible comparison with reality. Similarly Keen (1984) develops an upper atmosphere vorticity index to describe moisture transfer and release over Greenland. The modelled accumulation values produced by this model show only a reasonable correlation with reality. Despite its advantages in understanding the complexity of external controls, the inclusion of a model of this type would have involved another numerical solution routine, the development of which time precluded.

Instead, this work follows alternative approaches by Oerlemans (1981) and a study by Mock and Weeks (1966). These develop empirical predictive equations to model accumulation. If moisture fluxes are not modelled explicitly, and an empirical scheme is used, it is nevertheless desirable to relate predicted values of accumulation to physical quantities which are central to the process of snowfall. Oerlemans (1984) and Van der Veen make the general observation that physically, precipitation is strongly controlled by atmospheric moisture availability and that this is itself strongly influenced by air temperature (fig 4). This implies that two important values to include are the temperature of the local air mass and another value which relates strongly to the process by which moisture is given up by the atmosphere.

Using the same mass balance data as this study Mock (1967) formulates a set of three regression equations to describe mass balance values statistically. It was assumed that the mass balance largely reflected accumulation and the raw mass balance was regressed against latitude, longitude and altitude. These quantities were regarded implicitly as combined surrogates for air temperature, and the position relative to the main depression tracks along each coast, (as moisture supply controls), and the intensity of upper atmosphere vorticity (as release mechanisms). The equations covered a northern, intermediate and southern sector, and achieved R^2 coefficients of over 0.95 in each case.

The Northern and Southern equations were also adopted by Radok and others (1982) to yield similar results. Unfortunately, the match between zones is extremely poor, and if, as was done in the present study, the operation is repeated with the entire data set to obtain a continuous field, the best coefficient that can be obtained is 0.66. If two or three equations are used together, there are considerable discontinuities in what they predict in areas of overlap. Because these equations contain a number of quadratic terms, they are not very stable, particularly beyond the bounds of the source data areas. The inputs of latitude, longitude and altitude are complexly cross correlated with temperature and release factors and the nature of this cross correlation varies between zones. The equations therefore end up more as a statistical fit rather than a more direct representation of physical process.

In an Antarctic model, Oerlemans uses the following equation to replicate precipitation patterns.

$$P = max\left(0.05; \left(0.3 + 14s - 4 \times 10^{-5}h\right)/C\right) \tag{43}$$

where P=precipitation in cm/year, h=altitude in metres, s=slope, and C= a

continentality factor scaled between 1 and 2 to represent the proportion of ice cover within a certain radius : 1=no ice within radius and 2=complete ice cover within radius. Decreasing temperature with altitude is taken into account by the h term and s, the slope, accounts for orographic air mass uplift. Oerlemans obtained values for these coefficients by fitting the general equation to present-day observed accumulation in Antarctica. The whole of the equation is then multiplied by a function f(Ts) where Ts is sea-level temperature, to take account of non-elevational temperature variation. The value of Ts he derives from climatic data on snowfall in Scandanavia and Canada. This effectively reduces accumulation from the maximum 0.5m either side of $0°C$.

This Oerlemans scheme was more attractive because the terms are more easily attached to physical quantities. For pragmatic reasons described below, it proved easier to drop the altitude (h) term and the sea-level (T_0) term and substitute a surface temperature value (T_s) to produce directly the temperature variability. The equation can thus be reformulated :

$$V_a = (a + bS + cT_s)/C \tag{44}$$

Several different forms of this equation were used in a limiting exercise employing different definitions of continentality, slope and real and modelled surface temperatures. Whilst investigating correlations between individual variables it became evident that much of the modelled accumulation values can be accounted for by variations in modelled surface temperature alone. The equation (42) is of this form and was obtained as a least squares regression of gridded accumulation values against surface temperature values as obtained by equation (34), and their squares. The derived R^2 coefficient was 0.85 though this value is not very meaningful given the strong collinearity of the gridded data. It does not employ any slope term because, statistically, extra terms describing slope account for no further significant variability in accumulation rates. The implication is that over large distances, changes in moisture availability related to temperature are large compared with changes in moisture release mechanisms related to slope. The moisture release process appears relatively uniform. In part this may be because of the strong statistical correlation between slope and surface temperatures, particularly because the modelled surface temperatures used are of second order in altitude (eq 37). Some aspect of slope variability could therefore be present within the surface temperature values themselves.

Nonetheless, the geographical pattern of the model error (fig 6) shows no regular pattern that could be associated with slope or any other predictable physically

related quantity. Accumulation is underpredicted near to coastal indentations. It is possible that there is some unaccounted process relating to the way in which cyclones accelerate and thus deepen in accordance with coastline configuration.

The problem of intercorrelation

A methodological problem is introduced because of the nature of the two step procedure and because of the natural intercorrelation of the variables. Temperatures and hence accumulation drop toward the centre of the ice sheet. The question is how much of this temperature drop is due to altitude and how much due to increasing continentality? The surface altitudes and continentality are strongly correlated themselves; the middle of an ice sheet is both higher up and further from the sea than the edge. Since there is no independent check on equivalent sea-level temperatures the two effects are difficult to distinguish.

The problem of distinguishing between the two effects applies particularly to whether or not the vertical lapse rate over Greenland is linear or non-linear, and to the separate introduction of a continentality factor to model sea-level temperature. The experiments found that there was a progressive acceleration of cooling toward the centre of the ice sheet. Surface temperatures get colder at an increasingly faster rate toward the interior. One way of modelling this feature was to use a non-linear lapse rate (eq 39). This suggests that not only do temperatures drop but also that the rate of cooling increases with altitude. Another way of modelling the same feature is to suggest that there is a stronger continentality effect, that progressive cooling of surface temperatures is related to enhanced continetality effects at all altitudes. In other words, it is possible to produce a similar ice surface temperature model result by using a linear lapse rate and a strong dependence on continentality or by using a non-linear lapse rate and having a lesser dependence on continentality for sea-level temperatures.

It seems reasonable to anticipate a continental cooling purely as an effect of the land mass. This happens over other continental areas. Similarly, one could expect enhanced radiation losses from the high albedo surface ice sheet than equivalent land surfaces.

Winter-time continental cooling over ice-free areas occurs because of the reduced short-wave radiation input. Higher albedo snowy surfaces also reduce effective incoming radiation whilst long-wave ground radiation continues. Radiative heat loss is only partially balanced by advective heat gain from the warmer ocean air masses and

so areas furthest from the heat supply, the ocean, are coldest. The ice sheet tends to act similarly, but forms a permanent heat sink mainly because of the permanently high albedo surface. Just as over winter-time continental areas, toward the centre of the ice sheet there is more or less perpetual radiative loss; the only heat gain is by advection. The interior thus stays permanently relatively cooler. Some of the effect occurs purely as an effect of distance, but some relies on the permanency of the snow cover. The long-term combined effect for cooling toward the interior is thus greater than would be the case over ice free areas. In addition to altitude effects, temperatures are lower toward the centre because the distance from the coast increases, and the mean annual albedo is higher there. The two effects multiply.

A simple altitude effect for accelerating the rate of cooling is harder to account for. By making the lapse rate non-linear and dependent on altitude itself it may be that some additional albedo effect is being included rather than any actual dependence on altitude. A good fit in the sea-level temperature model derived either by the linear and non-linear lapse rates could only be achieved with a continentality factor in each case. This probably indicates that there is some land mass dependence on temperature. In the end, the non-linear lapse rate (eq 39) was employed in the main model partly to allow for the representation of both effects, and partly because it gave a better fit overall. This was used in the derivation of the final temperature expression (eq 34).

The end result of this approach is that mass balance is modelled solely in terms of latitude, altitude and the additional continentality factor. How good is such a model ? There are few pragmatic alternatives. We still know exceedingly little about real mass balance values and the physical processes that influence them. The error differences between the model and reality are consistent with the error limits of the real estimates themselves although these can only compound the overall error. It would be possible to include present-day values directly into the model and assume them constant but this would not allow a representation of some of the important feedbacks that operate as ice sheets evolve with forced temperature changes. These are included because of the strong dependence on altitude although this is not linear or simple. The model is certainly not completely accurate, but it is definable and easily comprehended.

Before applying the model over the ice sheet it is possible to do some simple static analysis to observe how the accumulation and surface ablation components combine and how the model is forced depending on the value of the surface ablation forcing

constant used. Figure 8 shows the how the accumulation and surface ablation patterns vary over the latitude:altitude space in Greenland. Mass balance is the simple sum of the two values. The figures for the mass balance show that a peak of maximum net accumulation rates exists in low latitudes ($65°N$) and high altitudes(2500m). Away from these peak areas, net mass balance will decline to the south and below largely because the melt rate increases, and to the north and above largely because snowfall is insufficient. Surface ablation is static with continentality and so it is only the variability of accumulation with continentality - C which gives rise to the different mass balance scenarios in the third panel of figure 8. Strictly, the surface ablation rate is only the potential surface ablation rate since the actual rate depends on having ice present in order for ablation to operate. In the model, maritime areas have mass balance rates up to 20cm/year greater than areas inland.

The figures 9 and 10 show the mass balance spaces that result when the model is forced using the $1.02°\Theta/°C$ and $2.5°\Theta/°C$ values of the surface ablation forcing constant respectively. A constant value of C=1.5 is used to calculate these. With the $F = 1.02°\Theta/°C$ constant, mass balance is largely unchanged for wide swings in temperature. Although the surface ablation and accumulation patterns are both affected the changes are relatively evenly matched. There is little net change in mass balance. By contrast, the surface ablation rates in figure 9 are forced comparatively more, and since accumulation rates increase here, the net result is to produce larger net mass balance rates with cooling. The shape of the mass balance space does not really change, but the position of equilibrium line is depressed by about 125m per degree centigrade cooling. The latitude of the maximum potential net mass balance rates does not change. Figures 11 and 12 extend this analysis for varying continentality and forcing temperature combined. The case of the $1.02°\Theta/°C$ surface ablation constant (fig 11) shows that in this scenario continentality accounts for more variability than temperature forcing. In the final case of the $2.5°\Theta/°C$ value, fig 12 the full range of variability for continentality and forcing temperature is apparent. The variation of mass balance values with topography and the effect of forcing the model from the present-day situation are considered as sensitivity experiments in the next chapter.

There are no sufficiently detailed studies of net mass balance over wide enough areas to be confident that the modelled result of peak net mass balance occurring at these intermediate altitudes is correct. Radok and other's(1982) compilation of measured surface balance rates seems to suggest that this is the case in some areas. For

instance, at $N65°$, on the east coast, Radok marks mass balance rates as decreasing inland from $80cma^{-1}$ to $40cma^{-1}$. This matches fairly close with the modelled result (Fig 8). Part of the problem of discerning this relates to the fact that the spatial resolution of changing mass balance rates is small near the ice edge where gradients are steep, and this is also the region where fewest mass balance measurements have been made. The maps of modelled surface mass balance (Fig 24) show that the modelled rates change quickly within a few cells near the ice margin and decrease toward the centre of the island. This pattern concurs with Radok's map.

2.8.2 Calving

It has been estimated that calving may be responsible for up to 50% of the total ice loss from Greenland. It is difficult to simulate as a mechanical process, but calving rates have been shown to be closely related to water depth (Brown and others 1982, Reeh 1982). Following Brown and others, calving was therefore calculated if the basal elevation of a cell was below sea-level, and was estimated as :

$$V_c = -28.75B \tag{45}$$

where V_c is in metres/year and B is in metres below sea level.

2.8.3 Sea-level

Water depth directly effects calving and sliding velocities. The zero altitude in the coordinate system used was present sea-level. The basal altitudes were allowed to fluctuate about this value and so introduce an isostatic component, but equally a 'eustatic' component needed to be introduced. An effective way of introducing this effect was to compare the total ice volume of the Greenland ice sheet to a generalised 'eustatic' sea-level curve which makes assumptions about the synchroneity of corresponding global ice volume changes.

2.9 Computational Stability, smoothing and constraints

Modelling inaccuracies derive from three sources : The breakdown of the assumptions needed for the ice dynamics equations, the representation of continuous media

as discrete points in the method of numerical solution, and the build-up computational errors involved in rounding variables within the computer. Such errors tend to become exponentially self- propagating once they start to become significant, so steps had to be taken to minimise their occurrence and propagation. This involved three approaches :

(a) The establishment of a stable time step.

Budd and Jensen (1975) formulate an equation which approximates the length of a time step for the non-propagation of error terms.

$$\Delta t_{max} = \frac{(\Delta x)_2 \, |\alpha'|}{2U'Z'n} \tag{46}$$

where $|\alpha'|$, U', Z' are estimates of maximum average slope, maximum vertically integrated velocity, and maximum ice thickness respectively. With the maximum ice thickness for Greenland of 3000m and a 20km grid spacing, this calculates a stable time step of about two years.

A further technique is used that allows the length of the time step to be dynamically changed during the model run based on the total flux state of the model. The time step is allowed to increase provided the overall flux rate of the model does not start to accelerate. This would indicate instability propagation. When this happens the time step duration is reduced quickly until flux rates resume more normal levels. This means time steps have different lengths. The time step was held constant in the first 100 steps of the model in order to gain an initial assessment of the flux rates in the model. Interestingly, the time step tends to settle at values close to the 2 year step suggested by Budd and Jenssen. The ability to adjust the time step should theoretically kill the propagation of major instabilities if these start to occur. It is important to have this facility because with constant time steps unstable conditions can still generate because of topographic circumstances which contravene the assumptions in the velocity equations.

(b) The limiting of ice velocities to within preset bands.

Both sliding and shear velocities were constrained to values approaching the fastest known to occur in nature. Typically these values were set to 2km/a.

(c) The periodic smoothing of the surface and bed to eliminate the propagation of a surface wave form which occurs as a result of the numerical solution.

The surface was smoothed using the following equation :

$$E^{+}_{i,j} = \frac{1}{16}\left(E_{i+2,j} + E_{i-2,j} + 10E_{i,j} - 4\left(E_{i+1,j} + E_{i-1,j}\right)\right) \quad (47)$$

This tends to result in a loss of ice mass, so this was redistributed in proportion to the existing thickness of the ice.

The effect of these procedures is shown in figure 13. These are shown for two runs identical but for the fact that in the one, Run 136, smoothing was turned off. The reason for doing this was because it became evident that calving was being triggered by the smoothing function and some assessment of the effect was needed. This is described in Chapter 4. For the time being, however, these two runs serve to illustrate more general effects in the model. The variability in time step duration is shown in figure 13. After an initial period in the model when the time step is held constant it fluctuates in both cases. Average time steps in the non-smoothed case are higher than the smoothed example. This is because, with smoothing, the ice sheet margin is thinned and so the ice becomes out of balance along the margin and this dramatically increases the ice flux rates. The time step is held constant again for a short period in order to let the model establish a more stable state but it still tends to reduce after this because flux rates still tend to be enhanced. Some of the enhancement is due to the calving being triggered into an unstable state in this instance. The effect on isostasy can also be seen. Smoothing the bed throws the isostatic model severely out of balance but it subsequently readjusts. The basic topographic outline does not change in the long term because the topography is always referenced back to the assumed relaxed state. Even though the smoothing throws local elevation by mean values of about 0.25m, in smoothing these quickly restore themselves to what is implied by the balance loadings (eq 16). The bed needs to be smoothed because otherwise, eventually, it picks up wave forms that exist in the more dynamic ice model. Conventional wisdom is to smooth rather than not. Occasionally, small amplitude wave forms were identified on the surface of the ice, but it never became catastrophically numerically unstable. However it seems that the introduction of a variable time step would allow smoothing to be less frequent and disruptive on the model. This fact was only fully appreciated at a late stage in the research and so, in the main, smoothing was applied every 200 years.

2.10 Input data

2.10.1 Topographic grid generation

Initial calculations indicated that it would be prudent to collate surface and basal data to construct grids of the order of 5km to 20km. From computing constraints, this was a resolution that the model was likely to be capable of dealing with. A further requisite given the paucity of information available for Greenland, was to obtain the best sources available, and at very least to establish a known level of data quality. If available, existing digital information was preferred.

The raw topographic information was obtained from four sources : Digital Airborne Radar and expedition survey data for subglacial and ice surface altitudes collated by the World Data Centre A for Glaciology, the U.S. Navy Digital Land, Sea and Ice surface altitudes available globally at 10' latitude by 10' longitude, SEASAT altimeter readings from southern Greenland, and the GGU 1:2M Quaternary map of Greenland from which relevant information was digitised. These provided information for four distinct data zones : The present ice surface, the subglacial surface, the presently exposed land, and submarine areas. The last three combine to comprise the base topographic grid and the first, by simple subtraction, yields ice thickness. In addition, polygon outlines of the existing ice sheet edge and the Greenlandic shoreline served as cutting frames when extracting data for each zone.

Because the ice sheet area was covered by more than one set of source data, a choice had to be made about which parts to use. The radar data for the subglacial altitudes is certainly the most accurate and is relatively detailed in some areas. However, there are substantial areas of NE Greenland, some parts in the SW, and parts of King Christian X's land for which no radar data exists. Therefore, it seemed desirable to interpolate in areas of dense radar data coverage, yet make an educated guess in the poorly covered areas. The subglacial contours on the 1:2M Quaternary map look attractive, but apart from one or two areas which incorporated early radar findings they are somewhat conjectural, though partially informed and well reasoned. It therefore seemed prudent to use the map contours in the areas not covered by the radar.

The 10' data gives the most complete coverage of the ice surface. It is digitised from the 1:1M air navigation charts and whilst the absolute accuracy is probably no

better than 50m, the continuity was preferable to interpolation from the partial coverage of the radar data or the SEASAT set. Because all these sources have relatively dense cover throughout, area combinations of them would probably have resulted in 'stepping' in the resultant data set. The alternative way to combine them would have been some complicated interpolation procedure in which an absolute reference frame was obtained from the radar data and relative altitude interpolation values were taken from either the 10' data or the SEASAT sets. Any minor gain in accuracy for the initial model did not seem justified by the time it would take to perform this complex procedure. Although the SEASAT and WDC-A radar ice surface values were read into ARC-INFO for observation they were not used in the model construction. The SEASAT data only covers an area south of about $68°N$ and the WDC-A whilst extending over many parts of the island provides only sporadic cover.

In practice, the first task was to digitize both the shoreline and ice sheet edge from the 1:2 Quaternary map as an ARC-INFO line coverage. This map, whilst based on a polyconic projection is actually a mosaic. In order to ensure sufficient accuracy during digitising, a grid of known latitude and longitude intersections was projected into a set of 60 reference or TIC points on a single polyconic projection. Coordinate pairs were then digitised into this framework using the EDIT command which forces a piecewise affine transformation of the coordinates based on the established TIC points. Whilst the base map and projected grid initially diverged by an equivalent of up to 20km in places the absolute positional accuracy of the points, once digitised was of the order of 1km.

Because, in some areas, the ice edge forms the shoreline, each segment had to be coded as shore, ice edge, or both. Separate ice edge and shoreline polygons were subsequently formed using the ARC-INFO SELECT command. The submarine and subglacial contours were also digitised at this stage as single coverages.

Some preprocessing of both the digital sources was necessary before they could be read into ARC-INFO. The World Data-Centre A material had to be read out from two different files, combined and thinned down from the initial 52,000 data points. ARC-INFO was physically unable to read in this much data and since some of the accuracy was superfluous for 5km resolutions a simple Fortran program was used to weed out points within a 5km tolerance along transect lines. From this reduced data set of 11,000 altitude points, Basal and Surface altitude files were separately rewritten. The US Navy 10' data for the area was unpacked from the base tapes, purged of a significant number of obvious errors, and rewritten into a single file. This

rewriting was necessary because the source files contained extra columns, which the GENERATE command, which was used to transport the data into ARC- INFO, will not accept.

The ARC-INFO TIN package was used interpolate grids from the data. It requires a third dimension attribute to be recorded for either contour lines or spot values. For the digitised contours, these values were entered directly into the INFO attribute table of the contour coverages. For the digital data, the altitudes were read in as the first column in the GENERATE source file which assigns the value as an ARC internal ID number.

The initial data were represented as five coverages : The WDC-A subglacial values, the WDC-A surface values, the 10' data for land and ice surface, the digitised submarine contours and the digitised subglacial contours. These had to be converted into a single coverage for ice surface values and a single coverage for basal values. Each coverage was firstly projected out of its original coordinate system into a common Albers projection. This is a secant conic, equal area projection, and so is particularly suitable for ice sheet modelling at high latitudes. The ice surface coverage was simply created by using the CLIP function which 'cookie-cuts' the altitude data within the ice edge polygon. Submarine altitudes were obtained directly from the digitised submarine contours once a few lines had been tidied up and removed by clipping with the external box and erasing values from the centre using the SHORE polygon. A coverage of values in the exposed land zone was obtained from the 10' data by erasing the internal ice surface points with the ice edge polygon, and clipping externally using the shoreline to remove any external points. Finally, a subglacial coverage was formed by combining the data from the WDC-A set with digitised subglacial contours that remained after clipping out the areas suitably covered by the WDC-A data. The submarine, exposed land and subglacial data was brought together using the UPDATE command.

Converting these coverages into grid formats suitable for use in the model was performed using the ARCTIN, and TINLATTICE commands. The grid origin, extent and cell size is defined and values are interpolated onto the grid using a linear or bivariate interpolation. Whilst a 10km grid, using a bivariate interpolation was defined at first, the production of other grid areas and resolutions is relatively simple. However they are only as meaningful as the original data and the interpolation routine allow. One final operation was to clip the ice surface lattice to remove false values which become interpolated beyond the ice edge. The grids were exported from

ARC-INFO using LATTICEGRID which sets up an SVF (Single Variable File) file containing the gridded information. A Fortran program was written to take both grid files as input, add additional rows and columns to the surface grid to match it with the base grid, subtract basal altitudes from surface altitudes to yield ice thickness, and output these grids again in an SVF format to which four further values were added : The cell size in kilometres, a projection code to indicate the projection used, and x and y shift values of the grid origin from the projection origin. These then became the topographic input files for the ice sheet program.

2.10.2 Non-topographic data

Grids of accumulation and temperature were interpolated in the same manner as the topographic data. Other non-locational inputs included the parameters used in the ice mechanics and climatic simulation equations and some values controlling the time steps used, the amount of smoothing required, how often to calculate mass balance or isostatic readjustment and some constraining values. These values were stored in external files and accessed by the main program.

The relationships specified in the equations themselves may be regarded as input, as is their method of solution. They are specified within the program as Fortran statements.

2.10.3 Output files and other output media

The model output files contained the same type of grid data but also contained sufficient details so that they could rerun a model using the same parameters and suitable topographic inputs.

2.11 Program Implementation

The solution of the ice flow equations using finite differences is computationally intensive because of the large arrays used and the small time step intervals that are demanded if stability is to be maintained. In fact, since the number of cells increases as the square of the linear grid separation and since the approximate length of a stable time step is also inversely proportional to the square of grid separation, the total computation time increases as the fourth power of this quantity. Consequently, it was necessary to reduce computing time as far as possible.

The main program was written in Fortran. By setting up the input variables as Fortran Parameters, and by structuring the program without subroutine calls in the main iteration loops, computation time was optimised at the expense of a certain degree of modularity and readability.

A front-end program, ICESETUP, was used to read the ice parameter and run control values from two separate files containing variables and character headings. This partially checked the consistency of these values, and rewrote them as parameter statements which were then incorporated in the main program during its compilation. This meant the array dimensions could be preset.

After reading in the main arrays the base grid was smoothed for a specified number of iterations, and any loss of mass was redistributed equally over the grid.

To start the main iteration of an entire grid logical operations were performed to calculate the values of logical operators that determined the operation of parts of the program. Mass balance was then recalculated if required. Similarly, smoothing of the ice surface was performed if necessary, and lost ice redistributed.

The main part of the grid iteration for a single time step then commenced and proceeded as standard nested row and column loops. The nature of the velocity and flux calculations is that they must always refer one row and one column ahead and behind and the velocity calculation must precede the flux calculation. Since the outer loop was by rows, a window four rows deep and the full grid columns wide was used to calculate velocity and flux and return a new value for ice thickness. New velocities were calculated in the front three rows, and fluxes in the back three, as the window advanced. This saved the need to operate two full- sized arrays and thus the time taken in accessing virtual memory. If any isostatic readjustment calculation was needed it was done on the basis of the elapsed time since the previous calculation. The base grid was updated accordingly.

The program made an assessment of the overall flux state of the model. In order to detect and overcome the instabilities which developed in the course of a model run, the time step was recalculated. The time counter was then advanced by this amount and another grid iteration started.

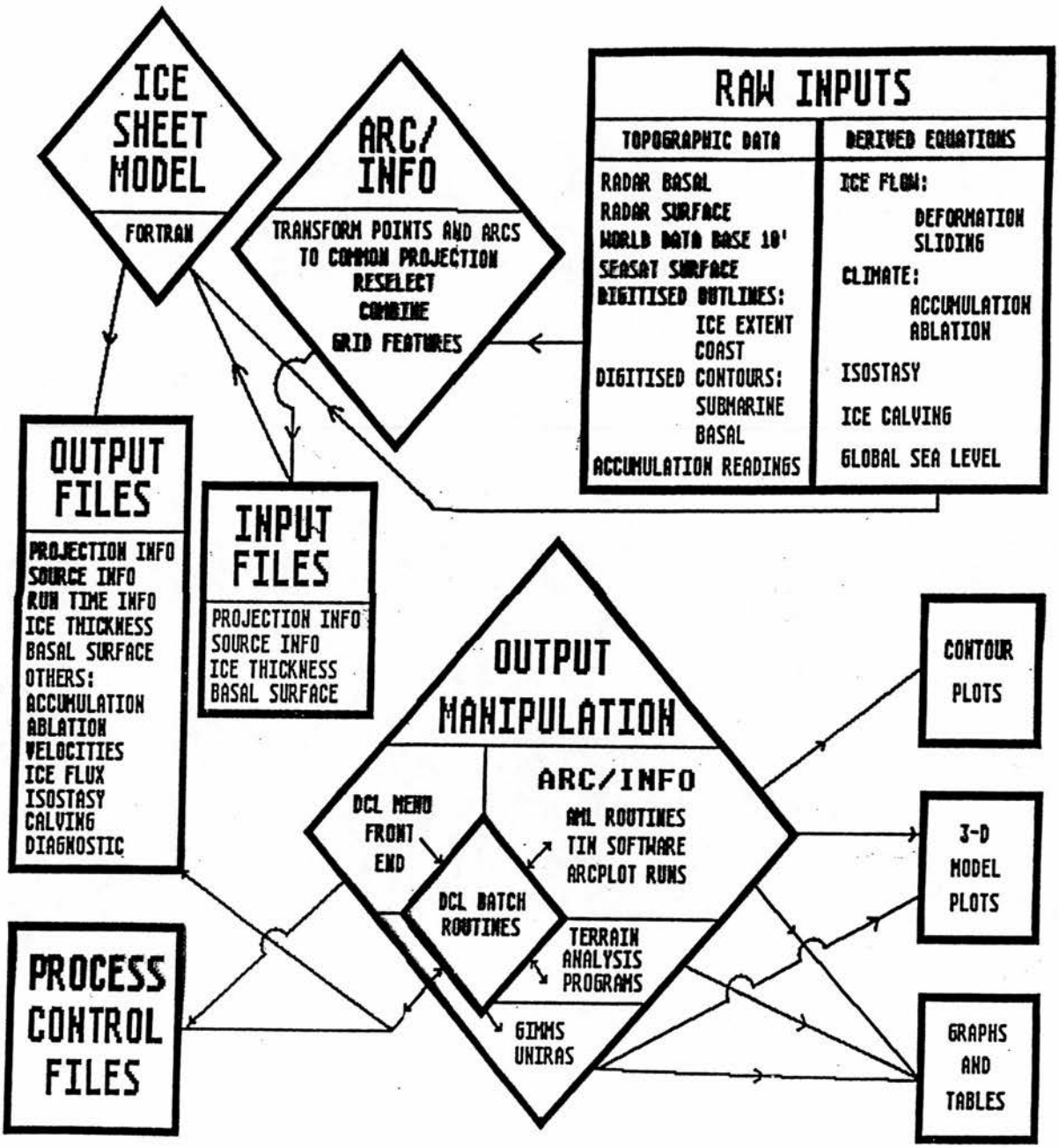

Figure 2: The modelling system architecture: A conceptual overview of the main elements of the system used to implement the model. Rectangular boxes denote data storage areas and diamonds processing steps

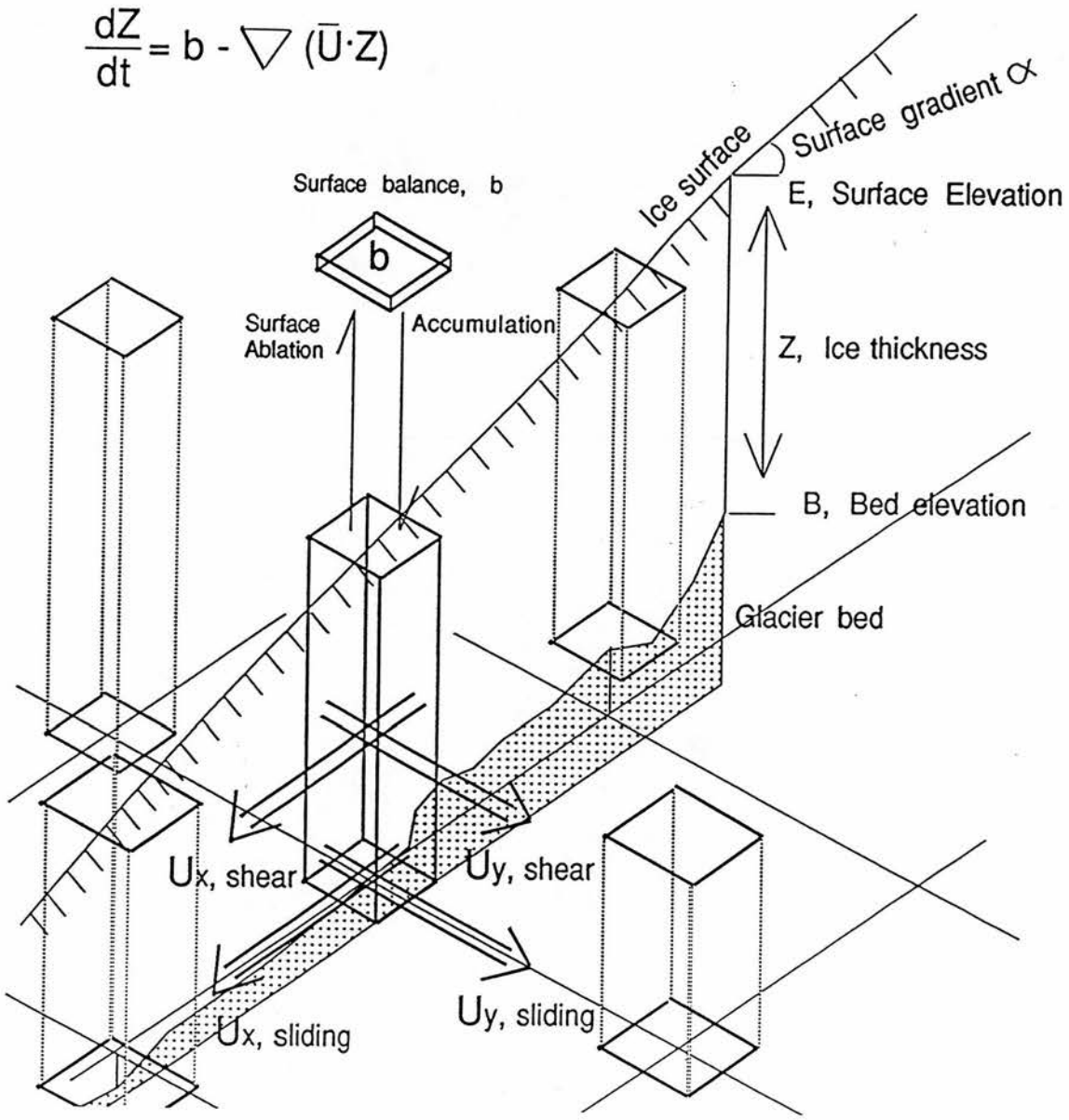

Figure 3: A schematic representation of the system used to implement the continuity equation and iteratively recalculate ice thickness. U is velocity, Z, ice thickness, E, ice surface elevation above sea-level, B, bed elevation and b, surface mass balance.

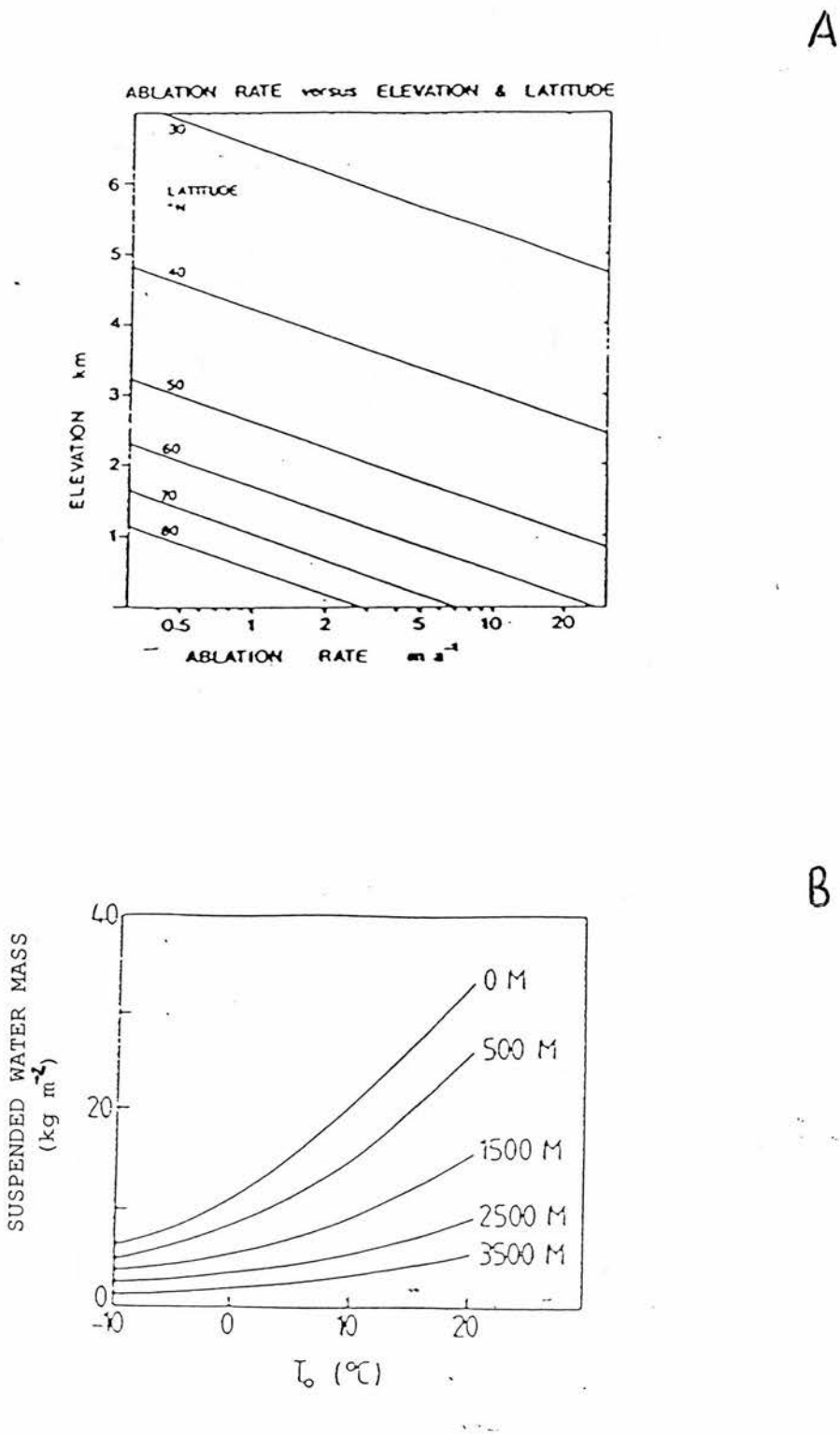

Figure 4: A, shows the ablation/altitude relationship derived by Budd and Smith 1981 for Northern Hemisphere latitudes. E_0 is defined as the 1m/a ablation altitude. B, shows the relationship of atmospheric moisture to air temperature. (From Oerlemans and Van der Veen(1984)).

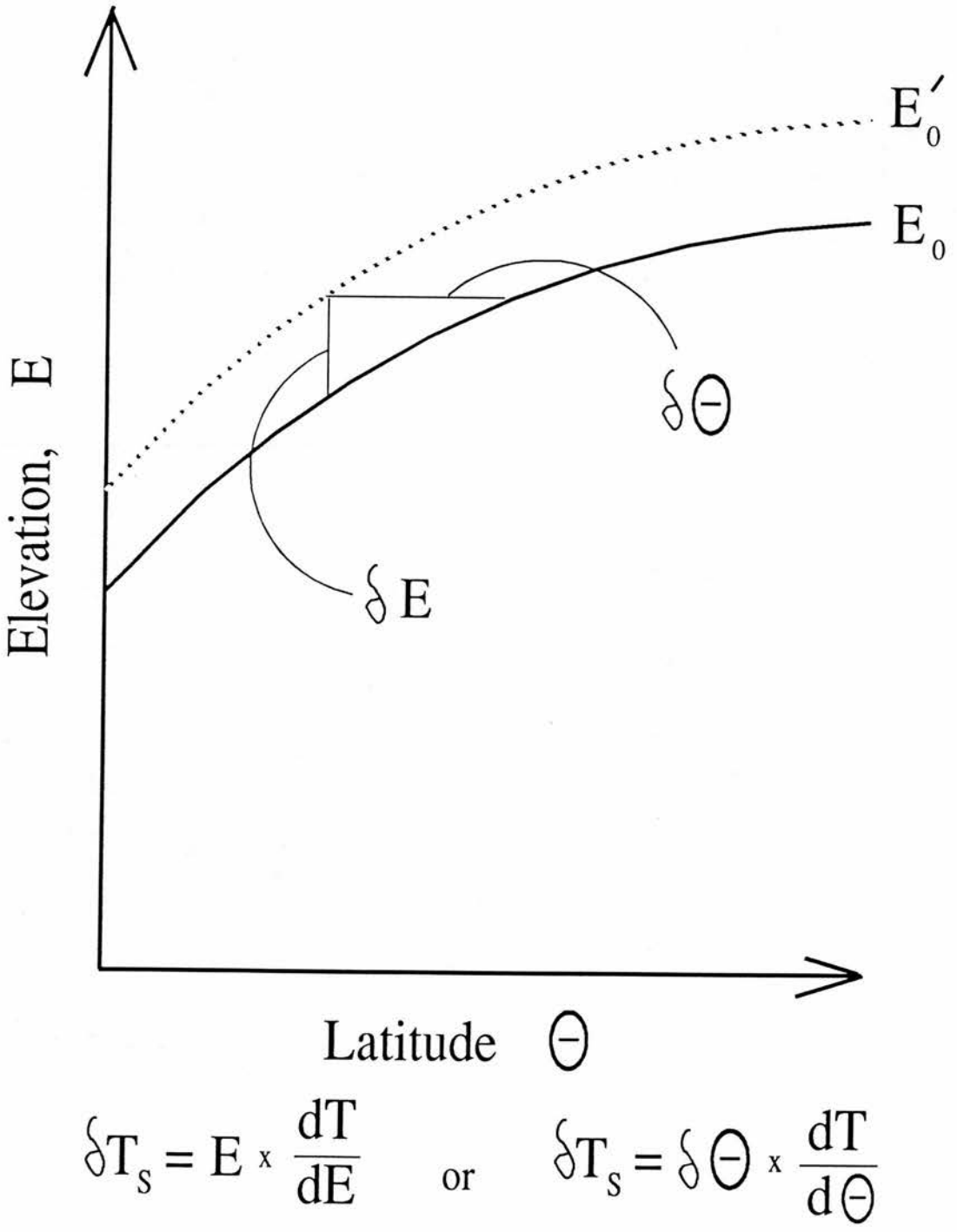

Figure 5: Changes in surface temperatures δT along the 1m/a ablation (E_0) line can be associated with either changes in latitude, $\delta\Theta$ or changes in altitude, δE. Forcing ablation change by movement of the E_0 line concordant with global temperature change can be done by considering the temperature equivalent gradient along E_0 associated with either latitude or altitude.

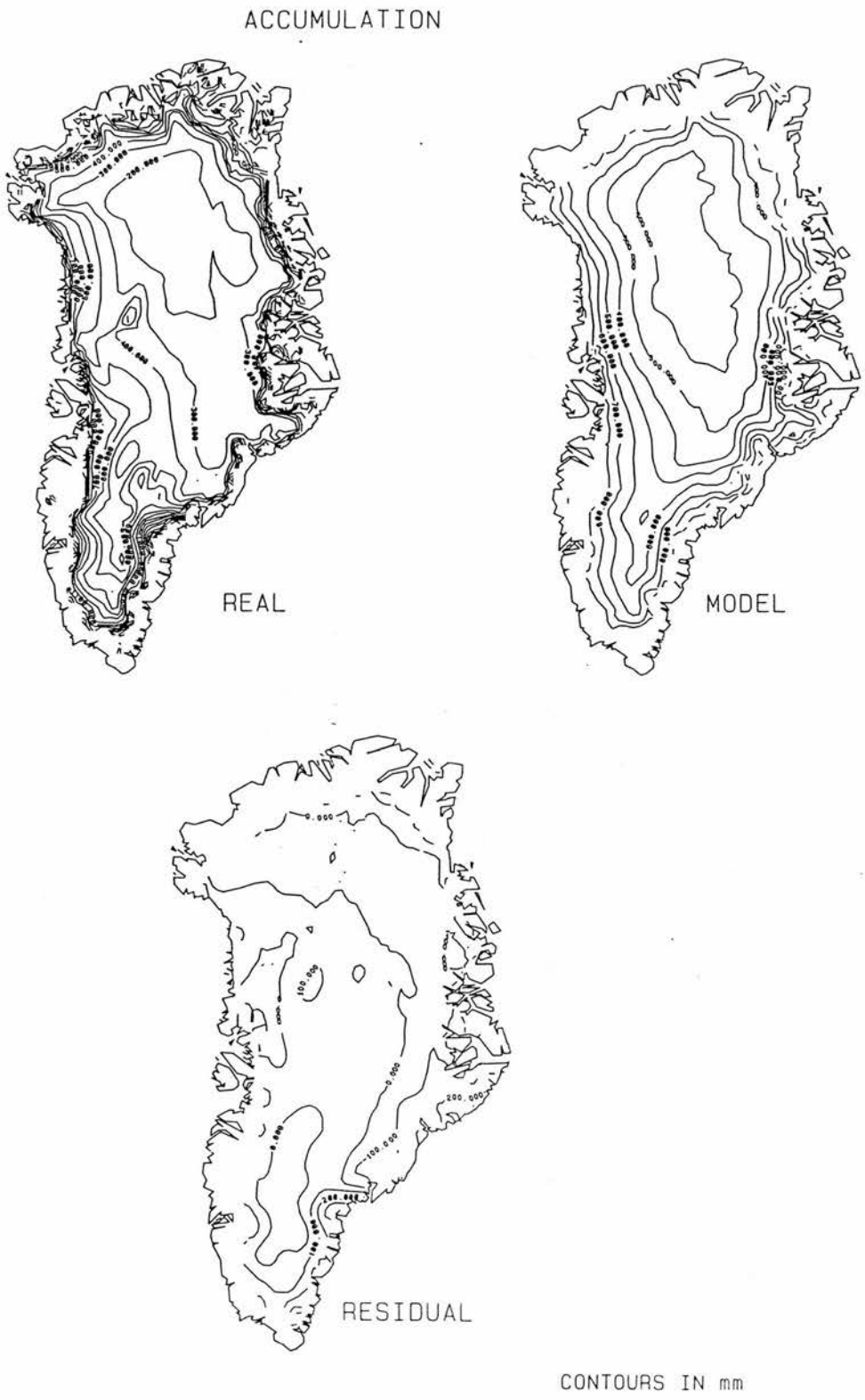

Figure 6: Real interpolated, modelled and model residual accumulation values for Greenland. Contours in cm/a.

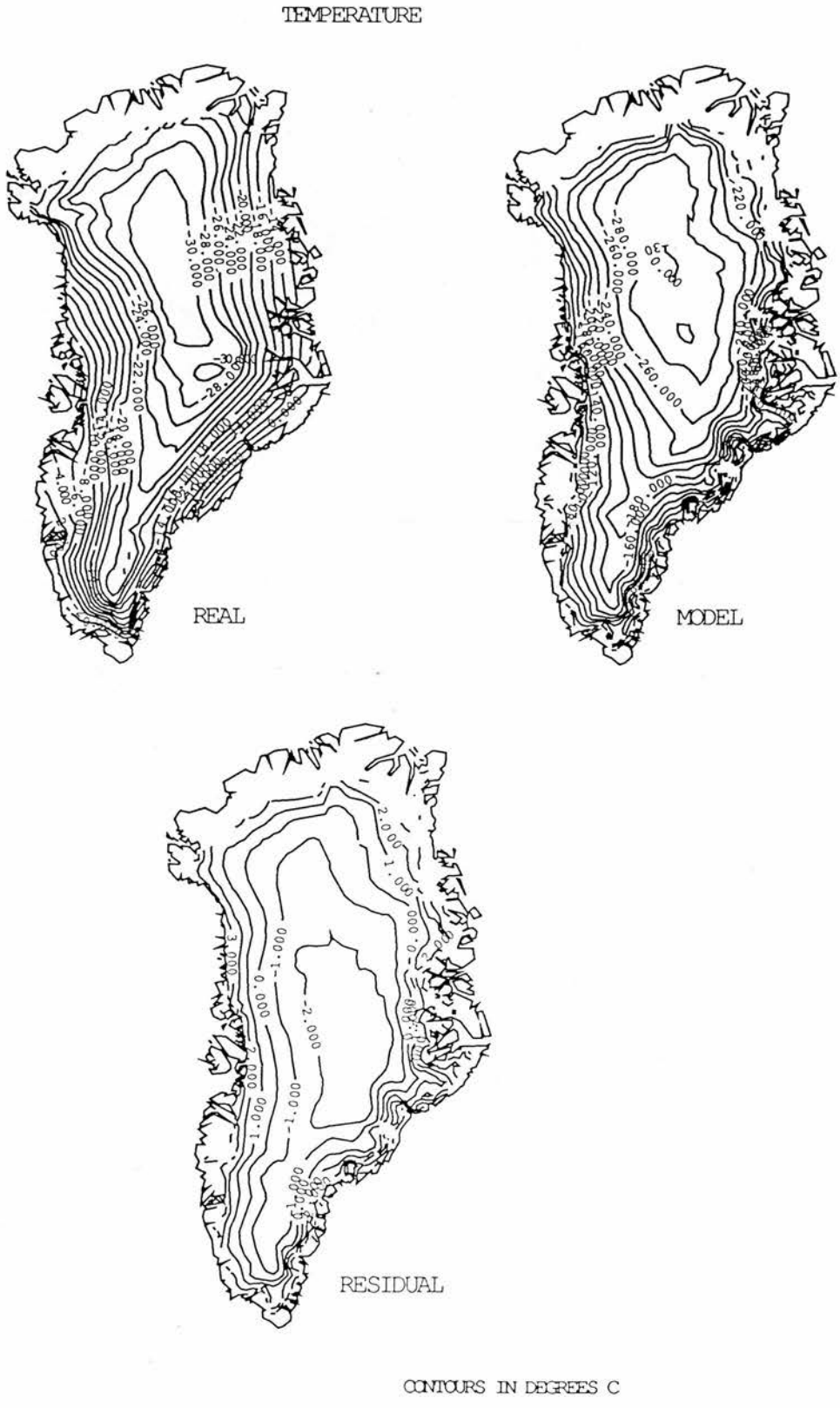

Figure 7: Real interpolated, modelled and model residual temperature values for Greenland. Contours in $°C$.

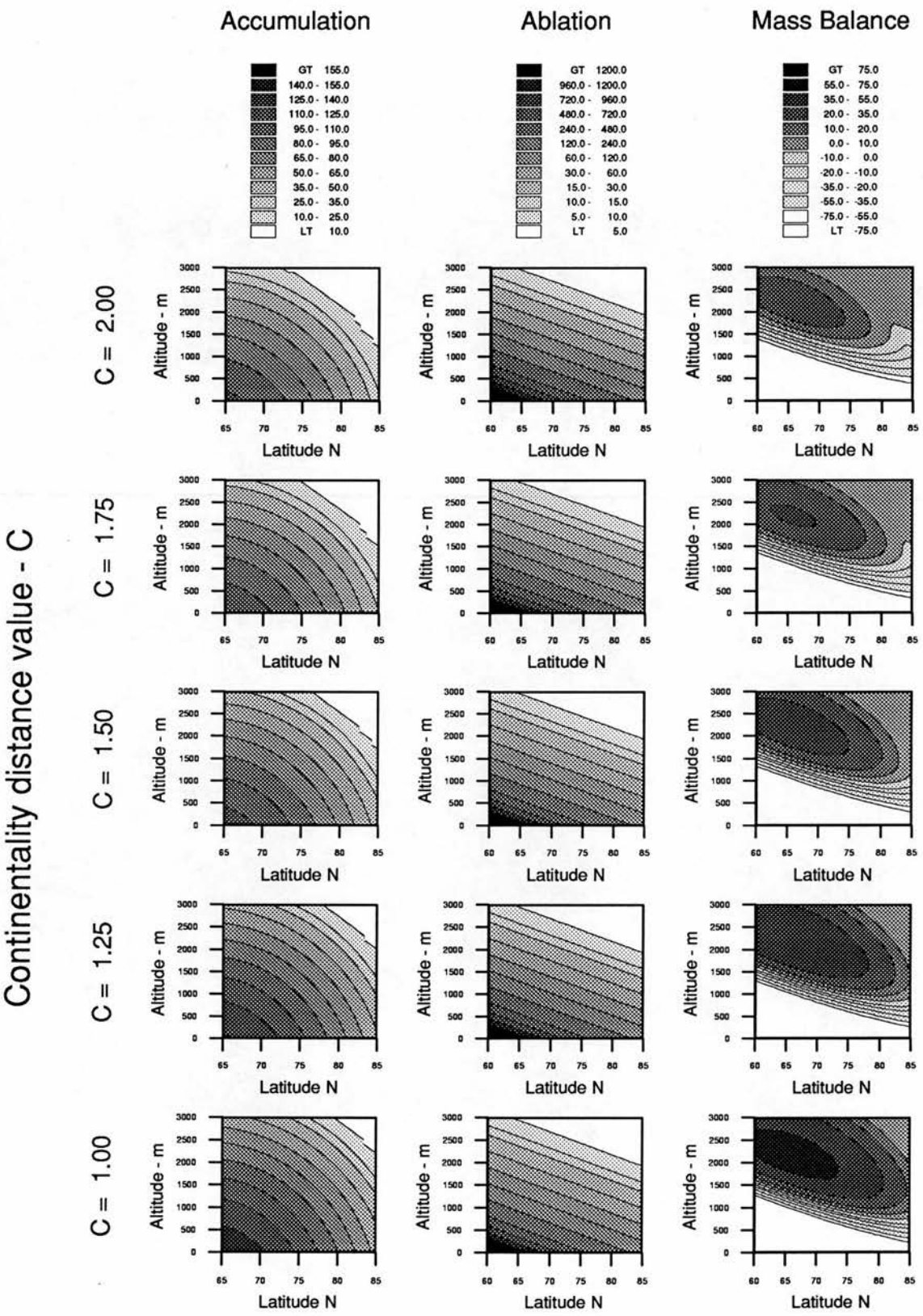

Figure 8: Hypothetical accumulation, ablation and surface mass-balance values in cm/a, shown varying with the latitude-altitude domain of Greenland and for variations in the continentality value, C.

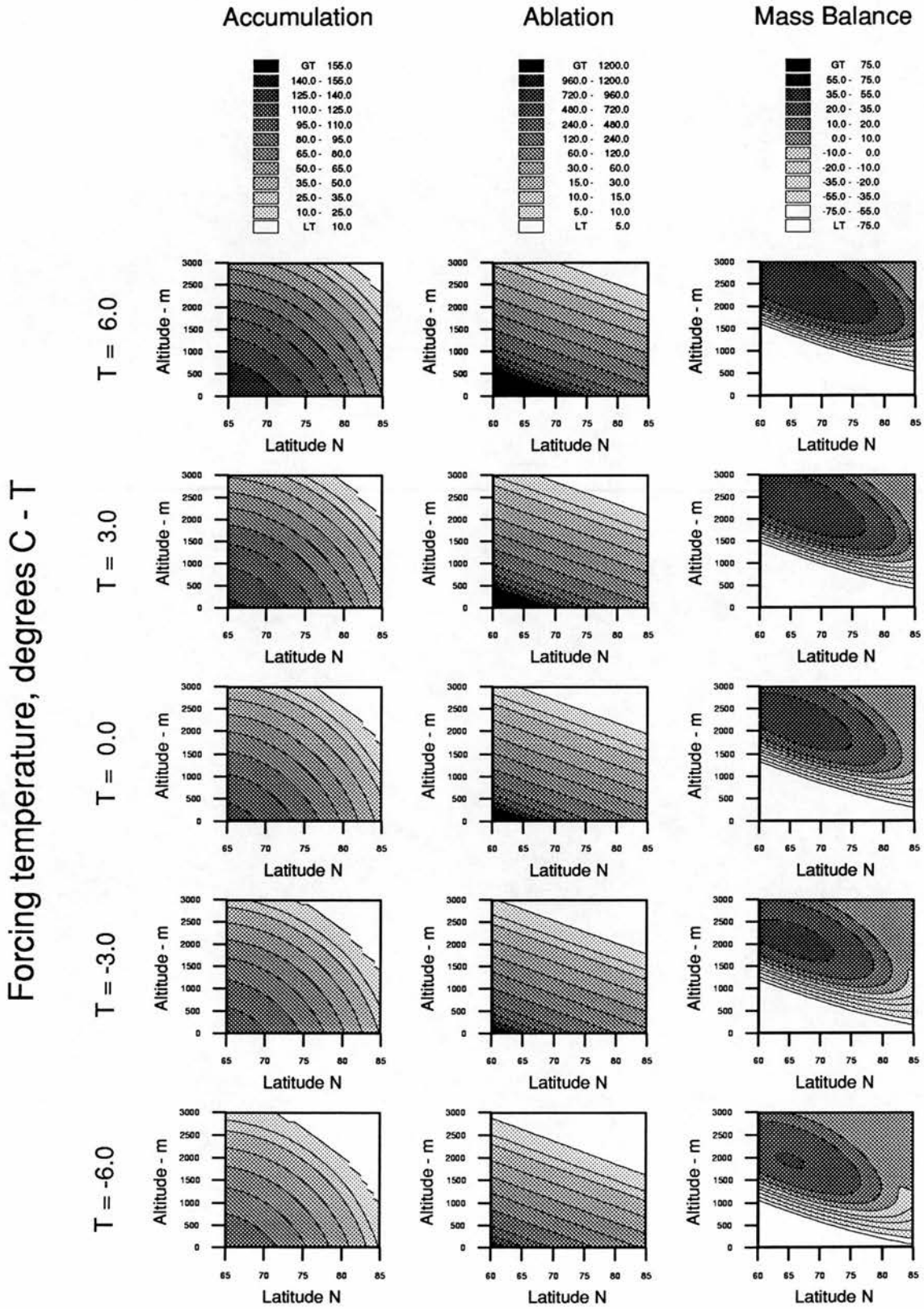

Figure 9: Hypothetical accumulation, surface ablation and surface mass-balance values in cm/a, shown varying with the latitude-altitude domain of Greenland and for forcing temperatures between $-6°C$ and $+6°C$ when the ablation forcing constant, F = 1.02. The divergence of accumulation and surface ablation with temperature is not large enough to force mass-balance greatly.

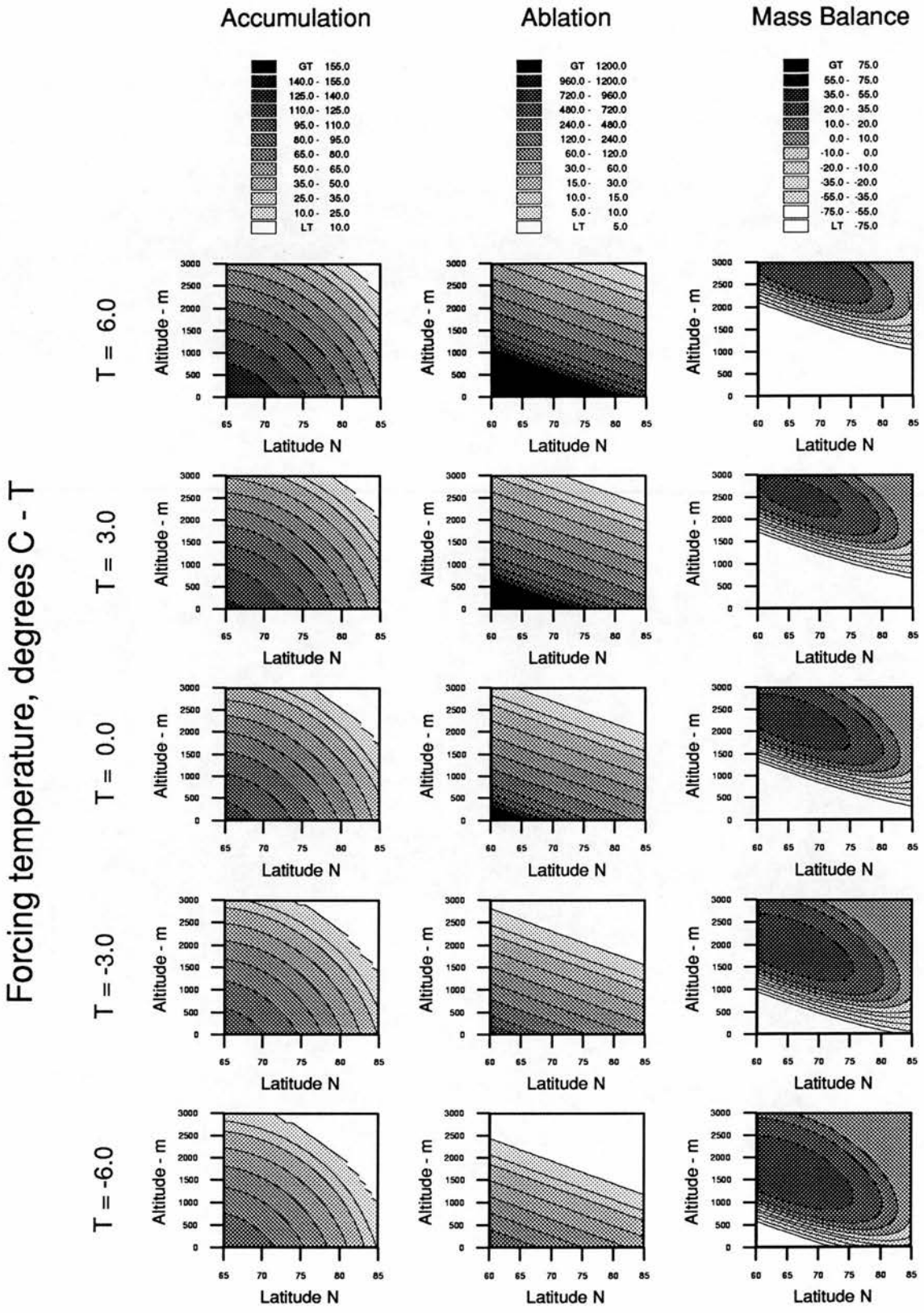

Figure 10: Hypothetical accumulation, surface ablation and surface mass-balance values in cm/a, shown varying with the latitude-altitude domain of Greenland and for forcing temperatures between $-6°C$ and $+6°C$ when the ablation forcing constant, F = 2.50. The divergence of accumulation and surface ablation with temperature forces large surface mass-balance change.

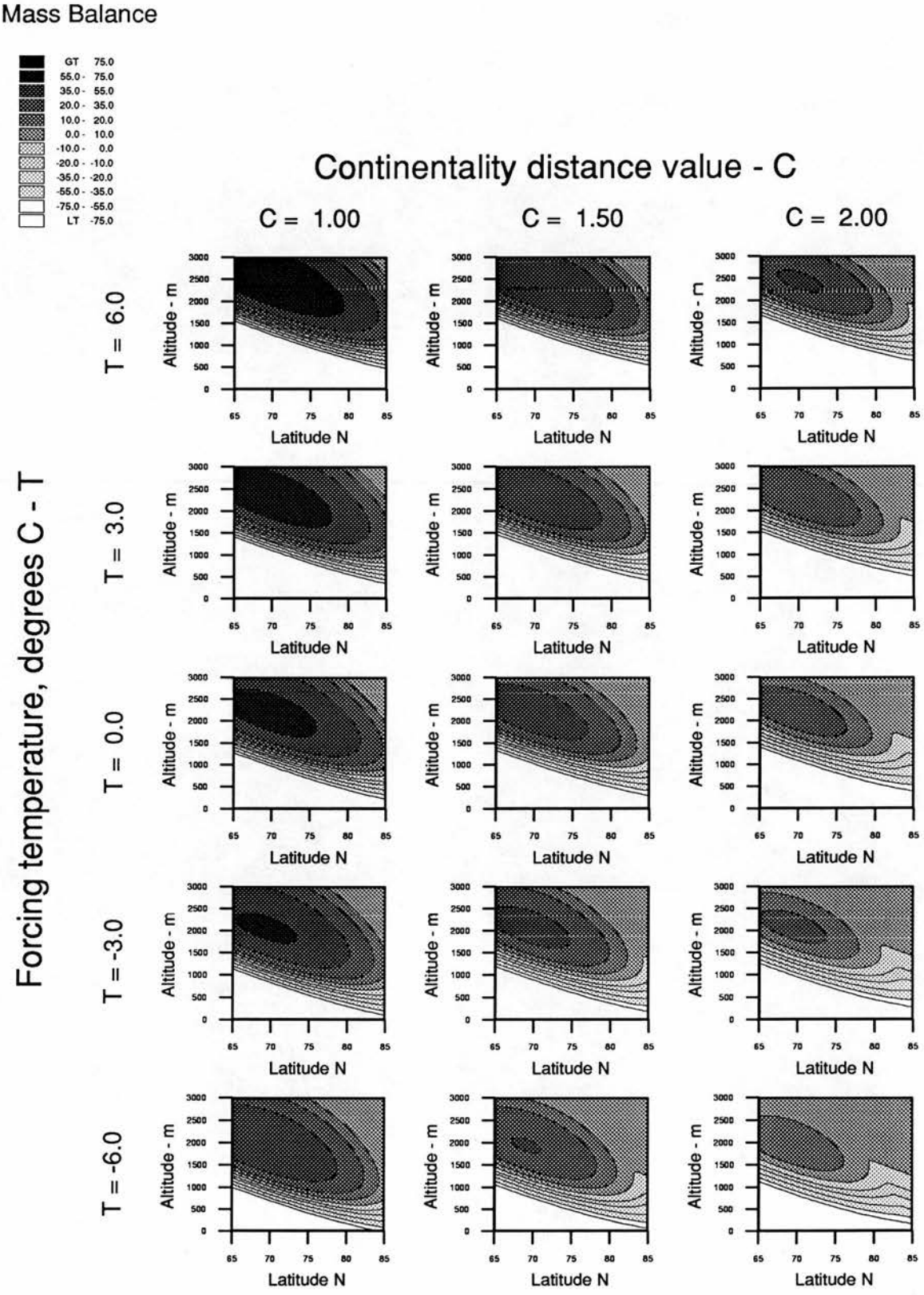

Figure 11: Surface mass-balance values (cm/a) for variation in latitude, altitude, continentality and forcing temperature with F=1.02. within the model domain. Warmer more continental areas are more mass positive but the altitude and latitude and intensity of the maximum mass-balance focus shifts through the other two variables.

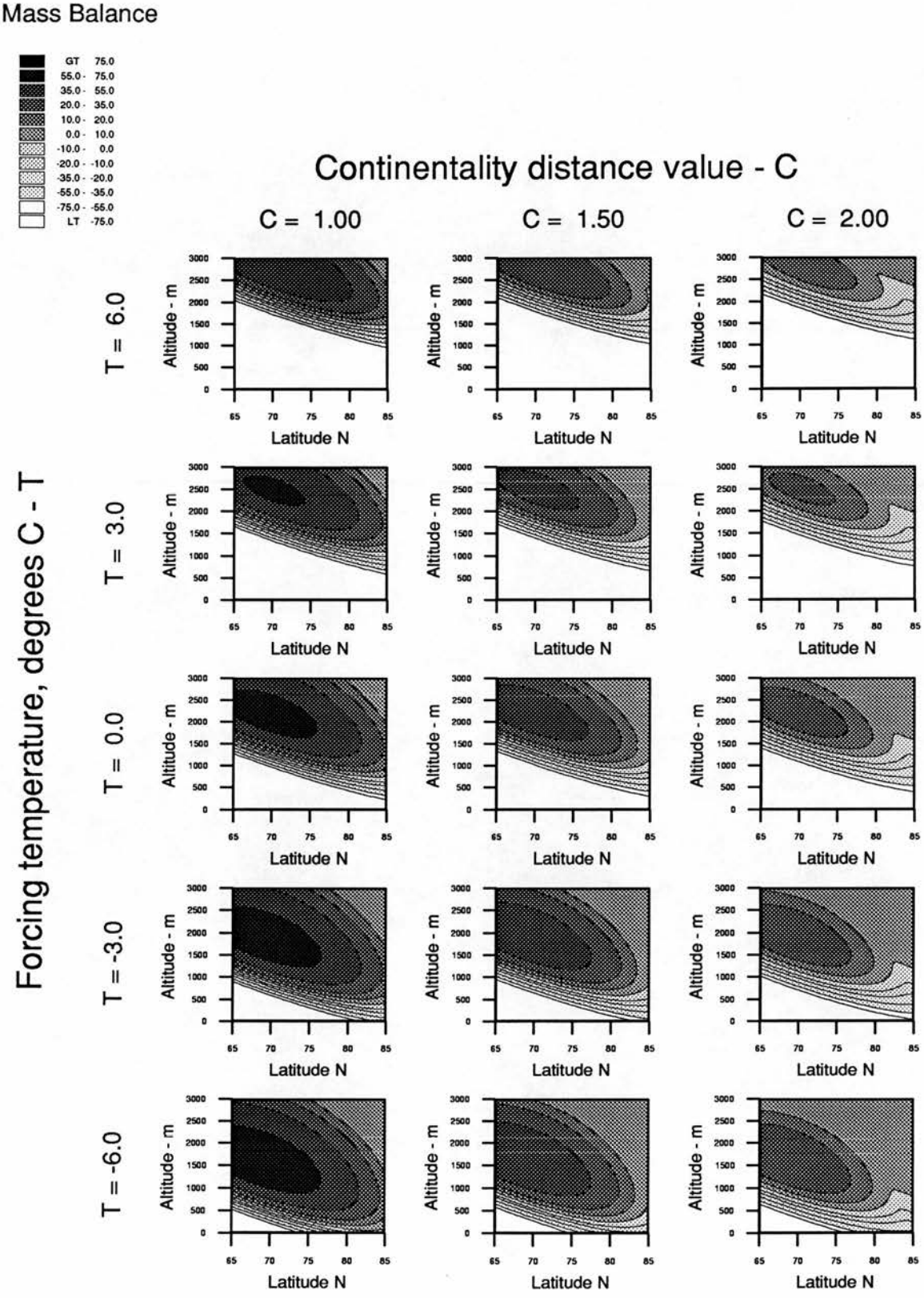

Figure 12: Surface mass-balance values (cm/a) for variation in latitude, altitude, continentality and forcing temperature with F=2.50. within the model domain. Warmer more continental areas are more mass positive but the altitude and latitude and intensity of the maximum mass-balance focus shifts through the other two variables.

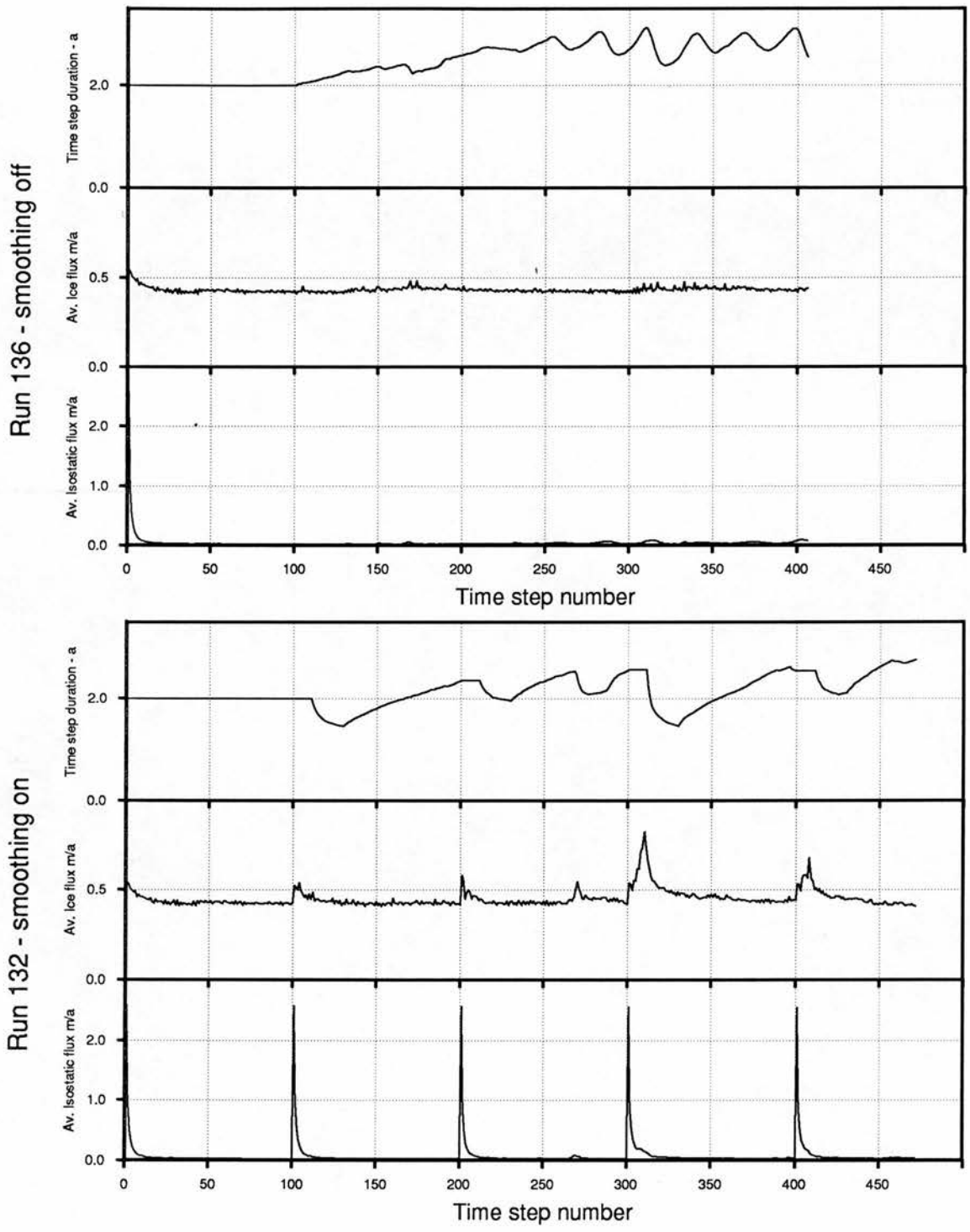

Figure 13: The relationship between the time step, and isostatic and ice fluxes in smoothed (lower) and unsmoothed (upper) models. The time step is held constant for the first 200 steps and then allowed to vary as a damped inverse function of the overall model flux state. Smoothing provides a regular trigger which stimulates catastrophic calving events and hence the overall ice flux and corresponding isostatic recovery

Chapter 3

SENSITIVITY TESTS AND QUASI-EQUILIBRIA

In order that the model could be used in a predictive or deductive manner, it is important to comprehend its inherent mechanisms. There are three key steps:

1. Checks on program coding and stable numerical behaviour.

   When viewing the maps and graphs produced by the model it is important to establish firstly, what effects are artifacts of the model or are the result of the way in which certain variables or relationships have been treated.

   Finite difference theory predicts a theoretical stable time step(equation 47), but other instabilities caused by the breakdown of the assumptions in the velocity equations can occur. Checks were performed to analyse the behaviour of the model throughout the solution routine, to detect inexplicable or erratic behaviour. These can be caused either by an unstable solution or by coding errors.

2. The sensitivity of the model to individual parameters or forcing variables. This is a crucial step because it points to both strengths and weaknesses in the model and thus influences interpretation of the results.

   The model contains a complex web of interdependent variables. It is important to establish which quantities influence the behaviour of the model most strongly, both directly and by introducing stability or instability to the action of other variables. This analysis can be used subsequently to help identify which factors accounted for the behaviour of the model in predictive situations.

3. The observations of trends towards stable or unstable states and the length of characteristic time lags within the model.

   If the model is to be used predictively, it is important to establish the response time of the model to a change in input and to identify any conditions leading to unstable behaviour.

There is no reason to assume that present-day topography or mass-balance conditions are stable and this needs to be established if one is to justify the use of present-day variables as input to the model. It is also important to discover whether conditions of quasi-equilibrium can be achieved and how long this takes. This is because it is necessary to be able to distinguish the effects of forcing from these. It is also inherited as an instability from the starting conditions. It is of secondary interest to see whether the model exhibits oscillatory behaviour even with stable parameters and to get an indication of the duration of the lags involved in ice and asthenospheric mass redistribution.

Whilst the second and third steps above were sought deliberately, it was hoped that any problems with the first would show up though a series of experimental runs. There were two parts to this analysis which were undertaken concurrently but are described separately for clarity. They are :- (a) Tests on the effects of individual non-forcing parameters such as those used in the velocity, isostasy and calving calculations. (b) Tests on the significance of the forcing values of temperature and sea-level by starting the model with present-day conditions and varying the forcing values systematically. These tests were carried out with reference to an 'Initial Standard Run'.

Values for parameters for the Initial Standard run and for subsequent experiments are given in Table 2 . In subsequent tests, parameters were altered singly in order to demonstrate their effect by comparison with the initial standard. The forcing tests were done likewise but when building the model towards a maximum condition it proved necessary to alter more than one parameter or forcing function. This was done in a piecemeal fashion to establish the additional effect of each parameter. Because it was not practically feasible to run the model for more than 20,000 years of simulated time in any one run, this latter procedure involved a succession of separate sequential tests. Typically, the model tended towards some equilibrium within a 20,000 year run, whereupon the end condition was used as the starting condition for the next run, using modified variables.

Run Number	Run Time years	Forcing Temperature °C	Forcing Sea-level m	Arrhenius Constant A kg³ km³ a⁻⁶	Sliding cut-off altitude m	Calving Constant	Artifical Accumulation Multiplier %
		Ablation Forcing Constant θ/C		Sliding Constant k m³ bar⁻¹ a⁻¹	Continentality Distance °C km		Artificial Ablation Multiplier %
32	10000	0	--	0	5.0E-26	2.0E4	300	350	28.75	0	0
90	20000	0	--	0	5.0E-26	2.0E4	300	350	28.75	0	0
107	1000	0	--	0	5.0E-26	2.0E4	300	350	28.75	0	0
49	10000	0	--	0	2.5E-25	2.0E4	300	350	28.75	0	0
59	10000	0	--	0	1.0E-24	2.0E4	300	350	28.75	0	0
48	10000	0	--	0	5.0E-26	1.0E4	300	350	28.75	0	0
58	10000	0	--	0	5.0E-26	4.0E6	300	350	28.75	0	0
74	10000	0	--	0	5.0E-26	2.0E4	150	350	28.75	0	0
75	10000	0	--	0	5.0E-26	2.0E4	600	350	28.75	0	0
77	10000	0	--	0	5.0E-26	2.0E4	300	350	20.00	0	0
76	10000	0	--	0	5.0E-26	2.0E4	300	350	40.00	0	0
78	10000	0	--	0	5.0E-26	2.0E4	300	700	28.75	0	0
99	10000	0	--	0	5.0E-26	2.0E4	300	150	28.75	0	0
63	10000	0	--	0	5.0E-26	2.0E4	300	350	28.75	-10	0
64	10000	0	--	0	5.0E-26	2.0E4	300	350	28.75	0	+10
95	10000	0	--	0	5.0E-26	2.0E4	300	350	28.75	-5	+5
91	20000	+6	1.02	0	5.0E-26	2.0E4	300	350	28.75	0	0
92	20000	-6	1.02	0	5.0E-26	2.0E4	300	350	28.75	0	0
93	20000	+3	1.02	0	5.0E-26	2.0E4	300	350	28.75	0	0
94	20000	-3	1.02	0	5.0E-26	2.0E4	300	350	28.75	0	0
119	20000	-3	2.50	0	5.0E-26	2.0E4	300	350	28.75	0	0
120	20000	+3	2.50	0	5.0E-26	2.0E4	300	350	28.75	0	0
121	20000	-6	2.50	0	5.0E-26	2.0E4	300	350	28.75	0	0
122	20000	+6	2.50	0	5.0E-26	2.0E4	300	350	28.75	0	0
123	20000	-1	2.50	0	5.0E-26	2.0E4	300	350	28.75	0	0
124	20000	+1	2.50	0	5.0E-26	2.0E4	300	350	28.75	0	0
60	10000	0	--	-200	5.0E-26	2.0E4	300	350	28.75	0	0

Table 2: Variable parameter values used in each run. ISR refers to the Initial Standard run values used in runs 32,90 and 107.

3.0.1 The present-day Greenland Ice Sheet

The topographic input yields a map of the present- day ice sheet (Fig 15) and values for the present-day ice volume (Fig 17). These are worthy of consideration in themselves and also because the difficulty of establishing the true ice sheet state bears on the model's ability to relate to reality. The input (real) ice volume is calculated to be $2.984 \times 10^6 km^3$, covering an area of $1.89 \times 10^6 km^2$. This compares to values given by Radok and others (1982) of $2.988 \times 10^6 km^3$ volume and $2.530 \times 10^6 km^3$ by Holtzscherer and Bauer (1954). Areas given by Radok and others(1982) are $1.674 \times 10^6 km^2$ and $1.730 \times 10^6 km^2$ by Bauer(1955).

Given that the ice volume is aggregated from point ice thicknesses, there are three potential sources of error in establishing the true ice volume at any given time.

1. Inaccurate mapping of the ice surface. Even with satellite or airborne radar altimetry, absolute relief is difficult to establish and little ground surveying is undertaken on a regular basis.

2. Inaccurate mapping of the bed This can only be inferred from radar or radio-echo soundings which may each suffer from measurement error.

3. Undersampling and interpolation. There are far too few properly surveyed points to establish the real surface or bed topographies with great confidence. The choice of different interpolation routines affects the values given at intermediate points. The point values used here were converged onto a regular 20km grid and the summation done at this resolution which introduces a further potential for error.

Moreover, the readings which do exist have been taken over many years when the ice-sheet may well be in a state of considerable flux. An instantaneous real value is difficult to establish. This research tried to reduce the error in calculating ice surface and bed topography as much as possible. The greatest errors are likely to exist in poor estimation of the bed topography rather than the surface. The main purpose of topographic input generation here was to establish continuous arrays of values for the model rather than to produce a detailed assessment of the true state of the ice sheet. It was felt that within the overall error potential of the model, the input grids provided an adequate representation of the present reality.

3.1 The Initial Standard Run

This was done in runs 32, 90 and 107. Run 32 recorded 1,000 year intervals over 10,000 years, Run 90 for 2,000 year intervals over 20,000 years and Run 107 for 200 year intervals over 2,000 years. Because most of the sensitivity tests were done over a 10,000 rather than 20,000 year period Run 32 is presented in the Initital Standard Run maps in order to give direct time interval comparison with the initial experiments, but the longer period of Run 90 is given in the total volume and flux charts (Figs 17,18). The behaviour of the model can be described with reference to time sequential maps of the derived outputs, and the volumetric charts. It should be noted that the initial input condition (t=0) is slightly different from the true present day ice sheet configuration. This is an artifact of the different and not very good data sources used and of the interpolation and grid formation procedures.

3.1.1 Ice sheet topography

The most notable feature is the lack of any vast change (Figs 14, 15 and 16). The greatest changes occur in the first 2,000 years as is shown in more detail in Run 107 (fig 16). This initial rapid change can be explained as a function of the mismatch between the mass balance model and the imposed initial condition. It is interesting, if fortuitous, to note that the initial tendency of the model is to move towards an equilibrium close to the present day form of the ice sheet. The change in thickness plots for Run 32 and Run 107, figures 19 and 20, show where the major changes in ice growth are as the system develops.

In addition, the initial tendency to adopt an overall smoother profile is a direct consequence of the surface-dependent equations used to solve ice flow. The raw data input has a series of higher frequency altitude fluctuations which the model smooths out rapidly in the very early stages (Fig 20). The apparent intense disturbance in ice thickness from t=0 to t=1000, results from this and is a common feature of all the runs but is not very important to the overall direction of the model run.

Following this initial smoothing, ice steadily grows in Northern Greenland whilst withdrawing from King Christian IX Land in the east and the most southerly tip. This is reflected in the total volume curves which show the loss of ice from the south eastern sector and its gain in the North East (Fig. 17). There is very little change after the first 6,000 years other than a steady elongation of the northern dome. This is borne out by the consistency of the thickness change pattern after this time (Fig

1). It is worth noting at the outset that once the rate of ice thickness change starts to decline, thickness changes in the major ice troughs become apparent. Ice continues to extend steadily northwards into Peary land. Overall, the 20,000 year condition is an extremely good representation of the contemporary ice sheet where the height and dimensions of the main ice domes are faithfully replicated. The over-prediction in the North East probably results from underestimating aridity there and the under-prediction in the South West is probably due to underestimating wetness. The model fails to predict details such as the local glaciation on mountains near Sukkertoppen and Disko Island, and the glacierization of the mountainous areas of the east coast has the poorest representation. The model is probably failing to predict sufficient precipitation to simulate local glaciations effectively. There is nothing in the precipitation model to represent steep orographic precipitation gradients near the coasts. These areas correspond closely to where underpredicition of accumulation takes place in the static present-day model. The subglacial topography of the east coast is poorly known and it may be that the modelled topography of Knud Rasmussen's Land is too low to maintain active glaciation at that latitude.

3.1.2 Mass balance

Given that, for a fixed sea-level temperature, mass balance is driven by topographic change, the surface ablation and accumulation patterns develop in a similar manner to the overall ice sheet morphometry (Figs 21 and 22). A dynamic equilibrium is reached when positive feedbacks in mass balance at higher, more continental locations, are adequately countered by the negative feedbacks in the ice dynamics which hinder ice thickening. In addition, the aggregate volume loss in km^3/a, and the time instantaneous mean maximum accumulation, surface ablation and calving are shown (Figs 17 and 18). The sectors refer to nominal east-west and north-south lines on the Albers projection of the model grid, and are shown as the rectangular quadrants in Figure 1. The smoothed chart (Fig 18) gives a better indication of the long term direction of the total mass balance.

The values in the mass balance flux plots do not add up exactly. This requires some explanation. Accumulation and surface ablation values were only recalculated and recorded on a 50 year interval. This is sufficient to allow feedback between the ice sheet's topography and its climate but creates problems in estimating the true mass balance components because the ice sheet's area changes continually within

the calculation period. The accumulation and ablation values are a summation of the individual values for all the cells within the ice sheet area at any one time. If the ice sheet area changes within the recalculation period, then newly created cells are not included in the existing mass balance sum, and cells which become ice free record ablation/accumulation values but no longer exist. Therefore there can be a mismatch between what potential mass balance is recorded as its constituent ablation and accumulation components and what is actually lost from the ice mass.

There is a secondary and more substantial problem. If the total negative mass balance sum in any one cell for any one iteration is greater than the amount of ice available for removal then the negative balance is over-recorded. Moreover, this problem is not easily tractable because the equations only describe the potential for surface ablation or calving to act on any one cell. If less ice exists than the potential for it to be removed then there is a need to define what proportion is removed by either mechanism. The magnitude of this problem was only discovered late-on in the research after many of the values had been recorded at fifty year intervals. Short of running each model again there was no way of reconstructing the detail of the mass balance history. Because of the problems in calculating mass balance contributions in sufficient detail it was necessary to describe the mass balance as the actual difference in ice volumes between time intervals. Ice volume was recorded exactly as the sum of all ice thicknesses within the ice sheet area. The accumulation and ablation values give the total calculated potential within the ice sheet area at the 50 year interval concerned but the calving flux is a running total of potential calving for each time step.

The way of avoiding this problem requires cell by cell running totals to be kept of each mass balance component at each time step once ice flux redistribution has been calculated, taking into consideration any new ice cells which are formed during the redistribution, and making assumptions about the proportions lost to calving or ablation if the potential for mass removal is greater than the available ice. Such a highly iterative summation process can introduce additional rounding errors. The numerical solution of the ice flux is prone to the same problem.

Nonetheless, the total balance charts show that as the ice sheet volume increases to a quasi equilibrium, the total mass of the ice sheet is controlled strongly by calving flux. The running mean graphs show that this balancing action becomes steadily more effective in limiting ice sheet size over an averaging period of 500 years (Fig 18), whilst at the same time producing overall negative balance periods over shorter,

50 year, time spans (Fig 17). An explanation of these short term fluctuations and their association with the thickness change in ice streams is given later in Chapter 4. Total long term equilibrium is not reached, even within the first 20,000 years of static forcing conditions. However, the rate of change steadily decreases and the ice sheet is close to equilibrium after 10,000 years. This overall trend can be understood with reference to the time sequence maps of temperature (Fig 23), surface mass balance (Fig 24) and surface ablation and accumulation (Figs 21 and 22). As the ice sheet expands to the north, the temperature field stays much the same in the south, whilst the area of colder temperature increases in the north as the interior becomes steadily more continental and higher. Consequently, both accumulation and surface ablation rates decline in the north, the combined result being to increase the area of positive surface mass balance. So, in summary, the equilibrium profiles toward the south are maintained mainly through the steep surface mass balance gradients, mainly as a response to surface ablation at low altitudes. In the north where the balance gradients decline, calving is dominant in checking further ice expansion.

3.2 Isostatic change

Changes in the sub-glacial topography over the 20,000 year period (Fig 25) reflect changes in ice accumulation and loss. This is entirely as would be expected for a diffusion model which seeks isostatic pressure balance over long time periods. The only persistent change is the lowering of the subglacial surface in NE Greenland below the areas of ice accumulation. There are no major changes in coastline configuration. The apparent large change in the topography of Ellsmere island is produced because it is represented as a plane at zero metres and very minor readjustments in base level cause a change of sign. By the end of the 1000 year period isostatic fluxes have begun to decline to rates below minimum 5m/1000 years that can be shown by the maps in most areas.

3.2.1 Ice velocity and mass flux

Ice velocities (Fig 26) are directly derived from ice sheet topography and this mirrors the development of the ice sheet. The shear velocity pattern derives directly from the surface slope and ice thickness driven shear equation (Fig 27). Maximum velocity occurs toward the edge and flow concentrates into concave depressions, decreasing

over ridges. Velocities tend to be higher in South and West Greenland than in North and East. The north-south difference is caused by the differences in mass balance profiles. The east-west is caused by the eastern mountain fringe reducing ice thickness over much of the marginal area. Velocities reflect a concentration of ice flow into a few major ice streams : Illulisat, Nuuk, Kangerdlugsuaq and Scoresby Sund. Sliding velocity shows more variation overall, in that high velocities occur toward the ice edge in all areas (Fig 28). There is little regional difference from sector to sector. This is explained because there is a strong dependence on ice thickness in the sliding equation and only a first order dependence on surface slope.

Topographic differences become more significant when considering ice flux rather than ice velocity alone. Highest ice flux occurs where the ice is thick and flowing fast; that is in deep troughs. It is the shear component of total velocity which is most significant in these ice streams until their weight is reduced by partial flotation and sliding becomes significant. Ice can then be removed effectively by calving at the terminus. This maintains thin ice and sliding at the end of ice streams and keeps relatively steep gradients into the ice stream which promotes shear.

A similar effect can be seen in the time development of shear velocity in NE Greenland. In each run, the ice expands there. As the ice position stabilises, stronger shear velocity profiles develop.

The importance of the Initial Standard Run is twofold. It demonstrates that over long time periods, using present day climate the ice sheet model predicts a stable ice sheet in a dynamic equilibrium which resembles that of the existing ice sheet. This equilibrium state can be explained in terms of the topographic configuration, surface mass balance and internal ice dynamics. Secondly, it provides a standard against which concurrent runs with different parameters and subsequent runs perturbed from equilibrium can be tested.

3.2.2 The significance of the Initial Standard Run.

The discrepancy between the input condition (0a) and the condition which is in balance with a dynamic climate model (20000a) can be interpreted in a number of ways. In part it reflects error both in the original measurement of the topography and climatic variables. Secondly it may reflect an inadequately detailed or incorrect climate model as a whole or in parts (eg N. Greenland). This needs only to be slightly wrongly defined in order for small inaccuracies to amplify over long time

periods. Because of the relatively good agreement between the modelled equilibrium and reality, it is reassuring to know that such errors are likely to be self-regulating rather than exponentially unstable; the modelled system tends to balance itself out at somewhere near the real situation. Thirdly, the present climate over the ice sheet may not be in balance with the topography and might indeed develop a new topography over sufficiently long time periods. The problem of ascertaining this is that climatic records themselves only relate to the last few decades, and the timescale of climatic fluctuation is far shorter than the adjustment period of ice sheet systems. The latter is always lagging behind changes in climate. Therefore to obtain a true picture of the instantaneous balance state one would have to model correctly and aggregate the totality of climate change and ice adjustment over long time periods. In many ways it is surprising and informative that the match between the modelled and real systems is as close as it is if the assumption that the present ice sheet is in long-term balance is made.

3.3 Sensitivity tests on single variables

3.3.1 Alterations in the Arrhenius constant A

Ice flow

From the shear velocity equation (equation 10) it can be seen that shear velocity varies linearly with the Arrhenius constant - A. Values of A have been derived from either laboratory experiments or by extrapolation from field data and it is difficult to ascertain a realistic value for n, the power constant in the flow law. The value used in the Initial Standard Run was derived as an approximated average from different field sources given by Paterson (1982) for a temperature of around $-10°C$. The value for A varies with temperature and for temperatures below but near to $0°C$, a 10 degree centigrade shift in temperature is roughly equivalent to a twofold variation in the value of A. Since one of the flow assumptions used in the model is an isothermal ice mass, it is important to discover how far gross change in A would effect the model result. The Initial Standard Run for 10,000 years (Run 32) was therefore repeated with decreased (Run 49) and increased (Run 59) values for the Arrhenius constant. Conceptually, these represent 'stiffer' and 'softer' ice. The development of the ice sheet and the associated shear velocities are shown in Figures 29 - 34. The difference in ice extent after 10,000 years between the reduced and increased Arrhenius value

runs is negligible but the overall shape is significantly different (Figs 29 and 30) with an increased Arrhenius value. The ice extends a little further and the overall profile is much shallower. Higher shear velocities lead to more ice flowing from the accumulation zones into the surface ablation zones, thus reducing the gradient and causing a slight extension of the margin.

The reverse applies to a decreased Arrhenius constant (Fig 29). The ice gradient increases and the margin retreats slightly as a result of lower shear velocities (Fig 30). This difference is perhaps best observed by the difference in the two thickness change plots toward the beginning and middle of the run duration (Figs 33, 34) The faster ice velocities of Run 59 cause relative reductions in thickness in the centre.

Further detailed output of Runs 49 and 59 is included in Appendix 3. One might expect a greater difference in ice extent given the large increases in velocity but four further factors can be called to account.

First, increases in shear velocity for the same ice surface slope tend to cause relative ice thinning near the margin and this causes more rapid ice sliding in the model.

Secondly, the shear equation is far more dependent on slope which varies according to the power of n (where n=3) than on the linear constant A. Therefore, for any of the values of A used here, a similar parabolic profile is maintained toward the margin where the ice surface is steep. Shear velocities become increasingly high, little influenced by small changes in the value of A. Only toward the centre of the ice sheet does a reduction in slope cause a significant difference in velocity and mass flux. Since the most dynamic effects of mass balance are noted near the ice margin, this insensitivity of the margin to changes in A means that the mass balance of the ice sheet as a whole is relatively unaffected.

Thirdly, the greatest change in topography occurs at altitudes where there is the least variation in mass balance, namely the ice centre where mass balance is weakly positive. The 'softer' ice model, whilst transporting more ice to the surface ablation zone, also reduces the altitude of the interior, enhancing mass balance in the source region. The reverse is true for the 'stiffer' model, which causes a decrease in accumulation in the interior as a result of increased continentality.

Fourthly, topography near the margin has an effect in 'pinning' the margin to certain locations in spite of different ice supply. If the ice margin retreats to an area of higher ground the edge surface gradient is reduced. This slows the ice and reduces surface ablation. The centre of Greenland covered by the ice sheet, is a large bowl

with relatively high areas fringing the present margin. Even where these high areas are broken by troughs the net effect is to provide a stable topographic pinning point for the ice sheet. This effect probably applies to all experiments. The dominance of this last effect is extremely hard to quantify but is considered later as one of the persistent model features influencing ice behaviour. Similarly, it is not possible with the present results to say which of these four effects is most important in influencing ice sheet extent.

Variations in the sliding constant - k

Sliding velocities are linearly related to the sliding constant k (equation 13). This equation is empirically derived from data in Antarctica (Budd and others 1984) and so, whilst the value used in the Initial Standard Run was a useful first approximation, it was important to determine the sensitivity of this parameter to variation. The value of k was halved and doubled in Runs 48 and 58 respectively. All other variables were identical to the Initial Standard Run. Once again it possible to observe that there is relatively little change in ice extent whilst differences develop in ice surface topography (Figs 35 and 36). Halving the constant (Run 48) produces 'stiffer' ice and a steeper ice profile. Doubling the constant (Run 58) flattens the profile. The patterns are very similar to the corresponding changes in the Arrhenius constant and it is possible to explain the different profiles in a similar way, namely that they are related to the more and less efficient removal of ice from the interior to the edge. Again these are best demonstrated by the thickness change plots (Figs 37, 38).

Increased sliding velocities reduce the overall gradient of the ice sheet, thus reducing the shear velocity in compensation. Details of these and the total and sector ice volumes are included in Appendix 3. Whilst the sliding equation is linearly related to surface slope, it is inversely proportional to thickness, which means that sliding velocities tend to become high toward the edge regardless of the sliding constant. Again these rapid velocities occur near the steepest and most dynamic part of the surface mass balance profile and can transport mass rapidly from the accumulation to the surface ablation zone. However, because a minimum thickness value of 300m is used for calculating sliding velocities in order to prevent them becoming exponentially and unrealistically large, this effect no longer applies at thicknesses near or below this minimum thickness.

As is the case with experiments changing the Arrhenius constant, the greatest changes in topography caused by varying the sliding constant are in the ice sheet

centre. Here there are compensatory mass balance mechanisms which counteract the effect of an increase or decrease in altitude, and thus there is little effect on the mass balance of the ice sheet as a whole. Topography, and particularly its role in providing pinning points, is likewise a factor discouraging changes in ice extent as a result of changing the sliding constant.

3.4 Reducing and increasing the sliding cut-off thickness

The cut-off thickness specified in the model sets an artificial thickness Z_* value for calculating sliding in thin ice. In the sliding equation (equation 13) it prevents exponential thinning of thin ice. The value was set arbitrarily at 300m in the first instance. By reducing the cut-off thickness to 150m the constraining velocities for a given slope are doubled and by increasing the cut-off thickness to 600m the constraining velocities for a given slope are halved. Although it was important to set this value high enough to constrain excessive sliding velocities relative to shear velocities, too high a value limits sliding velocites arbitrarily.

For instance, with surface slope of about 1:100, ice velocities at the cut-off thickness for the 150m, 300m, and 600m cases are about 100, 50 and 25 m/a respectively. It is possible to demonstrate that extreme values of the cut-off thickness produce unreasonable sliding velocities. For instance, (using the same 1:100 slope) if the cut-off thickness is reduced to 10m, the sliding velocity can reach up to 1800m/a. If it is increased to 1000m, all ice thinner than 1000m in constrained to flowing at 18m/a. In the first case the fast ice velocity has become assigned purely on the basis of very thin ice. Although such velocities are possible for surging ice, they usually occur in much thicker ice bodies, or at least in ones in which the sliding is not simply attributable to very thin ice. In the second case, constraining ice sliding in very thick ice to such small values is equally unrealistic. Therefore, the choice of some intermediate value is desirable and the sensitivity tests give some indication of appropriate values. In the range of test cases chosen, the value of the sliding cut-off thickness chosen seems to have little long-term effect on ice sheet development. Figure 39 shows the Initial Standard Run for 10,000 years with the sliding cut-off altitude at 150m and Figure 40 with the value at 600m. Comparison shows that the ice sheet extent varies little. However, as would be expected, the greatest observable effect is on sliding velocities

toward the ice margins (Figures 41 and 42). Velocities stay the same near the interior. In the model of the present day ice sheet, ice velocities within the surface ablation zone are probably those most affected by alteration in the cut-off thickness. Therefore the most noticeable effect is likely to be minor adjustments in the shape of the ice profile near and below the surface ablation line. However, since the surface ablation gradient is steep the effect is comparatively small. The cut-off thickness was held at 300m in subsequent experiments.

3.5 Mass Balance

3.5.1 Changes to the calving constant

The calving constant is another linear parameter, this time directly affecting calving flux (equation 45). Once again it is an empirically derived regression parameter. It is important to gain some perspective on its importance in affecting the modelled behaviour of the ice sheet, because calving is an important element in ablation. The value of the calving constant ($V_{c/b}$) in the Initial Standard Run is 28.75. In this sensitivity test the val e was reduced to $V_{c/b} = 20$ in Run 77 (Fig 43) and increased to $V_{c/b} = 40$ in Run 76 (Fig 44), while all other variables were held constant. Interestingly, the changes have little effect on the development of the contemporary ice sheet model. With reduced calving the 10,000 year examples show miniscule increases in extent. With increased calving, there is a slight decrease in extent. It is all but impossible to demonstrate the variations in calving flux in map form for two main reasons. Firstly, the high fluxes are confined to single cells at the margin and occur at a finer resolution than can be mapped at a Greenland scale. Secondly, as is illustrated in a graph of the total ice flux for the Initial Standard Run (Figure 14), calving varies cyclically over short periods and typical values may not coincide with a particular time record.

These experiments with the contemporary model show that the overall topography and evolution of the ice sheet are relatively little affected by varying the rate of calving. It will be shown later that after some experiments with simulated maximum conditions a reduced calving rate ($V_{c/b} = 20$) could be justified in some instances.

3.5.2 Altering the minimum and maximum mass balance rates

Both the accumulation and surface ablation equations are positional regression equations, parametrized on real world data. They therefore tend to become invalid beyond the spaces for which they are parametrized and towards the extremes of the real data values. A further problem is that the accumulation and surface ablation equations behave differently at their extremes. This is because they are both non-linear and differing relationships. But this problem is eased because high accumulation invariably coexists with high surface ablation and vice versa. Only one of the two constrains mass balance in any one situation.

In high accumulation/high surface ablation areas, with no constraints on accumulation and a maximum of 15m surface ablation, the highest net mass balance values occur in areas of only modest accumulation rates. In other words surface mass balance here is surface ablation limited. A maximum limit of 15m was adopted for surface ablation. This is sufficiently high a value since it is not exceeded under present day conditions. Limiting it below this level does not however seem reasonable since rates of comparable magnitude have been measured in West Greenland today (Braithwaite and Olesen 1989). In low accumulation/low surface ablation areas, the difference between positive and negative mass balance is quite fine. However the effect on the overall behaviour of the ice is potentially great, because of the large extent of the zone in the ice sheet interior and the north of Greenland. In Run 61, the minimum accumulation was raised to 10cm/a from the 5cm/a level used initially. The maps show that this seemingly minor change has a fairly dramatic effect on the development of the ice sheet. Over a significant area of the interior, accumulation increases from 5cm/a to 10cm/a (Figure 45). The effect on the topography of the ice sheet is to cause significant growth of the central ice dome and its northern flanks over 10,000 years (Fig. 46, 47).

3.6 Alterations to continentality

The continentality controls the rate of cooling toward the interior at sea-level equivalent altitudes and is derived by distance from the sea. It affects accumulation rates via the lapse rate and accumulation equation. Because a set distance is used in the parametrization of the accumulation equation itself, it is not really desirable to change

its value in normal circumstances. Nonetheless, it was important to check the operation and sensitivity of the parameter. The original value of 350km was the radius of a circle whose diameter was approximately half the mean width of the continent. This was to try and introduce the maximum possible variability of continentality temperature over the whole ice sheet. A larger continentality distance (Run 78) of 700km, decreases the rate and range of cooling towards the interior and tends to increase temperatures slightly overall; a decreased distance of 150km (Run 99) increases the rate of cooling towards the interior and tends to decrease temperatures. Increasing the distance (Run 78) causes a greater difference in the north than the south (Fig. 48) The southern dome does not extend much beyond the limits of the standard run, but it is slightly higher. The central and northern areas are more elevated too, and the ice extends more, than the Initial Standard Run towards the north. The research implication for the growth in the north is that the 'desertification effect' is being lessened. This has more impact in the North where ice growth is limited by low accumulation than in the south where high surface ablation controls growth.

Decreasing the distance (Run 99) makes the ice sheet drier, tending to reduce accumulation and lower the interior surface slightly overall. In the south, the drier climate cuts off the supply of ice sufficiently to reduce the extent of the ice (Figure 49) when compared to the Initial Standard Run(Fig 16).

3.6.1 Altering the global mass balance

The model includes a facility to apply a direct multiplication constant to either surface ablation or accumulation. This is in order to be able to equate ice sheet change with percentage perturbations of the mass balance terms. It allows the model to be forced whilst circumventing some of the feedbacks in the mass balance models themselves. Two experiments illustrate the effects of increasing the mass balance. Run 63 involves a reduction in surface ablation of 10%. Figure 50 shows the total increase in ice volume that results, with the main growth occurring in the north east. Run 64 increases the mass balance by increasing accumulation by 10%. The results are very similar but there is a slightly greater increase in ice volume in the north east (Figure 51).

A fuller experiment in Run 95 shows the effect of reducing mass balance by increasing surface ablation and decreasing accumulation simultaneously by 5% (Figure 52). In this case there is an overall reduction in ice volumes, especially in the south and west but an increase in the north. Mapped output of these changes over the

10,000 years of the run is included in Appendix 3. The experiments confirm that the form and stability of the ice sheet are sensitive to relatively small changes in mass balance.

3.7 Summary

The sensitivity tests on individual parameters show that the internal ice dynamics are fairly insensitive to alterations in the parameters which control them. Where differences occur they concern the profile rather than lateral extent. However, the tests in the Initial Standard Run are fairly heavily biased in favour of land based ice and the situation may not be the same for extensively marine terminating glaciers. In contrast, all forms of alteration of the mass balance model have noticeable effects. This is an important conclusion. It means that in subsequent tests it is reasonable to assume that the ice dynamics model is fairly robust and reasonably good at simulating flow under a range of conditions. Changes in the ice sheet occur because of changes in mass balance and the geography of Greenland, rather than because of some artifactual internal condition in the dynamics model.

3.8 Forcing the model as a whole

This section describes a series of experiments in which the forcing variables of temperature and sea level are changed systematically. The aim is to explore the sensitivity of the model as a whole to perturbation, in particular the amount of change, the time lags involved and the geography of the change.

3.8.1 Forcing the model using global temperature

The Initial Standard Run was forced using different values for the surface ablation forcing constant. The 20,000 year condition in the Initial Standard Run was taken as the starting point for these experiments because the ice sheet virtually achieved equilibrium with present climate and any change can be ascribed to the additional forcing away from this state.

Two values of the surface ablation forcing constant were used in the temperature forcing of the surface ablation equation. The value of $0.973°C/°\Theta$ was used in runs 91-94. It simply equates a temperature shift at sea level to a latitudinal shift.

The value of $0.4°C/°\Theta$ was used in runs 119-124.

The effect of temperature forcing with a surface ablation forcing constant of $0.973°C/°\Theta$ is summarized in Figure 53 which shows that even with fairly major imposed temperature changes the net effect is rather minimal and in the opposite direction to that intuitively expected. The forcing includes one-step temperature reductions of $-6°C$ and $-3°C$ and stepped rises of $+3°C$ and $+6°C$. The $-6°C$, and $-3°C$ scenarios demonstrate minor volume losses, chiefly because of the reduction of accumulation in the centre with cooling. Elsewhere, reduced accumulation is not equally matched by reduced surface ablation and as a result the ice expands in the south. In contrast the $+3°C$, and $+6°C$ models show considerable mass gain over the central dome caused by enhanced accumulation. In terms of total volume this more than compensates for the slight retreat of the southern fringe. These total differences show up again on the mass balance charts. The $-6°C$ scenario shows reduced accumulation and surface ablation rates but the net effect is to cause initial negative total mass balance (Fig. 54). For the $+6°C$ scenario both accumulation and surface ablation rates increase but the net effect leads to mass gain (Fig. 55). The lower, flatter profile of the $-6°C$ scenario leads to a greater marine contact area and enhanced calving rates. The $+3°C$ and $-3°C$ are simply intermediate cases of these extremes and details are also included in the Appendix.

Whilst these models predict the anticipated direction of change in mass balance for accumulation and surface ablation separately, the combined effect is intuitively wrong. Cooling leads to a reduction in the volume and warming to an increase. The reason for this is that the model matches forced alterations in accumulation and surface ablation too evenly. One way to get a less even match is to alter the ablation forcing constant. Using the reduced value of $0.4°C/°\Theta$ makes the surface ablation terms more responsive to temperature; warming causes relatively greater melting and cooling leads to less melting. The reduced latitudinal lapse rate of $0.4°C/°\Theta$ produces an entirely different set of results. There is now marked differentiation both in the magnitude and rates of change. At one extreme, the $+6°C$ model causes the removal of all but two small residual ice caps over an 18000 year time span (Fig 56,57). At the other, the $-6°C$ model reaches a maximum state within 4000 years when further growth is constrained by calving at the continental edge (Fig 63,64).

In the warmest scenario (Run 122) rapid ice loss in the initial phases becomes progressively slower as the ice margin approaches more stable areas (Fig 57). Almost 50% of the ice loss occurs within the first 4000 years (Fig 57). Overall, the direction

of ice margin retreat is back toward a centre which shifts progressively north and east during deglaciation (Fig. 56). Southern Greenland becomes ice free within 2000 years. Eventually, permanent ice can only be maintained in the highest mountain areas of the east coast. The pattern of retreat can be related directly to topography. Ice tends to persist not only on the mountainous east coast but is also held preferentially by mountains to the north east of Disko Bay. The West coast does not deglaciate uniformly, but responds most rapidly in areas of low elevation and low amplitude. This experiment provides useful information about the response of the crust to isostatic uplift. Whilst the ice has been completely removed from the southern-most part of the island within the first 2000 years, basal uplift, though most rapid in the initial phases, remains observable for at least the next 6000 years.

The maps which show the progressive change in basal elevation over 1000 year intervals demonstrate well the complex behaviour of the isostatic model (Fig 58). In the first thousand years of run 122 there is rapid uplift where ice loss is greatest. With the removal of pressure on the lithosphere these areas become isostatically light, and the surrounding areas feed mass into the region of uplift. Therefore there is initial rapid downwarp of areas near to the deglacial front. Under the diffusion equation (equation 18) which governs asthenospheric flow, a mass potential gradient is set up into areas away from the initial ice removal. Once the initial unloading has stopped, the areas which are just outside the deglaciating margin now tend to become isostatically light, because they have lost so much mass in the early phases of adjustment. Consequently, these areas start to receive mass and now undergo relative uplift. The process of isostatic adjustment is therefore characterised by a wave of initial downwarping and then uplift moving away from the source unloading area with progressively reduced amplitude. If the pattern of deglaciation is uneven then such waves interact complexly as they move away from their source regions.

This is precisely the case in Figure 58. After the initial phase of deglaciation, most of the unloading is concentrated into two bands on the southwest and northwest flanks of the shrinking ice sheet. Unloading is relatively greater here than on the east side because the ice thicknesses involved are much greater. Therefore, two major readjustment waves propagate away from these two flanks as the ice sheet shrinks. In the process they interact with the pattern of readjustment set up from the deglaciation of the first 1000 years. Some areas inevitably go though multiple sequences of depression and reemergence as these waves pass by. The pattern also indicates that adjustment concentrates back towards the area of most recent ice removal. In doing so

ice free areas are as much affected by the continued deglaciation at a distance as they are by their own recovery. This highlights both the advantages and disadvantages of modelling isostasy in this way. Complex effects involved in uneven deglaciation are easily represented. However because the asthenosphere is assumed to be perfectly viscous no interruption or slowing of adjustment occurs because of the rigidity of the lithosphere. These effects continue to be observable in subsequent experiments.

In view of the catastrophic response to warming of $6°C$ it is worth examining the response to lower amplitude changes. Run 120 shows the response to warming of only $3°C$ (Figs 59, 60), again with the same surface ablation forcing constant of $0.4°C/°\Theta$. The $+3°C$ model retreats to a stable but reduced ice volume. The southern dome collapses within the first 8000 years and subsequently ice sheet continues to waste (Fig 59). The ice sheet does not seem to reach a stable state after 40000 years at the end of the run. The ice manages to maintain similar thicknesses in the north despite some edge retreat; it achieves this by steepening the profile. This can be attributed directly to an increase in the mass balance gradient with warmer temperatures. The situation over the northern dome can be roughly equated with the situation over a more southerly area in the present day Initial Standard Run. The accumulation isoclines have moved north by about 3.5° of latitude, and the surface ablation isoclines north by about 7° of latitude. In an attempt to check the response of the same model to cooling, Run 119 shows the response to a temperature depression of $-3°C$, again with an surface ablation forcing constant of $0.4°C/°\Theta$ (Figs 61, 62). In this run the model achieves a dynamic equilibrium after about 4000 years (Fig 62). In this state, the ice sheet edge has advanced offshore over a significant part of northern Greenland, but remains land-terminating over significant areas of the south. The mass balance charts show how the calving flux becomes more effective once the equilibrium state is reached. The variability in the accumulation and surface ablation curves relate to minor changes in ice cover triggered by cyclic calving fluctuations. The ice overburden near the margin is sufficient to cause some uplift along the proglacial shoreline which helps keep the ice edge inshore, particularly in the south. The effect is illustrated in Figure 61 which shows the changing in altitude of the bedrock topography in Greenland throughout the course of the run (119). The forcing in the model is still not sufficient to cause local glaciation on Disko Island.

In a more extreme case of cooling, the model was forced by a temperature change of $-6°C$, again with an surface ablation forcing constant of $0.4°C/°\Theta$ (Figs 63,64). The ice sheet reaches an equilibrium state in the first 2000 years of the run. Ice goes

offshore everywhere except in the extreme southern tip of Greenland. The balance charts demonstrate how the initial surface mass balance is highly positive and leads to rapid ice growth (Fig 64). Growth is curtailed only when calving assumes a dominant role in the total mass balance regime. The irregularities in the volume plots for this run show that the variability in calving activity occurs in all sectors of the ice sheet, although it is dominant in the north eastern sector. The sequence shows that the coastline is by no means stable, particularly in and around the major marine troughs. For example, the ice extent and the water depths south of Disko Island in West Greenland and in Scoresby Sund in East Greenland are oscillating throughout the last years of the run.

The $-1°C$ and $+1°C$ experiments produce similar results but to a lesser degree. In the $-1°C$ model, it takes 8000 years to reach a new equilibrium (Fig 65). The most noticeable feature is ice expansion in the south west, but it also takes place to a lesser extent on the north east. There is an overall increase in the altitude of the central dome as a result of reduced surface ablation. In the $+1°C$ model, there is an overall loss of mass, mainly in the far south (Figure 66). As in the warming case, the main ice dome in the north increases in thickness, but in this case it is a result of increased accumulation. These two experiments illustrate again that some areas are more susceptible to minor adjustments in global mass balance regimes because of their geographies. There is no simple relationship between the initiating climatic change and the ice sheet response. A summary of the effects of varying global temperature and its effect on ice volume are shown in Figure 67. In all cases the surface ablation forcing constant is $0.4°C/°$. The main feature is the sensitivity of the ice sheet to warming, but this assumes that mass balance is dominated by surface ablation. This is admittedly one extreme and the other is represented by the minimal response to temperature change as indicated in Figure 53 where a very conservative estimate is assumed of the role of surface ablation. As will be discussed later, there is a case for assuming a relationship closer to that illustrated in Figure 67 rather than that in Figure 53. At present the experiments seem to demonstrate the extreme sensitivity of the model to changing assumptions about mass balance, particularly surface ablation.

3.8.2 Forcing the model by changing sea level (Run 6O)

Sea level has two major effects on mass balance. Firstly, it affects the importance of calving as a proportion of total surface ablation. A change in sea level can increase or decrease the calving flux. Secondly,sea level governs the altitude of sea level temperatures and thereby affects the surface mass balance. In Run 60, present sea levels were reduced by 200m to see if this would induce ice growth. Comparing the mass balance charts of this (Fig 69) and the Initial Standard Run shows that there is little overall difference in surface mass balance. During the course of the model run, however, mass balance remains positive because calving has been reduced. As a result ice advances towards the retreating shoreline, increasing in volume but adopting a lower profile relative to absolute altitude than in the Initial Standard Run. In essence the whole ice sheet has dropped 200m, consistent with the lowered sea levels, but in doing so it spreads out more because there is more land to occupy (Fig 68).

3.9 Conclusion

The sensitivity tests in this chapter have looked at both individual parameters and the response of the model as a whole to forcing. The main conclusions in the first part are firstly, that the behaviour of the ice sheet is relatively insensitive to the choice of ice flow parameters, but sensitive to the way mass balance is parametrized. In the second part of the chapter it was shown that stepped temperature changes, positive or negative, cause the ice sheet to grow or decline in a predictable way. If the importance of surface ablation on mass balance is emphasised, then at one extreme a warming of $+6°C$ removes the ice sheet completely. Also, the experiments show that the main response can be achieved in as little as 2000 – 4000 years, although slower changes continue as long as 20,000 years after the perturbation. Calving emerges as a major factor controlling ice sheet behaviour, particularly after growth to a maximum extent which increases the proportion of marine margin. This latter relationship, the way the attitude of the underlying topography influences ice retreat, and the differing responses of different sections of the ice sheet, points to the importance of geography in the understanding of ice sheet response to change.

An important supplementary point to emerge from about 30 separate sensitivity tests is that none of the alterations has yielded a better model of the contemporary ice sheet than the Initial Standard Run. A better model of the contemporary ice sheet

has not been explicitly sought during these tests, but yet it gives some corroborative confidence that the Initial Standard Run is quite a good model of present situation. One further independent test for this is that the total flux values compare favourably with other estimates of the health of the present day ice sheet, although derived differently (Table 1.1). The accumulation values are similar to previous estimates, if slightly higher. Whereas the model predicts accumulation of $650 km^3/year$, other estimates range from $425 km^3/year$ to $630 km^3/year$ (Loewe 1934, Loewe 1964, Bauer 1955, Bauer 1957, Bader 1961, Benson 1962). The major difference is that the present model predicts much higher surface ablation relative to calving than in the present day situation. For example, the model predicts potential surface ablation rates of about $400 km^3$ and calving rates of about $70 km^3$ of whereas the measured estimates are nearer to $200 km^3$ for calving and $300 km^3$ for surface ablation.

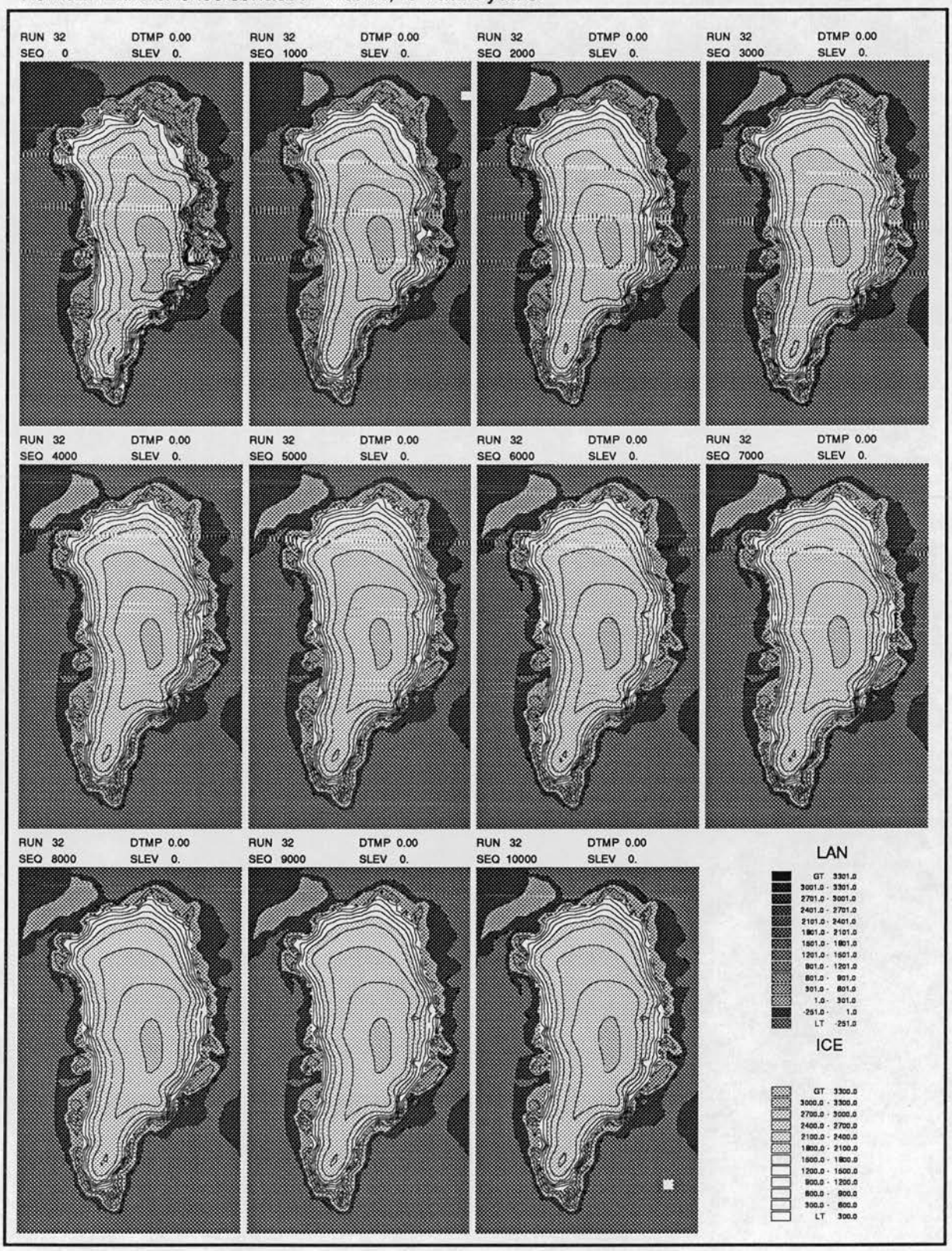

Figure 14: Modelled exposed land and submarine surfaces with superimposed ice surfaces for the Initial Standard Run (32 - 10000 years). The ice expands to a dynamic equilibrium with the modelled climate. The dimensions of this state are close to the real input condition.

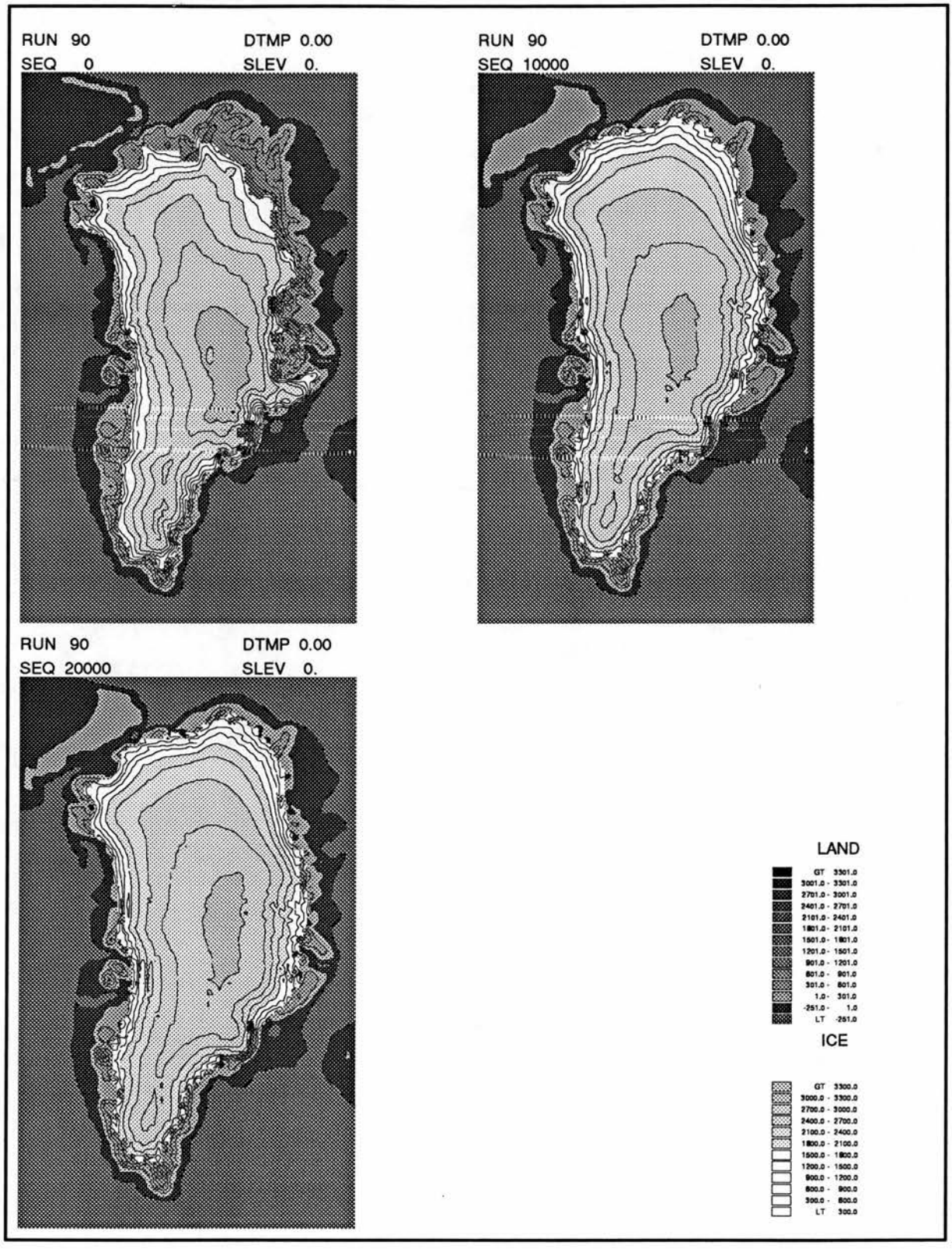

Figure 15: Modelled exposed land and submarine surfaces with superimposed ice surfaces for the Initial Standard Run, 0a, 10000a and 20000a (Run 90). The continuity of the equilibrium form betweeen 10000 and 20000 years is clear. The 0a map represents the 'real' input condition of the model.

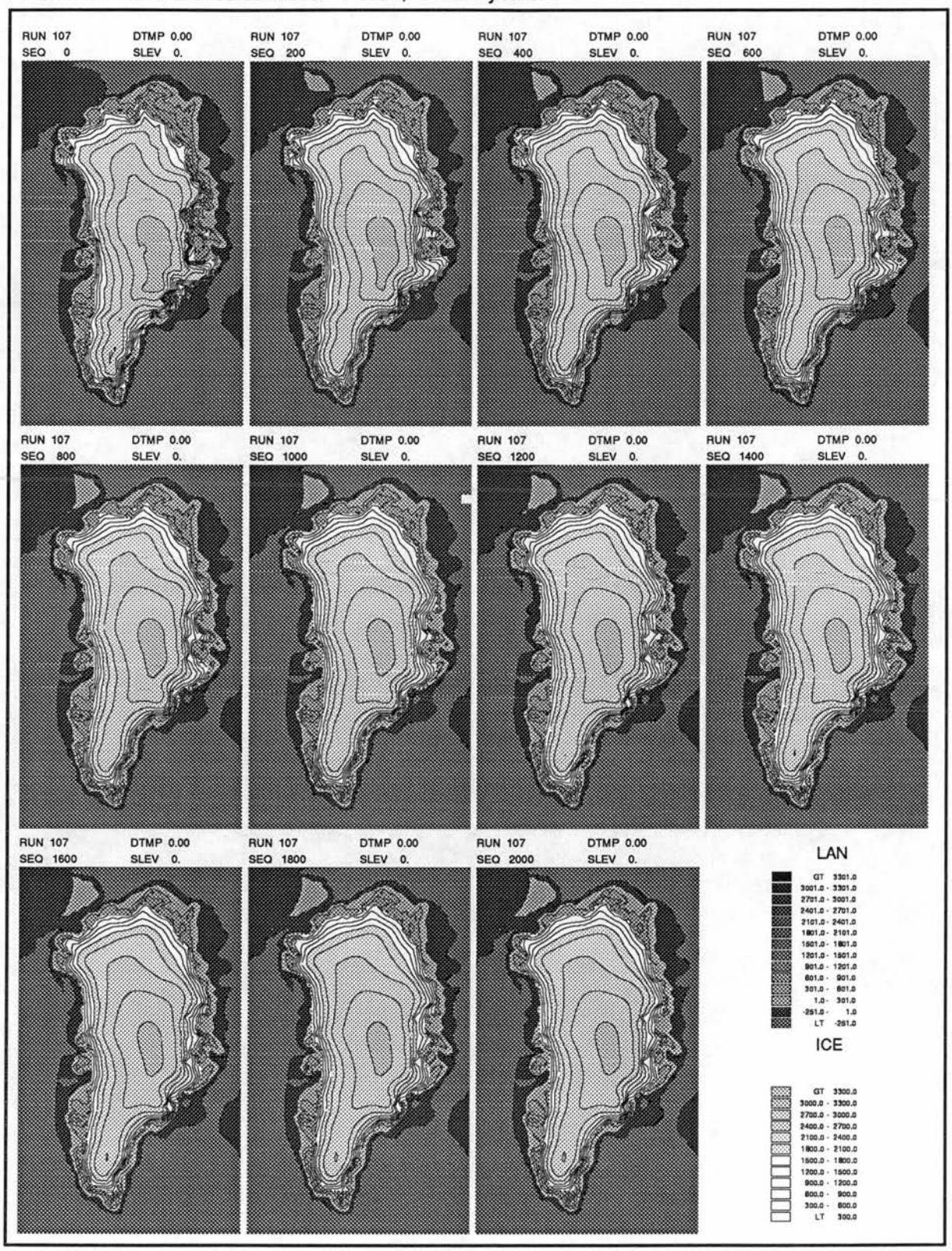

Figure 16: Modelled exposed land and submarine surfaces with superimposed ice surfaces for the Initial Standard Run (107 - 2000 years). With the shorter time resolution the initial smoothing of the modelled ice which results from defining ice flux as a slope dependent differential equation can be seen.

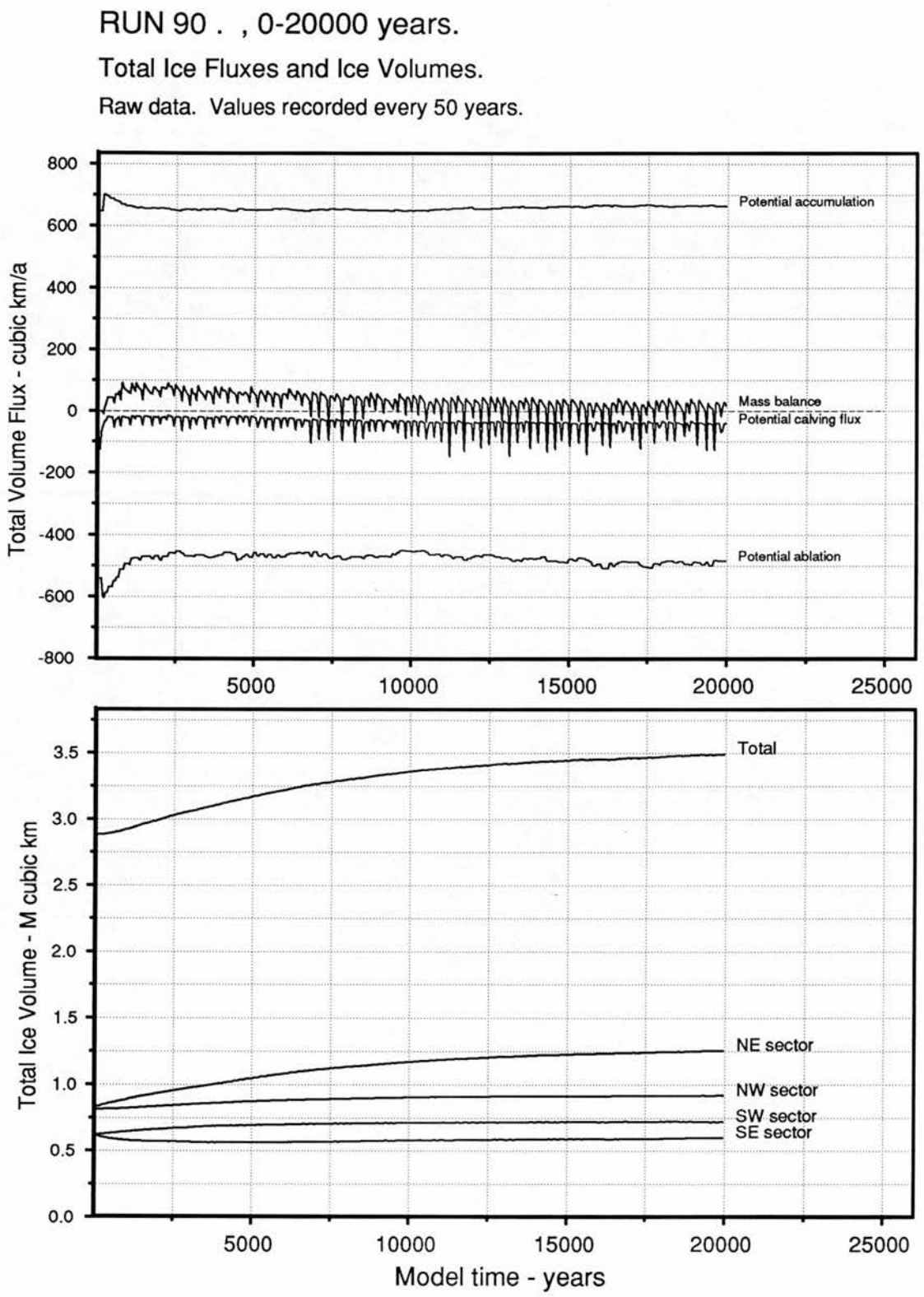

Figure 17: Ice volumes and mass balance values for the Initial Standard Run (90) given as raw data. This shows the total volume adjustment towards equilibrium. The mass balance rate fluctuates around zero, dependent on calving intensity.

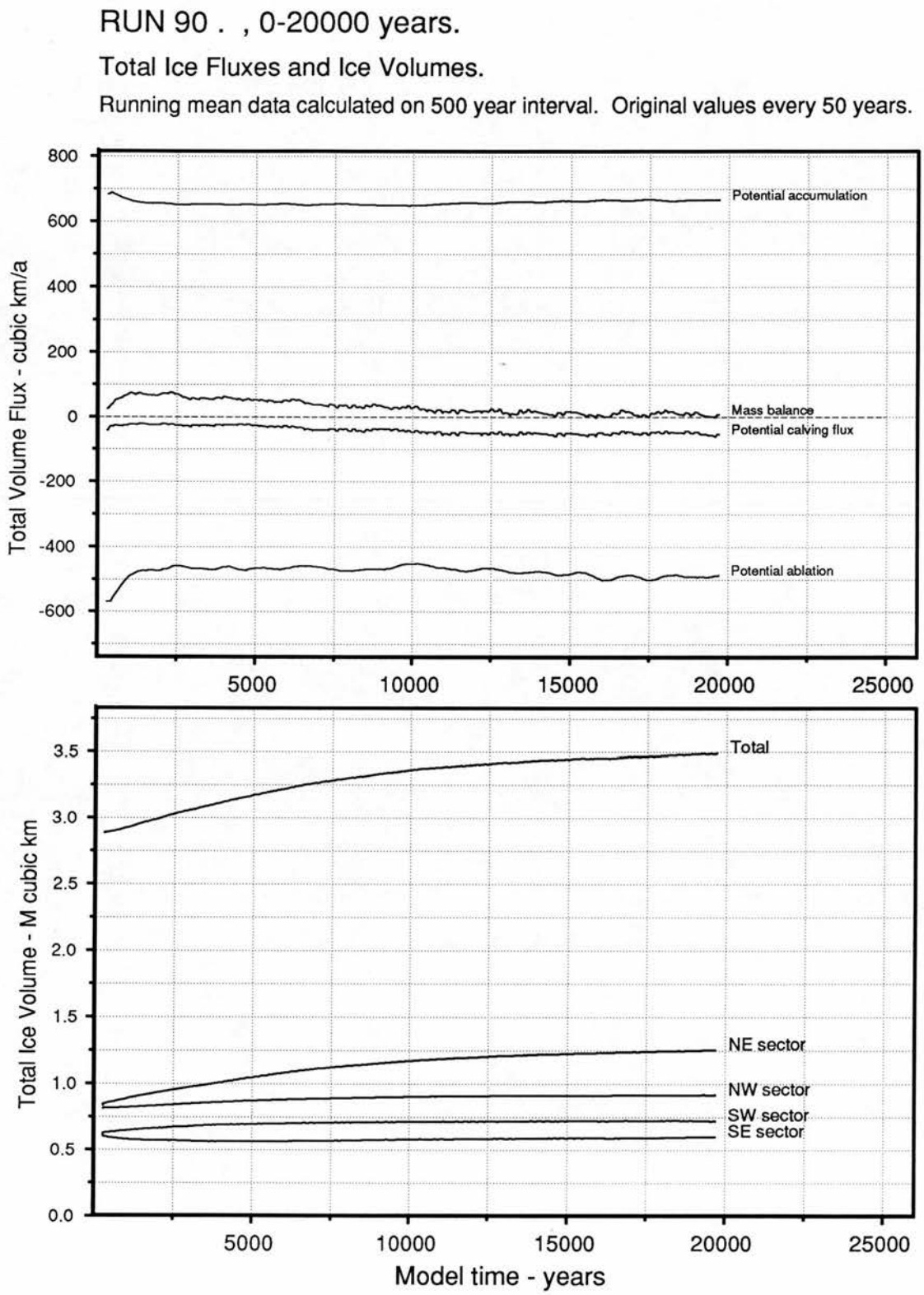

Figure 18: The figure shows ice volumes and mass balance values for the Initial Standard Run (90) calculated as a 500 year running mean. The smoothed graph shows the tendency toward equilibrium more clearly.

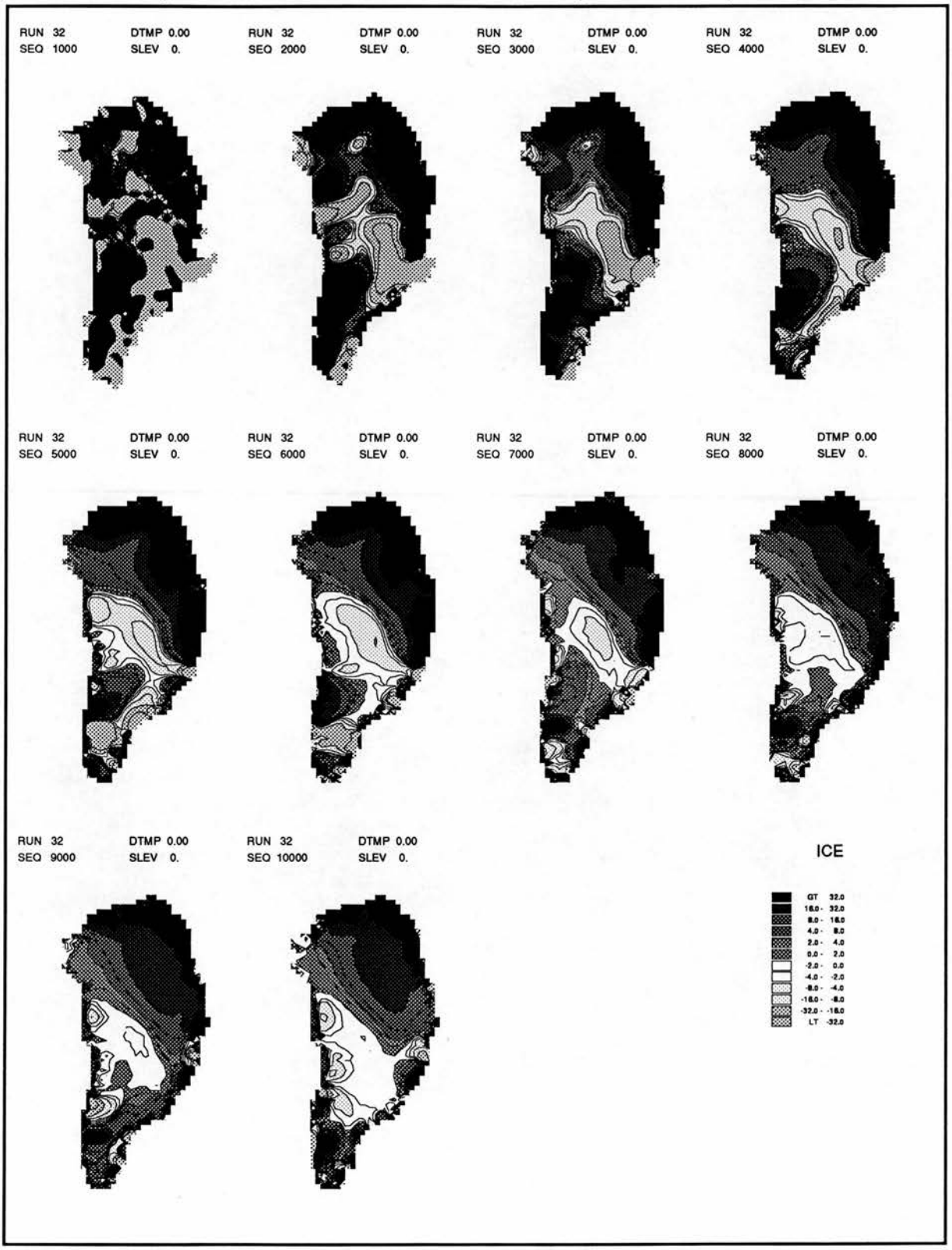

Figure 19: The figure shows changes in ice thickness for successive time steps for the Initial Standard Run (32).

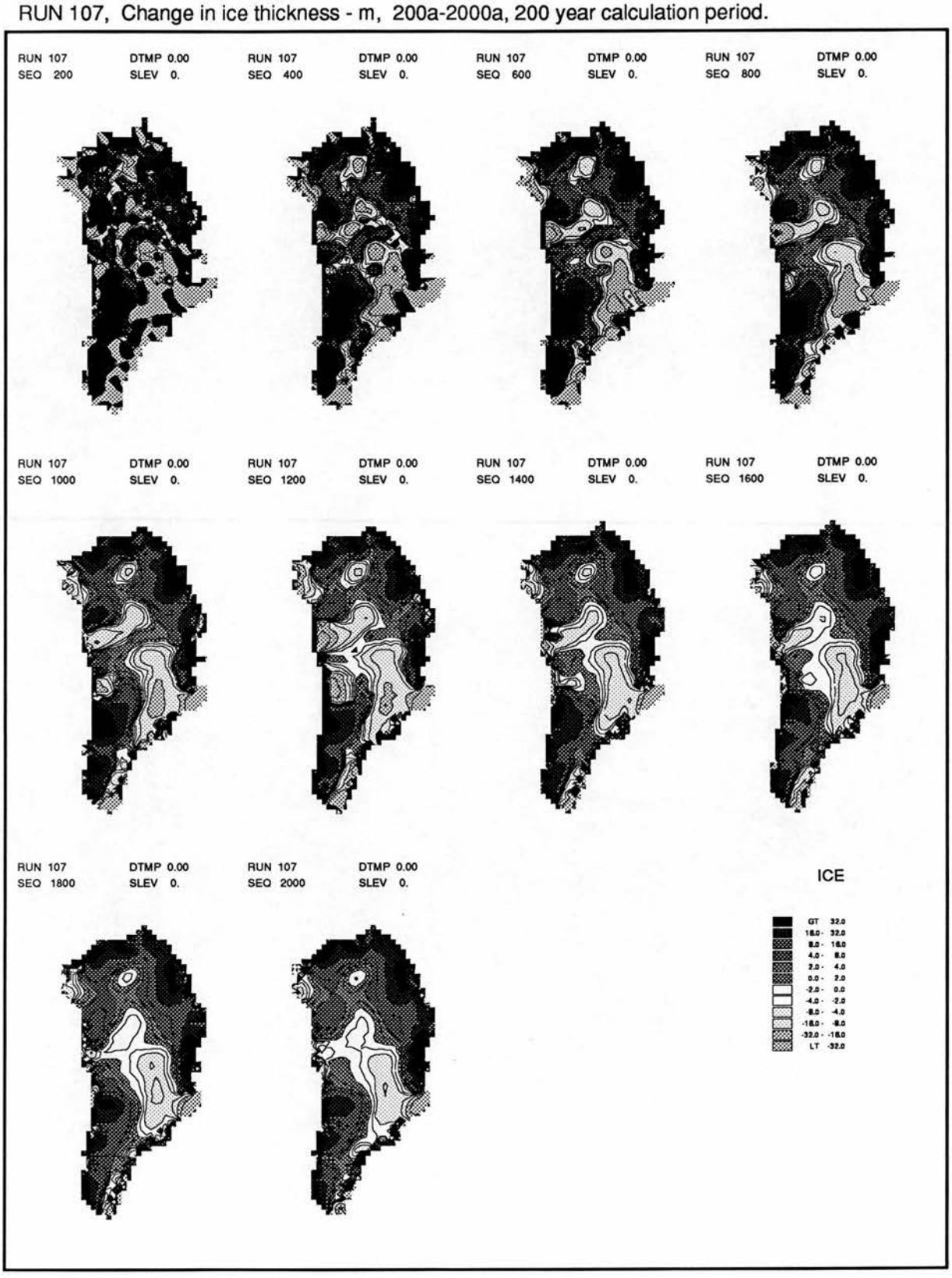

Figure 20: The figure shows changes in ice thickness for successive time steps for the Initial Standard Run (107).

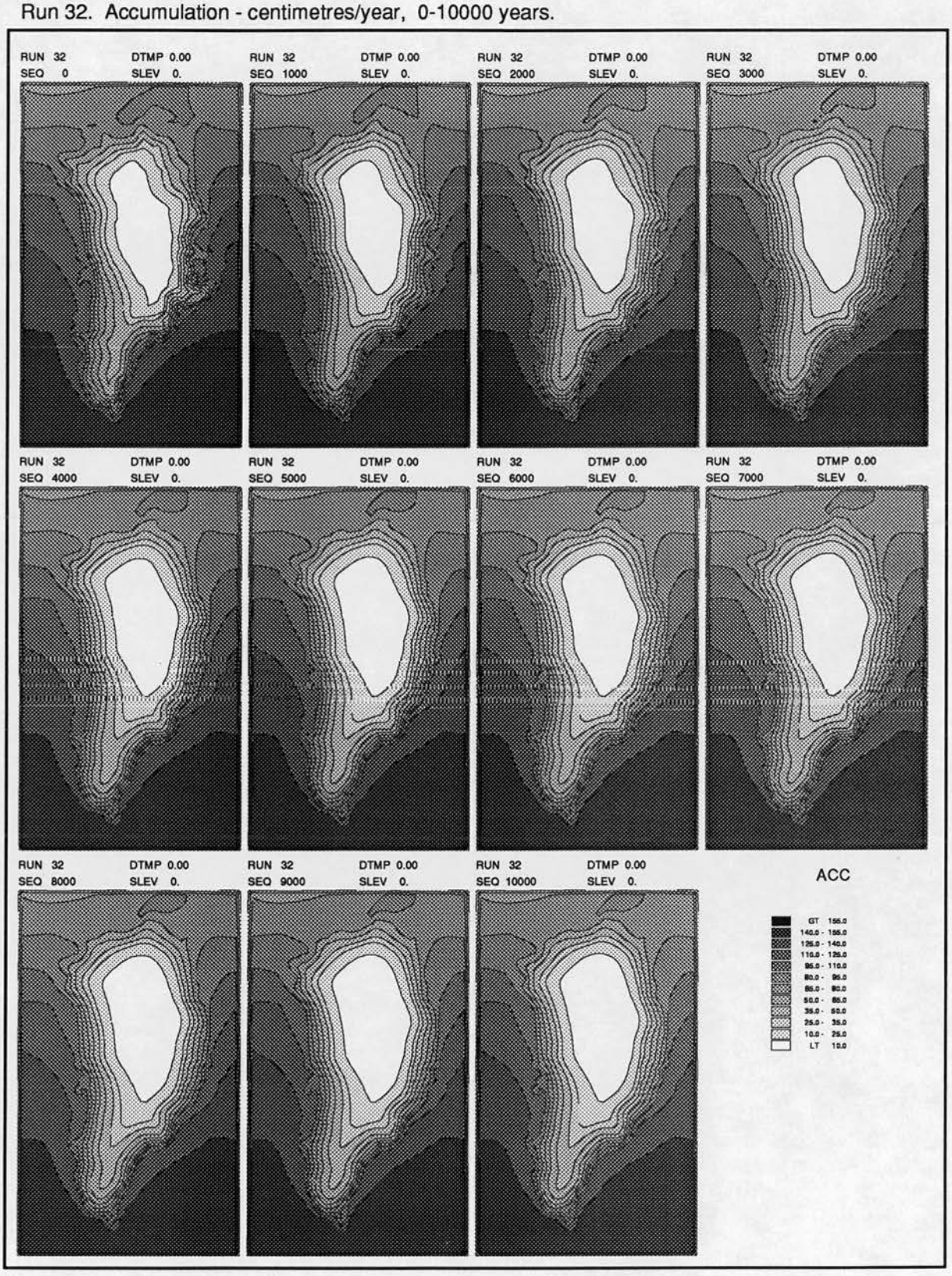

Figure 21: Modelled accumulation rates in cm/a for the Initial Standard Run (32). Modelled accumulation is predicted as a function of surface temperatures (eq 42). With a static forcing temperature, the development of this pattern is a reflection of the surface adjustment.

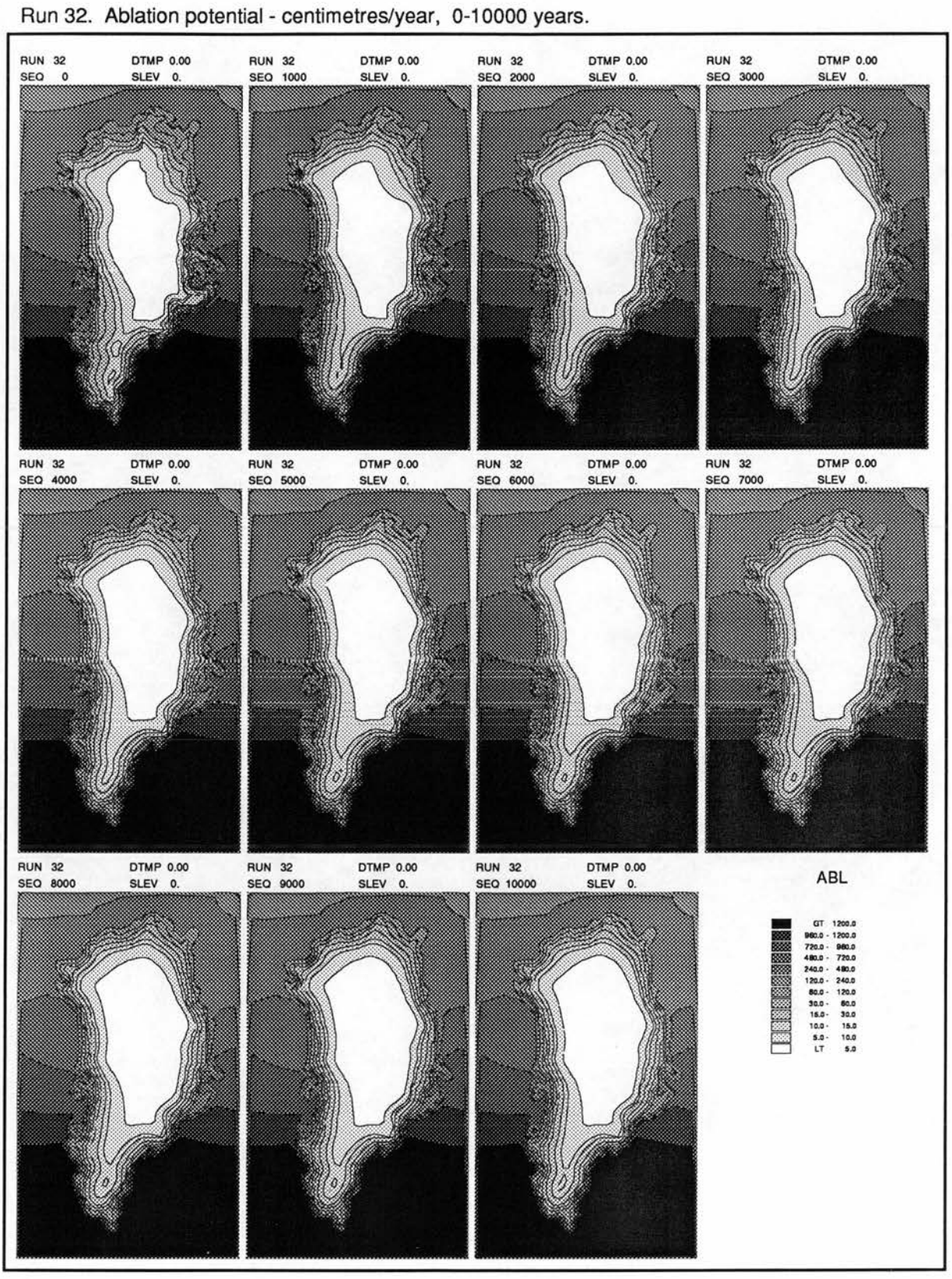

Figure 22: Modelled ablation rates in cm/a for the Initial Standard Run (32). Modelled ablation is predicted as a function of elevation and latitude (eqs 27,28).

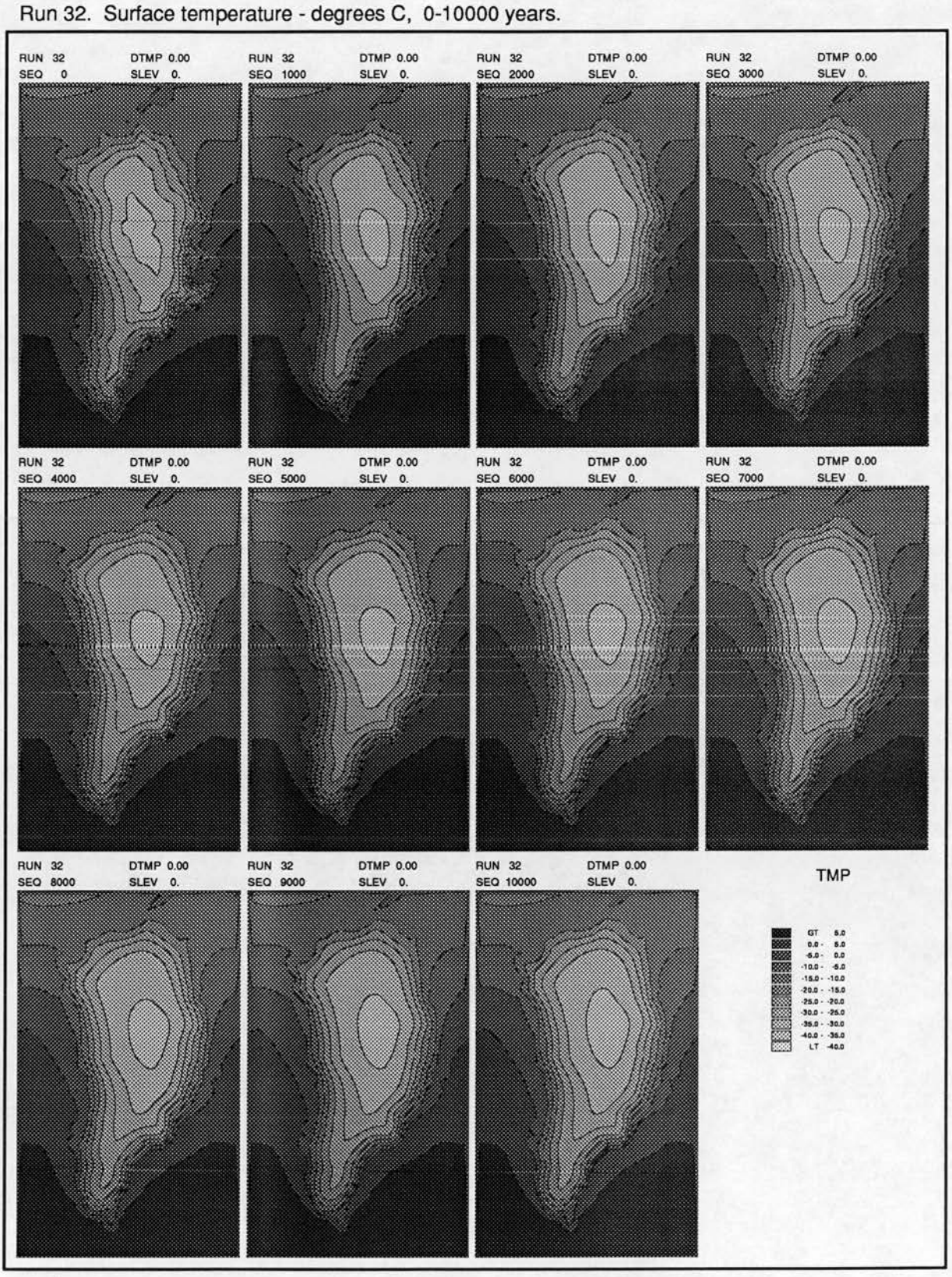

Figure 23: Surface temperatures $°C$ for Initial Standard Run (32). Modelled surface temperature is a function of latitude and elevation (eqs 34,35).

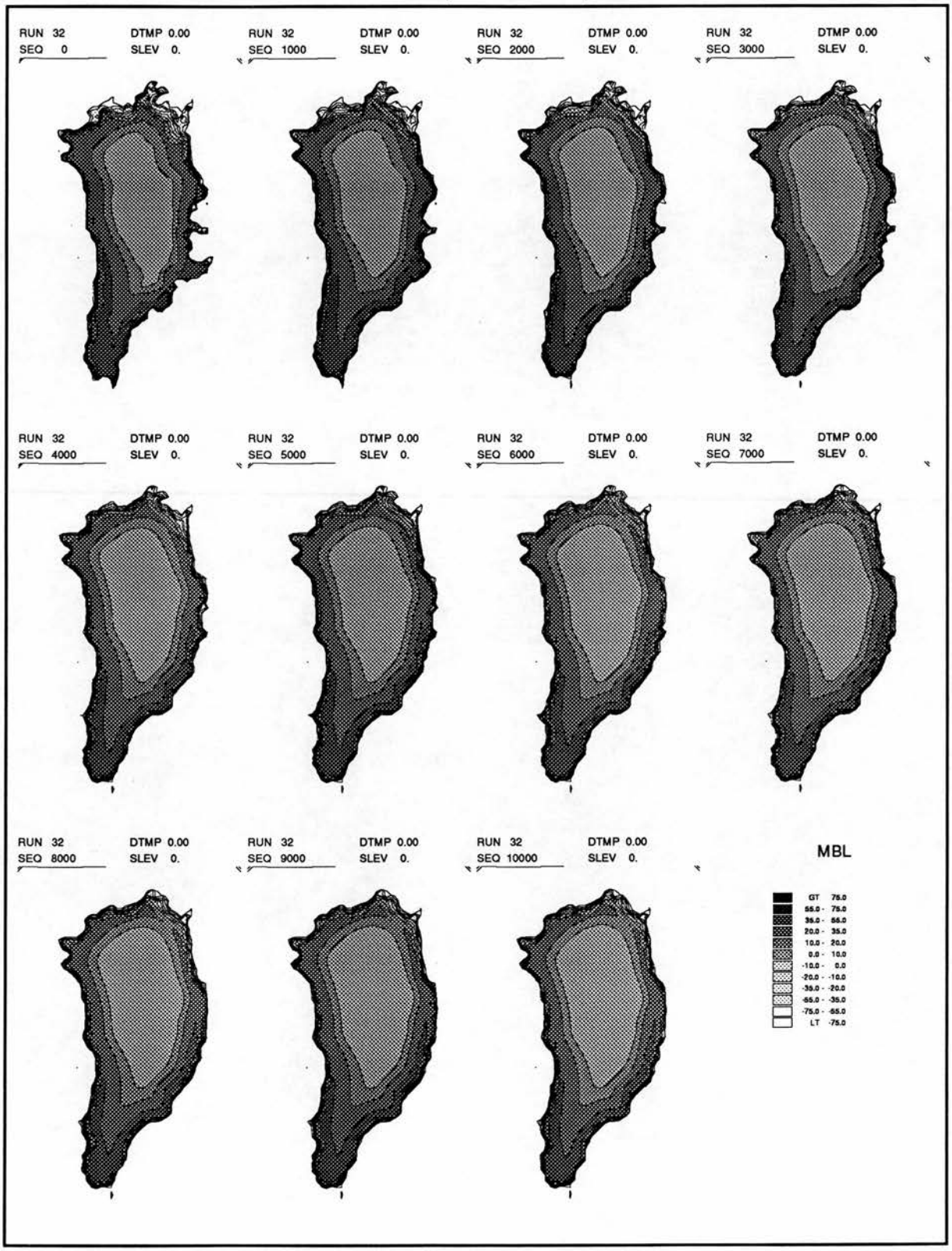

Figure 24: Modelled surface mass balance rates in cm/a for the Initial Standard Run (32). Modelled mass balance is the sum of accumulation and ablation.

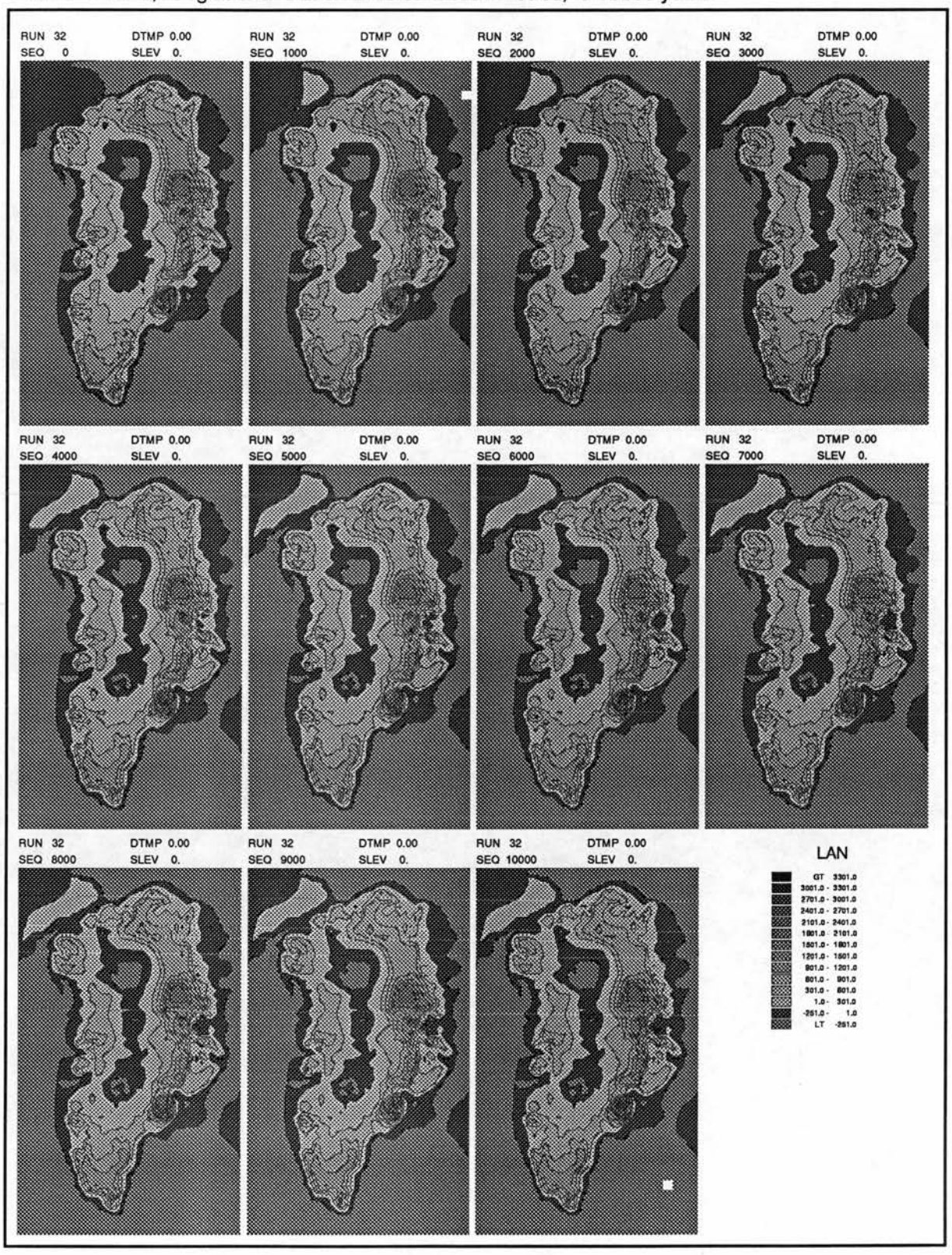

Figure 25: Modelled exposed land, subglacial and submarine surfaces for the Initial Standard Run (32). Values are recalculated throughout the run to account for isostasy (eq 16).

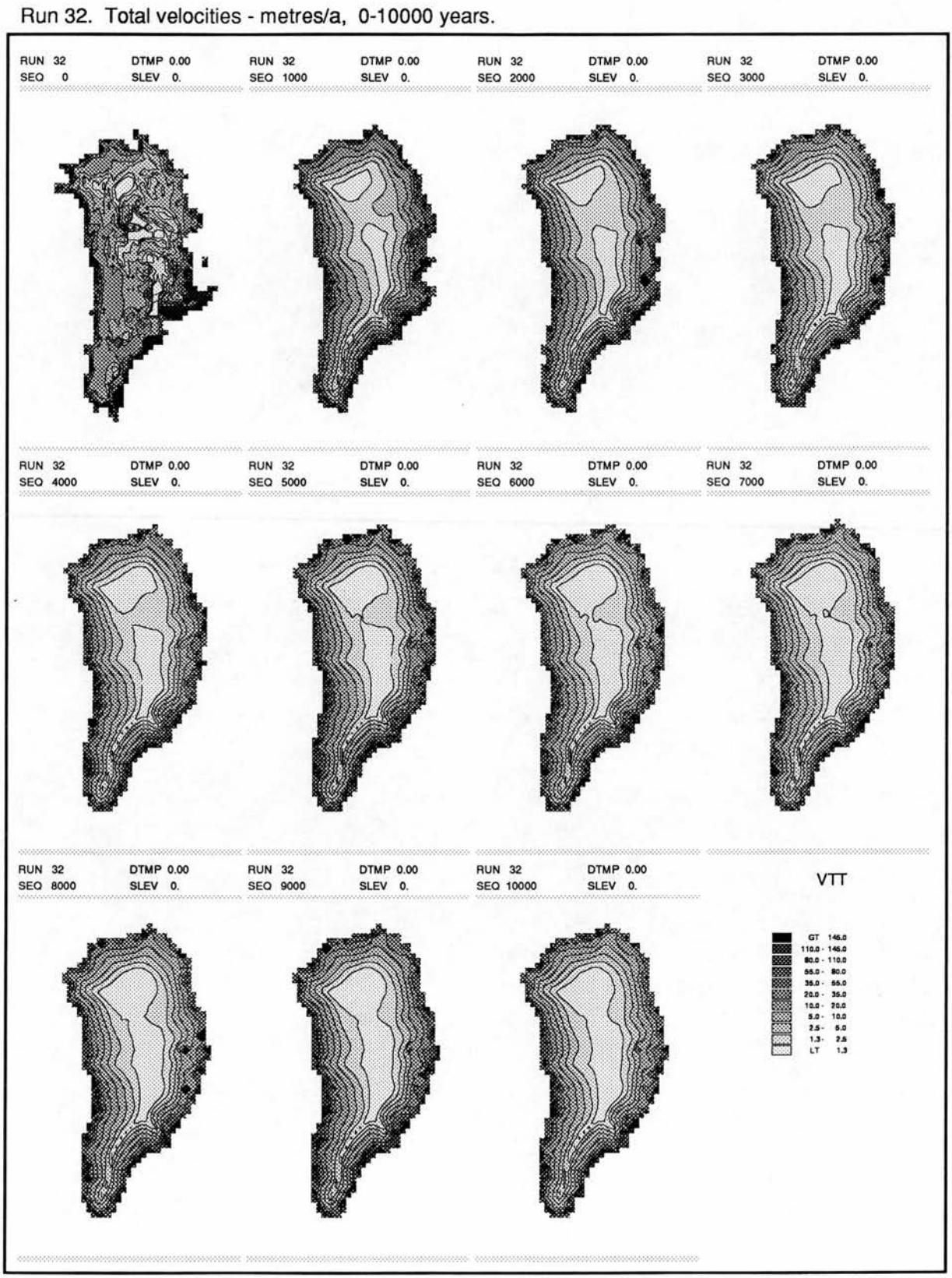

Figure 26: Derived average total ice velocites m/a for the Initial Standard Run (32). Values are calculated as the sum of sliding and shear components (eq 8,11).

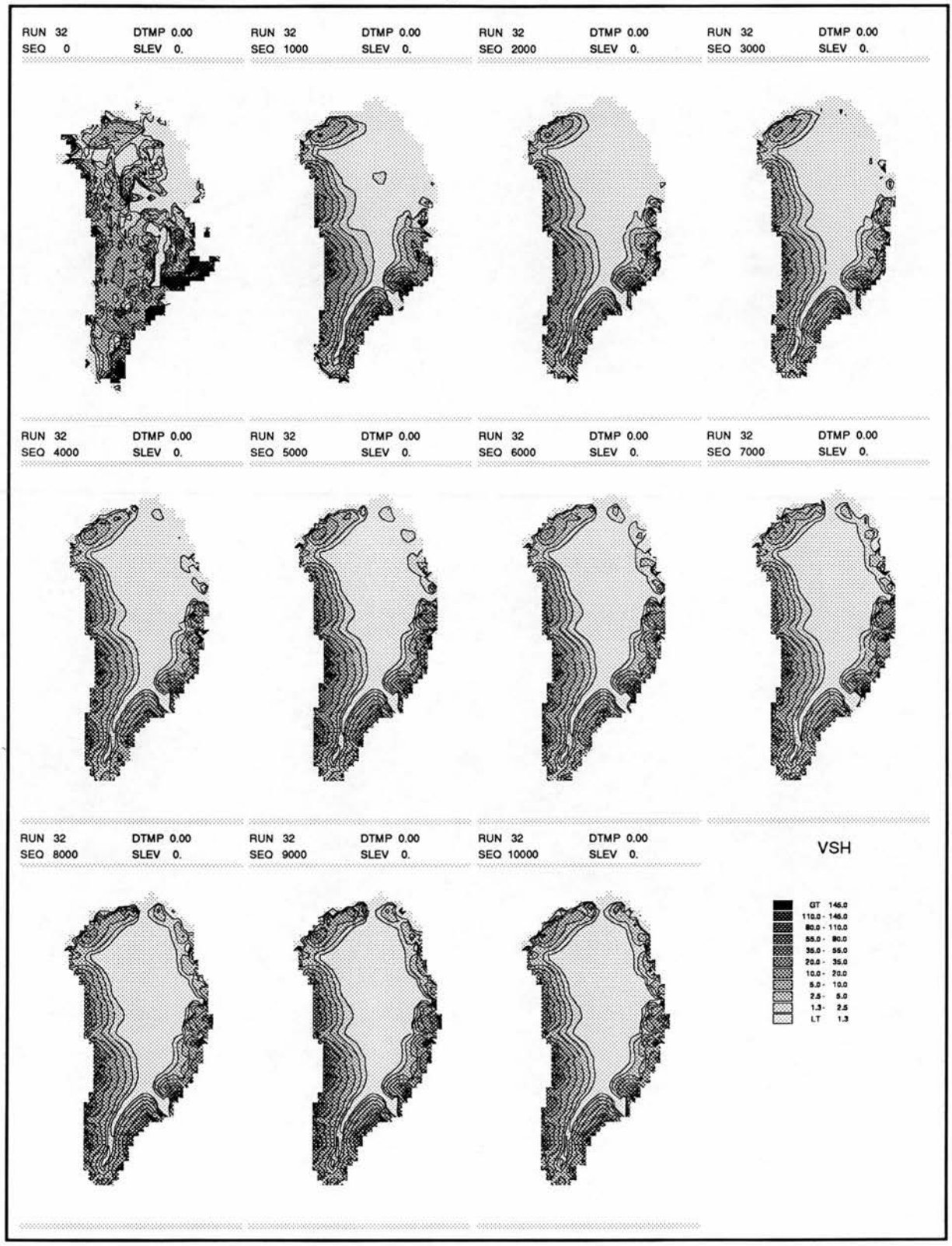

Figure 27: Derived average shearing velocites m/a for the Initial Standard Run (32). Values are as a function of surface slope and ice thickness (eq 8).

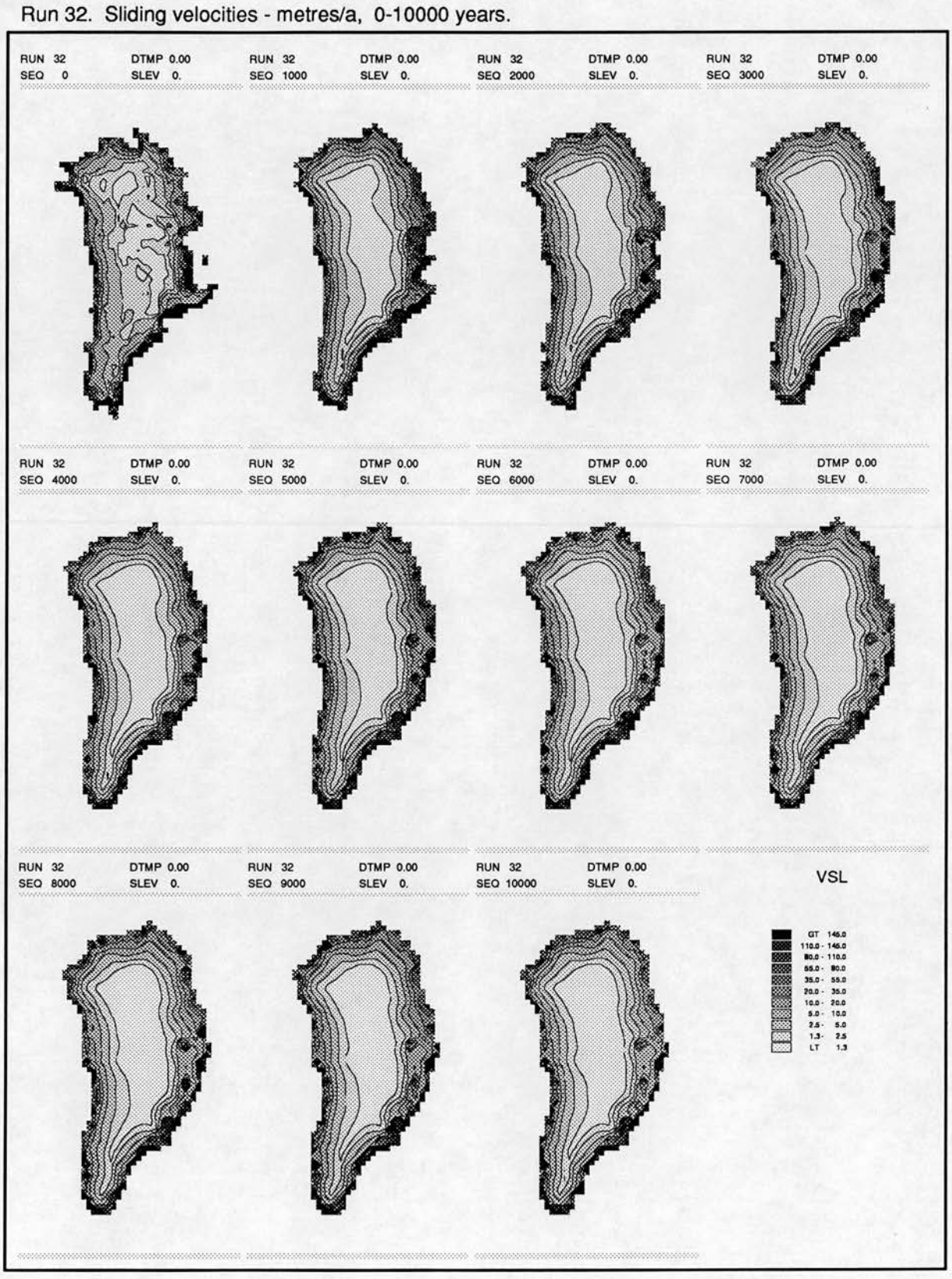

Figure 28: Derived average sliding velocites m/a for the Initial Standard Run (32). Values are as a function of surface slope, ice thickness and relative buoyancy (eq 11).

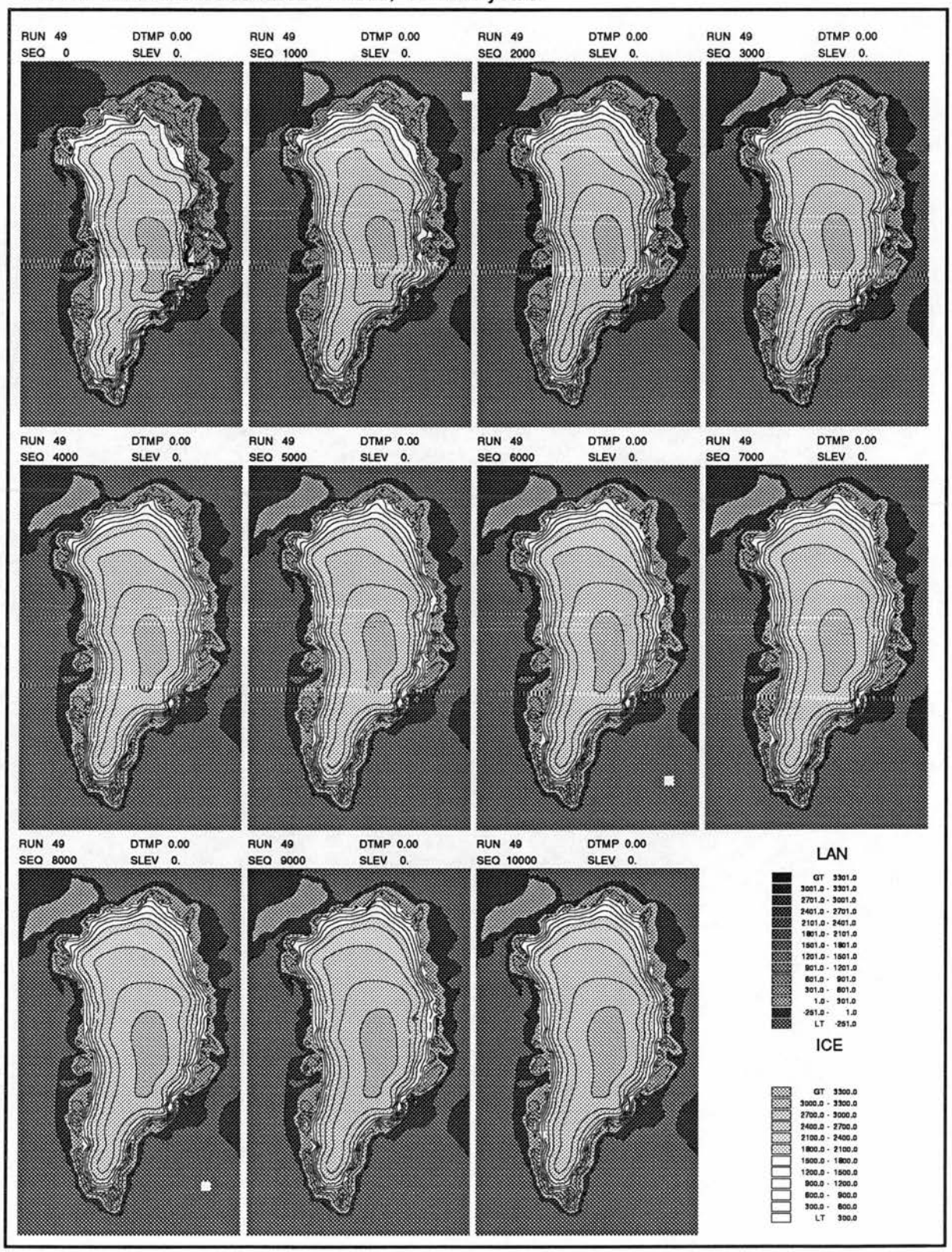

Figure 29: Modelled exposed land and submarine surfaces with superimposed ice surfaces for the sensitivity test with a reduced Arrhenius constant = $2.5 \times 10^{-25} kg^3 km^3 a^{-6}$ (Run 49). The equilibrium profile differs little in extent to the ISR, but maximum elevations and ice gradients are steeper with stiffer ice.

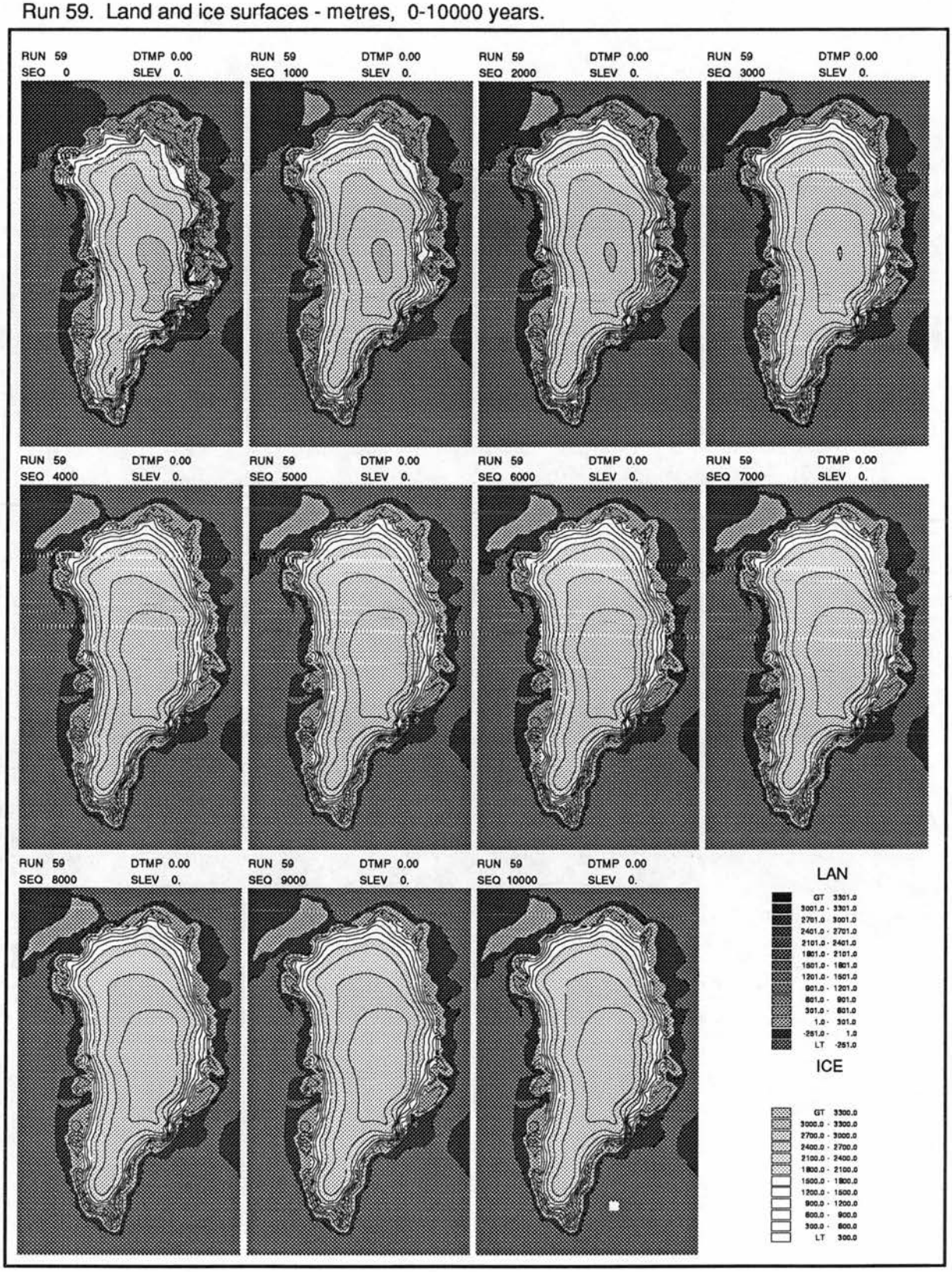

Figure 30: Modelled exposed land and submarine surfaces with superimposed ice surfaces for the sensitivity test with an increased Arrhenius constant $= 1.0 \times 10^{-24} kg^3 km^3 a^{-6}$ (Run 59). The equilibrium profile differs little in extent to the ISR or Run 49, the reduced Arrhenius case, but maximum elevations and ice gradients are reduced with less stiff ice.

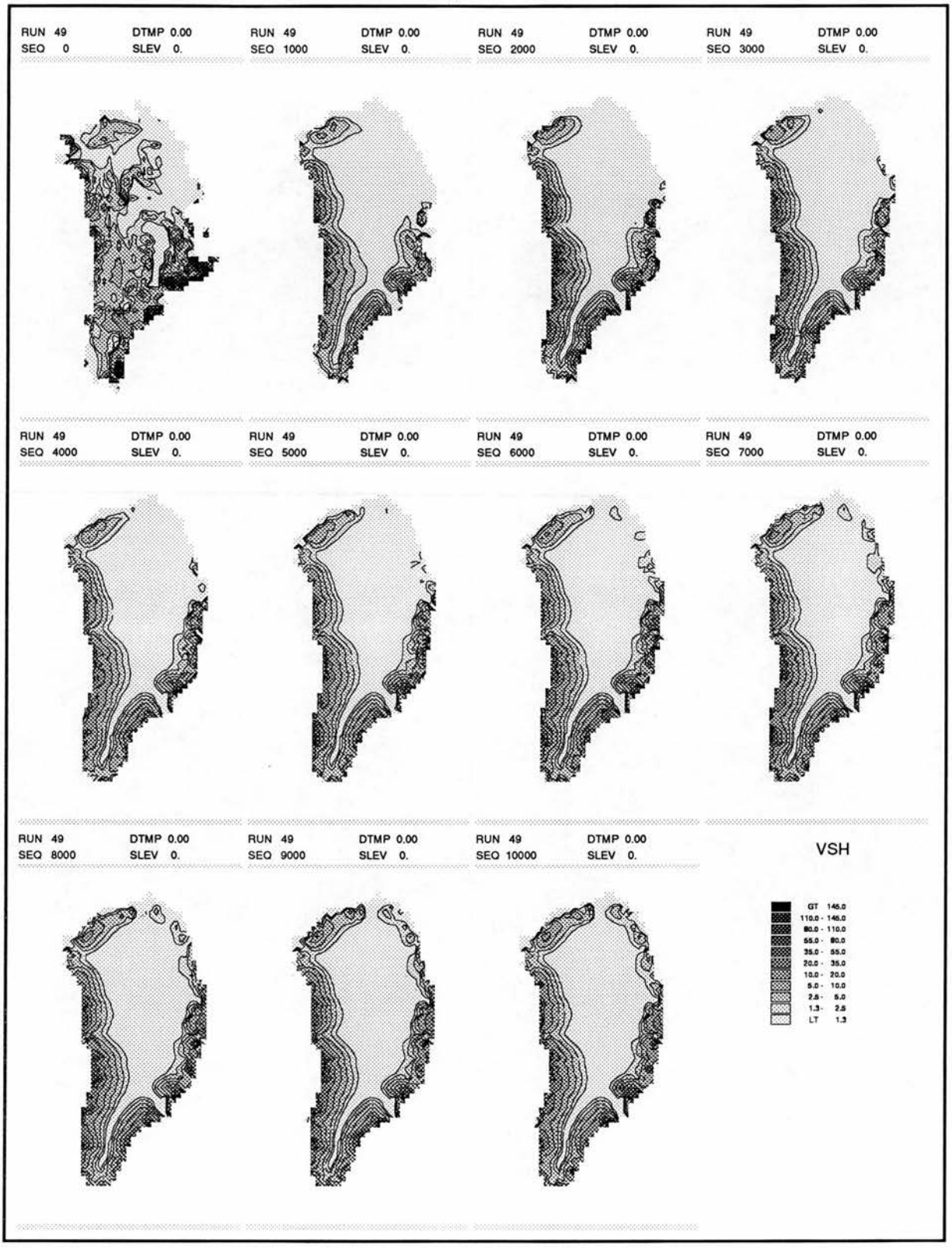

Figure 31: Derived average shearing velocites m/a for the sensitivity test with a reduced Arrhenius constant $= 2.5 \times 10^{-24} kg^3 km^3 a^{-6}$ (Run 49). Values are as a function of surface slope and ice thickness (eq 8) and are less than the ISR.

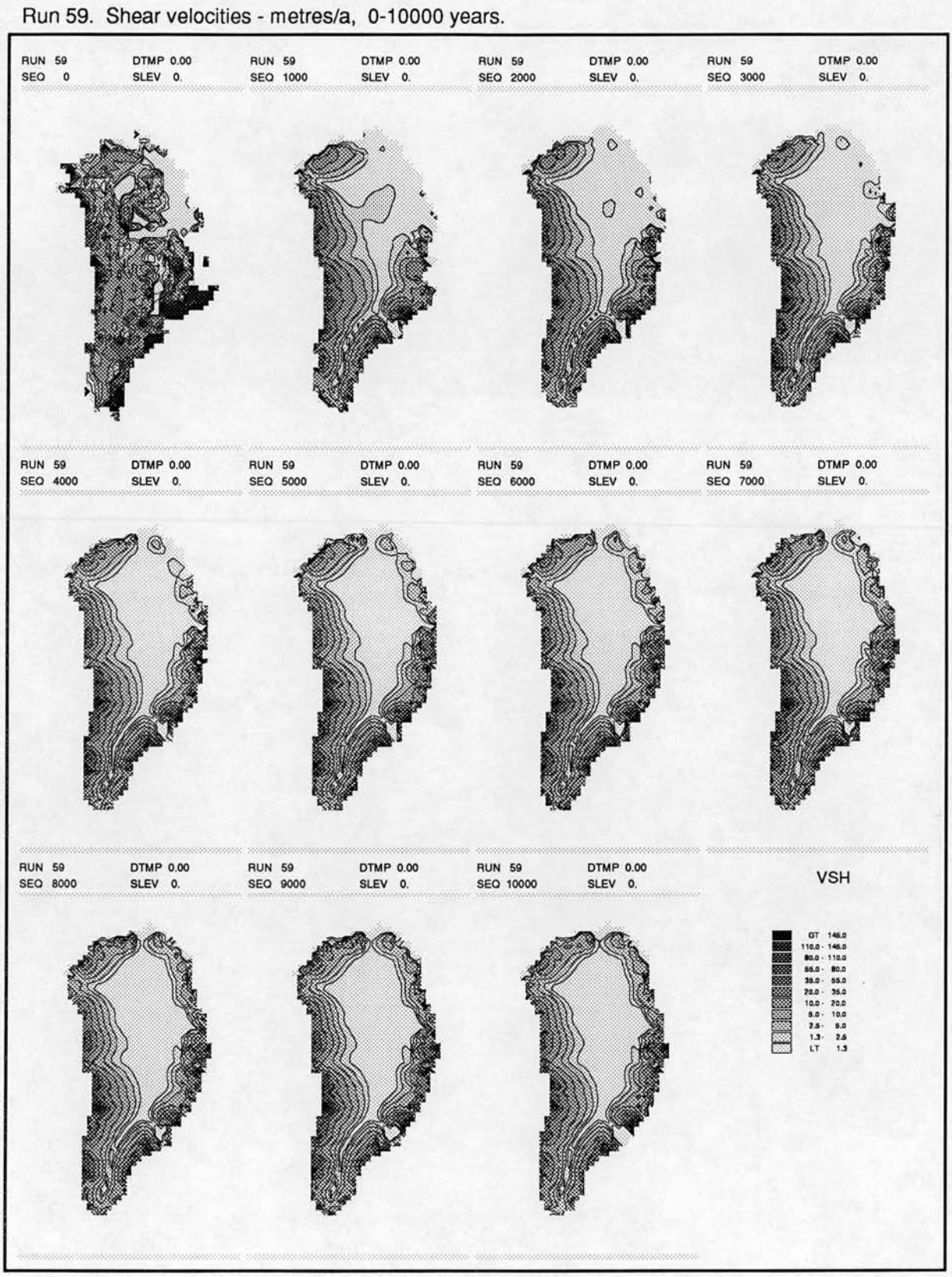

Figure 32: Derived average shearing velocites m/a for the sensitivity test with an enhanced Arrhenius constant $= 1.0 \times 10^{-24} kg^3 km^3 a^{-6}$ (Run 59). Values are as a function of surface slope and ice thickness (eq 8)

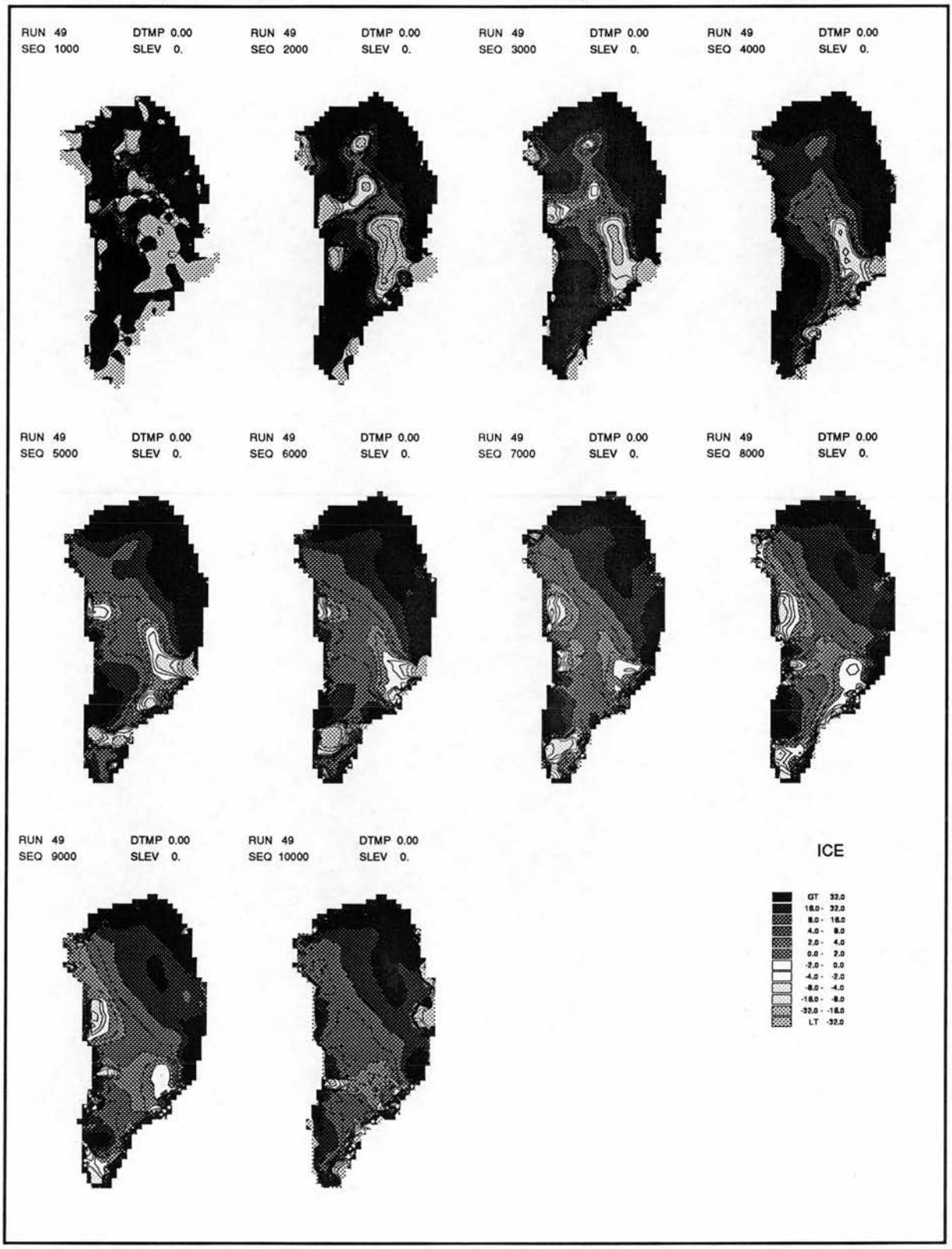

Figure 33: Changes in ice thickness for successive time steps for the sensitivity test with a reduced Arrhenius constant $2.5 \times 10^{-25} kg^3 km^3 a^{-6}$ (Run 49). The stiffer ice tends to thicken more throughout the run.

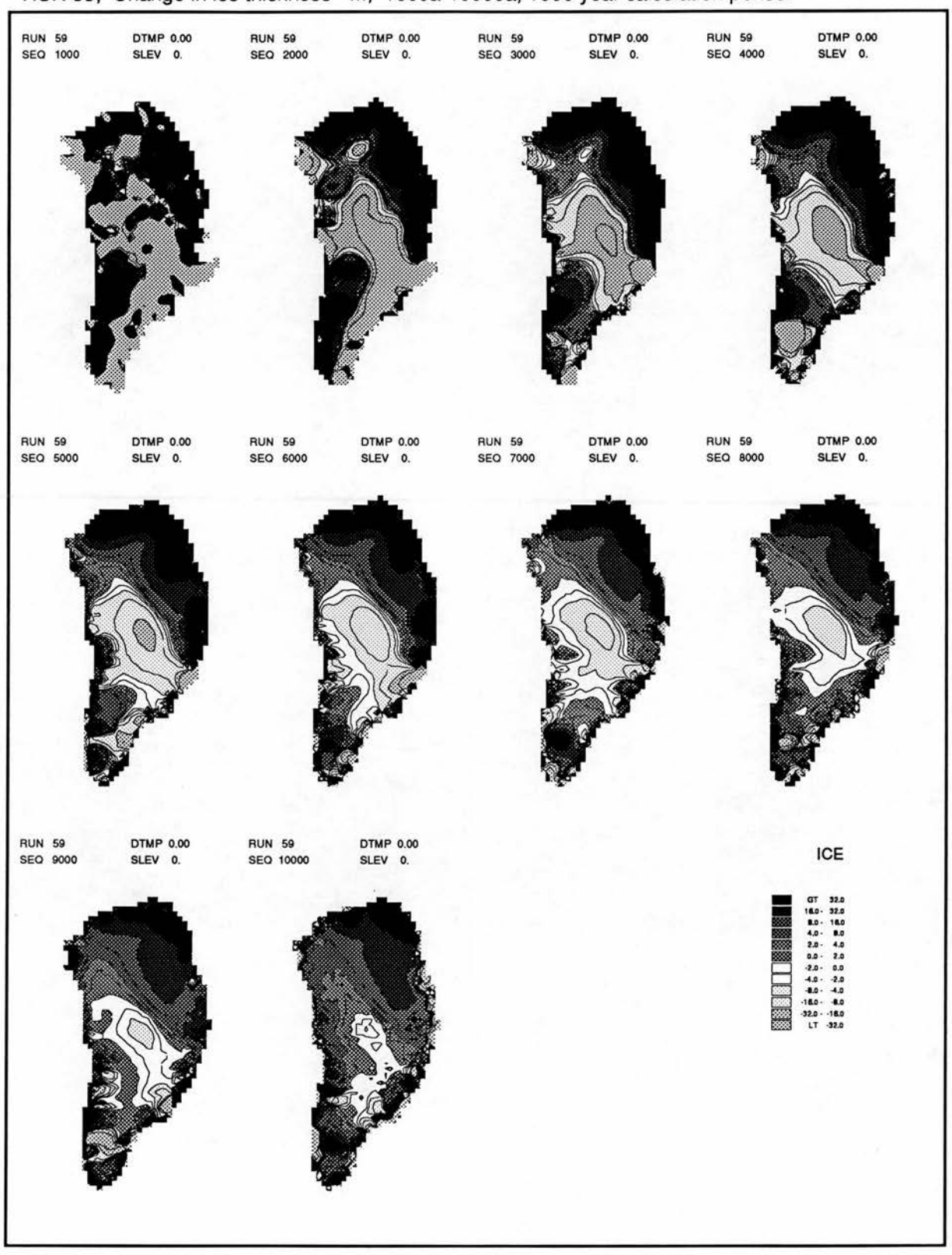

Figure 34: Changes in ice thickness for successive time steps for the sensitivity test with an enhanced Arrhenius constant $= 1.0 \times 10^{-24} kg^3 km^3 a^{-6}$ (Run 59). The softer ice tends to drain the central band more effectively causing thinning there.

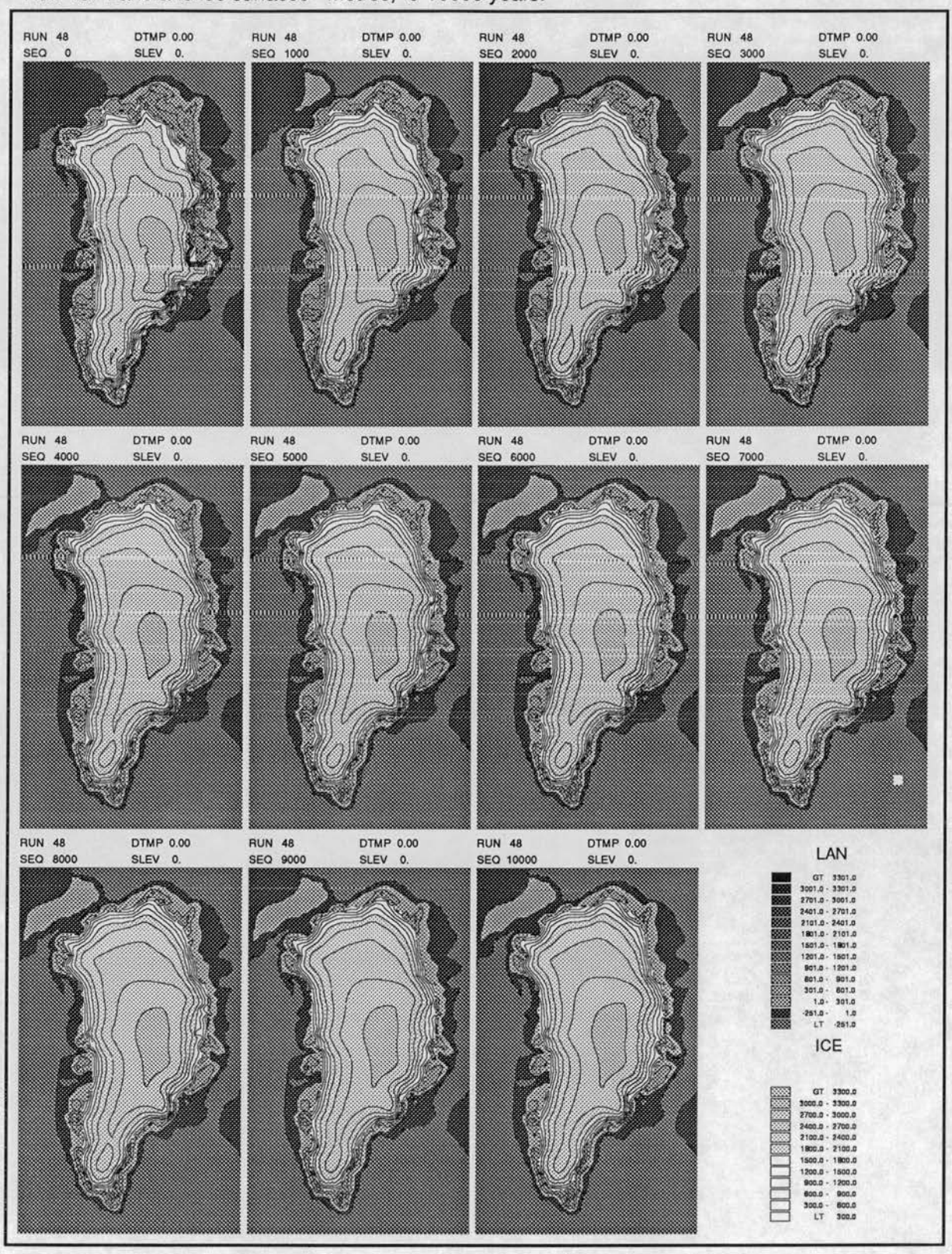

Figure 35: Modelled land and submarine surfaces with superimposed ice surfaces for the sensitivity test with a reduced sliding constant, $k = 1.0 \times 10^{-4} m^3 bar^{-1} a^{-1}$ (Run 48). The effect is to stiffen the ice causing steeper profiles.

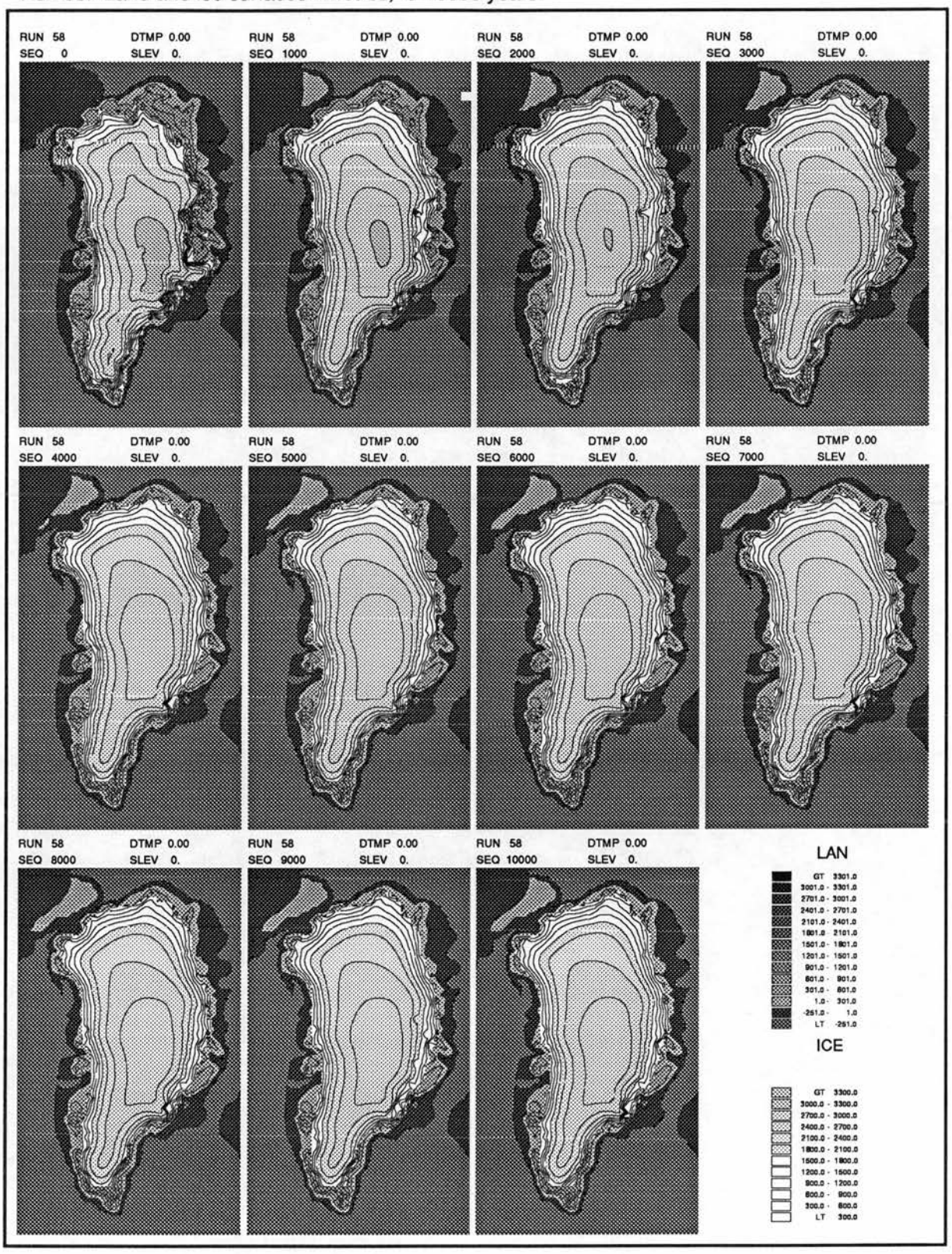

Figure 36: Modelled land and submarine surfaces with superimposed ice surfaces for the sensitivity test with an increased sliding constant, $k = 4.0 \times 10^{-4} m^3 bar^{-1} a^{-1}$ (Run 58). The effect is to soften the ice causing gentler profiles.

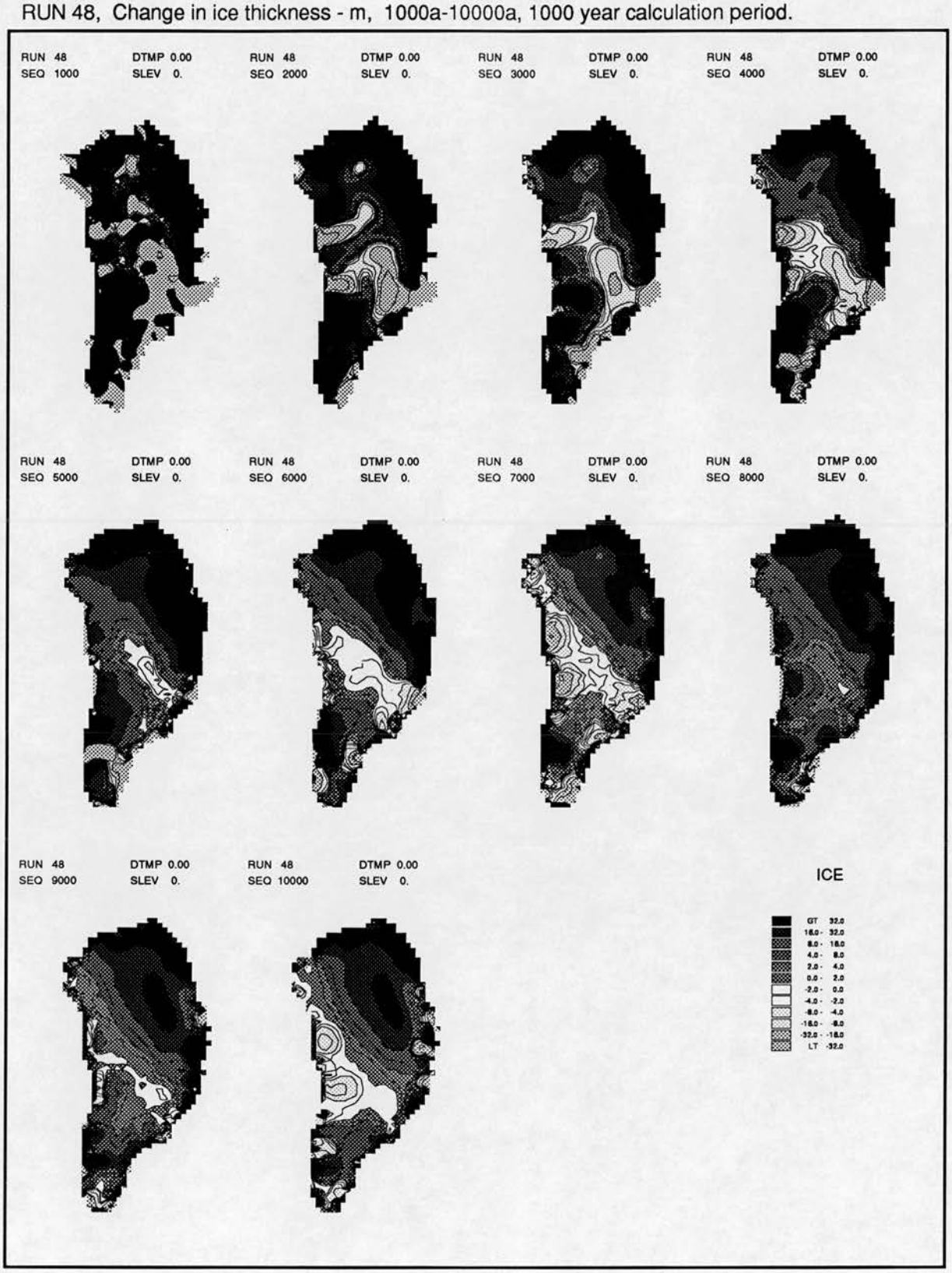

Figure 37: Changes in ice thickness for successive time steps for the sensitivity test with a reduced sliding constant, $k = 1.0 \times 10^{-4} m^3 bar^{-1} a^{-1}$ (Run 48).

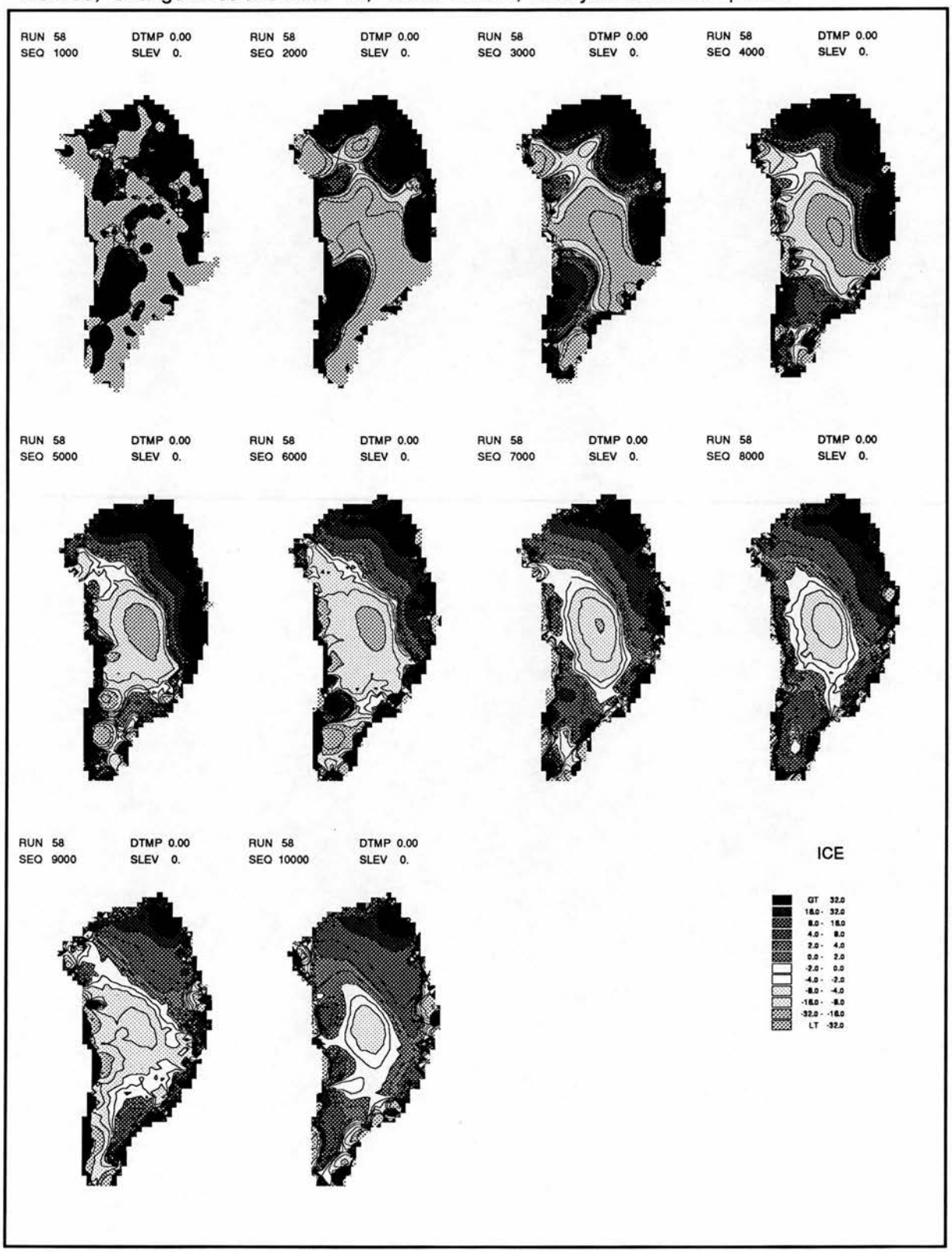

Figure 38: Changes in ice thickness for successive time steps for the sensitivity test with an increased sliding constant, $k = 4.0 \times 10^{-4} m^3 bar^{-1} a^{-1}$ (Run 58).

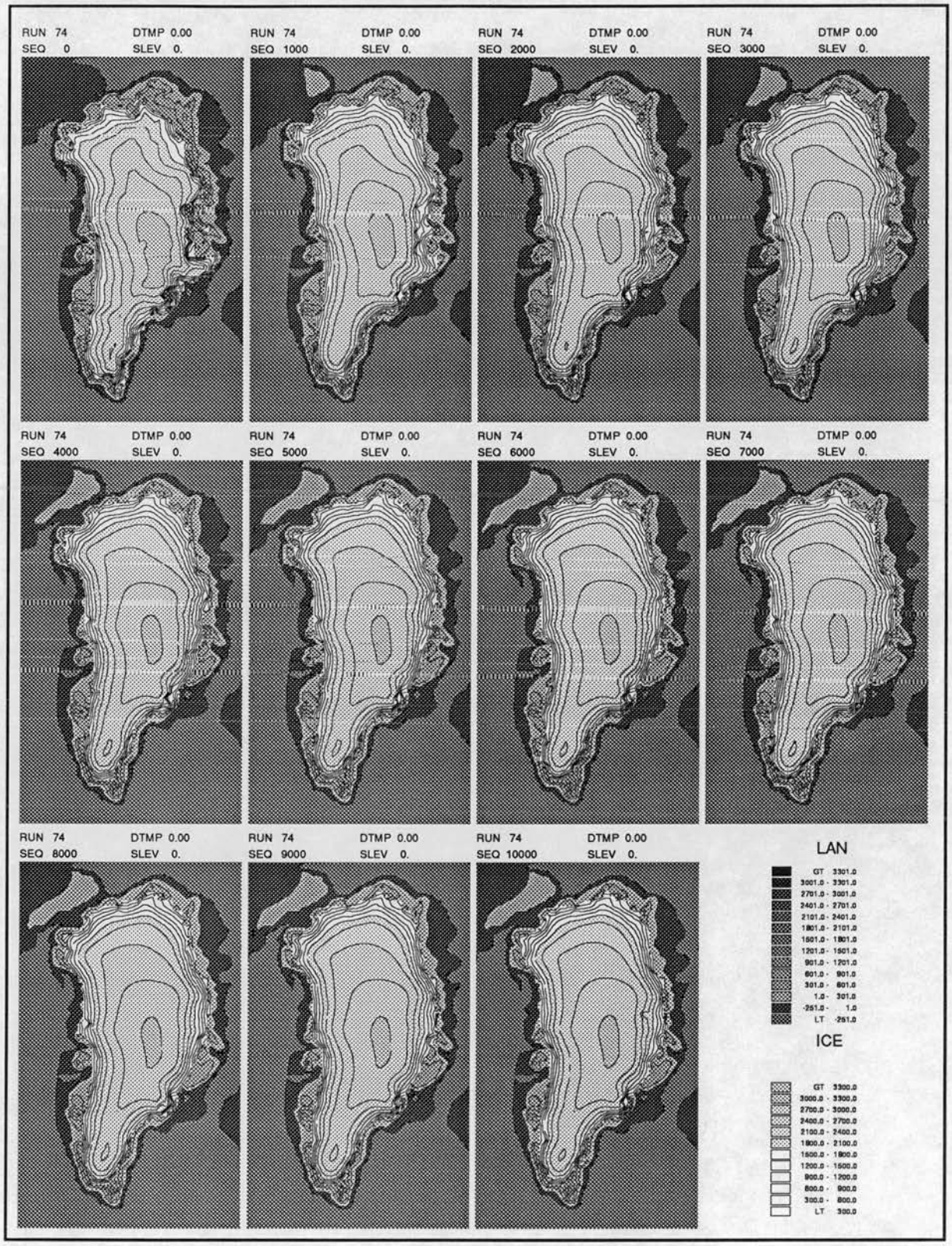

Figure 39: Modelled land and submarine surfaces with superimposed ice surfaces for the sensitivity test with a reduced sliding cut-off altitude = 0.15km.

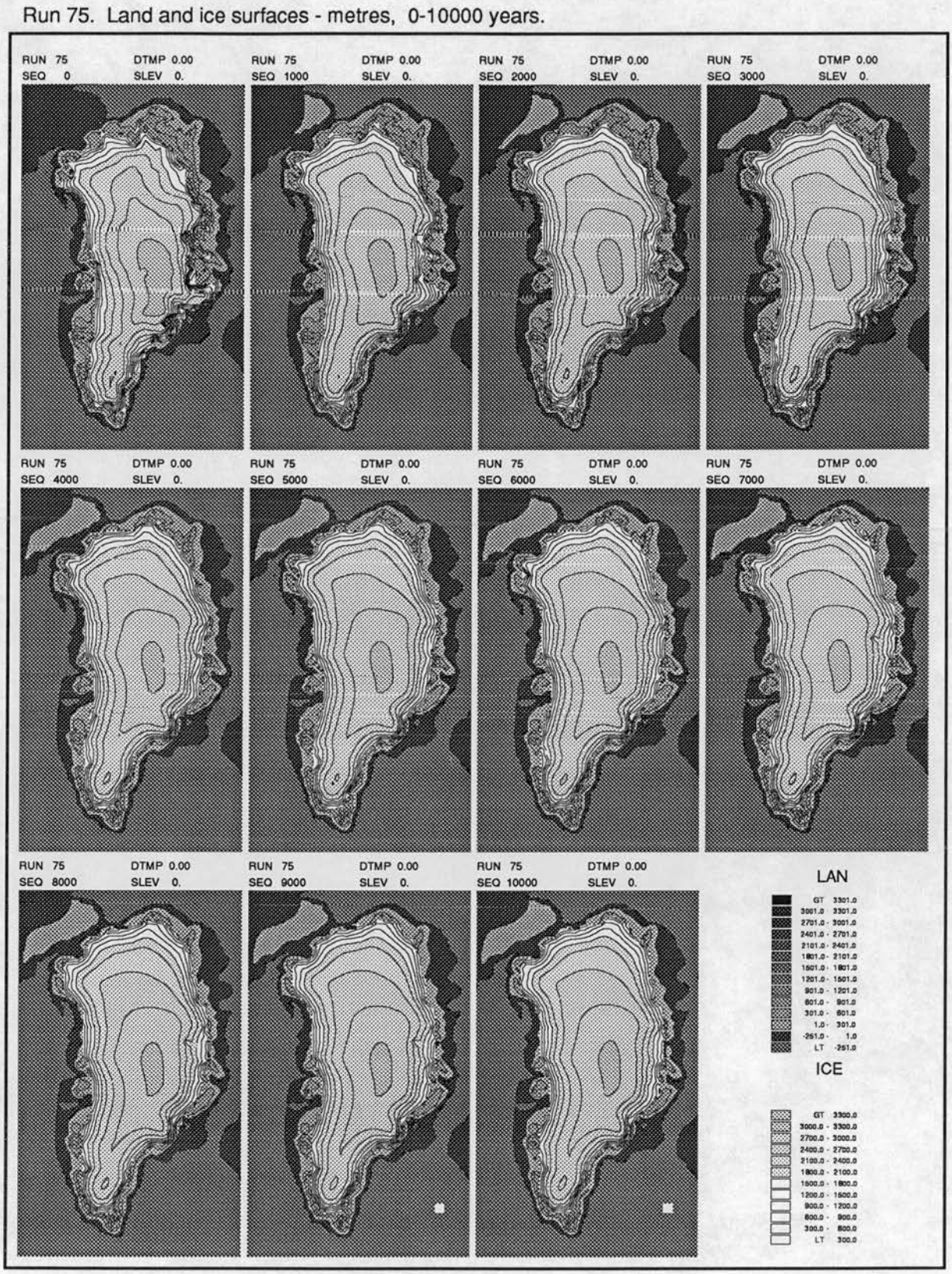

Figure 40: Modelled land and submarine surfaces with superimposed ice surfaces for the sensitivity test with an increased sliding cut-off altitude = 0.6km.

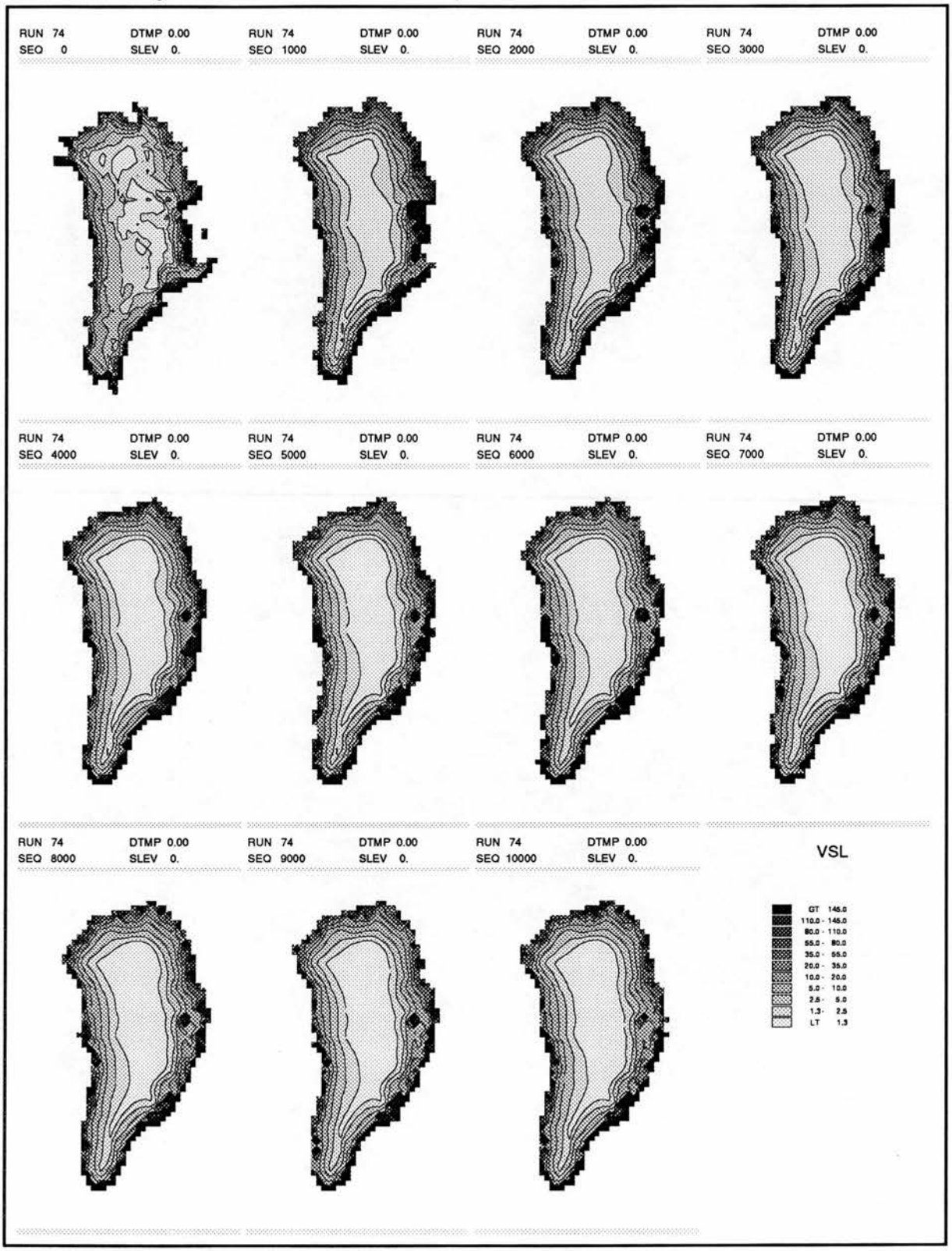

Figure 41: Derived average sliding velocites, m/a, for the sensitivity test with a reduced sliding cut-off altitude = 0.15km. Sliding velocities are enhanced toward the margin.

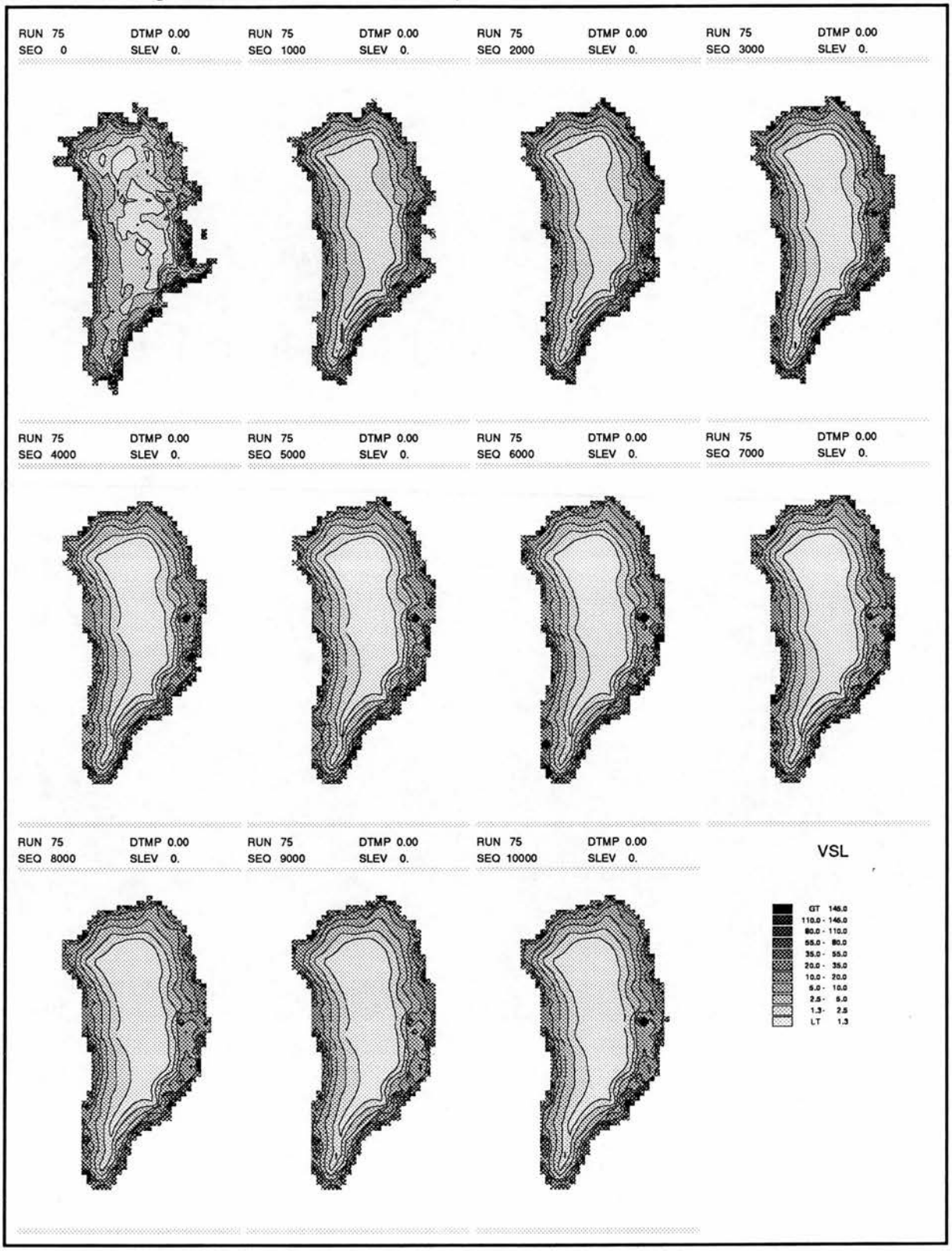

Figure 42: Derived average sliding velocites, m/a, for the sensitivity test with an increased sliding cut-off altitude = 0.6km. Sliding velocities are reduced toward the margin.

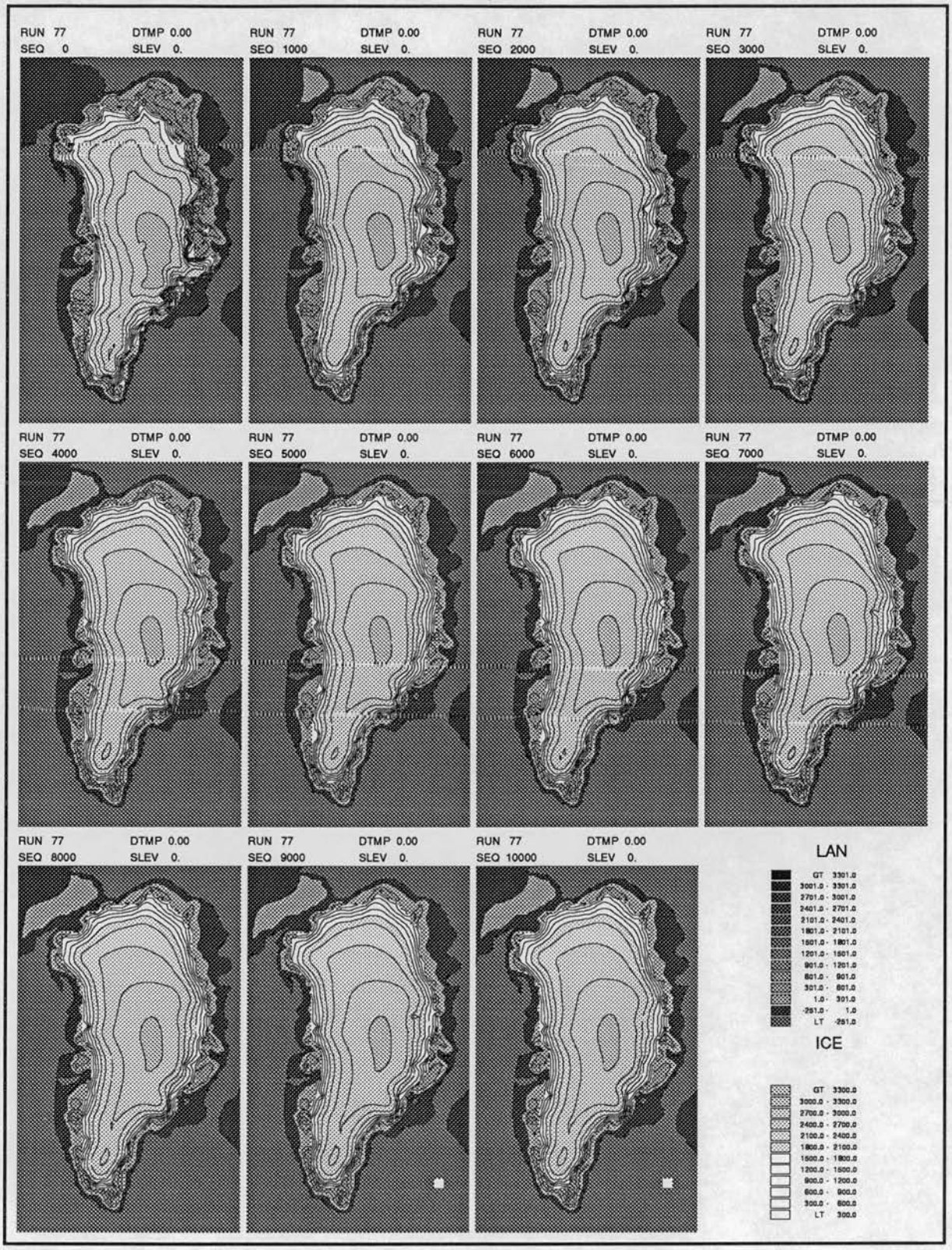

Figure 43: Modelled land and submarine surfaces with superimposed ice surfaces for the sensitivity test with a reduced calving term = 20. This has minimal effect compared to the ISR. The ice margin is slightly more extensive near calving lobes.

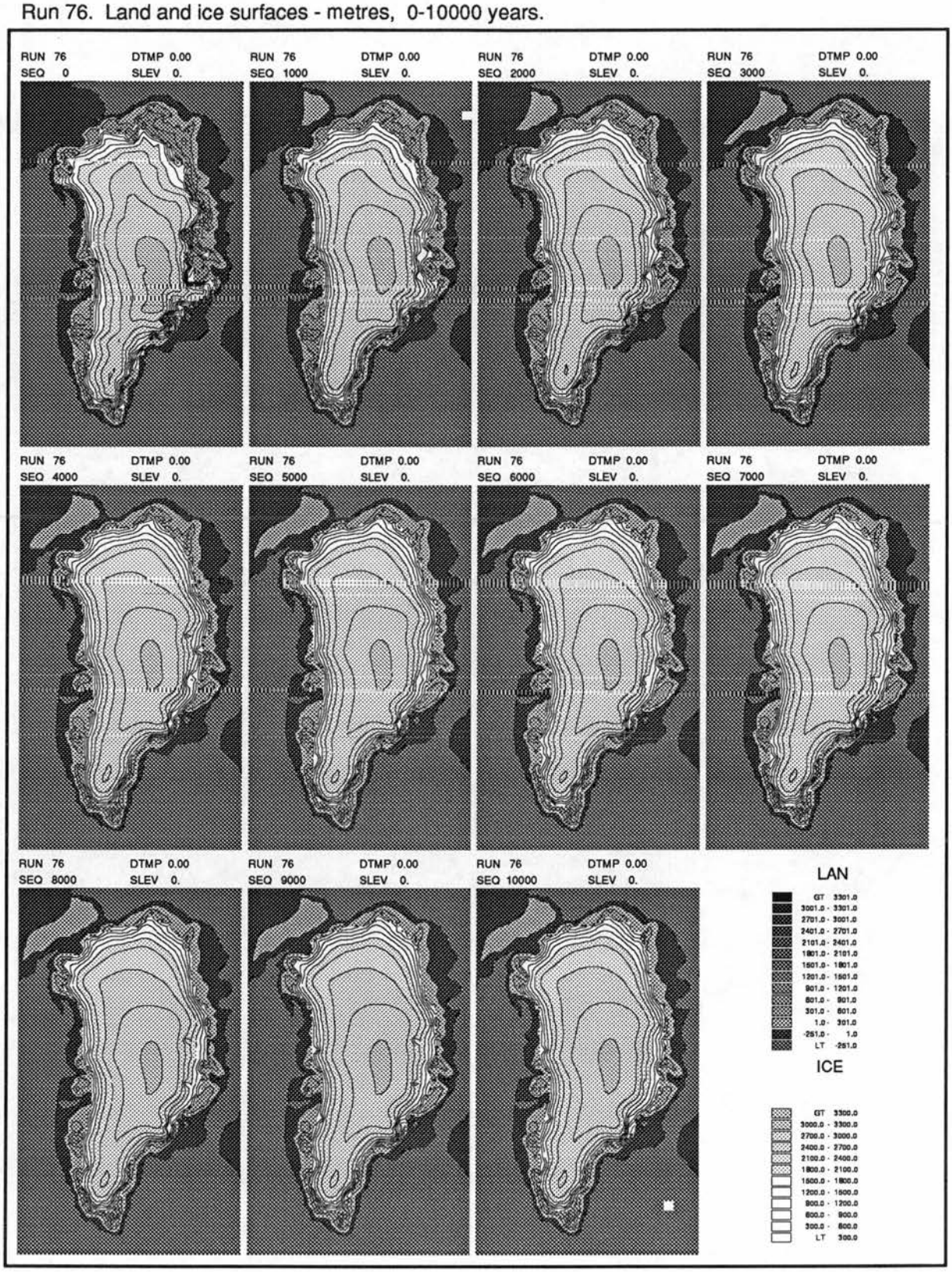

Figure 44: Modelled land and submarine surfaces with superimposed ice surfaces for the sensitivity test with an increased calving term = 40. There is a slight decrease in ice extent compared to the ISR.

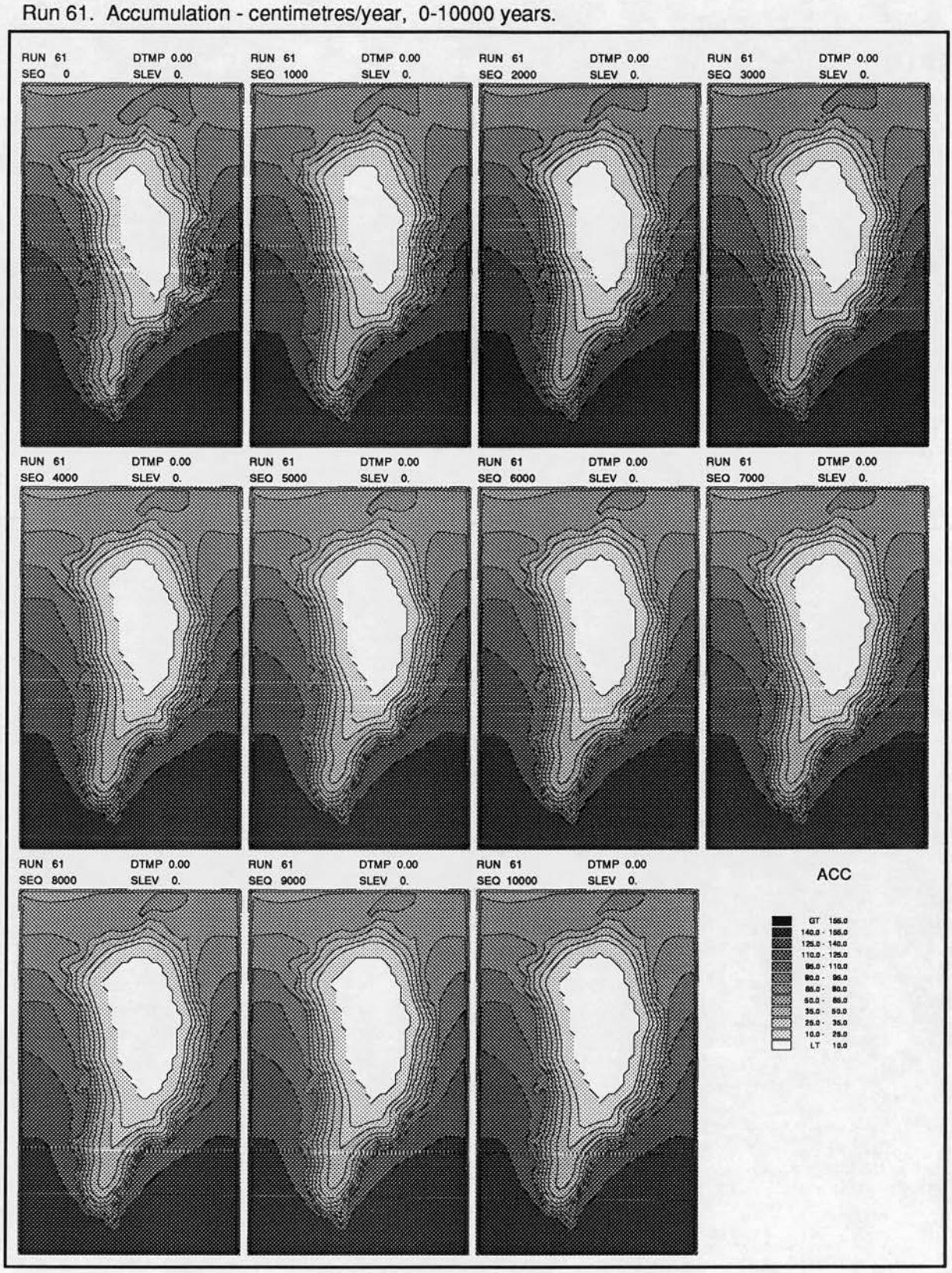

Figure 45: Modelled accumulation rates for the sensitivity test with minimum accumulation set to 10cm.

Run 61. Land and ice surfaces - metres, 0-10000 years.

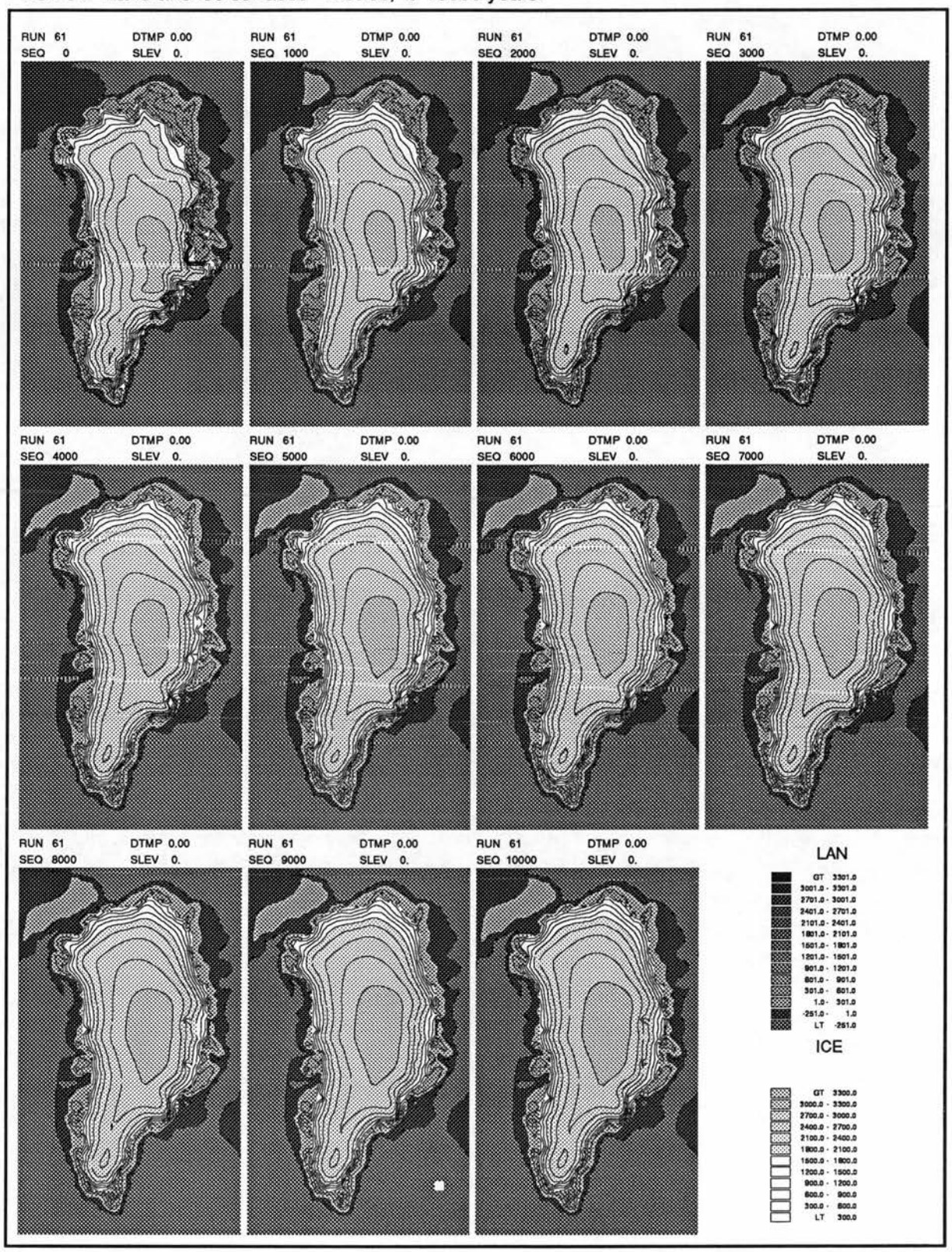

Figure 46: Modelled land and submarine surfaces with superimposed ice surfaces for the sensitivity test with minimum accumulation set to 10cm. Ice volume is significantly increased over the central dome and in Northern Greenland compared to the ISR.

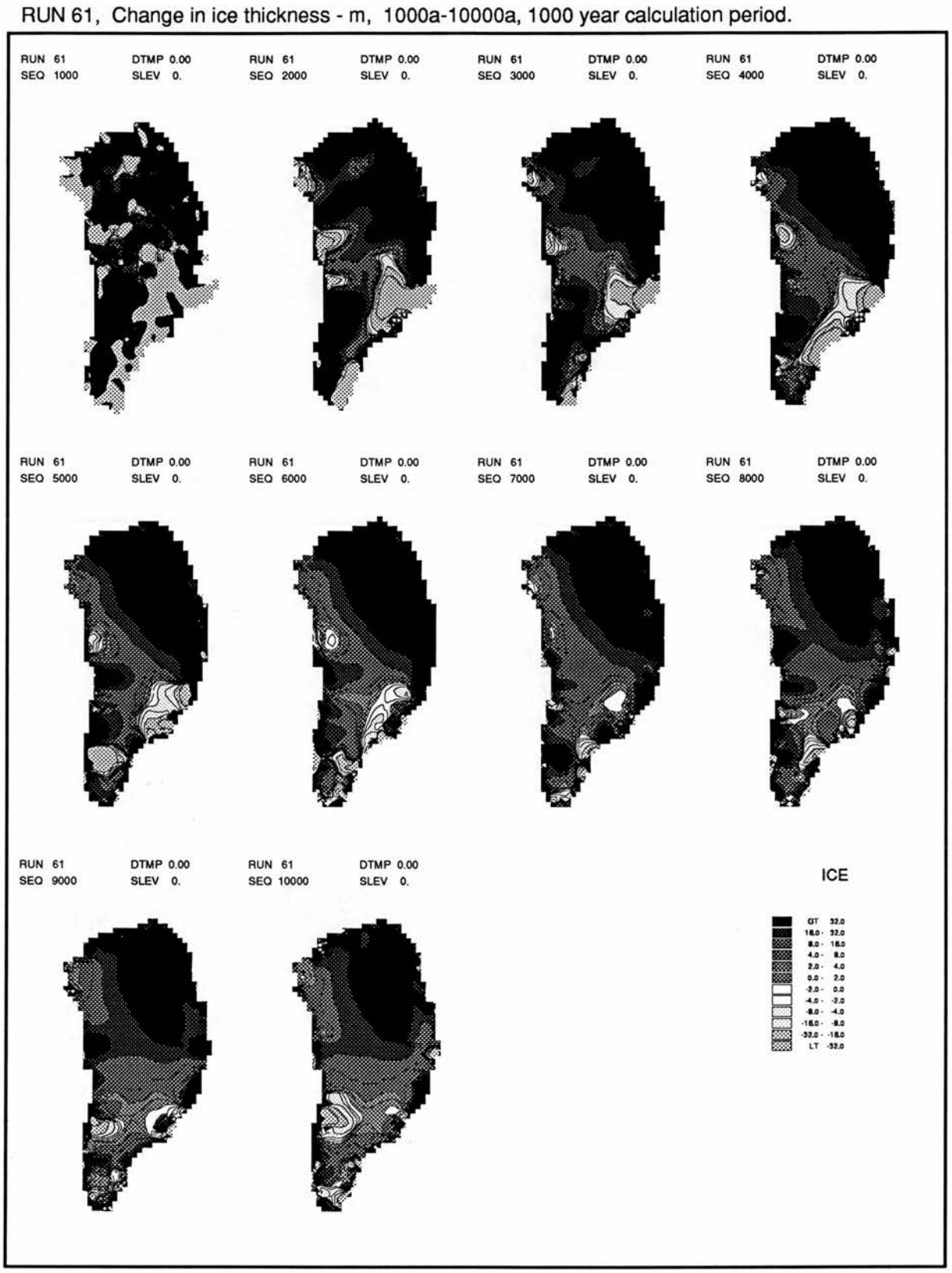

Figure 47: Changes in ice thickness for successive time steps for the sensitivity test with minimum accumulation set to 10cm (Run 61).

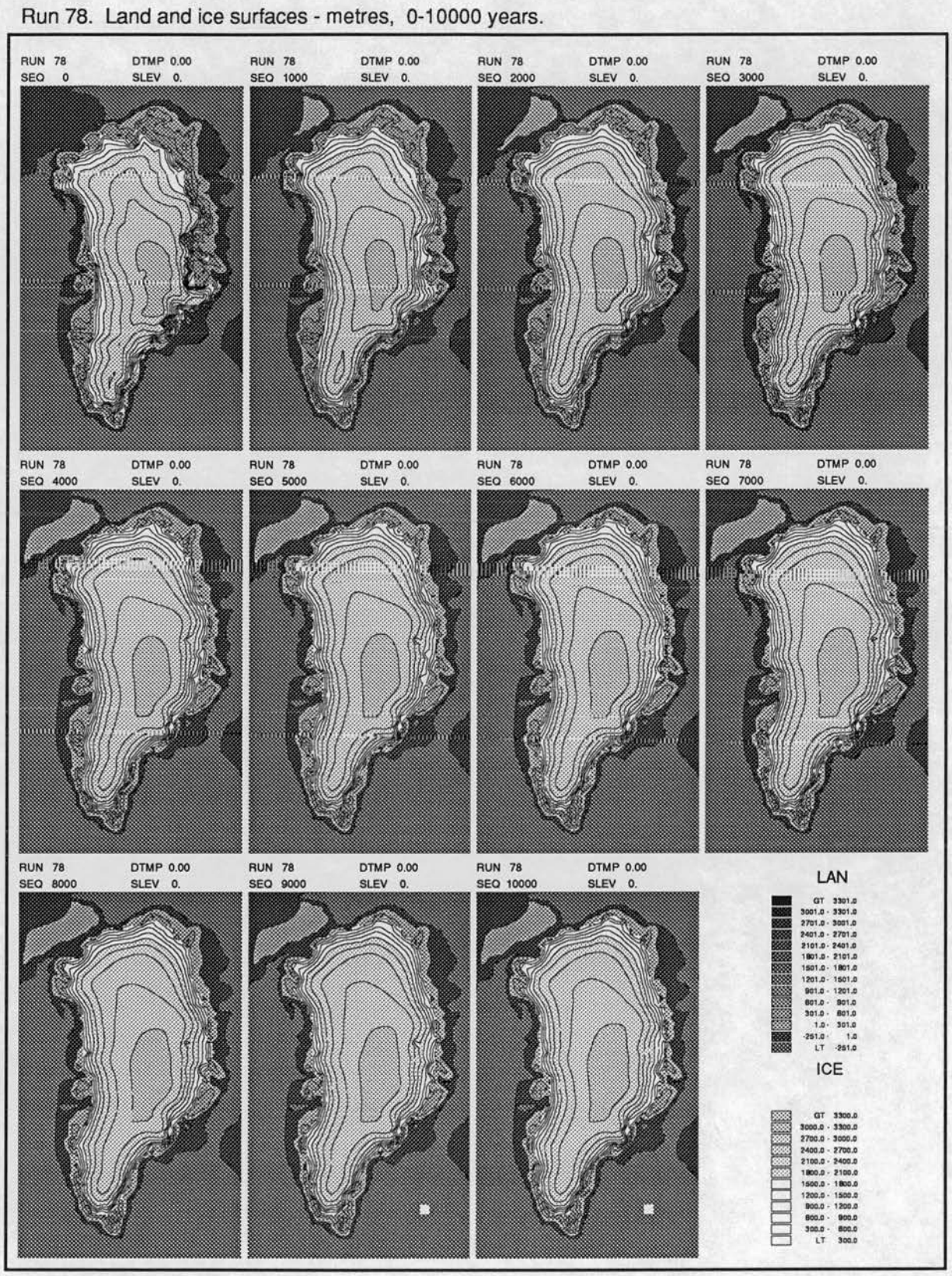

Figure 48: Modelled land and submarine surfaces with superimposed ice surfaces for the sensitivity test forced with an increased continentality distance = 700km (Run 78). A lessening of the 'desertification effect' causes ice to expand more in the drier central and northern areas.

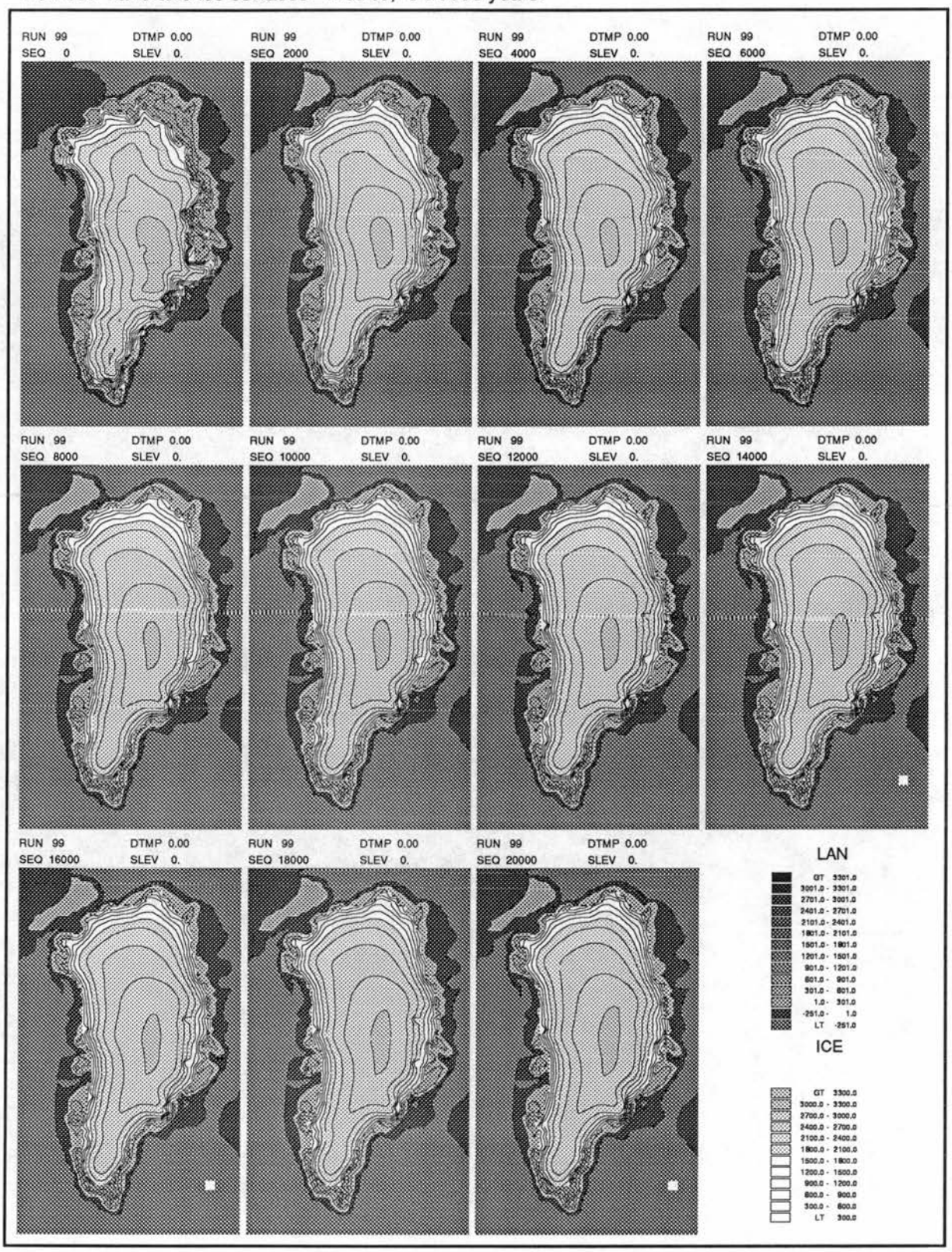

Figure 49: Modelled land and submarine surfaces with superimposed ice surfaces for the sensitivity test forced with a reduced continentality distance = 150km (Run 99). This tends to make the ice sheet drier and lowers the interior slightly. In the south,the additional dryness is sufficient to reduce the ice extent.

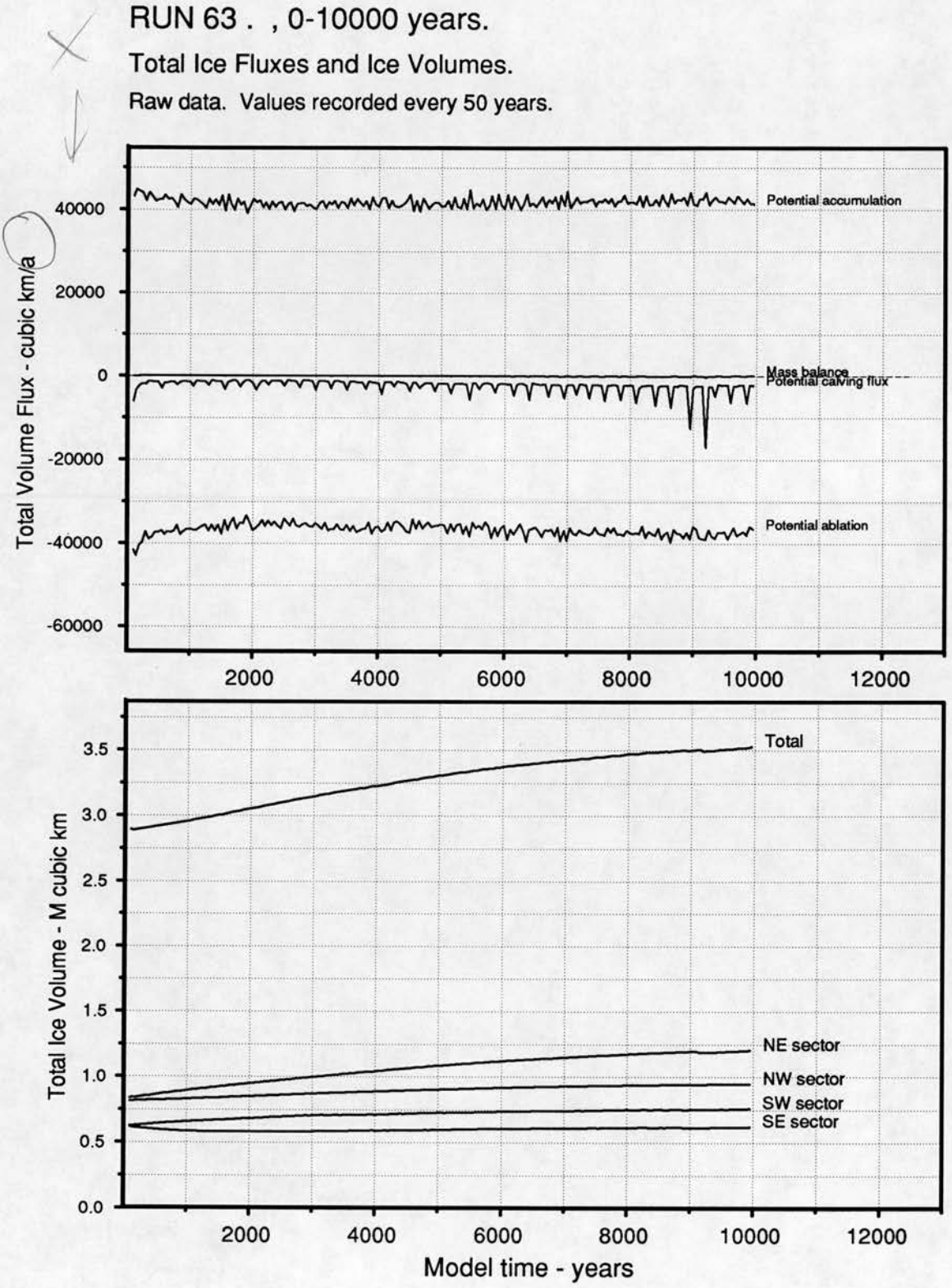

Figure 50: Raw data ice volumes and mass balance values for the sensitivity test with 10% decreased ablation rates (Run 63). This increases the overall mass balance and total ice volume.

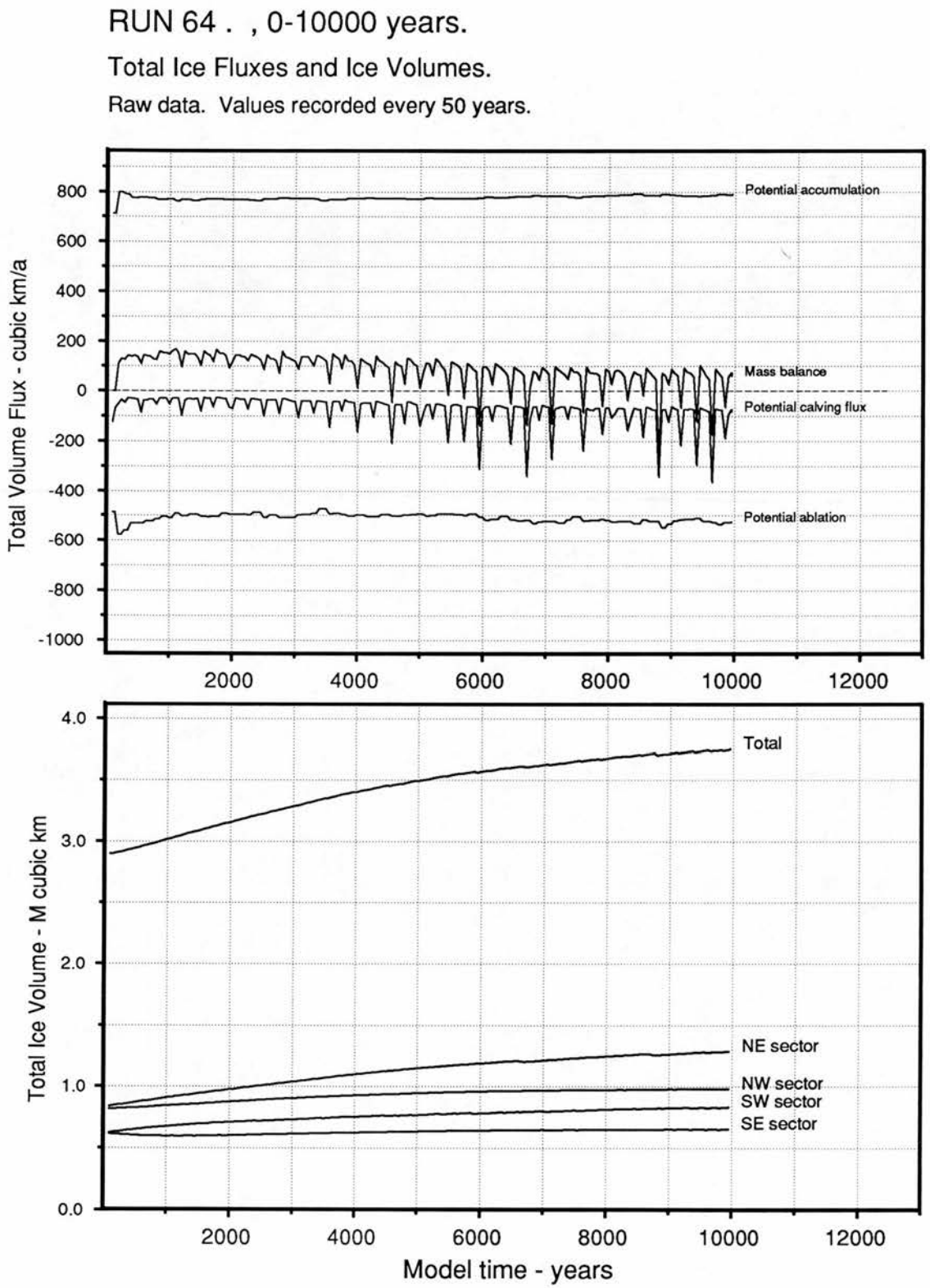

Figure 51: Raw data ice volumes and mass balance values for the sensitivity test with 10% increased accumulation rates (Run 64). This increases the overall mass balance and total ice volume.

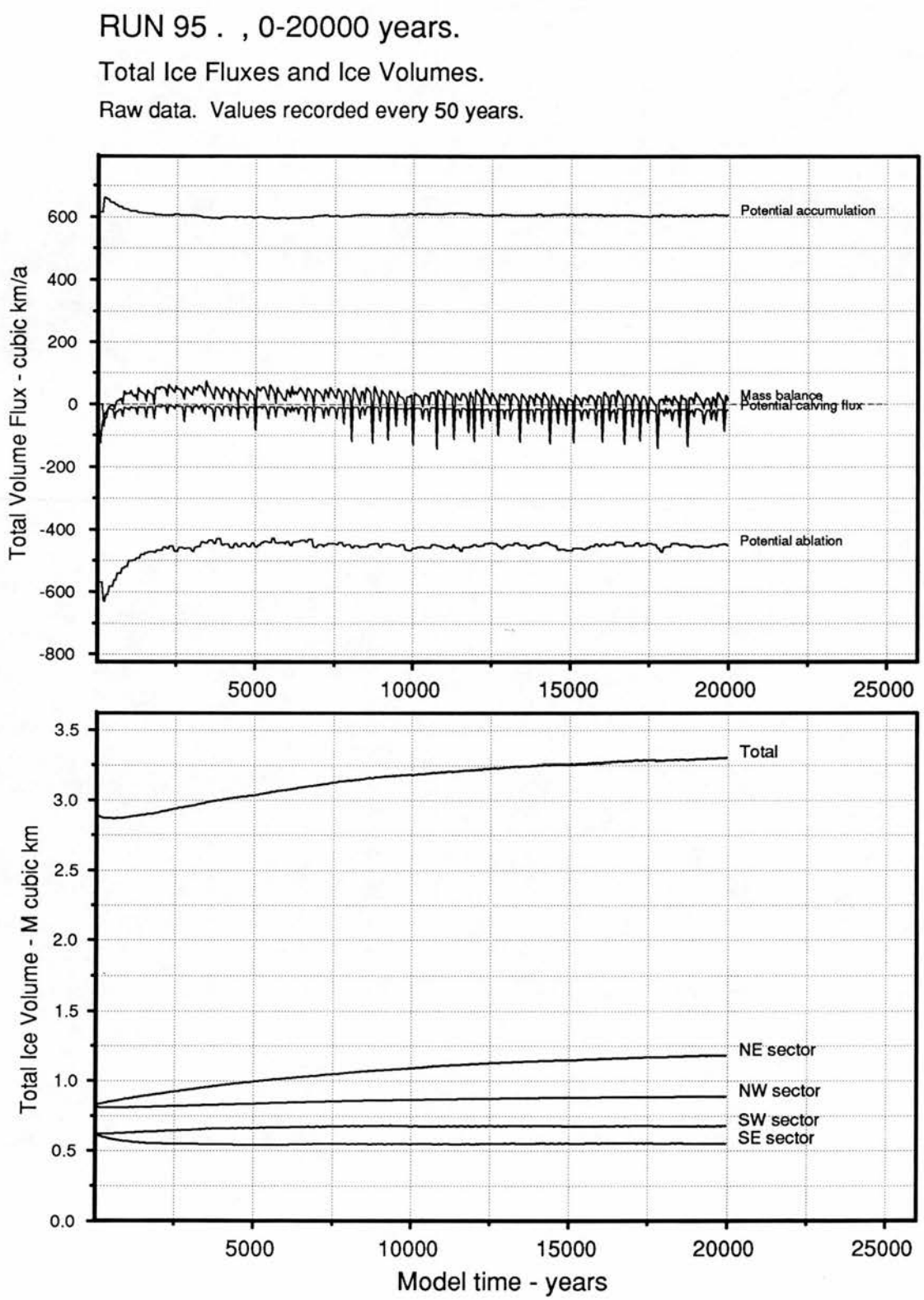

Figure 52: Raw data ice volumes and mass balance values for the sensitivity test with 5% decreased ablation rates and 5% increased accumulation rates.

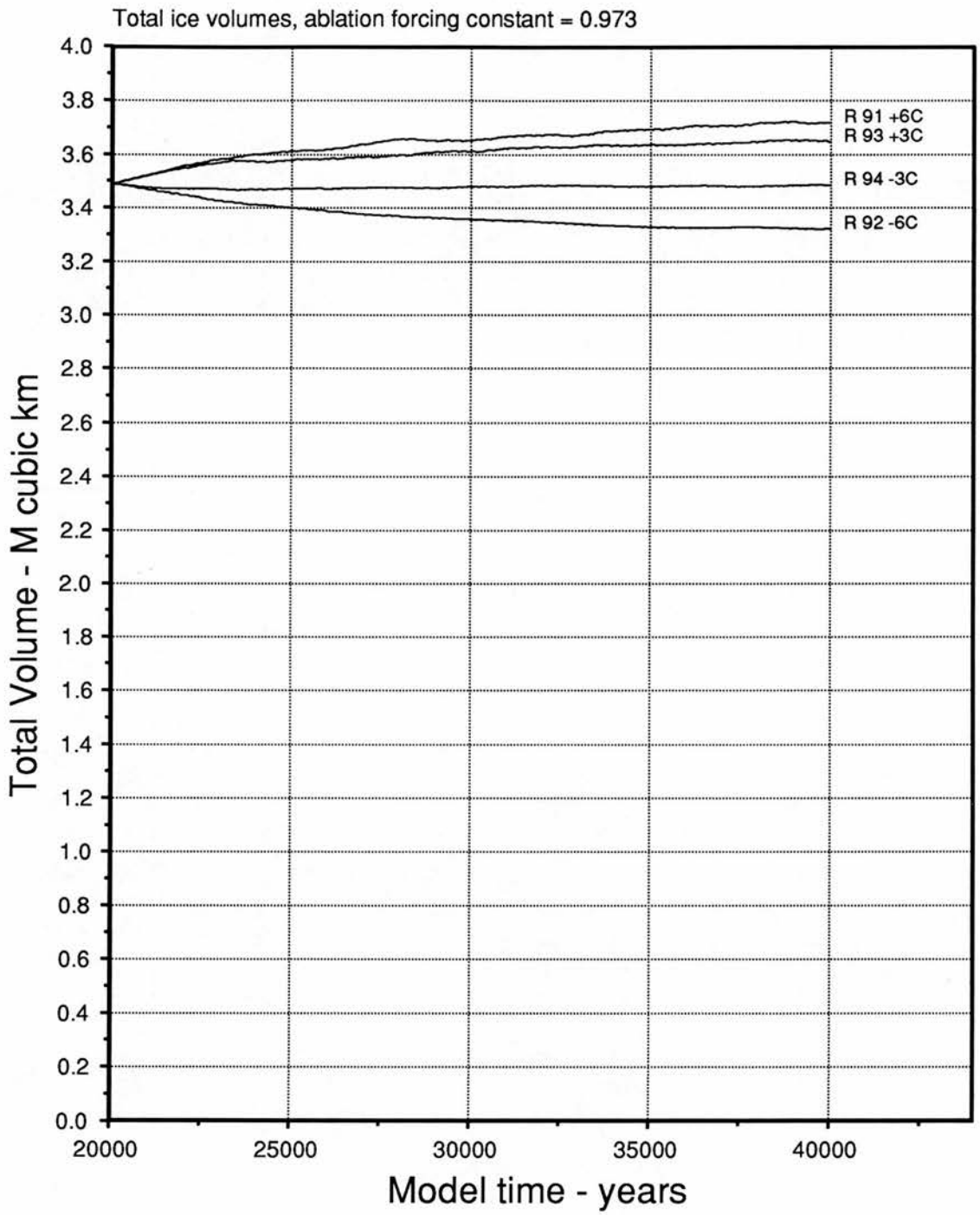

Figure 53: Raw data ice volumes for each of the runs 91-94, covering forcing between $-6°C$ and $+6°C$ for an ablation forcing constant, $F = 1.02°\Theta/°C$. There is little divergence in ice volumes and the ice grows in warmer scenarios.

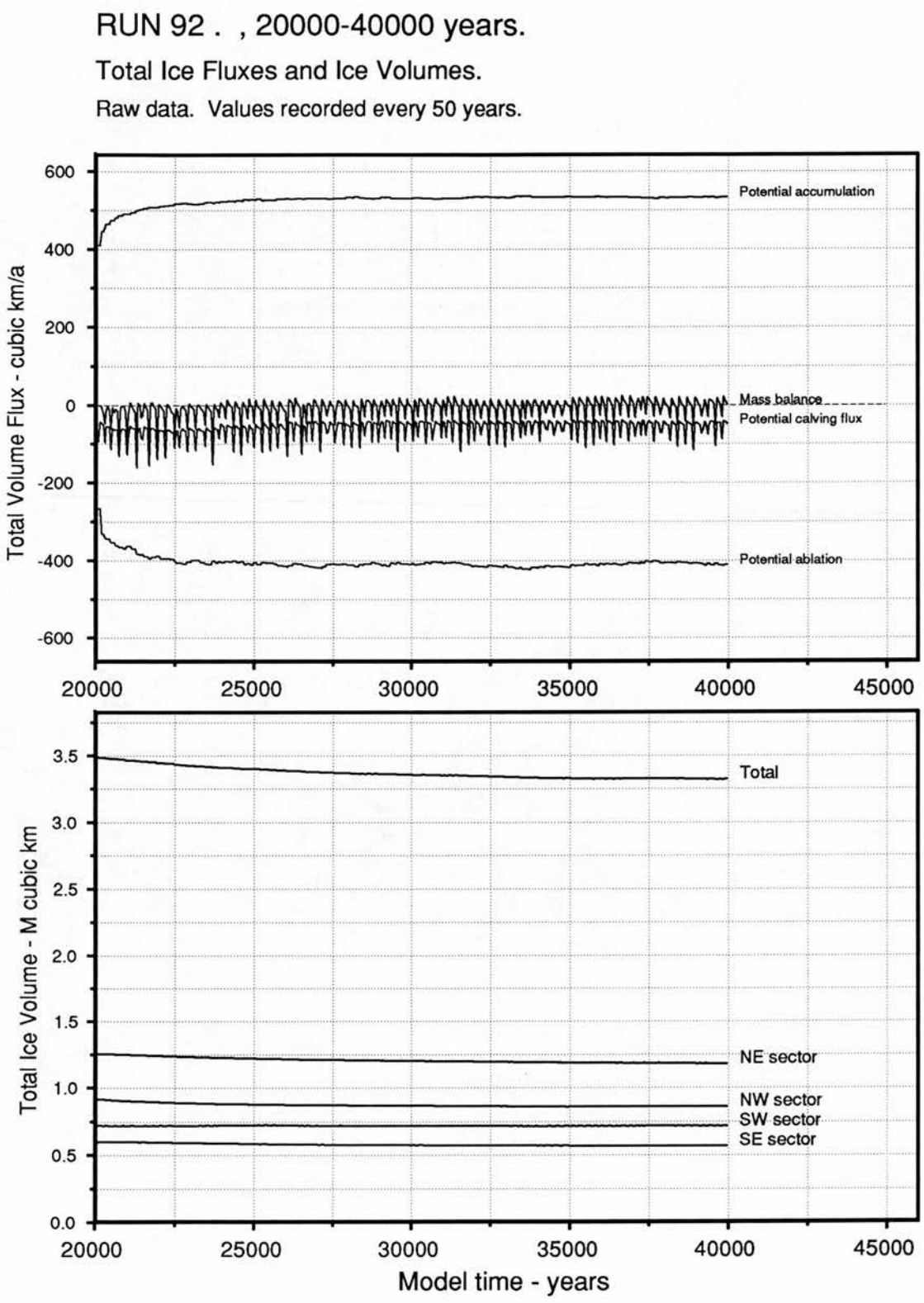

Figure 54: Raw data ice volumes and mass balance values for the forcing test with an ablation forcing constant, $F = 1.02°\Theta/°C$ and $-6°C$ forcing temperature.

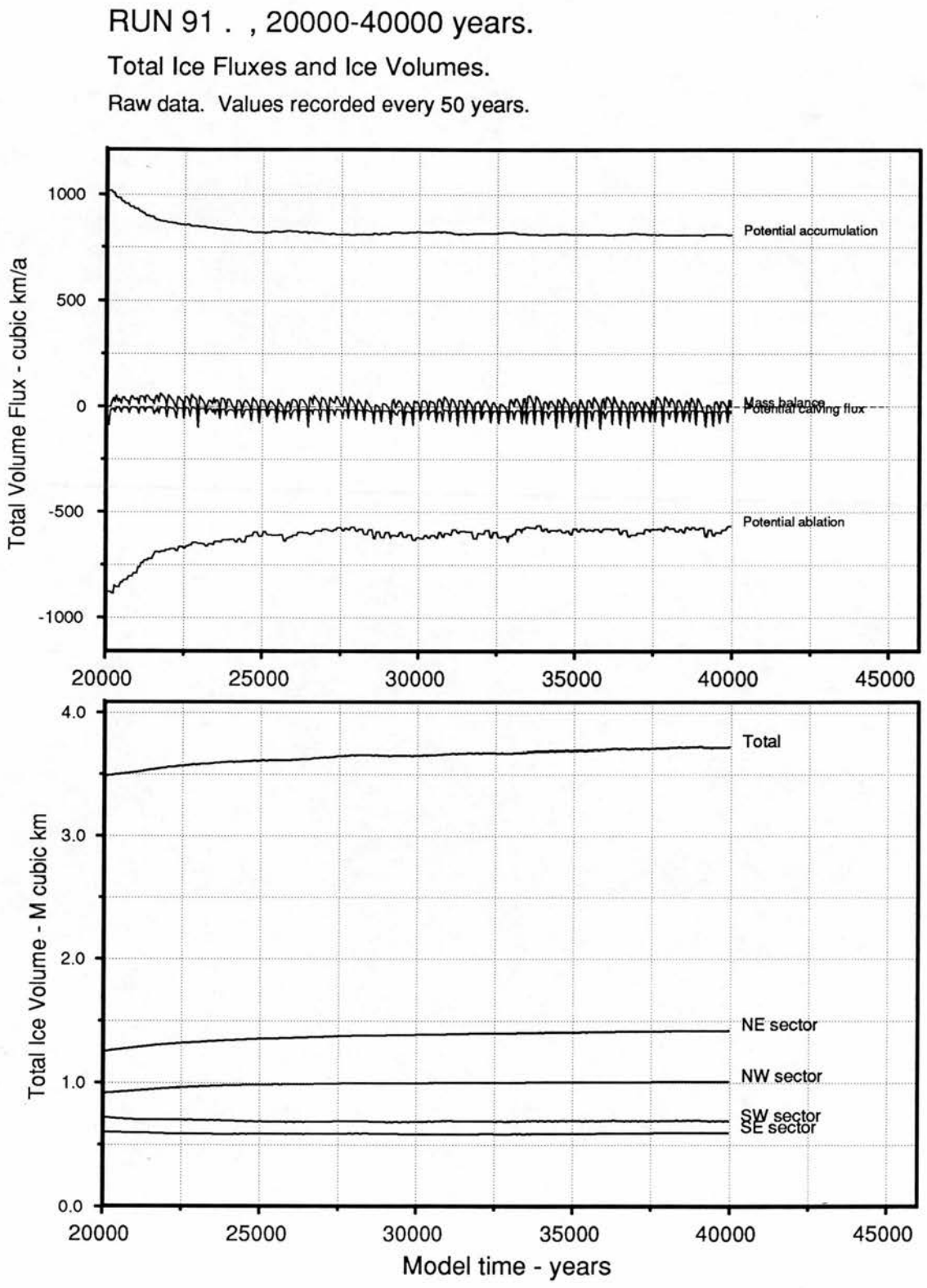

Figure 55: Raw data ice volumes and mass balance values for the forcing test with an ablation forcing constant, $F = 1.02°\Theta/°C$ and $+6°C$ forcing temperature.

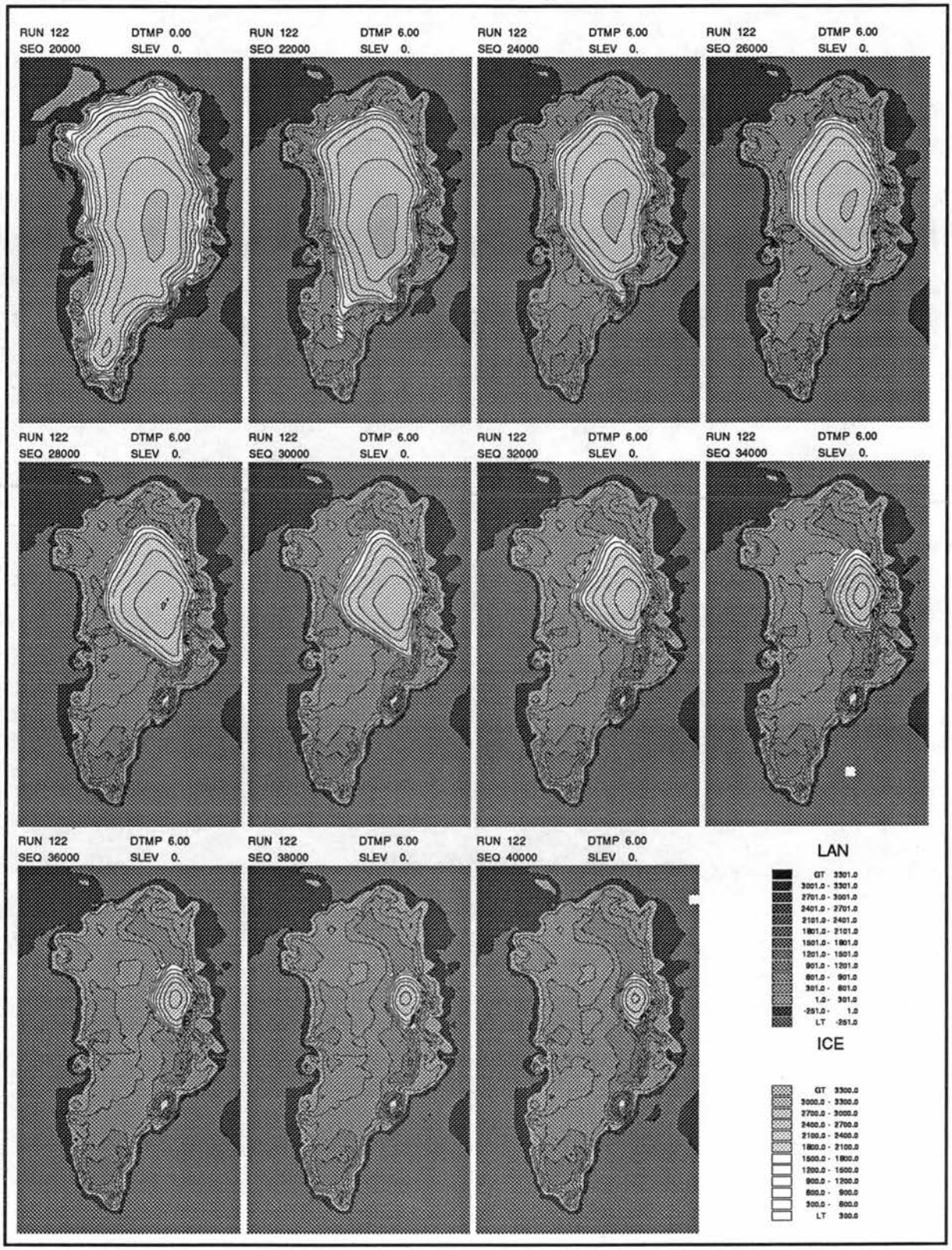

Figure 56: Modelled land and submarine surfaces with superimposed ice surfaces for an ablation forcing constant, $F = 2.50°\Theta/°C$ and $+6°C$ forcing temperature.

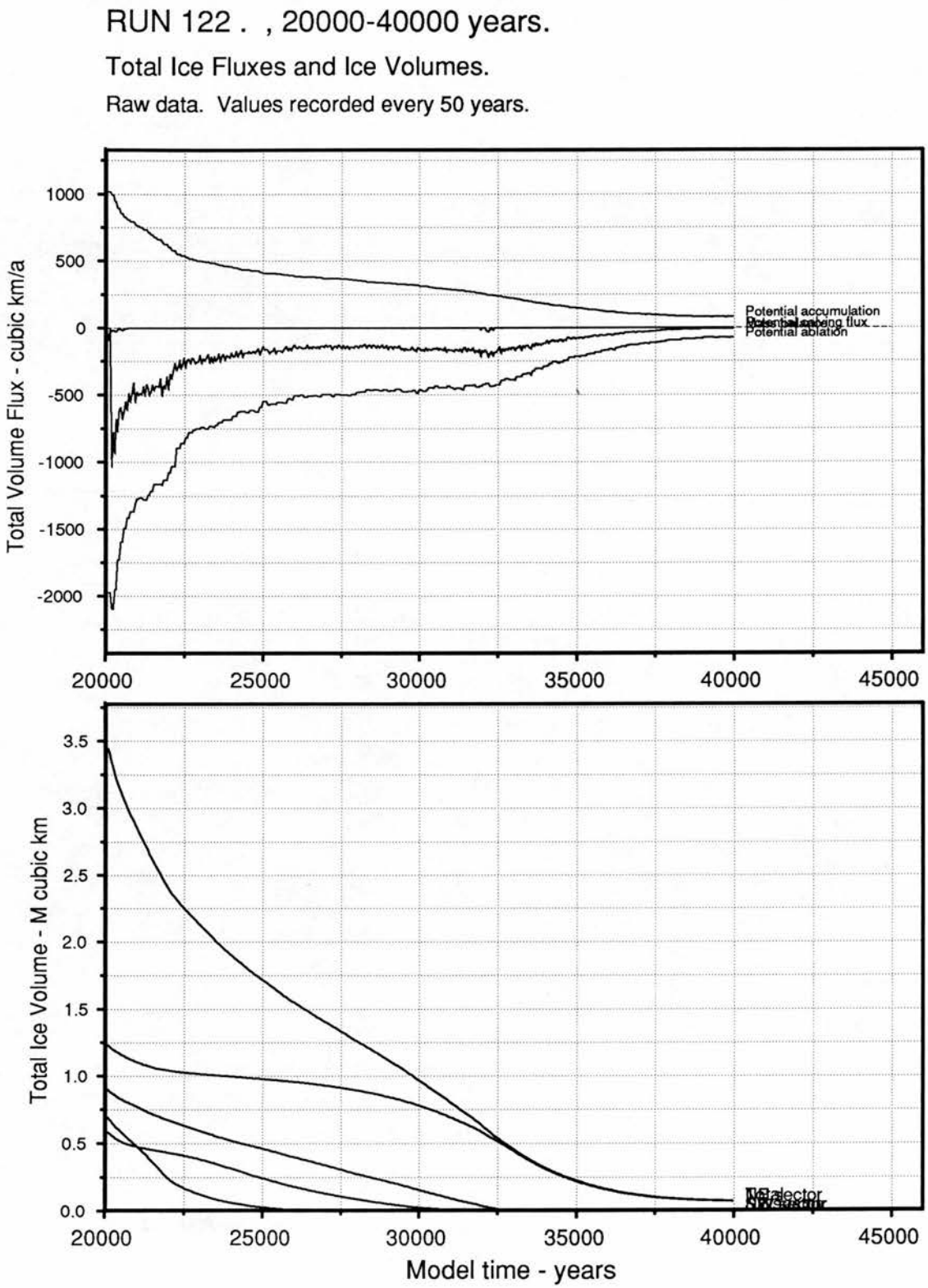

Figure 57: Raw data ice volumes and mass balance values for an ablation forcing constant, $F = 2.50°\Theta/°C$ and $+6°C$ forcing temperature.

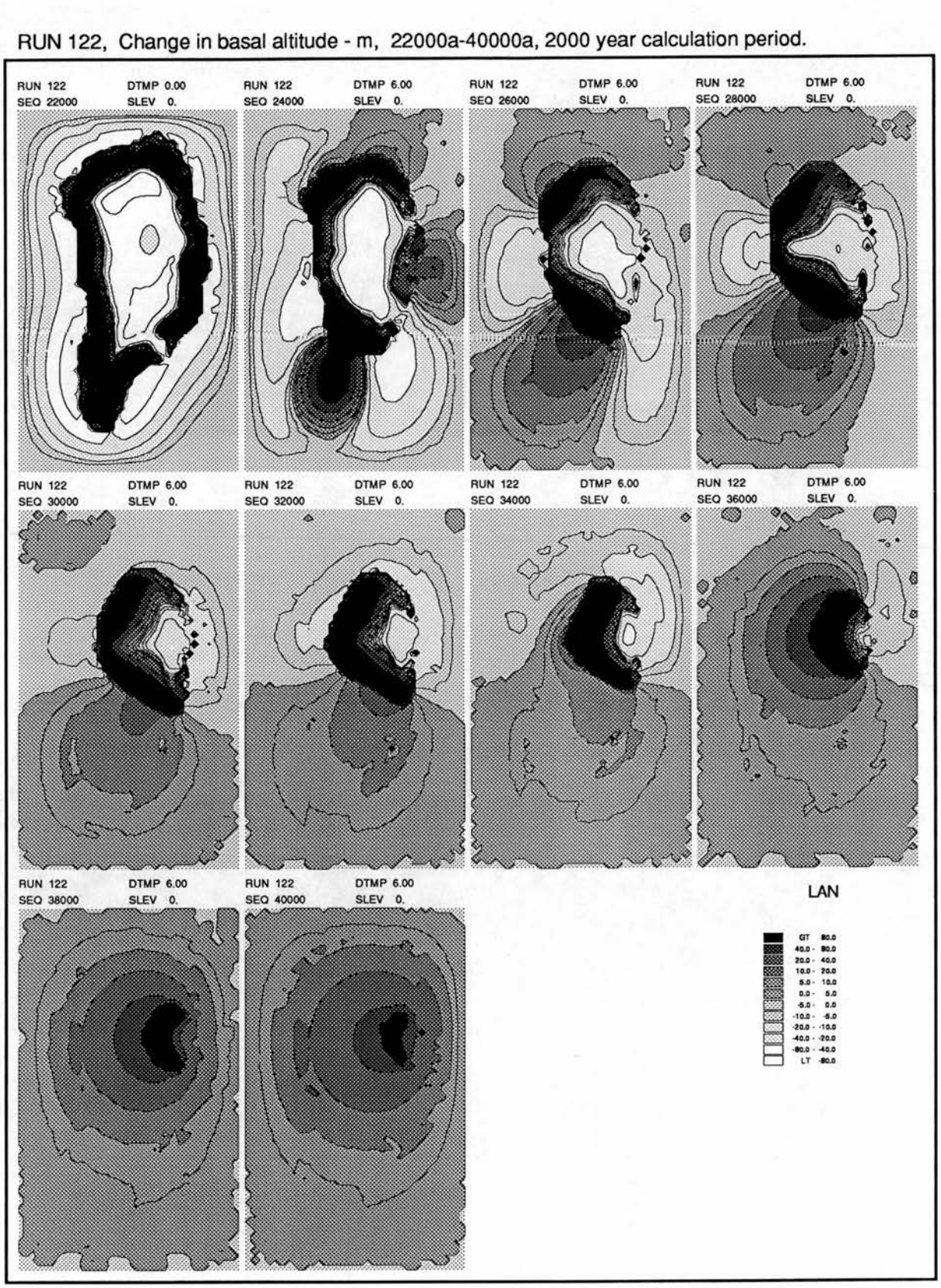

Figure 58: The deflection of ground elevations as changes in basal altitude caclulated over successive time steps for the forcing test with an ablation forcing constant, $F = 2.5°\Theta/°C$ and $+6°C$ forcing temperature. A wave of rising then falling ground passes behind the deglaciating margin. This is due to the initial advection of lithospheric mass into unweighted areas and then subsequent mass loss as new areas unweight.

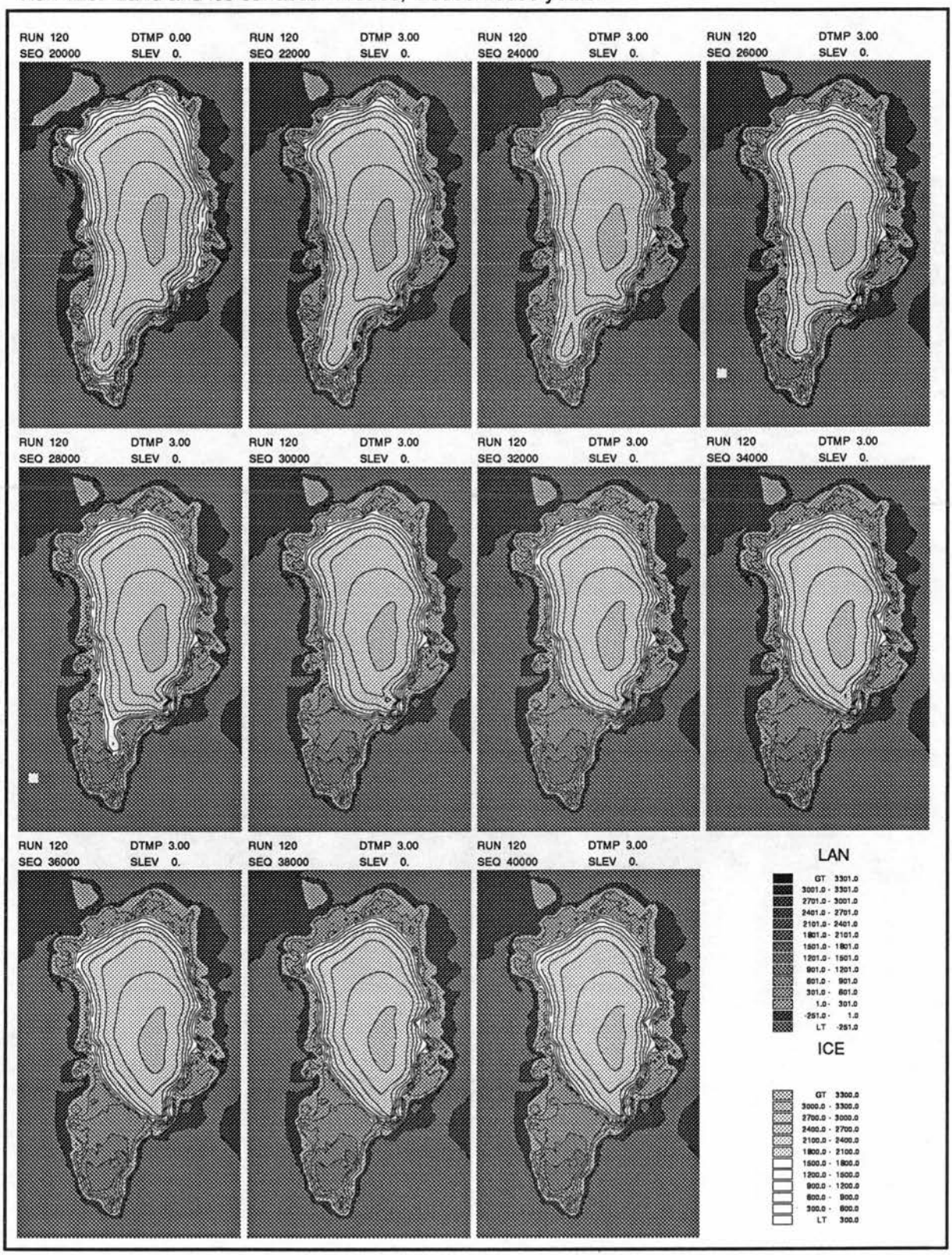

Figure 59: Modelled land and submarine surfaces with superimposed ice surfaces for the forcing test with an ablation forcing constant, $F = 2.5°\Theta/°C$ and $+3°C$ forcing temperature (Run 120). The ice wastes quickly within the first 10000 years and then reaches a stable equilibrium with a more northerly, smaller ice sheet.

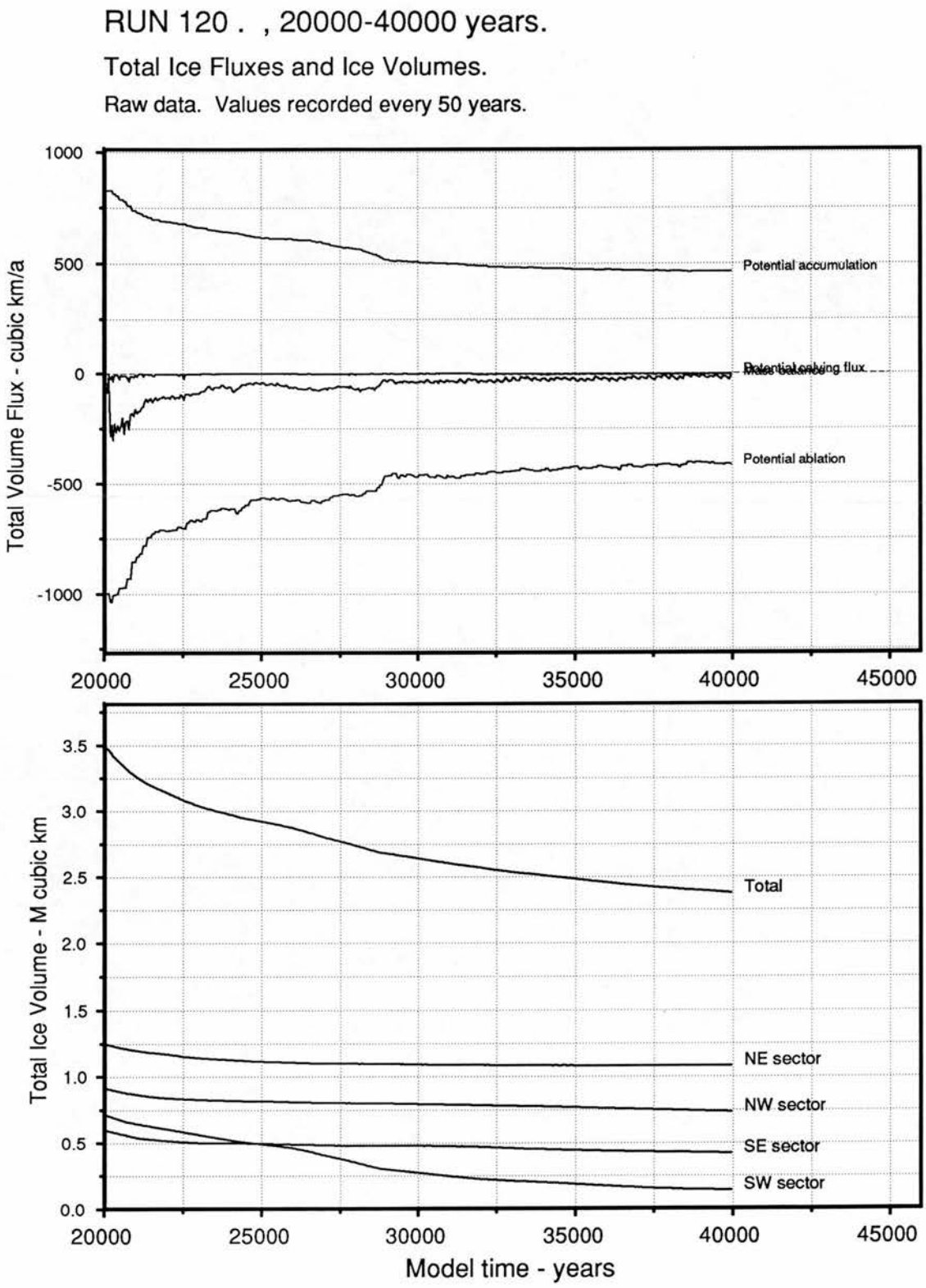

Figure 60: Raw data ice volumes and mass balance values for the forcing test with an ablation forcing constant, $F = 2.5°\Theta/°C$ and $+3°C$ forcing temperature (Run 120). After initial rapid change the ice sheet attains a new equilibrium.

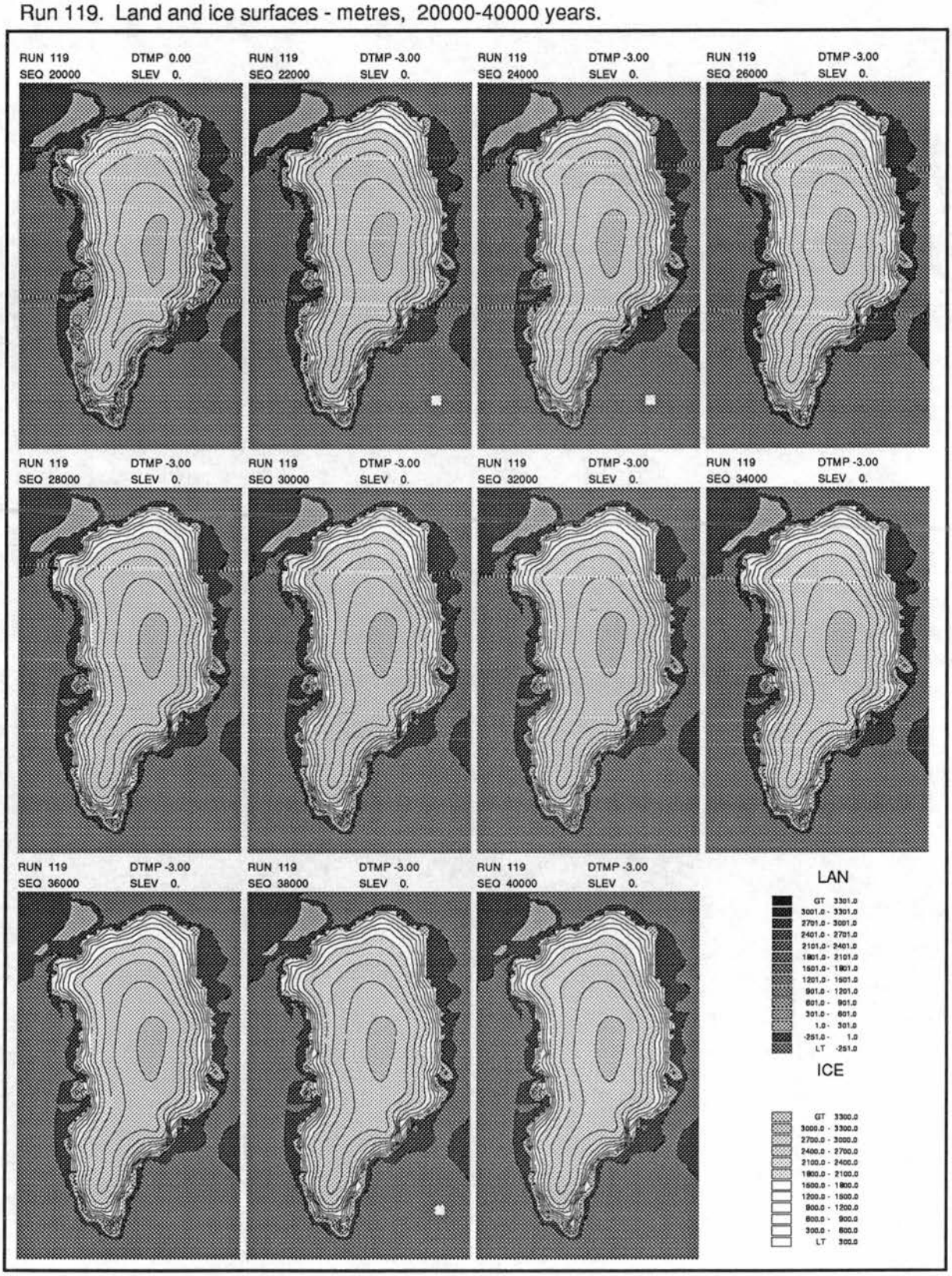

Figure 61: Modelled land and submarine surfaces with superimposed ice surfaces for the forcing test with an ablation forcing constant, $F = 2.5°\Theta/°C$ and $-3°C$ forcing temperature (Run 119).

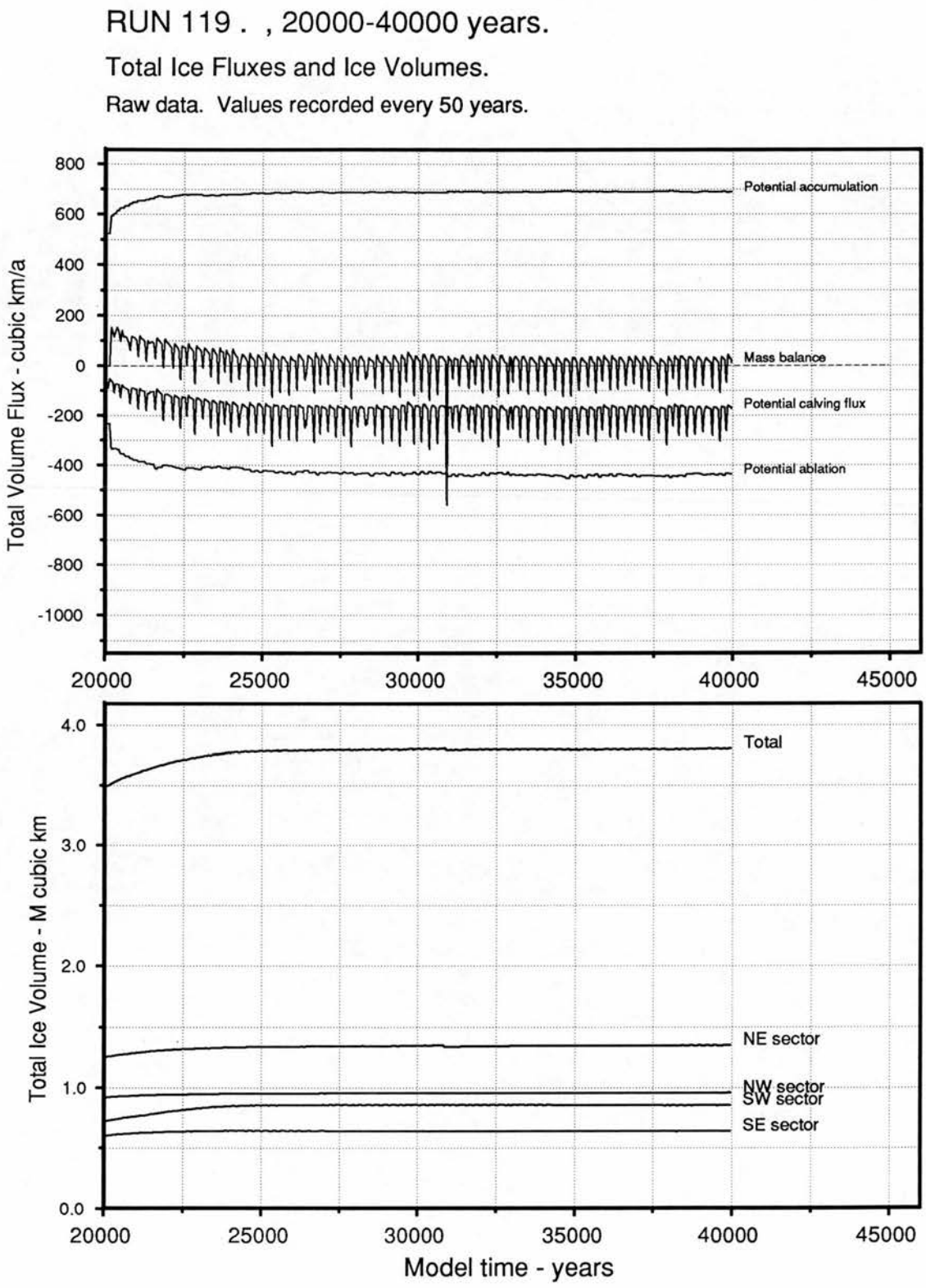

Figure 62: Raw data ice volumes and mass balance values for the forcing test with an ablation forcing constant, $F = 2.5°\Theta/°C$ and $-3°C$ forcing temperature (Run 119). Calving becomes steadily more constraining as the ice extends offshore. A new equilibrium results after about 5000 years.

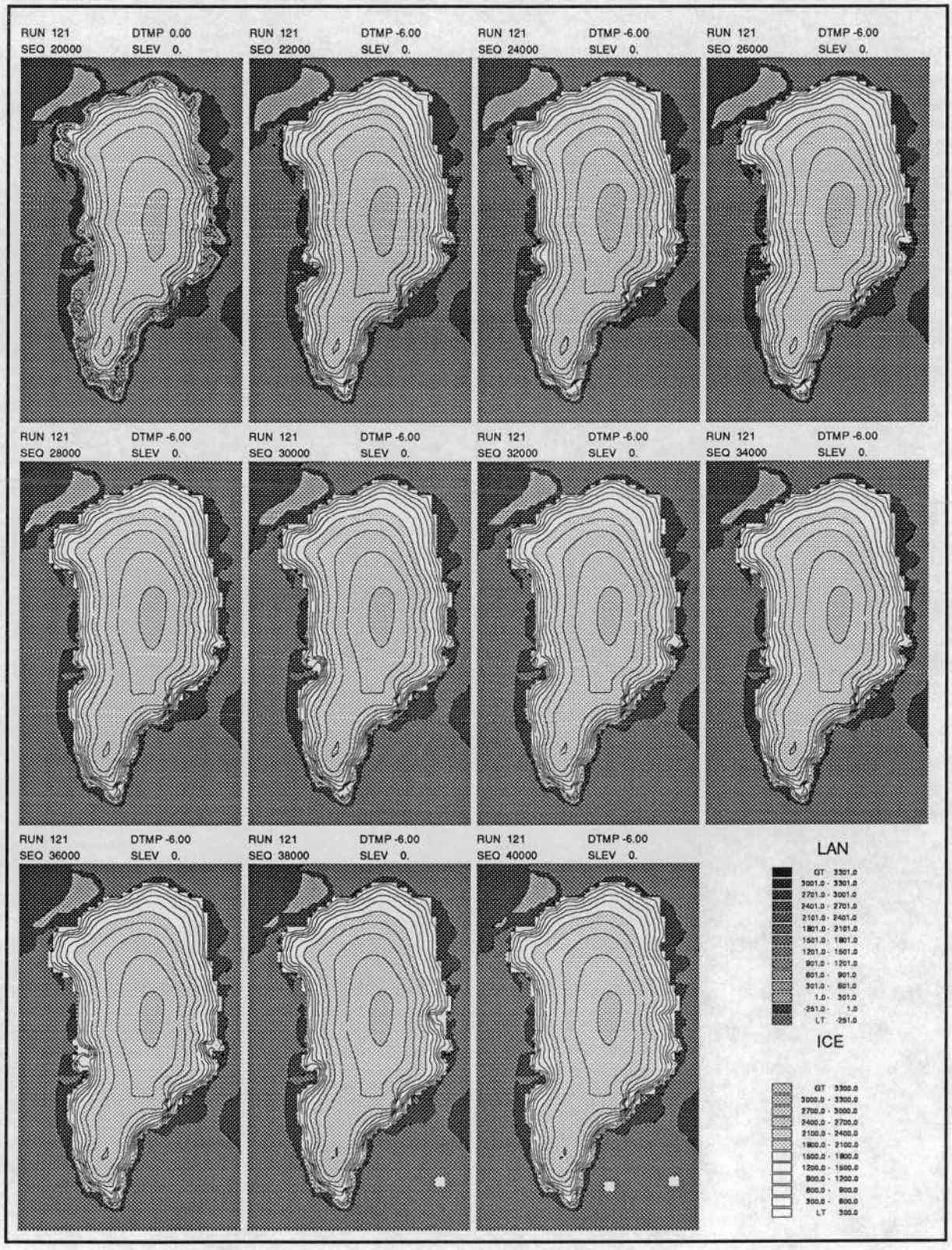

Figure 63: Modelled land and submarine surfaces with superimposed ice surfaces for the forcing test with an ablation forcing constant, $F = 2.5°\Theta/°C$ and $-6°C$ forcing temperature (Run 121).

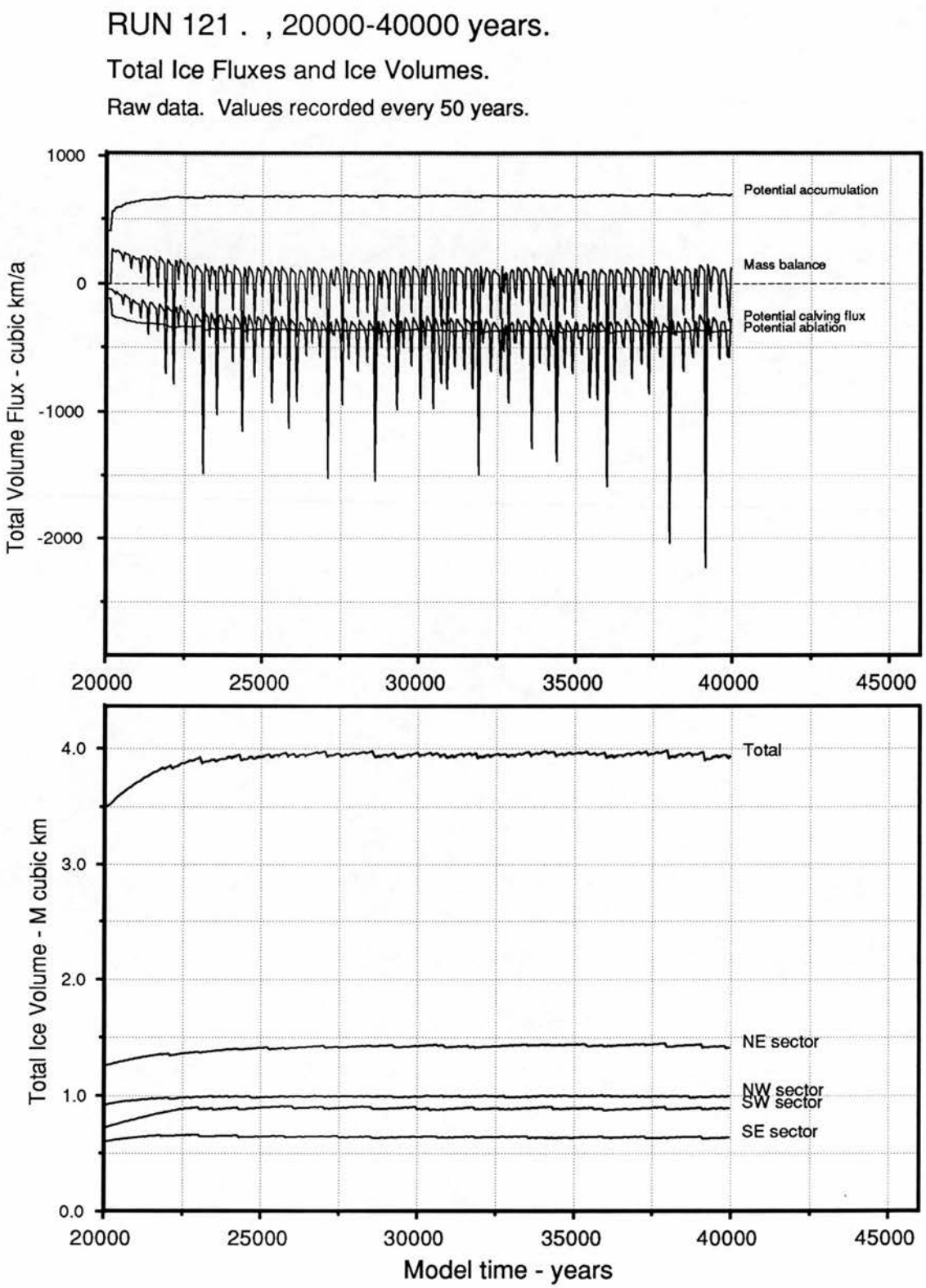

Figure 64: Raw data ice volumes and mass balance values for the forcing test with an ablation forcing constant, $F = 2.5°\Theta/°C$ and $-6°C$ forcing temperature. The model reaches an equilibrium which has significant volume flux due to calving activity.

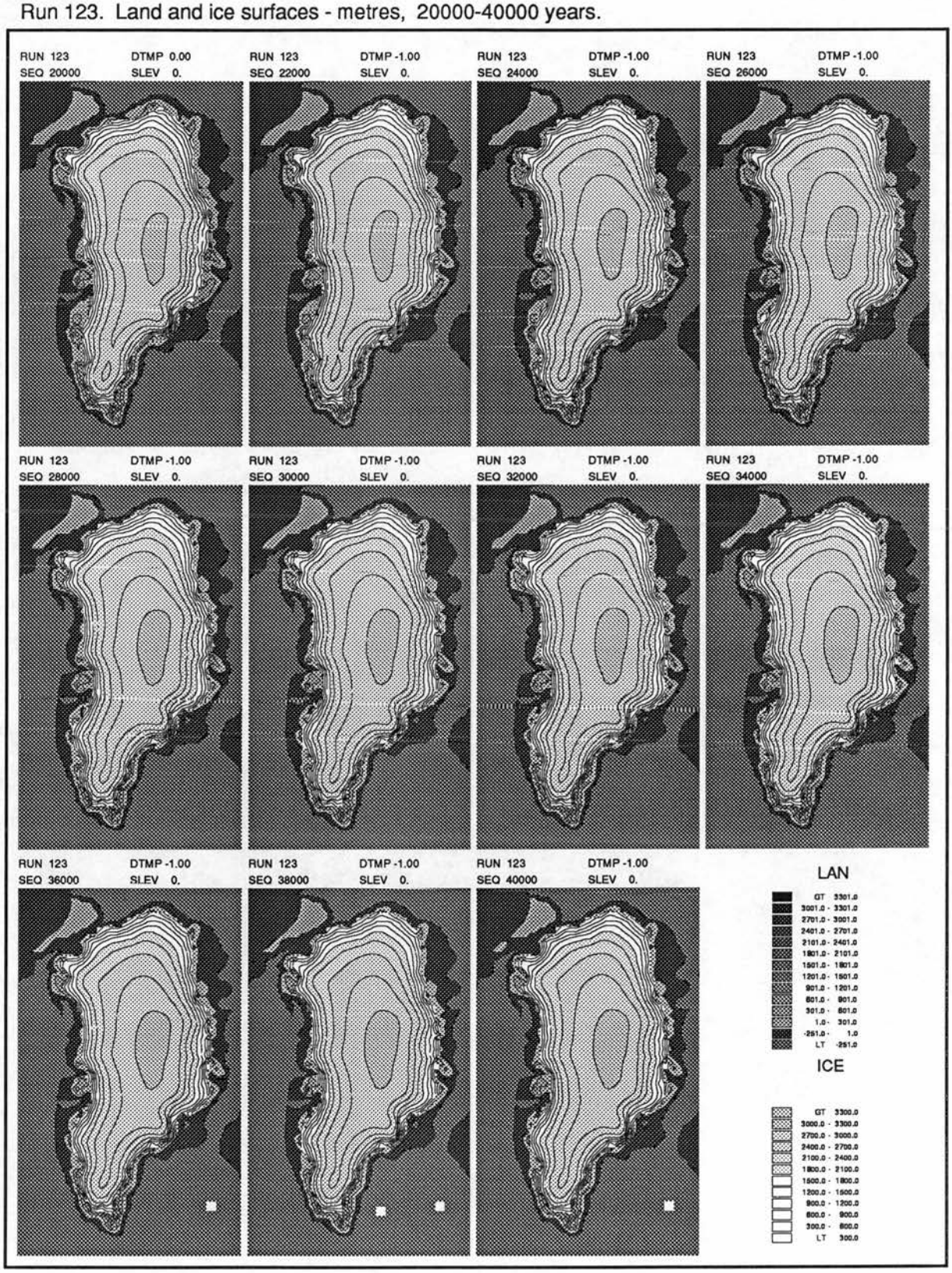

Figure 65: Modelled land and submarine surfaces with superimposed ice surfaces for the forcing test with an ablation forcing constant, $F = 2.5°\Theta/°C$ and $-1°C$ forcing temperature.

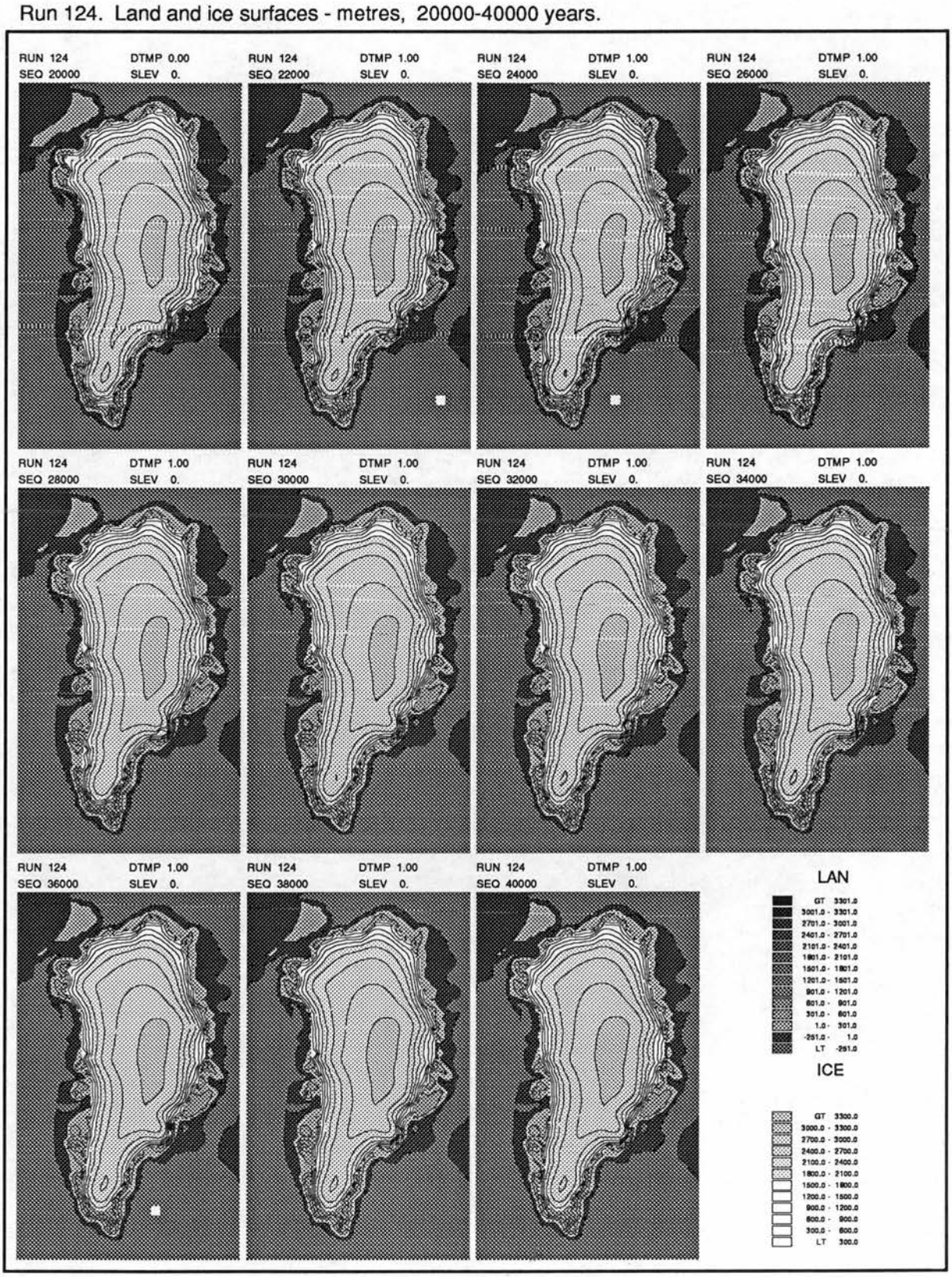

Figure 66: Modelled land and submarine surfaces with superimposed ice surfaces for the forcing test with an ablation forcing constant, $F = 2.5°\Theta/°C$ and $+1°C$ forcing temperature.

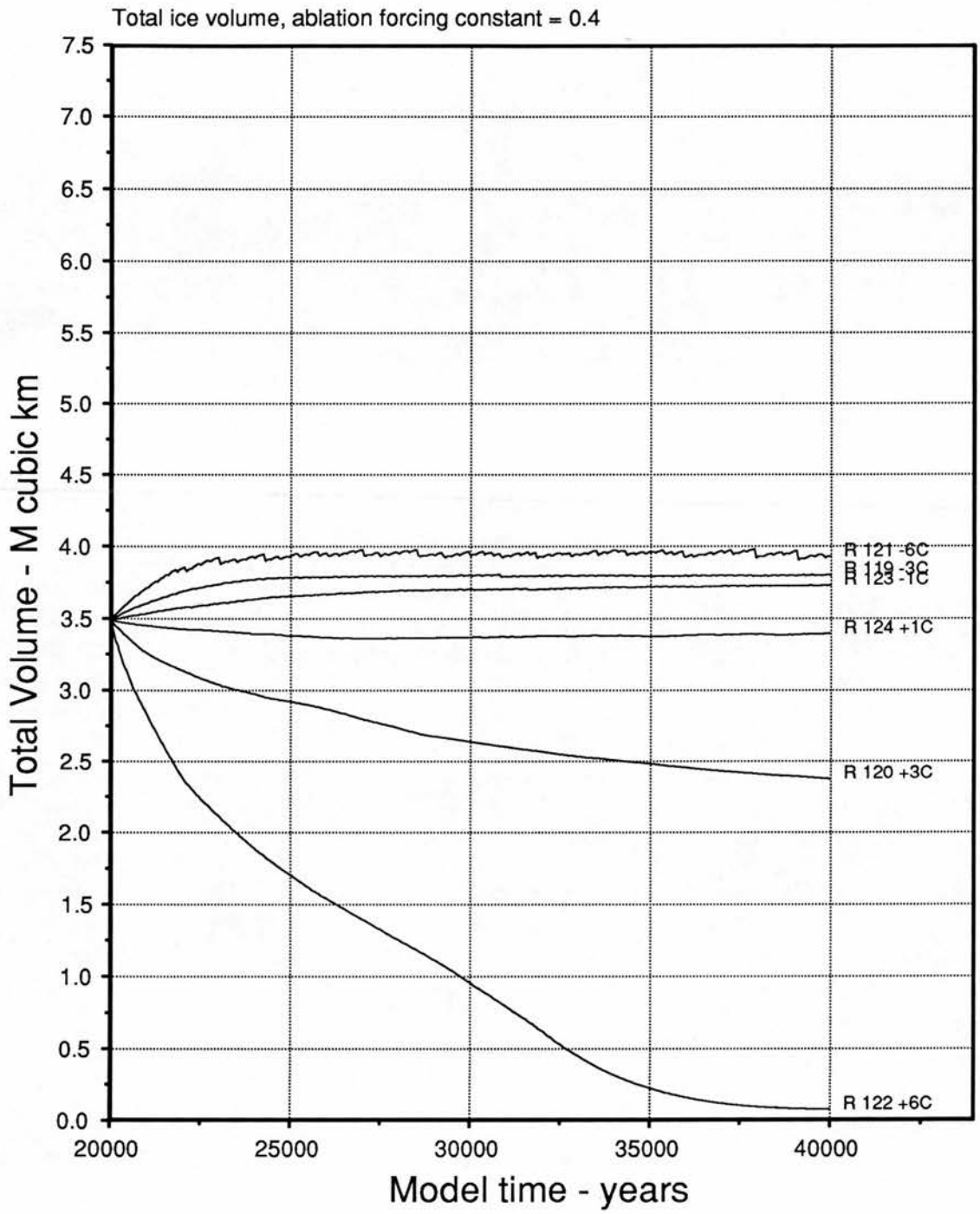

Figure 67: Raw data ice volumes for each of the runs 119- 124, covering forcing between $-6°C$ and $+6°C$ for an ablation forcing constant, $F = 2.5°\Theta/°C$. The large sensitivity to warming contrasts to the smaller sensitivity to cooling. With growth, the ice sheet becomes limited by the influence of sea-level on calving once the marine limit is reached.

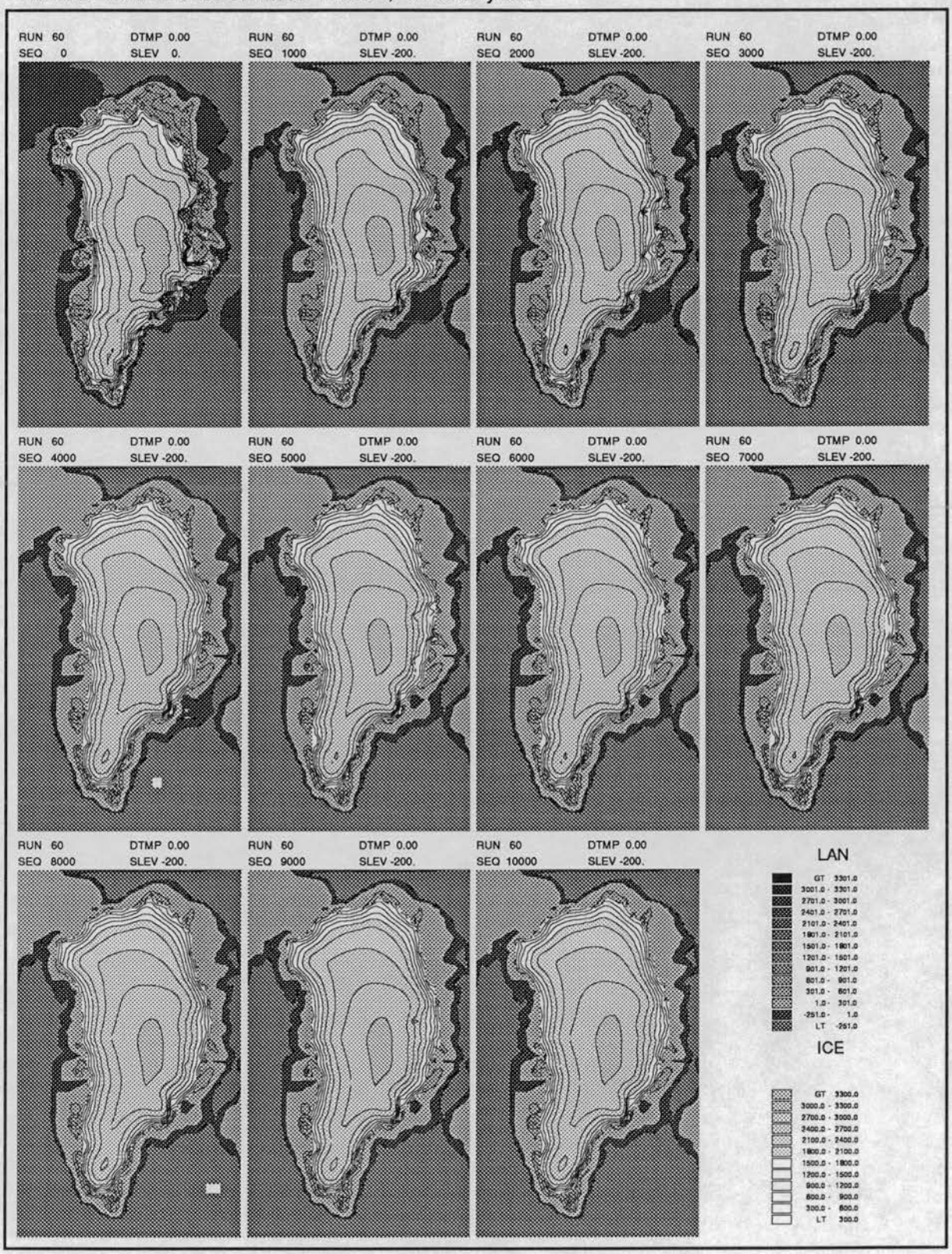

Figure 68: Modelled land and submarine surfaces with superimposed ice surfaces with sea-levels reduced to -200m below present. Ice volumes can increase, particularly in northern areas. There is an additional isostatic effect from water load removal.

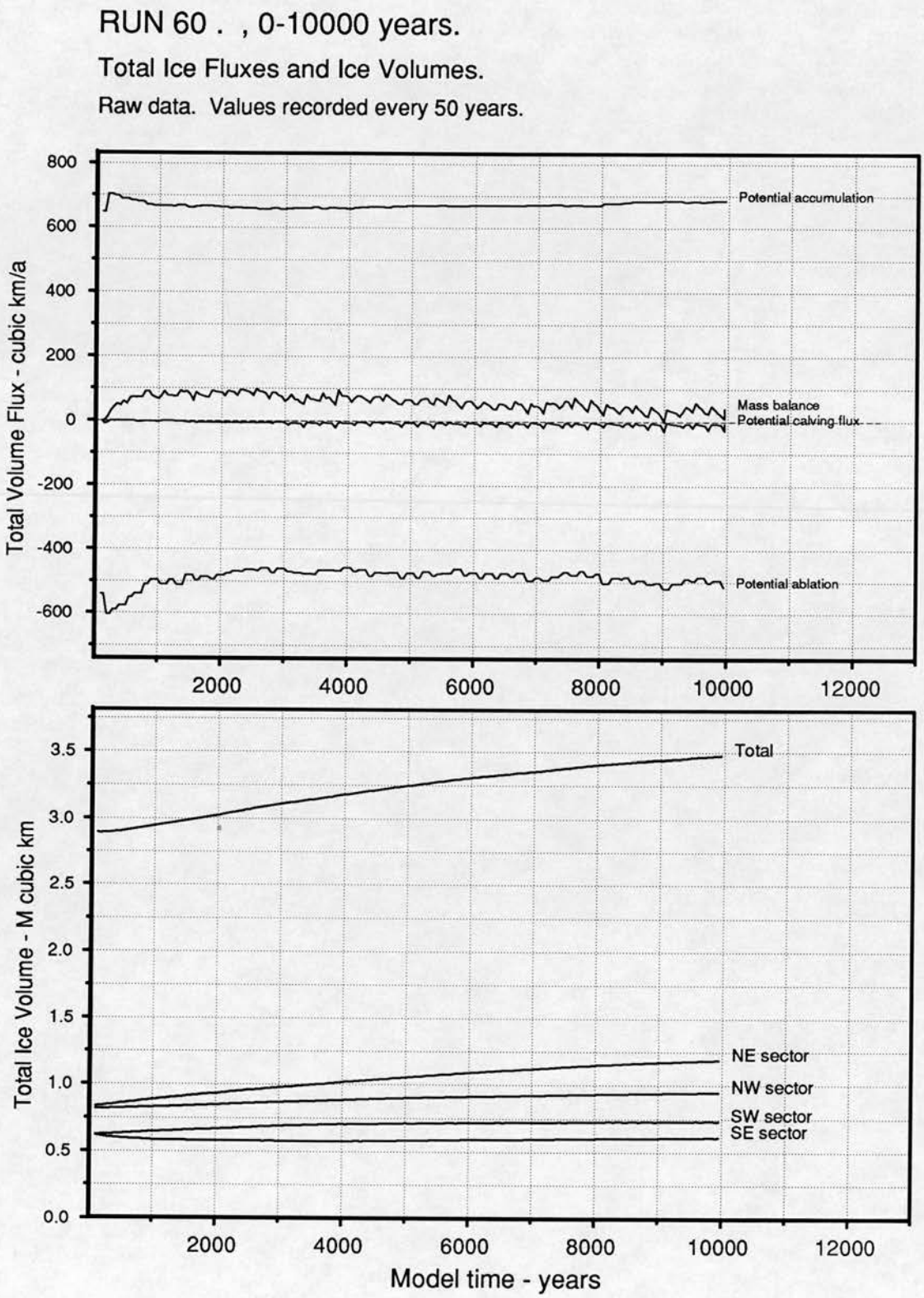

Figure 69: Raw data ice volumes and mass balance values with sea-levels reduced to -200m below present.

Chapter 4

MODELLING HOLOCENE ICE SHEET CHANGE

4.1 Introduction

This chapter looks at how the model can be used to evaluate actual glacier fluctuations through time and make predictions for future change. The model is used to predict the redistributions of ice mass which result from given amounts of sea-level and temperature forcing. It is of interest to work out why these modelled changes occur and what bearing they have on real behaviour. The argument in the preceding chapters demonstrates that confidence in these predictions depends on understanding the model's sensitivity to alterations in its internal parameters and forcing functions. This analysis shows that the model is most sensitive to the nature of the climate model applied, and in particular to the difference between modelled accumulation and ablation for different temperature changes. This dependence is most strongly influenced by the ablation forcing constant.

Because the gradients in the climatic model are parametrized using static present-day values, time dependent predictions are difficult to interpret. When forcing the model by temperature change, the present-day spatial gradients in mass balance are assumed to hold order to reposition the various climatic gradients relative to the topography of Greenland. This allows the use of a single 'global' forcing value but ignores the possible changes in the shape of these gradients over time from being applied in the forcing. Variables which might act in such a way as to enhance or hinder temperature-induced variations in accumulation and ablation gradients, are not accounted for. Examples of such additional influencing variables are cloud cover and

wind speed. For instance, overall warming increases ablation rates but the increase in cloud cover that might accompany warming would reduce them. Altitude-ablation gradients would be preferentially reduced whenever there was relatively high cloud cover. One might anticipate that any northward movement of Atlantic depression tracks as a result of warming would lead to more cloud, but that this would be unevenly distributed. Whilst it would be possible to apply a spatially varying forcing temperature, this was avoided. The extra level of sophistication brings up further uncertainties in interpretation.

It is probably better to regard the forcing values as general surrogates for climatic variations which lead to mass balance change. Whilst it is possible to relate forced mass balance patterns to present-day characteristic temperature distributions, there remains the difficulty of having no external means of establishing the likely persistence of the present-day climatic gradients over time.

This chapter is divided into three sections. The first section looks at the response of the present-day ice sheet to forcing. The second examines the nature and characteristics of the ice sheet at its maximum and compares the modelled predictions with geomorphological evidence. The third and longest section looks at the process of deglaciation from the maximum; again the modelled predictions are compared with geomorphological reconstruction.

4.2 Response of the present-day situation to forcing

It is worth considering what response today's ice sheet might be expected to have to climatic change. The sensitivity tests show that almost any long-term perturbation away from present day conditions will have a measurable effect. A cooling of the order of $-6°C$ would cause the model ice sheet to approach glacial maximum conditions within 2,000 years, and a warming of $+6°C$ would cause it to all but disappear over 15,000 years.

Given the present concern over possible warming induced by increased Carbon Dioxide and other greenhouse gases in the atmosphere, it is worthwhile repeating the sensitivity tests for short time intervals over the next 100 years. Runs 129,130 and 131 simulate warmings of $+1°C$, $+3°C$ and $+6°C$ respectively. The start condition for these experiments is again the quasi-equilibrium condition achieved at the end

of Run 90 after 20,000 years with static present-day parameters. It is particularly important to start from such a stable state of equilibrium because the short term changes are small. It is important to establish that they are genuine responses to the initial perturbation. The sensitivity analysis of the quasi-equilibric condition gives some confidence that this will be the case.

4.2.1 Modelled results

The basic results show the ice sheet surface change after 200 years (Fig. 70). They demonstrate that very little significant change occurs even over an extended human lifetime. The modelled total volume plots (Figs 71) predict that over 200 years the ice sheet is barely affected by a $+1°C$ warming; that it will lose 0.8% of its total mass with a $+3°C$ degree warming; and that it will lose 2.8% of its total mass with a $+6°C$ degree warming. The equivalent volume in terms of global sea-level is given. This progressively accentuated response fits with the idea that changes in mass balance rates are not linearly related to temperature deviations because of the differential gradients relating accumulation and ablation to temperature forcing. The relative accumulaton and ablation values increasingly diverge with greater temperature forcing.

Figures 72 – 75 show the change in ice sheet thickness over the 200 year period for the three scenarios. Each show change in ice calculated over successive 50 year periods. They demonstrate that redistributions in ice mass are brought about by the new mass balance regimes. Each of them shows a broadly similar pattern, which becomes clear in the first 50-100 years. At this time ice thickness reduces at the margins and increases over the centre of the ice sheet. The net mass loss at the margins can be attributed directly to the increased ablation rates and the net mass gain over the centre to increased accumulation rates. Both are directly caused by the warming. More significantly, this pattern shows that the ice sheet does not achieve a balanced profile within 100 years. The overall surface mass balance changes act in each case to steepen the centre-margin gradients. This, in the first instance, leads to faster ice flow and counteracts the surface mass balance trend until a new dynamic equilibrium and its associated ice gradients are established.

Eventually a situation should develop in these circumstances where mass loss occurs in the centre as well as at the margins, but this would need testing over much longer time periods. This does not occur within the initial 100 year period. In each case the centre gains mass over the first 100 years. So the ice sheet dynamics have yet

to respond even to the initial surface mass balance changes during this time. From 100-200 years, the ice sheet is beginning to establish a new dynamic equilibrium. Mass loss at the edges is reduced and mass gain over the centre also falls compared to the first 100 years. The ice sheet effectively increases its turnover and speeds up to cope with the new mass balance regimes. The increase in ice flux starts to counterbalance the altered mass balance regimes by increasing the rate of ice evacuation from the accumulation zone into the ablation zone. This reduces effective thickening rates over the centre and thinning towards the edge. The contrast is most marked if one compares the shape of the ice sheet after 50 years (Fig 74) and after 150 years (Fig 73). However, even after 200 years, the ice sheet is far from reaching equilibrium.

There are differences between each temperature scenario. The $+1°C$ model takes the shortest time to react. After 200 years, it has come close to achieving a new dynamic equilibrium. The $+6°C$ model, by contrast, is further from achieving a new balance state. There is still significant mass accumulation over the last 50 years, and it is still losing far more mass at the edges. The implications of these experiments are that the response time of the Greenland ice sheet to even small climatic changes is of the order of hundreds of years or more. Furthermore, the larger the perturbation, the longer the response time will be.

4.2.2 Implications for the future

It is worth considering in more detail, the predicted magnitude of the changes within the first 100 years. Even under the $+1°C$ scenario, when there is little significant change in the total mass gain and loss, significant centre-margin mass balance differences occur. In this case, much of the centre increases in ice thickness by 2-8m, whilst the margins lose about 30m of ice in the same period. However, there is considerable local variation. Most overall mass loss occurs in the south.

The pattern is repeated in the $+3°C$ and $+6°C$ scenarios, but with the higher forcing values emphasizing the broader centre-margin trend at the expense of local variation. In the $+6°C$ scenario, most of the edges lose in excess of 32m in thickness, while most of the centre increases in thickness by 8m over the same period. This is equivalent to an annual thickening of 0.16m. In each situation, the effect of warming on the ice sheet in the short term is to cause mass wasting at the margins but without significant positional retreat, and an increase in surface altitudes over central areas.

It is interesting that these predictions agree with the latest satellite measurements

of recent changes in the altitude of the ice sheet in South Greenland. By measuring changes in ice elevation with the SEASAT radiometer Zwally and others (1989) calculate that the southern dome of the Greenland Ice Sheet is thickening at a rate of 0.23m/year. Zwally (1989) argues that this is a response to global warming. The model suggests how the ice sheet may develop if this warming is sustained for a few centuries.

4.2.3 Maximum ice scenarios

One of the primary intentions of research was to model the glacial maximum condition for Greenland. In the first instance, this was to see what such an ice sheet might look like, what its associated physical characteristics might be and what climatic conditions are required to produce it. In the second instance, it was to provide reasonable scenarios from which to produce deglacial sequences.

Much of the research effort was directed towards trying to find a good or even believable maximum condition. Initially, it involved searching out a set of parameters that would allow the model to achieve a credible equilibrium maximum state. This is not to say that in reality the ice sheet ever reached equilibrium during the maximum glacial, but it was useful to establish this condition to observe the full effect of applied deglacial forcings. This was a multi-stage procedure. A first 'guess' was made at the set of conditions that might allow the ice sheet to evolve to maximum conditions. The model was then run for a set period, usually 10,000 years. At the end of this time the results were observed and if the model had not reached an equilibrium state it was allowed to run for a further period. If it had, then the end condition was assessed and additional changes made to the parameters to try and force ice growth further.

In searching out the parameters for maximum ice growth the model was allowed to evolve from one hypothetical maximum state to another, rather than grown from the present-day condition each time. This saves on processing time because the ice is already built up close to the equilibrium levels of the new run and so the model does not spend so much time generating new ice. Because the model tends to evolve to the same equilibrium condition over long time periods this short-cut does not alter the maximum conditions reached for a given set of parameters. One of the benefits of this work was that it provided pointers about the nature of the model as a whole, particularly the role of parameters in the climate simulation. A detailed description and analysis of each of these runs would not lend much to the major thrust of the

analysis and so they are not discussed in the text.

As result of this refinement exercise some understanding was obtained of what the model needs in order to grow to maximum. The basic set of conditions is as follows: The $2.5°\Theta/°C$ value of the ablation forcing constant must be used. If a value of this level is not used, it proves impossible to produce sufficient difference between the ablation and accumulation rates for a given temperature forcing to make the mass balance sufficiently mass positive for ice growth to occur. The basis of this fact has already been discussed in the previous two chapters. All that happens if the $1.02°\Theta/°C$ value is used is that the model's energy balance status changes; it does not grow. By using the $2.5°\Theta/°C$ value of the ablation forcing constant and a forcing temperature of $-6°C$, the model will produce a good maximum state. However, the Camp Century data used to run one of the real simulations starts at $-8°C$. In order to provide an equilibrium condition to start this real simulation, the model is forced further to $-8°C$ from $-6°C$ in Run 134. A description of this run follows. The last condition needed to achieve maximum is a lowered sea-level. This allows the marine margins of the model to extend and so the ice sheet reaches a larger size before calving starts to limit its growth. Two static sea-level values were used to find maximum conditions: -120m and -200m. Whilst the latter produces a larger maximum, both yield good maximum states with sufficient temperature forcing.

Having grown the ice sheet to maximum ice conditions, it is possible to look at what the ice sheet does in order to maintain itself at maximum. This is done for a 1,000 year time span in Runs 132 and and Run 136, described later. Two further experiments are presented here which were carried out toward the end of the refinement process when seeking out maxium conditions. These show two things. Firstly they give examples of the refinement process, how the model is forced from one nominal maximum condition to another and how long it takes the model to do this. Secondly they give some indication of the model behaviour over long time periods when it is at conditions which are close to a notional maximum. No one modelled maximum can be said to be absolutely correct. These experiments serve to illustrate that the model can evolve from one notional state to another, and subsequently, some assessment can be made both about why the model itself behaves as it does and what this might imply for real maximum conditions.

Maximum conditions for equilibrium at $-6°C$ and sea-level of -120m. Run 118

The refinement process revealed that significant increases in ice volume could be obtained from a lowering of sea-level to -200m, lowering temperatures to $-6°C$, the use of the $1.02°\Theta/°C$ ablation forcing constant, a mass balance enhanced by the use of artificial gross multipliers, and a lowering of the E_0 levels in South Greenland. This set of conditions provided an equilbrium condition which was used as the start point of Run 118. The start condition itself had evolved through successive refinement over the course of six runs, starting with the end condition of the Initial Standard Run at 20,000a (Run90).

The problem with this starting equilibrium is that the same set of conditions, but using present-day sea-levels and temperatures, produces large ice volumes compared to the present-day reality. Run 118 restores the artificial parameters, such as the gross multipliers to accumulation and ablation, to the Initial Standard Run values but sets the ablation forcing constant to $2.5°\Theta/°C$. Using the 2.5 value allows sufficiently positive net mass balance to counteract the resetting of the other parameters. In addition the forcing temperature was allowed to remain at $-6°C$ and sea levels at -120m. This means that a maximum state model can be produced whose present-day parallel is the Initial Standard Run. One can associate the difference between the present-day and maximum states in terms of the forcing temperature, rather than in a more artificial alteration of other model parameters. The time period is recorded as 80,000 – 10,0000 years which follows sequentially from the end point of the previous run.

Results

Figures 75, 76 and 77 show the major volume changes, total mass balance values and ice surfaces for the run. The total amount of ice growth is relatively small, from 4.80 to around 5.15 million km^3, about 7% of the total initial mass. Most of it is taken up by the formation of an ice dome over the Ellesmere Island area. However, there is significant ice expansion in the central and northern areas and some ice is removed from the Southern Dome as part of the adaption process between maximum states. Figures 78 and 80 shows that the main redistribution seems to have finished at 90,000a. After this, changes in ice distribution are associated with non-linear, cyclic calving behaviour at the marine margin rather than adjustment to the altered mass

balance regime. This shows what the model is doing at this stage of the refinement process. Overall, it progresses from the equilibrium of the previous run to a new dynamic equilibrium which it gets close to after about the first 10,000 years of the run. The total volume change is small, so time is saved in building up ice mass, but still there is a relative redistribution of mass involved. However, within the long-term equilibrium considerable fluctuation still occurs as a result of calving activity. The scale of these fluctuations is large compared to the adjustment due to the change in model parameters.

After this time there are two sustained characteristics in the ice sheet behaviour. The first of these is the continued growth of the ice over Ellesmere Island even though this trend is complicated by substantial ice removal in Nares Strait and adjacent areas after 16,000 years (96,000a).

The second feature is that whilst there is little overall long term major change in the ice sheet configuration, there is still shorter term variability. For example, from 10,000-12,000 years after the start of the run the change in ice thickness is less than $\pm 2m$ over much of the ice sheet (Fig. 78). However, in many areas, particularly near the margin and in places draining into marine terminating major depressions, there is often switching between periods of significant mass loss and significant mass gain. This seems to be related to the presence of marine termini and calving activity. The total mass balance graphs show massive swings in the mass balance flux brought about by periodic calving (Fig 76). There is a regular signal interspersed with far more major events. This is shown best by the running mean graph (Fig 77).

It is interesting to examine the state of isostatic balance at the maximum. Figure 79 shows that, whilst there is some substantial response to the initial starting conditions, this has mainly finished after 10,000 years. The lithosphere responds mainly to the additional ice loading at all areas along the margin, and to a lesser degree to the removal of ice from the southern dome. After the primary readjustment, ice development over Ellesmere causes continued isostatic loading, and the instability at many points on the ice margin produces corresponding isostatic movement along it, as for example in the area around Disko after 16,000a and 18,000a years on the diagrams.

Run 134, a maximum state produced from the $-6°C$ model at present sea-level.

The Camp Century temperature record suggests a 'global' temperature value of $-8°C$ during the last glacial maximum (Robin 1983, Dansgaard and others 1982, Dansgaard

1984). Run 134 was carried out to explore the maximum conditions with this level of temperature depression. For practical reasons the run was started from the 40,000a scenario of Run 121, which used present sea-levels and a temperature change of $-6°C$. The simulation in Run 134 was forced to a maximum with a further $-2°C$ temperature drop and a drop in sea level of -120m. The simulation ran for 10,000 years (40,000a – 50,000a in the diagrams).

Results

The total mass balance plots (Fig 81) show that the initial temperature drop of $2°C$ produces increased surface mass balance. Some is due to the increased exposed land area, some to the direct temperature forcing and some to the effect of a lower sea-level reference in the mass balance model. Because of the sea-level drop calving rates are severely retarded at first, only really reaching rates similar to the previous higher sea-level after 2,000 years.

Maps of the change in ice thickness (Fig 82) show that ice flows from the upper areas onto the newly exposed continental shelf. In the south this results in an initial thinning of the southern dome whilst net accumulation in the north is sufficient to compensate for any loss to the edges and causes slight thickening. Towards the end of the run, the n hern dome has more or less expa d into the newly exposed continental shelf. Elsewhere, the appearance of successive phases of thickening and thinning is once more associated with the development of periodic catastrophic calving behaviour near a major ice stream. As in the previous maximum example, ice over Ellesmere Island accumulates through the duration of the run, suggesting that things are not yet in equilibrium there.

The changes in basal elevations show features of the isostatic response (Fig 83). The first is the initial change in sea-level. This causes uplift in areas below sea-level. These are enhanced by the lithospheric mass being forced out from under areas newly occupied by ice. Subsequent to the initial movement there is some return flow back from the submarine and subglacial areas as the distribution of ice overburden evens out. In later phases this pattern is modified by isostatic responses to changes in the location of the ice margin and the continued growth of ice over Ellesmere Island.

4.2.4 Comparison of maximum state conditions with the geological record

Figure 84 shows a map of the Late Wisconsinan Glaciation and Holocene marine limits based on a review of existing geological and geomorphological evidence by Funder (1989). Figure 85 shows the present topography and the modelled ice morphology at the end of Run 118 ($-6°C$ -120m sea-level fall). There is a good match between the modelled ice maximum and empirical evidence of the last ice maximum. In both cases the ice sheet extends to the edge of the continental shelf round most of Greenland and links with ice on Ellesmere Island. The agreement is particularly good in West Greenland. Even some detailed matches are clear. Ice extends relatively further offshore from Nodre Strømfjiord than further south because the continental shelf is wider here. Ice seems never to extend far off Nanortalik where the water is deep and the ice supply limited. The main divergences occur in East Greenland. In the vicinity of Anmasalik, Funder shows the ice reaching to the edge of the continental slope while the modelled limit is much further inshore. The position is reversed in Northeast Greenland where the modelled limits extend further offshore than Funder's limits (Funder and Hjort 1980). In this area, however, there are insufficient field observations to know if this is a real difference between model and reality. It is interesting that breaks in the geological record occur in the model as indentations in the line of maximum extent. These coincide with troughs, such as Disko Bugt, which are deep and the sites of dynamic fluctuations in the ice margin.

4.3 Maximum state conditions and calving

Calving becomes a steadily more important control on total mass balance as the ice expands towards its maximum and the length of the marine margin increases. It is important to explain what effect calving has on the overall behaviour of the ice sheet as its controlling influence increases. One of the most striking features is the short term variability of the calving fluxes. The characteristic calving pattern is fairly stable but has increasing background value interspersed by major calving events. Moreover, as overall calving intensity increases, the magnitude of major calving events becomes larger. The implication is that the ice sheet develops longer marine margins which become progressively more unstable as they move into deep water. This variable calving behaviour influences the short term configuration of the ice sheet when it

is near maximum conditions. During retreat phases, the same variable affects the pattern of retreat. It is therefore worth looking more closely at how these calving events operate in the model and how good they are at representing real behaviour.

Run 132 was in part set up to do just this. The experiment took the maximum equilibrium condition with an imposed temperature change of $-6°C$ and a sea level fall of -120m, as established at the end of Run 118. This was run forward for a further 1,000 years with surface data recorded at 25 year intervals and volume and mass balance data at 5 year intervals. The aim was to pinpoint exactly when and where calving took place and why.

It was important to distinguish possible physical events from artificial instabilities introduced in the solution routine. It turns out that calving is related to the periodicity of the smoothing function used to control numerical instabilities. Figure 86 shows the relationship between smoothing and the calving events and Figure 87 the total ice volumes involved. To check the relationship betwen calving and smoothing a control run (Run 136) was set to be identical in all ways except that the smoothing function was omitted. The effect of omitting smoothing is shown in Figure 88.

The differences between the two mass balance records demonstrate the clear relationship between model smoothing and calving activity when smoothing is switched on (Run 132, Fig 87). However, with no smoothing (Run 136, Fig 88), calving activity is still irregular, but without the major calving events. To examine this behaviour further, it is necessary to associate the calving events with model locations.

Peak calving events occur in the model with smoothing at around 630 years and 840 years (Fig 87). Figure 89 shows the development of the ice sheet from 625-875 year points for the Western ice sheet, and Figure 90 for the entire ice sheet. It is evident that the calving activity is extremely localised. After 650 years, the increase in calving activity is associated with the formation of a major ice embayment at Umanaq to the north of the Nugssuaq Peninsula. After 850 years, it is associated with a similar, though smaller, feature to the south of Disko Island. Elsewhere, a small glacier tongue develops around Nuuk.

These three locations have offshore topographies in common, in that they allow very thick ice to flow into deep water close by. This is the key to why the areas are sensitive to catastrophic behaviour, and why this behaviour is triggered by model smoothing, even if it cannot be entirely explained in this way.

One of the model assumptions is that calving only occurs when the ice is floating. This, and the fact that floating and partially buoyant ice can flow more rapidly, sets

up a potential trigger mechanism for catastrophic behaviour. Once calving starts, ice thins rapidly. This tends to sustain calving at the margin. Ice is evacuated across the floating ice shelf at a constantly high strain rate and this thins the ice at the grounding point. The calving front has to retreat because it is losing more ice than is being supplied. At the same time, if the supply of ice at the grounding line cannot match the loss at the ice shelf to the calving front, the ice here thins too. As a result it becomes more buoyant and flows faster itself, thereby accelerating the process back up the ice stream until a point is reached where the subglacial surface is above sea-level. When this happens the ice can no longer flow faster through flotation. The situation stabilises either when the calving front reaches the terrestrial margin, or when the supply of ice to the ice shelf matches the calving loss at the ice front. This tends to happen if the ice enters shallower water or it if it thins.

The important controls on this mechanism are the depth of water at the point of calving and the magnitude of the ice loss which initiates flotation and calving. If the water is deep, the model allows ice removal to a maximum of 2km strain/year. If, alternatively the water is shallow, calving is much less intense, and a stable calving front can extend until the water is sufficiently deep for the calving loss to match ice flux to the ice shelf. However, if ice is advancing into deep water, it may cross a theoretical depth which initiates a calving cycle and temporary retreat. This catastrophic behaviour will only happen if a sufficiently large amount of ice is lost initially for the ice not to be able to reground quickly.

It is now possible to ask why the smoothing function can trigger this mechanism. Why is it that grounded ice in deep water becomes destabilised by smoothing when it is not in other circumstances? The effect of the smoothing function is to cause edge thinning of the ice sheet, because, by definition, edges are not smooth. No global mass loss is caused because a check is kept on the amount before and after smoothing and any loss of mass is reassigned over the entire ice sheet surface as a function of existing thickness. However, since more mass is lost at the edges than elsewhere, the effect of smoothing is to remove ice from the extreme edges towards the centre, every 200 years. Overall, this means that there is an artificial backflow of ice and increase of surface gradient. To estimate the effect, the edge of the ice sheet can be considered as a flat plateau 50m thick and 4,000km or 200 edge cells in length. The mean loss per edge cell would be about 7.5m and the total ice volume loss at the edges would be about $0.0075 \times 4000 \times 20 = 600km^3$. This is roughly equivalent to an annual total ablation figure, but given the steep ablation gradients right at the edge and the

approximate 200 year smoothing interval, ice removal by smoothing is probably less than one per cent of the ablation budget near the edge. Since no mass is lost under normal circumstances, the smoothing merely tends to steepen the energy gradient of the ice sheet for a short period. Within around three time steps, the edge gradients restore themselves to pre-smoothing levels (Fig 87).

Despite the minimal effect of smoothing to normal operation, it works as a calving trigger because of the localised ice removal from places which are normally grounded below sea-level. This can be illustrated by the example of Umanaq Bay to the north of Nugssuak, which is deeper than 500m, even under reduced sea-levels. The modelled ice at the edge reaches around 100m above sea-level and therefore, would lose around 15m of ice thickness under smoothing. If, under normal running conditions the ice built out beyond a stable grounding line where calving flux matched ice flux onto a narrow ice shelf, the situation could be balanced. With smoothing, the instantaneous loss of ice right at the edge is sufficient to enhance calving and flotation and to instigate unstable feedback.

4.3.1 Change in ice thickness

Further perspective on the modelled process of periodic calving comes from analysis at a higher resolution. The 25 year calculation period maps show that thinning and thickening from calving occurs over variable time periods, depending on the magnitude and duration of the original calving event (Figs 91-94). In many cases thinning is more rapid than the subsequent thickening which restores ice gradients. For instance in Figure 91 some calving takes place near Melville Bay and the ice surface gradient in the surrounding basin declines at 25a and 225a. In the period between, the basin regains mass slowly. In other areas, mass loss is sustained, for instance around Nuuk. Other areas display more complex patterns of gain and loss operating over longer periods. The most noticeable example is the large phase of deglaciation in Umanaq Bay where the initial thinning by calving is large (Fig 93). The thinning is at first contained to the bay area but then a zone of thinning spreads upslope for the next 200 years whilst the bay area simultaneously thickens. Clearly, there is no single set pattern for calving and its associated surface effects, but the different trends are identifiable even for the smaller basins.

When the model is seen on a longer calculation period of 100 years, it is clear that the subtleties become obscured (Fig 95). For instance, the cycle of thinning

after 25a in the Melville Bay area, followed by thickening at 50a, 75a and 100a, is lost in the 100a map for the same area. Even the major changes at 600a-700a around Nugssuak become rather condensed. It is nonetheless possible to see the transition from thinning to thickening, for instance, around Umanaq Bay.

When the calculation period is increased further there is a greater loss of information. The summary map of changes after the 1000 year run (Fig 96) suggests that most activity has occurred at Nuuk and Melville Bay. Although these undoubtedly saw calving, they are less important locations than elsewhere. The only feature faithfully recorded over these calculation times is the infilling over the Nares Strait, which continues throughout the sequence.

To conclude this discussion of the process of periodic calving, it is clear that if the model output shows ice thinning or thickening associated with a calving terminus it could be for one of two reasons:

1. There has been genuine thinning or thickening associated with the process acting over a particular time period. This could indicate a single cycle switching of the calving state at just one time in the calculation period.

2. By chance, the time periods picked for the calculations show strong thinning or thickening associated with the most recent event. Other earlier events may have occurred, but their effects are obscured.

It is equally possible for all sorts of interesting things to happen within a particular calculation period and the net effect to show nothing. However, if changes show, it is likely some calving effect is present. Judging the scale and duration of the event is another matter. It seems likely that switches in calving activity occur at much shorter time scales than the 1000 year time intervals used for some of the analysis below.

Isostasy

Calving induces an adjustment in isostasy. In particular, the overall increase in margin calving rates associated with the 200 year smoothing signal shows up in each relevant step as a wider ring of isostatic change. Because the isostasy model does not take account of lithospheric strength, the effects of ice unloading can be fairly localised and quick to operate over small distances if rapid unloading occurs. In the locality of immediate deglaciation, using the smoothed model, there is more than

80m of rebound within 25 years and further adjustment for the next 300 years. As an example of the likely magnitude of the effect of deglaciation the calving cycle removes about 2,000m of ice from Umanaq Bay of which around 1,500m is originally above sea level. This is the equivalent of about 400m of lithospheric uplift, but full recovery is never reached because the ice reoccupies the area quickly.

However, this scale of localised unloading sets up very steep modelled diffusion gradients over the short distance of the fjord width and isostatic readjustment is extremely rapid. The figures identify big calving events at Disko Bay (525-550, Fig 98; 825-850, Figs 99-100) and at Umanaq (625-650, Fig 99). The diffusion gradients are sufficiently strong to force lithospheric mass back into the fjord and create more than 100m basal uplift within 50 years. The uplift is rather too fast to be realistic but the rapidity stems directly from the lack of modelled lithospheric strength, the perfect diffusion and the modelled localisation of major unloading. These enhanced isostatic movements are a common feature in other experiments whenever locally variable calving activity occurs. The extreme values do not spread far; only very small areas are affected at first, so little total mass is involved.

In the 100 year calculation maps some of the longer term trends become rather more obvious, particularly the dissipation of isostatic readjustments away from the source disturbance (Fig 101). The difference between disturbed and stable areas becomes more evident than with the shorter calculation period. The effect is clear on maps representing a 1,000 year calculation (Fig 96). The 1,000 year calculation aggregates changes over long time periods. It yields a map of all areas affected within the calculation span. As such, it provides a better record of the glacial changes than the thickness change maps do over the same period.

4.3.2 The action of isostasy with calving

The nature of the isostatic model adds a further instability to the modelled calving process. The effect of isostasy on calving behaviour is to make the water from which the ice has just retreated shallower, and thus it helps grounded ice to expand back over the area. Whilst the isostatic influence is most noticeable in catastrophic situations, it undoubtedly acts as a stabilising influence on less deep, more stable margins.

The realism of the calving process

It is important to ascertain whether the calving instabilities are wholly an artifact of the modelling. The conclusion is that they are not and that the model is highlighting a potentially important process, though over-emphasising it. Whereas the initial trigger is artificial, the magnitude of the calving effect and its location can only be accounted for by the existence of certain topographically favourable locations. The non-smoothing model does not demonstrate such major events because there is no strong triggering device, but it demonstrates unstable behaviour nevertheless. It is possible that calving cycles could be self-triggering over longer time periods in favourable locations.

The apparent cyclicity of enhanced calving is brought about by the regular smoothing of the ice surface. However, the actual areas affected are not the same and the variable magnitude of calving events over longer time periods reflects the operation of modelled assumptions played out in certain favourable geographical situations. It has already been pointed out that over longer time periods the overall calving flux varies little, whether or not it is artificially triggered by smoothing (cf Figs 87 and 88). The model contains no stochastic elements but they would be easy to introduce as variations in mean accumulation and ablation patterns, or enhanced calving caused by wind shear or favourable ocean currents. It could be argued that if such were included they too could trigger unstable calving behaviour. All that the smoothing is doing is putting an artificial trigger on an already unstable situation. In other words, the propensity of the ice sheet margin to adopt an unstable condition is a direct consequence of the isostatic and calving relations embodied in the model. Through the natural processes of the model, ice flowing into deep water, particularly embayments, is inclined to become easily destabilised if there is sufficient instantaneous thinning near the ice edge. The artificial smoothing in the model provides just such a hefty trigger and the calving consequently adopts a regular cyclicity in accordance with it. However, there are additional cycles associated with the collapse from and rebuilding to unstable situations in a number of different localities which do not all become unstable at the same instant. The period between catastrophic calving and rebuilding to another unstable state varies with margin topography. The modelled calving system contains, by definition, the same physical elements, but the manifestations of it are geographically differentiated.

The effect of calving on ice sheet development

The combined effect of the smoothing - calving sequence of events is best observed in the maps showing changes of thickness (Fig 93) in the 25 years preceding 625a and 725a in the model run. The smoothing occurs shortly after 625a. There are a number of different features to note.

In the north, in the Nares Strait Channel, smoothing after 625a affects flow at the outer edge of the ice shelf, but in general ice growth is sustained. The effect of the momentary steepening of ice gradient after smoothing is observed as the upper parts of the ice sheet become at first marginally thicker (black) and then as time progresses start to thin again as the gradient restores to pre-smoothing levels. The area of steepening affected by the calving event to the north of Nugssuak appears clearly at 650a and then increases in spatial extent, whilst decreasing in magnitude value at 725a. An expanding bowl of ice is tapped to replace the ice lost in the channel. Whilst the area affected stretches back to the ice divide, the magnitude of the effect is relatively small beyond the local area.

Other calving termini behave in a similarly complex fashion. Generally speaking they gain mass prior to smoothing, lose mass immediately after smoothing and then return to gaining mass once again. Some of them affect the ice sheet in the vicinity.

The long term effect of cyclic calving shows up slightly better with progressive integration of the period over which thickness change is measured after 650a (Fig 102). The cumulative effect of major calving events at the margins removes substantial volumes of ice there. The areas most affected are in the south west draining into the Nuuk region. Calving can influence ice thickness as far as the ice divide but the effect lessens considerably away from the margin. Rather than causing uniform ice thinning, the mechanism is characterised by the steepening of ice gradients from the calving focus towards the ice centre. Unless high calving rates are maintained, this gradient is reduced again as the margin readvances. Overall, the model appears to embody a limited mechanism for ice down-draw from unstable marine termini (Hughes 1985,1987).

When the model is run with no smoothing, the overall effect is similar. The major difference is that, with smoothing, the ice thins to a greater extent and recovery takes longer. Secondly, the differentiation between areas of thinning and thickening is less marked, particularly near to the ice shelf - ice sheet junctions. This is as one would expect if the model is not being ogged into periods of such marked calving activity

and relative quiescence.

4.3.3 What the maximum state models show

In summary, these maximum state models show the nature of short term variability during periods of long term equilibrium. The smoothed and unsmoothed scenarios demonstrate the effect of different calving regimes upon the short term behaviour. Calving termini show at one extreme continuous steady ice loss and at the other intermittent catastrophic ice loss. The tendency toward one form of behaviour or the other relates directly to the presence of suitably sensitive topographic basins, and to the magnitude of external or internal triggering mechanisms. In the unsmoothed model it appears that strong internal triggering is difficult to produce, but the introduction of a regular smoothing function can provide a dominant triggering effect if suitably sensitive margins exist. The nature of the calving regime affects the ice mass towards the centre but the response is reduced and delayed with progressive distance from the calving focus. The result is that in a more stable calving regime the ice sheet surface shows little short term change attributable to calving. Longer term patterns dominate. In a more unstable calving regime, the centre-margin ice gradients constantly adapt to calving activity through time and this becomes the dominant control on overall surface form.

The articial smoothing in the model tends to emphasise the overall affect of calving. The question is whether this effect is overemphasised relative to reality. The smoothed and unsmoothed models yield calving conditions which are on the one hand, catastrophic, and on the other, relatively even-paced, yet with a similar net calving rate. The most important point to make here is that the model is easily configured into situations which are inherently unstable. The actual propagation of a major calving event is achieved with a relatively small disturbance of the ice edge, albeit artificially introduced.

Moreover, these situations are not random. They relate entirely to particular characteristic topographic circumstances, namely calving bays. In other words, they occur at precisely the kinds of locations where workers like Mercer (1961), Hughes (1987) and Brown and others (1982) have argued that the catastrophic calving occurs in reality. The model supports the general view expressed by these authors that catastrophic calving events can cause the rapid evacuation of ice under favourable topographic circumstances. Further, the mechanisms inherent in the model suggest that

this process can occur even with simple expressions describing calving as a function of depth and enhanced sliding velocity as a function of buoyancy.

In addition, the model demonstrates the way in which the loss of ice by such a mechanism is conferred to the rest of the ice sheet. Under maximum conditions, the gradient of the ice basins involved is cyclically steepened and reduced; there is no major evacuation of ice over grounded areas. Under deglacial conditions, it will be shown that once an area calves, the balance is not restored. Calving bays and these associated drainage areas deglaciate first.

If there is concurrent warming, the steepened ice gradients that result tend to be closer to equilibrium deglacial mass balance profiles, and so are relatively stable once calving has occurred. Because of the limited spatial resolution, the model can only replicate such processes with large features but there is no reason to suggest that more finely resolved models could not be equally successful for smaller features.

4.3.4 Ice streaming behaviour in the model

The ability of the model to simulate ice streaming behaviour is best examined in maximum state situations. Because the model is isothermal, true frictional heat feedbacks in streaming behaviour cannot be replicated. However, the model does seem to be able to concentrate flow into major depressions and it is able to transfer mass loss at the calving margin back into the ice body. When a margin calves rapidly the gradient of the ice upstream of the calving front becomes steepened and therefore accelerates. This causes the ice in the depression to be evacuated more quickly and reduces the surface elevation and ice thickness. Because of the dependency of the sliding term on buoyancy, if the ice thins and is marine based, ice velocities are further enhanced.

The major deficiency in this respect is the inability to produce true streaming behaviour in non-marine-based situations. This slows down the potential to evacuate ice to the calving front and therefore maintains higher elevations and ice thicknesses. The higher elevations so caused are likely to over-predict surface mass-balance. The net conclusion is that the inability of the model to evacuate ice through fast-flowing ice streams to calving fronts gives it the tendency for greater stability. Within this context the fact that the 20km grid in the model can only represent streams of a minimum of 40km width is secondary. Ideally one would want to be able to model streaming behaviour with some resolution within the narrow (5-20km) corridors within which

it is known to occur.

4.4 Deglaciation tests

Five different deglaciation tests were carried out. The purpose of these was to examine the behaviour of the model in retreat scenarios, and in particular to identify common patterns in the retreat behaviour of the model that could be attributed to interplay of topography and climate elements. The first four of these experiments used the $-6°C$ temperature, -120m sea-level equilibrium model as the start condition (Run 118,100,000a), the fifth experiment (R135 - 'Deglaciation 2') used a $-8°C$ temperature, - 120m sea-level equilibrium state (R134, 50,000) to start the model. These starting conditions were assumed to represent glacial maximum equilibrium conditions in Greenland.

4.4.1 Stepped deglaciation using temperature only (Run 125)

The forcing temperature was set to $0°C$ at the start and the sea-level to -120m for the duration of the run. This means that all model forcing occurs right at the start of the run. The experiment predicts the 10,000 year lagged response to a single, stepped warming and the patterns associated with the readjustment.

The total volume plot for this run shows a total ice loss of about 21%, from 5.15 to 4.05 million km^3 (Fig 104). Most of the deglacial activity occurs within the first 1,000 years accounting for about 60% of the total ice volume loss. After about 5,500 years the model reaches a new equilibrium state closely approximating to the present day extent of the ice sheet. The maps of the ice surface and those of thickness change show the geographical distribution of the forced deglaciation (Figs 105-106). Within the first 3,000 years, the ice retreats from a largely marine-terminating to a mainly land-terminating state. The effect of warming is to steepen ice gradients throughout Greenland. Within the first 1,000 years, ice thins rapidly at all points on the margin. There is an intermediate annulus of ice thickening which is interrupted in areas draining into regions of significant calving activity. The southern ice dome centre thickens and the northern dome centre thins slightly.

The initial steepening gradients are interpreted as a direct result of the progression

to a warmer and hence higher energy ice model. The continuing effect of continentality and low temperatures over the northern dome fails to provide sufficient means to maintain the dome and it thins. In the south, central ice thicknesses actually increase during deglaciation. Throughout the period, additional drainage by calving is sufficient to modify the wider climatically induced trend.

There is a progressively slower evolution toward more stable conditions. Some of the thickening in the area immediately to the north of the southern dome may be a delayed response to reduced calving activity. Much of the subsequent change is associated with the remaining calving areas, but even in areas with land termini, the constant climatic signal produces variable retreat patterns.

In the remaining period from 5,500a-10,000a, the overall surface pattern appears largely unchanged in Figure 106. This is consistent with an overall equilibrium state. Such change as there is can be attributed to variable calving activity or to the application of the smoothing function.

The single forcing event gives a good opportunity to look at isostatic response to a perturbation (Fig 107). There is a rapid and marked response to the initial deglaciation. Fundamentally this is a mirror image of the pattern of ice thinning trend, but the removal of ice from the margins causes the model to draw lithospheric mass from considerable distances into the adjacent submarine and subglacial areas in order to allow uplift in the deglaciated areas. In the case of south Greenland this process of ice margin uplift is aided by the additional ice mass that builds up in the centre. There is some lag in isostatic adjustment. Significant uplift consistent with the initial deglaciation is still proceeding after 5,000 years, but it becomes modified by changes associated with ice growth after that time. Subsequently, isostatic movement is much less and can largely be related to continuing ice fluctuations near the margin.

It is worth noting that the near-equilibrium condition produced here is in all respects the same as that produced by taking a present day model and simply lowering sea-level; compare this run (Fig 105) to Run 60 (Fig 68). This convergence of forms suggests that the model tends towards the same equilibrium condition, from whichever direction or previous state it is forced.

4.4.2 Stepped deglaciation using sea-level only (Run 126).

Using the same starting conditions as above, this experiment was forced by raising sea-level at the start of the run from -120m to 0m. The forcing temperature was held

constant at $-6°C$ for the duration of the run, which lasted 10,000 years (Fig 110).

Perhaps the most important feature to note here is that the total magnitude of ice sheet change is less than the temperature-forced equivalent simulation. The ice volume falls from 5.15 to about 4.60 million km^3, a 11% reduction compared to the 21% reduction of the temperature-forced model. Just as with the temperature-forced model, there is rapid initial deglaciation, progressively decelerating to an equilibrium after 3000a-4000a, although the equilibrium reached is far less stable. About 72% of the total volume lost during deglaciation is removed within the first 1000 years ($5.15 - 4.75 Mkm^3$ total, Fig 108).

Deglaciation occurs because the water depth at the margin increases, thus enhancing calving, and because the sea-level reference used for the climate calculations shifts. The latter is only of minor significance, since the total accumulation and ablation rates show little change. The effect is to raise the entire mass balance theatre by only 120m.

Running mean calving rates (Fig 109) over an 1,100 year interval increase from around $400 km^3$ prior to deglaciation to over $1,000 km^3/year$ at the start of deglac ion. Much of this is associated with a single 50 year period toward the start of the run recording over $5000 km^3/year$. This $0.25 Mkm^3$ in 50 years, is about 5% of the entire ice sheet mass at that time. This loss coincides with the first smoothing application in the run. The ice thickness change maps (Fig 111) indicate that major ice loss occurs from all the margins in the first 1000 years. In particular, a sizeable chunk is removed from King Frederik VIII Land in northeast Greenland which could account for the majority of the single event mass loss.

After the first period of very high calving rates, there is an intermediate period during which the medium term (1,100 year mean) calving rates remain high and the total mass balance rates stay negative. Then, after the 3,000 years, the mass balance rates show medium and long term variability about an equilibrium. The shape of the ice sheet and the overall nature of the equilibrium state is more or less identical to the equilibrium condition of Run 121, also at $-6°C$ and 0m sea level. (Fig 63)

The isostatic response to deglaciation shows a similar pattern to that caused by temperature-forced deglaciation (Fig 112). The main differences are: the overall level of isostatic adjustment is less because less ice is removed; areas of initial adjustment are more localised than the broader patterns of the temperature forced model, reflecting the concentration of calving activity; since a marine margin with cyclic calving is maintained, unstable patterns of alternating uplift and depression continue

throughout the model run.

4.4.3 Stepped deglaciation using $0°C$ and 120m sea-level forcing (Run 127)

The stepped deglaciation model forced by both a temperature rise of $6°C$ and a sea-level rise of 120m is characterised by an initial rapid deglacial phase in the first 1000 years, followed by progessively slower deglaciation until the ice sheet approaches equilibrium after 6,000-7,000 years (Fig 113,114). As expected the overall volume loss is greater than the previous two experiments and falls from 5.51 to $3.80 Mkm^3$, a reduction of 26%. This is less than the sum of the separate effects (21%-temperature, 11%-sea level). The initial rate of deglaciation is much faster, with about 81% of the deglacial volume removed within the first 1,000 years. This represents a larger volume of ice and a larger proportion of the total volume than the total loss in the same period caused by the models forced by temperature alone (70%) and sea level alone (-12%).

The geographical distribution of the ice removal not surprisingly shares features common to both of the individual cases (Fig 116). The change within the first 1,000 years is so large that most ice thickness changes are greater than 32m. This makes comparison difficult, but, in general, the pattern seems to be dominantly controlled by the climatic signal as in Run 125. In other words, the initial tendency is to produce steepened gradients throughout. This allows the same thickening of the southern dome and a similar though less developed annulus of relative thickening around the centre. This annulus is interrupted to a greater extent in the vicinity of major ice basins than in the temperature deglacial model (Run 125), presumably because of the increased calving at the margins of those basins. The model is less close to an equilibrium state at the end of the 10,000 years, however, since it continues to lose ice mass.

The relative importance of the two mechanisms of deglaciation changes during the course of the cycle (Fig 113). At the onset both increased calving and increased surface ablation operate in tandem to produce rapid rates of ice removal. Up to 1000a in the run, the relative importance of calving is high. This is because the ice surface has been lowered and is closer to equilibrium with the warmer climate, while at the same time there are still active marine margins favouring high calving rates. The latter effect is transitory as isostatic recovery soon reduces the extent of marine

margins. After this stage, towards the end of the run, surface ablation dominates once more, though the magnitude is greatly reduced.

Isostatic readjustment following deglaciation has similar features to both previous models (Fig 116). The rebound is much stronger at 1,000a as can be seen by comparison of Figures 107 and 116. Subsequently, the three major areas of readjustment are associated with calving termini, in the Nares Straits, NE Greenland, and around Disko Island. These areas show a readjustment lag of the order 5,000 years. After this, the model shows very little isostatic major scale readjustment, but there is still considerable local movement associated with calving termini fluctuations.

4.5 Summary of the different aspects of the simple deglacial models

Before turning attention to more realistic, smoother deglacial scenarios it is worth summarising what the stepped models reveal about the response of the model to deglacial forcing. The combined effect of sea-level rise and a temperature increase produces a larger imbalance than each operating singly. With a larger initial imbalance, not only is there a larger eventual response, but also the speed of the response is faster, in both absolute and relative terms. The model responds quickly to large disturbances and settles as an inverse exponential. The duration of the lag also seems to increase with the magnitude of the initial disturbance. Since the pattern of ice retreat and isostatic readjustment is spatially uneven, this implies that the pattern will vary according to the magnitude and speed of deglaciation. Therefore, it is not reasonable to expect to find a similar retreat pattern for different scales of ice sheet disturbance played out over longer time scales. The pattern of retreat could conceivably vary with the speed of deglaciation. Therefore, any attempt to emulate or simulate real deglacial conditions needs to reflect not only the correct magnitude of forcing but also the correctly timed signal. Doubling the forcing function is unlikely to provide the same retreat patterns in half the time.

A second important implication which can be drawn from the stepped models is that the direction from which equilibria are achieved does not seem to matter. Over long time periods, models with the same defining parameters will eventually tend to the same end condition, whether they grow to that state or decline from a larger state. All the deglacial models achieve a quasi-equilibrium state which is similar and close

to that reached from building the ice sheet through use of the Initial Standard Run. The implication of this is that there is something about the geography of Greenland which favours an ice sheet equilibrium resembling that of the present day.

4.6 'Real' Simulations

Two attempts were made to produce realistic deglacial sequences. 'Deglaciation 1', Run 133, took the global sea-level curve taken from dated coral reefs in Barbados(Fairbanks together with an extremely simple three point temperature curve for the last 18,000 years based on interpretation of marine and intertidal shell fauna evidence from coastal waters (Kelly, 1985). 'Deglaciation 2', Run 135, uses the same Barbados sea level curve and a 30,000 year temperature curve based on the Camp Century ice core temperature record following an interpretation by Jenssen (1983) and Dansgaard and Johnsen (1969). The sea-level and temperature curves for both runs are shown with the total volume and mass balance plots (Figs 117, 118 and 125, 126)

'Deglaciation 1' produces topographic records at 1,000 year intervals, 'Deglaciation 2' at 250 year intervals. Both record total volume and mass balance information at 25 year intervals.

4.6.1 'Deglaciation 1', Run 133. The overall deglaciation of the ice sheet

The dominant influences on the total volume and mass balance graphs are the two temperature shifts at 6,000 and 13,000 years into the run (Figs 117-118). Figure 117 shows raw data values and figure 118 shows smoothed data calculated on a 500 year running mean. The first shows the full scale of the calving events but the second illustrates longer-term trends. Forcing by sea-level change makes far less evident impact. Up until the temperature change at 6,000 years, the total ice volume drops slightly from 5.15 to $5.00 Mkm^3$, about 3%. The volume loss is relatively constant, punctuated by substantial calving loss events. The rise in temperature of $+7°C$ at 6,000 years accelerates mass loss dramatically, removing $1.0 Mkm^3$ of ice in the next 1,000 years. The overall ice sheet loses 20% of its total mass during this process. At 13,000 years into the run a drop in temperature of $1°C$ causes a slow and steady increase in ice volume until the end of the run at 18,000 years.

The changes in ice thickness and configuration (Figs 119-120,121-122) reflect the total volume changes (Fig 117). In the first 5,000 years of the run, the only significant changes in the ice thickness resemble the dynamic fluctuations studied in detail in the maximum model cases. There is only 14m change of sea-level in the first 5,000 years, so sea- level forcing is small. The major ice streams show strong alternating ice gain and loss, whilst the central area slowly but continuously loses mass. Significant locations, such as around Disko Island, Ellesmere Island and NE Greenland periodically destabilise. When the temperature rises sharply at 6,000 years, the ice sheet surface is dominated by the new surface balance pattern. The pattern of change in ice thickness at 7,000 years is all but identical to that for the stepped temperature model 1,000 years after warming (Fig 121). Given the large and sudden change in temperature, this is to be expected.

The situation from 6,000a-13,000a can be thought of as intermediate between the two stepped deglaciation models, one forced by temperature alone, the other in combination with stepped sea-level rise. There is strong temperature forcing, and calving remains an important element in the overall loss. The differences in the ice sheet development can be explained almost entirely by the timing and nature of the sea level signal relative to the temperature changes. In the continuous Deglaciation experiment, sea-level change has already had an effect by 6,000 years, and so the warming impact affects a smaller ice mass than in the stepped experiments. Thus there is less loss related to temperature change. Another difference is that sea-level forcing continues for longer and is gradual and delayed rather than total and complete. This means that the importance of calving persists longer into the deglacial cycle, though at a lower level. Calving continues to be influential for at least 8,000 years into the run.

In the 13,000-18,000 part of the run, with the forcing temperature falling one degree to the present-day level, minor ice sheet regeneration takes place (Fig 122). This shows itself as increasing ice thickness in almost all sections, followed by continued growth to the north and a more balanced situation in the south. The growth pattern associated with this cooling is more or less an inverse mirror of the warming pattern.

When the pattern of deglaciation is viewed by section, it is clear that the overall loss of ice varies from place to place. In the course of the complete deglacial cycle the northwest sector loses 35% the total, the southwest 30%, the northeast 23% and the southeast 21%. The northwest sector is enhanced by the rather artificial loss over Ellesmere Island and without this the figure would probably be closer to the

north east sector volume. The conclusion is that the southwest sector has a higher proportional loss of ice during deglaciation than the others. This is mirrored in the maps which show that from 7,000a-13,000a in the run and with the single exception of Watkins Mountains area on the east coast, the land- based retreat distance in southwest Greenland is greater than in other areas.

Another important point to emerge from the simulation is the contrast in the rate of retreat in marine and terrestrial margins. After the initial loss from marine areas, subsequent retreat over the exposed land is far slower and fairly steady from 7000a-13000a years.

The isostatic adjustments associated with the deglaciation (Figs 123-124) are best interpreted in the light of the previous deglacial experiments. The first 6,000 years show little isostatic adjustment. Local changes are associated with major calving centres. The largest change occurs after the sudden warming at 6,000a, then follows a similar readjustment sequence to the other stepped experiments. The major deglacial isostatic pattern diminishes in magnitude 3,000-4,000 years after the temperature forcing and becomes dominated more by local effects. There is a small reverse trend causing depression associated with slow ice sheet expansion after 13,000 years.

4.6.2 'Deglaciation 2', Run 135.

The previous experiment showed that changes in temperature still dominate the pattern of retreat. To simulate smoother deglacial sequences the model requires smoother temperature forcing. This was achieved in Deglaciation 2 which runs for 30,000 years using the smoother temperature curve derived from Camp Century.

Total volume and mass balance trends

Figs (125-126) show the total volume and mass balance trend, together with the sea level and temperature forcing curves. For the purposes of analysis, it is helpful to consider the run as constituting four separate phases:

Phase 1 0-16,000a. Total volumes remain high but fluctuate.

Phase 2 16,000-21,000a. Sharp decline in total volumes.

Phase 3 21,000-26,000a. Low total volumes, minor loss.

Phase 4 26,000-30,000a. Low total volumes, minor gain.

4.6.3 The general development of the ice surface and global changes in ice thickness.

Phase 1: 0-16ka (Fig 127-128,130-131)

Total mass balance is more or less static during this phase but the negative balance moves from being calving-controlled to being ablation-controlled. The calving and ablation curves diverge increasingly through this phase but the net effect on total mass blance is minimal. Only right towards the end of the phase do the large amplitude calving events give way to a steadier ablation loss.

There is very little change in the ice configuration for about the first 13,000a. At this time, the majority of the ice sheet remains marine-terminating. As a result, the basins draining into major calving areas show alternate thickening and thinning ice as described before. Only from 13,000a-16,000a do significant areas in the south, south-west and parts of the east coast start to develop land termini. There is no great change in the profile of the ice sheet. The thickness change maps show that throughout the period there is slight thinning of the northern dome, whilst the southern dome thickens at a progressively faster rate. Once land termini start to appear in the south at around 13,000a this process accelerates noticeably, and the pattern of ice sheet thickness changes at 17,000a (Fig 131) resembles those related to the stepped temperature forcing pattern seen above.

Phase 2: 16-21ka (Figs 128,131)

At the start of this phase, calving rates start to increase again, pulling the entire mass balance curve sharply down. The changes in the thickness (Fig 131) show that at 16,000a and 17,000a the mass loss attributed to calving is associated with enhanced calving rates in a number of areas. Since the sea-level trend shows no breaks at this time the increased reversal is difficult to explain. When calving rates decline again the surface ablation rate is sufficiently high to keep the mass balance strongly negative. The second calving increase at 19,000 years can be directly attributed to the collapse of ice over Ellesmere Island. Subsequent to this point, calving rates drop to almost zero. This has to be treated with caution though because the model represents Ellesmere Island as a flat plane and so destabilisation can occur more easily than one would anticipate in reality. However, it reaffirms the ability of the model to produce catastrophic effects in certain situations.

The significant feature of this period is that the ice sheet retreat is dominated

by the strong warming. The ice limits pull back from the coast and become almost entirely land terminating. In some places the margins pull back behind the present day limits of the ice sheet. The ice sheet is still noticeably losing mass at the end of this period and thinning.

Towards the end of this phase a pattern of thinning develops which is indicative of warming. The southern dome loses mass in all areas, and the annulus of thickening around the northern dome retreats upslope. Consequently large areas of the lower flanks of this dome begin to lose ice.

Phase 3: 21-26ka (Fig 129,132)

The steadying of the mass balance rates in phase 3 is because the ice sheet is approaching a new equilibrium with warmer conditions and a high sea-level. So much mass has been lost within the ablation zones that the ice sheet has taken on a new profile and both ablation and accumulation rates are reduced because there is less ice covered area. But because the lower areas, suffering the most loss are mainly within the ablation zone, ablation rates are most affected by this process and total mass balance rates increase. Ice loss resumes towards the end of the phase after further warming to reach a minimum volume of $3.0Mkm^3$, $0.8Mkm^3$ less than the model records for present day conditions.

The ice topography does not change greatly in this phase. The slight cooling at about 21,000a, slows the thinning process in many areas, but the overall tendency for mass loss remains. Thinning almost stops around 24,000a, at a time when temperatures fall by $1.9°C$. At the end of the phase the ice sheet achieves its minimum size. The ice volume is $3.0Mkm^3$, about 55% of the maximum glacial size.

Whereas many areas of the ice sheet stabilise in this phase, the southern dome shows persistent ice loss in all areas. This results in a noticeable retreat of the southern ice to areas well within present day ice limits. It is possible to identify areas where calving occurs. In the early, relatively warm part of this phase, calving is nonexistent. With the slight cooling around 23,000 years, some of the larger calving basins infill with ice. With renewed warming around 25,000 years, all the calving areas reactivate, causing their feeder basins to thin.

Phase 4: 26-30ka (Fig 129,132)

The ice sheet is closer to balance, but there is renewed cooling which leads to further mass gain.

The ice sheet starts this phase from its minimum size at any stage in the run. The initial slight cooling causes the ice to start to thicken around the edges (27,000a). The pattern is similar to the one at 22,000a when the forcing temperature declines further, but the ice sheet is larger. However, this later cooling is more rapid and so the glaciation is quicker. The calving basins refill during the latter period of cooling.

With the most intense cooling in the middle of this phase, ice growth is strongest. The margins expand outward in all areas, most noticeably the southern dome. The expansion is slowing toward the end of the run, but nevertheless is still active. Some of the calving margins reactivate, particularly in the last 1,000 years.

4.6.4 Climatic vs calving influences

Overall, the passage from the maximum glacial state to the minimum mass and subsequent regrowth is climatically dominated. In particular, strong deglaciation only takes place once ablation rates become more influential than calving rates. When deglaciation is proceeding most rapidly during phase 2, calving has a comparatively small effect on the total balance. However, the increase of calving at 16,000a still largely accounts for the inception of rapid deglaciation. This occurs as a distinct and additional effect to the increasing ablation accompanying the temperature rise. In these early phases it is calving that keeps total mass balance strongly negative. Clearly, whilst much of the deglaciation, particularly later on, can only be ascribed to climatic warming, some additional process speeds up calving in the early part of the major offshore-onshore retreat at around 17,000a. The shape of the curve suggests that calving rates would steadily decline with continued deglaciation but here they are interrupted by the break up of the Ellesmere Ice dome which causes total calving rates to accelerate.

The conclusion is that calving, as an effective and major deglacial agent, is restricted to a very narrow time band. But within this short period its action can remove large amounts of ice. From 16,000a-18,000a, net surface balance loss is barely negative; at 16,000a it is positive, at 18,000a it has become negative. The calving is the most significant ablation mechanism from 16,000a to 18,000a during this period and accounts for much of the net total loss of about 0.6Mkm. This is over one third of

the total loss of about $1.5Mkm^3$ in the whole of phase 2, the most important deglacial period.

4.6.5 General isostatic trends.

Isostatic effects are shown by the maps showing the changes in bedrock altitude (Figs 133-135). There are distinct patterns related to each phase.

Phase 1, (Fig 133-134)

The changes in basal altitude resemble those of other maximum state scenarios. The only significant changes are associated with localised unloading from calving fronts and the flow of lithospheric mass into and away from these zones. They reflect the ice thickness changes taking place above them. As before, the main areas affected, are the Nares Strait, around Disko Island and Umanaq, Scoresby Sund, and King Frederik VIII's Land.

Phase 2, (Fig 134)

The onset of rapid deglaciation leads to a progressively stronger isostatic readjustment from 16,000a-20,000a. This is similar in form to the adjustments seen for the stepped deglacial models. However, the effect is more or less continuous throughout deglaciation, and the total deflection at any one time is less. This corresponds with the slower loss of ice. It is a shrinking concentric wave initiated inside the retreating margin. Rates of uplift increase to a maximum as the ice margin approaches and can decline more gradually once the area has become free of ice.

Phase 3, (Fig 135)

The overall adjustment in this period is fairly minimal. The most interesting fact is that the minor thinning and thickening associated with the small temperature fluctuations in this phase are reflected in corresponding isostatic trends near the margin. These patterns dominate any residual effect from the main deglaciation.

Phase 4, (Fig 135)

The isostatic patterns correspond to renewed glaciation. Because absolute fluctuations in bedrock topography become reduced with the smoother forcing signals, the

extent and lag time of continued readjustment are less. But long term effects clearly persist. Figure 135 shows the change in basal altitude after 23,000a in this run. Certain areas which were exposed before 18,000a still show steady adjustment over 22,000a-30,000a. For example, the area of strong uplift ($> 80m$) over Ellesmere Island expands.

4.7 Smaller areas - a detailed consideration of SW, S and E Greenland and comparison with the geomorphic record

These paragraphs look at the extent to which the pattern of deglaciation predicted by the model 'Deglaciation 2' can be related to the geomorphic record for the areas concerned. In particular, the large scales can be used to examine how the model relates to topography. At first, the discussion is concerned only with similarities in pattern. The problem of matching real and model chronologies is dealt with subsequently.

Detailed maps showing the deglacial sequence at 1,000 year intervals for south-western, eastern, and southern Greenland are given in Figures 136 – 144.

4.7.1 South West Greenland (Figs 136-138)

Phase 1 (Fig 136-137)

In the first 10,000 years, the margin shows very little change. There are some adjustments such as the small calving event in Disko Bugt at 3,000a, and the ice margins over Disko Island fluctuate in response to change in the ice streams to the north and south. Only after 11,000 years does the outer ice margin start to move back permanently. The marine terminus off low-lying Lersletten and Nodre Strømfjiord moves back as a parallel front, but remains a mainly marine terminus up until 16,000a. The ice margin due west of Sukkertoppen moves back and becomes grounded sooner than the ice to its south or north. By 15,000a, the Sukkertoppen massif becomes permanently exposed (Fig 137). From 11000a onwards, ice starts to disappear from Disko Island. The ice in the Disko Bugt embayment barely shifts position through this early phase of deglaciation.

Phase 2 (Fig 137)

In this phase, the ice becomes entirely land terminating. This transition mainly affects the low lying areas, and in general, it is achieved by isostatic uplift of these areas rather than by ice moving into areas already above sea level. This applies particularly to Søndre Strømfjiord. The ice margin is reluctant to move off the higher areas of Sukkertoppen and the Nugssuak peninsula but once it starts to withdraw back into lower areas, retreat speeds up. By the end of the phase, the ice has formed a fairly straight ice front compared to the more distinctly embayed form at the start of the phase. By the end of the phase the ice sheet margin south of Sukkertoppen has moved further back than the model's present day position predicts. To the north of Sukkertoppen the modelled ice margin is just slightly forward of the present day line.

Phases 3 and 4 (Fig 138)

The ice terminus retreats in warmer periods and advances in cooler ones, though the overall change is small and uneven. The maximum retreat position occurs at 25,000a-26,000a, after which the ice readvances closer to the present-day position. The furthest retreat of the ice behind the present-day position is about 100km and occurs due east of Sukkertoppen. By comparison, the retreat and advance in the Illulisat area is less marked The modelled position at the end of the run there is slightly further out than the present-day line.

4.7.2 East Greenland. (Figs 139-140)

Phase 1, (Fig 139-140)

As in SW. Greenland, the model predicts very little change in the earlier part of this phase. There is some minor fluctuation of the calving fronts. The ice margin starts moving at about 13,000a, somewhat later than in the southwest. Most noticeable is the retreat by the ice calving into Scoresby Sund, and the parallel retreat of the ice shelf off the coast of King William Land. The margin in the areas to the south moves onshore fairly rapidly, and then shows very little further change.

Phase 2, (Fig 140)

It is worth noting that the low area of Jameson Land, with two major calving bays to the North and south, has its ice supply cut very soon and deglaciates early. Further retreat occurs in and around Scoresby Sund and Knud Rasmussen Land. This region develops a mainly land terminating margin by 20,000a, similar to the situation in the southwest. The ice margin retreats slowly back off the Watkins mountains area. Again, retreat in the southern area is far less pronounced. In particular, the ice hardly moves from the high areas of King Christian IX Land compared to its full glacial position. By the end of the phase, the ice has become almost entirely land based.

Phases 3 and 4, (Fig 141)

There are minor fluctuations of the ice front associated with the minor relative warmings and coolings. By the end of the phase, the ice is close to that predicted for the present day.

4.7.3 South Greenland (Figs 142-144)

The modelled situation is a little simpler here than on either coast. As before, there is virtually no change in the first 10,000a, whereupon the ice margin moves fairly rapidly on-shore along most of the margin. It becomes land based by about 16,000a. In the warmest period at about 25,000a and again at 27,000a, the margin has retreated well inside what the model predicits for the present day. In the last 3,000 years of the model it starts to expand fairly rapidly once more.

4.8 Comparing the patterns of retreat with reality

This is a hazardous task. The disparities between the present-day real and modelled conditions have already been noted. At small scales, these appear relatively small. Naturally, at larger scales, they become rather more glaring. What is more, the overall resolution limits are being reached. Significant topographic features, like Disko Island or the Nugssuak Peninsula are covered by only a few model grid cells.

Moreover, whereas the best geomorphic records tend to concentrate on change between very narrow geological time bands (eg Ten Brink and Weidick 1974) the model is best adapted to looking at entire glacial-interglacial sequences. The geomorphological record for the early part of the retreat in southwest Greenland is the least well known yet the model results emphasise this part as the most dynamic part of the deglaciation. From a modelling point of view, evaluation at this scale is tenuous because the simplifying assumptions used mean that the poorest representation of the ice sheet is at the margin. It is likely to produce poor simulation in very detailed considerations of the margin. Therefore detailed comparisons are approaching the limits of testability. As a result, broad regional trends of the overall geomorphic record are used for comparison rather than detailed, site specific, examples. The best geom orphological evidence comes from southwest Greenland because the ice retreat is spatially the best resolved there.

4.8.1 South West Greenland

Figure 145 shows a summary of the main stage positions in South West Greenland from a review by Funder (1989). The major similarities between the modelled and geomorphologically interpreted situations are as follows:

1. The ice deglaciates from the Disko Bugt area much earlier than the surrounding land both in the model (Fig 137) and according to the geological record.

2. There is a tendency for ice to linger to the north of Disko and on the Nugssuak Peninsula in the model (Fig 137) as is the case at the Taserqat stage.

3. In both the model and the geological record the ice margin retreats over Lersletten (Fig 137) before moving off the Sukkertoppen plateau.

4. Retreat over Lersletten and Nodre Strømfjiord is relatively rapid and in the early phases is characterised by a marine front moving back into isostatically depressed submarine areas.

In the middle of the retreat sequence isostatic rebound is sufficient bring the land back above sea level within a time span of about 1,000 years. This does not however seem to greatly affect the overall speed of retreat since temperatures attain high levels at this time. Nonetheless this pattern of retreat phased with marine transition fits the pattern of the early and middle part of the latest deglaciation in Greenland (Ten Brink 1974).

4.8.2 East Greenland

Knowledge about the actual sequence of events in East Greenland is far more scant. Figure 145 shows a known ice position in the Milne stage at 10,000BP and Figures 139-141 retreat positions predicted for the model.

The major similarity here is the prior deglaciation of Scoresby Sund before the ice goes completely from Jameson Land at the 10,000 BP Flakkerhuk stage (Funder 1990). Some authors (Hjort 1979) argue that the geological record in S Jameson land indicates the presence of an unglaciated enclave there towards the end of the last glaciation. The model results suggest the contrary, that given the glaciological situation in East Greenland under maximum ice conditions, the presence of such an enclave is not tenable (Fig 136). This agrees with the most recent review by Funder (1990) (Fig 145).

4.8.3 South Greenland

The major model mismatch occurs in South Greenland. At maximum it does not really extend as far as the geological record seems to show. It retreats rapidly under warming but there is no way of telling whether the extreme retreat it reaches at 27,000a in the model had a real equivalent. It certainly does not expand out as far as the present limits, but then neither does it in the present day modelled equilibrium. Overall this seems to suggest that in Southern Greeenland the model tends to under predict glaciation in most scenarios.

4.9 Chronological matching

Even from these limited comparisons, it is evident that the model predicts deglaciation far earlier than seems to be the case from dated geomorphological features. The West coast Tasersuat and the East coast Milne stage are both dated at around 10,000BP. The closest model equivalents occur at 14,000a and 15,000a respectively, or 16,000BP and 15,000BP. The model equivalent of the 80,000BP stage on the West Coast occurs at about 20,000a or 10,000BP.

In each case here the modelled changes seem to occur far earlier than the real equivalents. Further, the time gap is wider for the earlier example. This suggests one of three things:

1. The timing of one or other of the forcing signals is wrong. This applies partiularly to the Camp Century core dates, since they are derived from assumptions about ice flow and strain rates.(Dansgaard and Johnsen S.J. 1969).

2. The model responds more quickly to the forcing than it should.

3. The dating of the geomorphological evidence is wrong.

Of the three possibilities, the first is the most likely cause of the mismatch.

4.9.1 How well does the model replicate real ice sheets ?

To conclude this chapter, it is important to summarise the extent to which the model can be assumed to be saying something about real events and real processes. It is worth highlighting areas of agreement between what the model predicts and what is known about the Greenland ice sheet.

Given that the ice dynamics and climatic parts of the model were formed separately from fundamental analysis, and given that there was only a limited predetermined connection between these and the topographic input, the model tends to produce extremely close imitations of the ice sheet, both for the present day and for maximum ice conditions. The temperature deviation required to force the model between these states is consistent with what is known about the present climate and palaeotemperatures (Kelly 1985, Dansgaard et al 1971, Radok et al 1982). There is a certain reassurance that, after the complexities of model formulation and testing, the results are consistent and corroborate one another.

In addition to this agreement between the present-day and maximum there are a number of ways in which the model appears to agree with views about the nature of deglaciation in Greenland, both in form and process. The extent of the topographic 'fit' between stages of the model in simulated deglaciation and those that are indicated by the geomorphological record has been shown. The model cannot record fine detail but modelled regional trends have parallels with the real evidence. One problem remains. The stages of the geomorphological record are generally interpreted as being caused by relative standstill or readvance of the glacier margin (Kelly 1985). On the other hand, the snapshot views of the model produced pictures which look like the real 'stages' but are in fact a single record of a continuous retreat.

Debate occurs over whether the geomorphological 'stages' in Greenland are caused dominantly by climatic perturbations or whether they merely reflect the fact that the

ice sheet margin halts at topographically favourable locations. In general, the former view, whose main proponent is Weidick (1968, 1972b), has received more attention, although other authors (Warren and Hulton 1990, Kelly 1985, Funder 1979) have suggested that the latter is equally or more important. Because, in Run 35, the model is driven by a smooth climatic signal, whose gradient does not reverse during the main deglaciation, it cannot be expected to show standstills from climatic reversals. On the other hand, it does support the conclusion that certain topographic features, in particular, calving bays and high ground, tend to encourage and retard the rate of retreat, thus creating areas of relative standstill. Over other areas, retreat is continuous. The core of the argument then returns to the geomorphological record and the way in which regional stages are constructed from actual features. In certain areas, the geomorphological record is characterised by an overall sparse covering with intermittent large features which tend to occur at topographically significant points. Such is the case in the Iliminaq region immediately to the south of Illulisat (Jacobshavn). Here it is argued that the identification of regional patterns is somewhat tenuous because the correlation of, and interpolation between the major features is speculative. Only relative, rather than absolute, synchronicity can be established. The reality of large scale contemporaneous stages is doubtful. In the Søndre Strømfjord area, however, it is extremely difficult to suggest that the large continuous features which exist are anything other than contemporaneous.(Weidick 1968, Ten Brink 1971[a]) Whether this synchroneity is related to climatic effects or, for instance, from the stemming of retreat higher up as calving intensity in fjords declines is difficult to establish. Moreover, the record in this area is unique. The problem, therefore, of trying to establish whether the model might indicate the cause of such standstills is more poignant. The question of whether standstills are real in the first place, however, depends on the interpretation of the evidence. The model suggests that limited extent regional standstills can occur because of topographic configuration alone.

In addition to these conclusions about the large-scale deglacial pattern and its causes, the model provides some other ideas about the nature of deglacation. It suggests why, in general, raised beaches dated around 5,000 BP are close to present sea- levels. Ten Brink(1971[b])and Sugden(1972) show that in southwest Greenland, relative uplift is greatest for beaches dated near the start of glaciation at around 10,000 BP and the shoreline came progressively closer to present sea-levels up until about 5,000 BP. The model indicates that isostatic rebound in the early postglacial was very rapid, exceeding rates of sea level change, but, by a stage which equates

roughly to 5,000 BP, both isostatic recovery and sea-level rise had slowed to smaller and similar rates.

Weidick (1968) concluded from evidence of peat-rich present-day moraines that, in South Greenland, the margin retreated behind the present ice front after about 5,000 BP. The model indicates similar events, and, if the Camp Century climatic record is correct, shows that this is climatically induced. Moreover, even though the deglacial model does not restore the margin to present conditions, it gets to a position close to the present-day modelled simulation. In general, the model also shows that the south of Greenland is more sensitive to climatic perturbation. This again concurs with Weidick's (1968) conclusion that the margin readvance during the 17th century 'little ice age' is best observed in South Greenland. Deglaciation over Sukkertoppen and Disko occurs in the model . Geomorphic evidence suggests this occurred and that local glaciation is a more recent feature (Sugden 1972) . The model requires conditions cooler by about $-1°C$ from present to restore ice cover in Sukkertoppen and by about $-7°C$ for Disko. The mismatch here is between present conditions in the model and the real world but it nevertheless suggests that, during overall deglaciation, ice removal over the area is likely to occur.

There are some final points that can be made about large scale controls on the overall stability of the ice sheet. In addition to the dynamism of the model's calving bays, it also indicates the link between mountains and mass balance. If the ice sheet margin is pushed into high ground with deglaciation, retreat stalls because the glacier margins head into relatively mass positive areas. The opposite applies to retreat into lower areas. Higher areas show less sensitivity overall. It is the basic interaction of the climatic model and the topographic surface at any one time that determines the stability of the model in grounded conditions. In marine conditions, extent is controlled by water depth. Therefore, as the Quaternary record also indicates, the maximum modelled extent is essentially confined to the continental shelf because beyond this, water depths create calving at magnitudes greater that the mass flux which the limited ice sheet surface can supply. Even under maximum conditions, Greenland has a smaller area of net accumulation than Antarctica relative to its calving front length. Calving can act as a more effective limit on size.

These processes go some way to indicating the differences between East and West Greenland during retreat. The west is low and flat with an extensive continental shelf, whereas the East is relatively mountainous near the coast and has a narrower shelf. On the East, the ice can never build out as far, never deglaciates as far into

the mountains, and is relatively thin over the mountains. On the West, the ice builds out further, deglaciates further and is relatively thick. Upon glaciation, much larger volumes of ice are involved on the West than the East, the deglaciation spreads further and there is more uplift. The relative enrichment of the geomorphological record on the west and its attractiveness for research is easily explained.

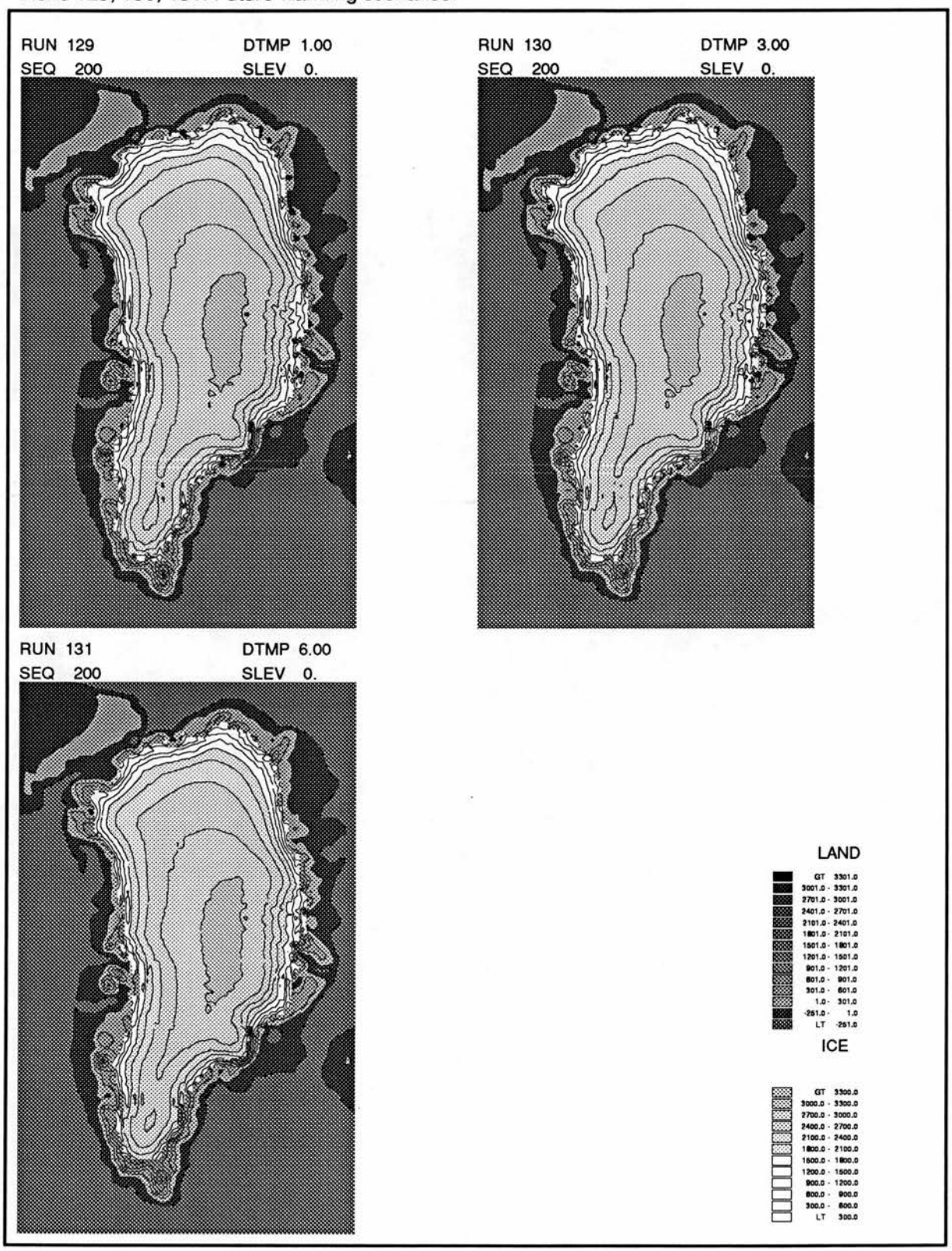

Figure 70: Modelled land and submarine surfaces with superimposed ice surfaces for forcings of $+1°C$,$+3°C$ and $+6°C$ modelled for 200 years into the future.

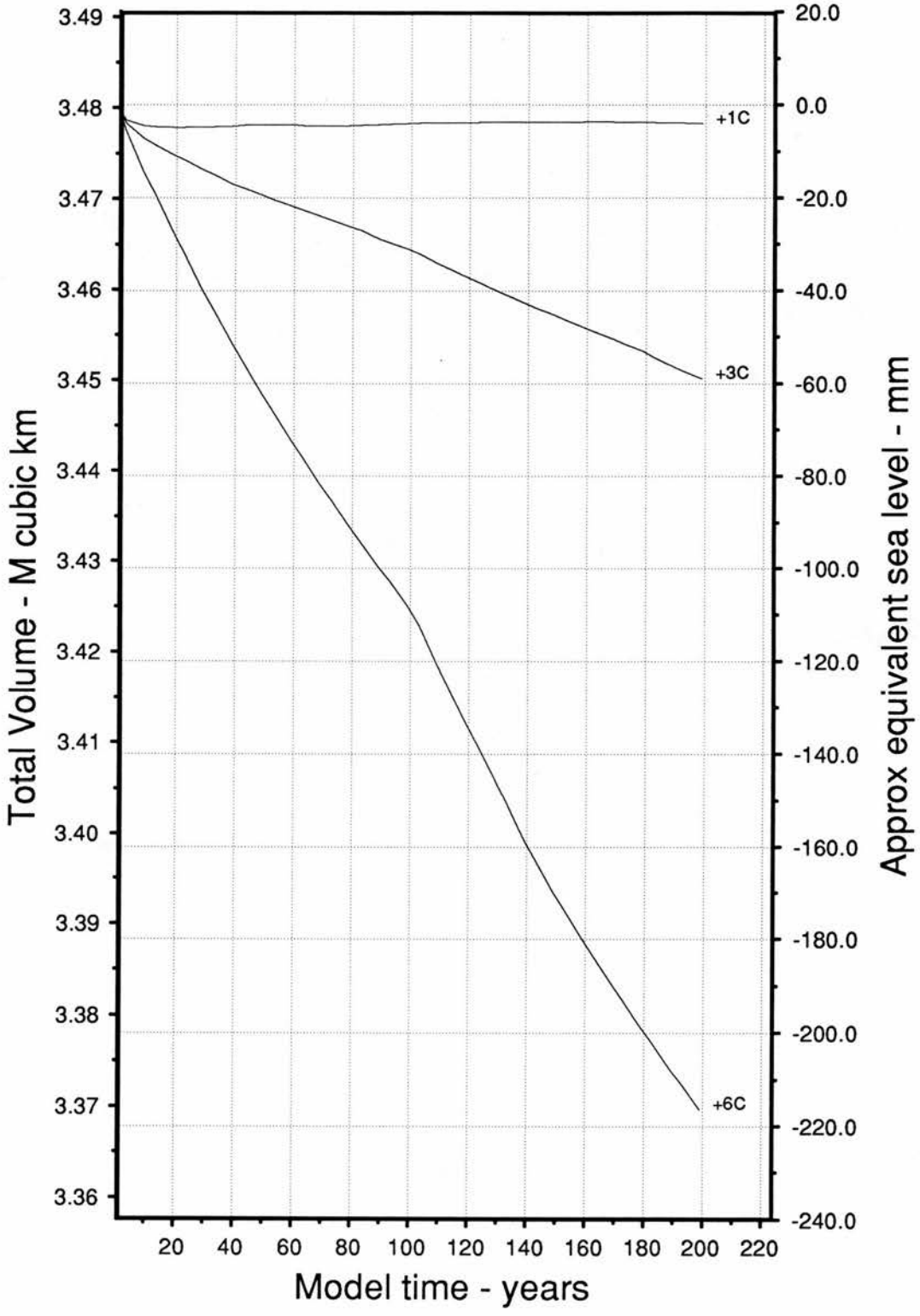

Figure 71: Total ice volumes for forcings of $+1°C$,$+3°C$ and $+6°C$ modelled for 200 years into the future using the ablation forcing value of 0.4 (Non-zero y-axis Runs 129, 130, 131).

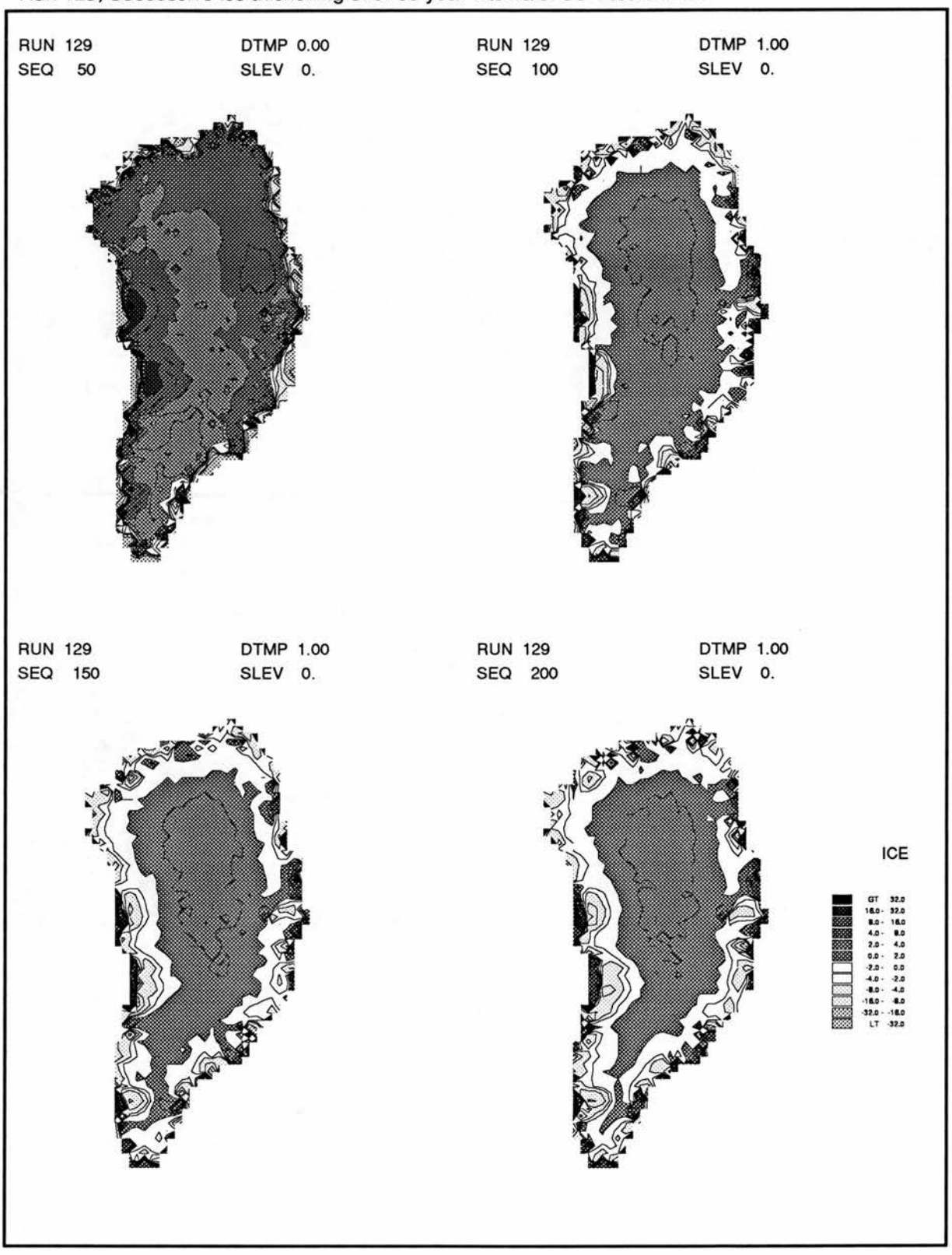

Figure 72: The change in ice thickness over 50 year intervals for 200 years forward from the modelled present-day equilibrium. A forcing of $+1°C$ is used with an ablation forcing value of $F = 2.5°\Theta/°C$ (Run 129).

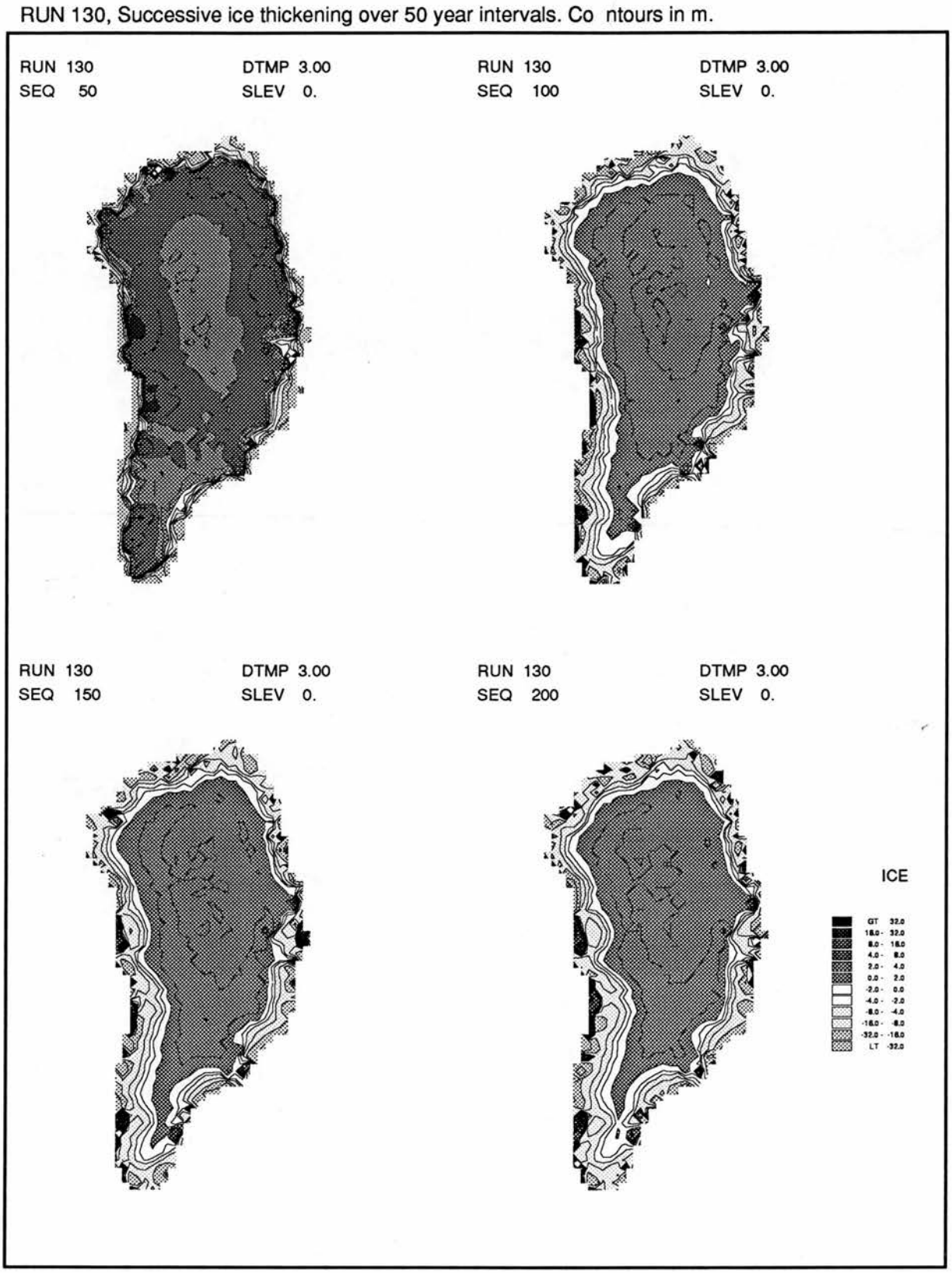

Figure 73: The change in ice thickness over 50 year intervals for 200 years forward from the modelled present-day equilibrium. A forcing of $+3°C$ is used with an ablation forcing value of $F = 2.5°\Theta/°C$ (Run 130).

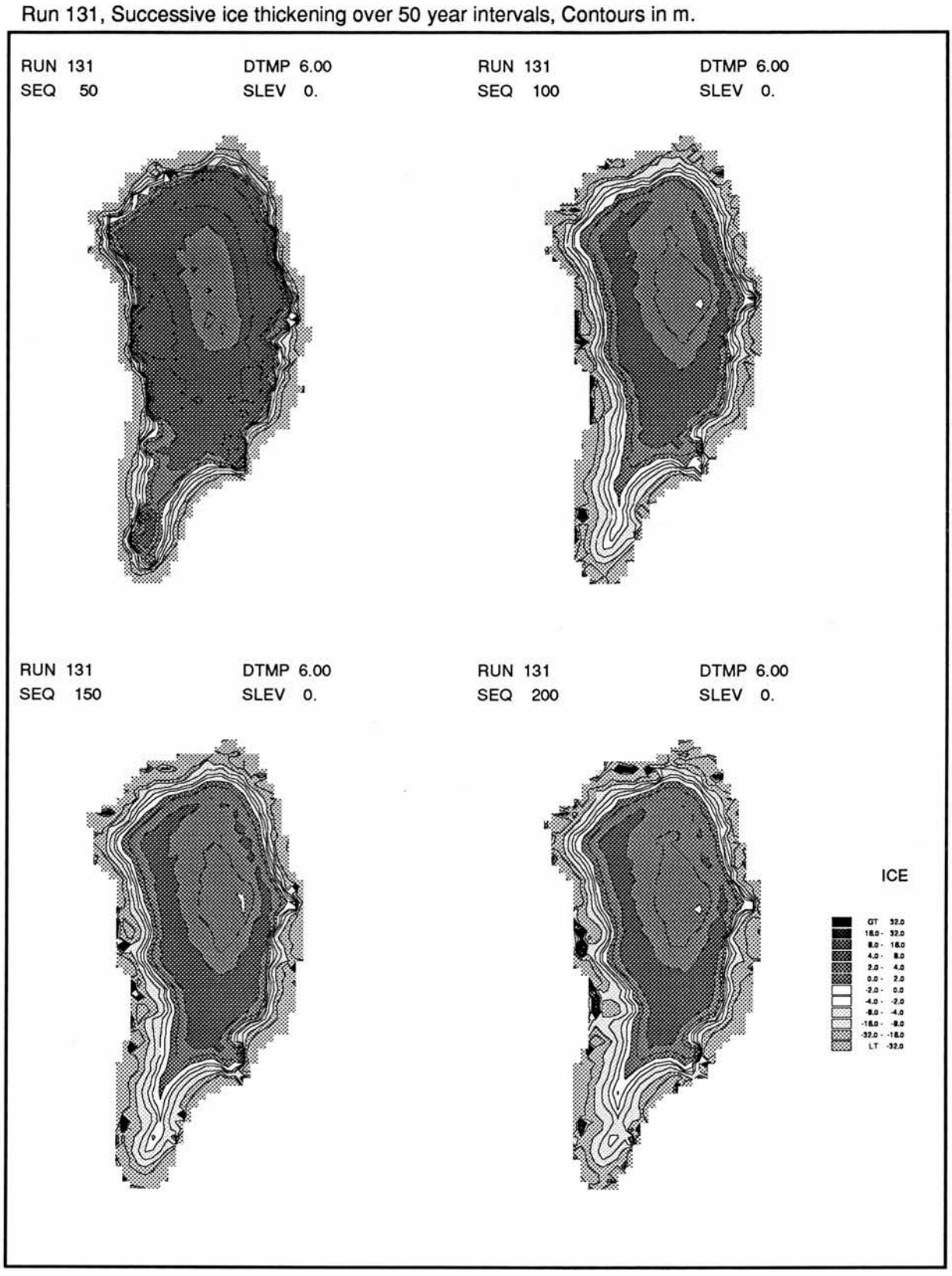

Figure 74: The change in ice thickness over 50 year intervals for 200 years forward from the modelled present-day equilibrium. A forcing of $+6°C$ is used with an ablation forcing value of $F = 2.5°\Theta/°C$ (Run 131).

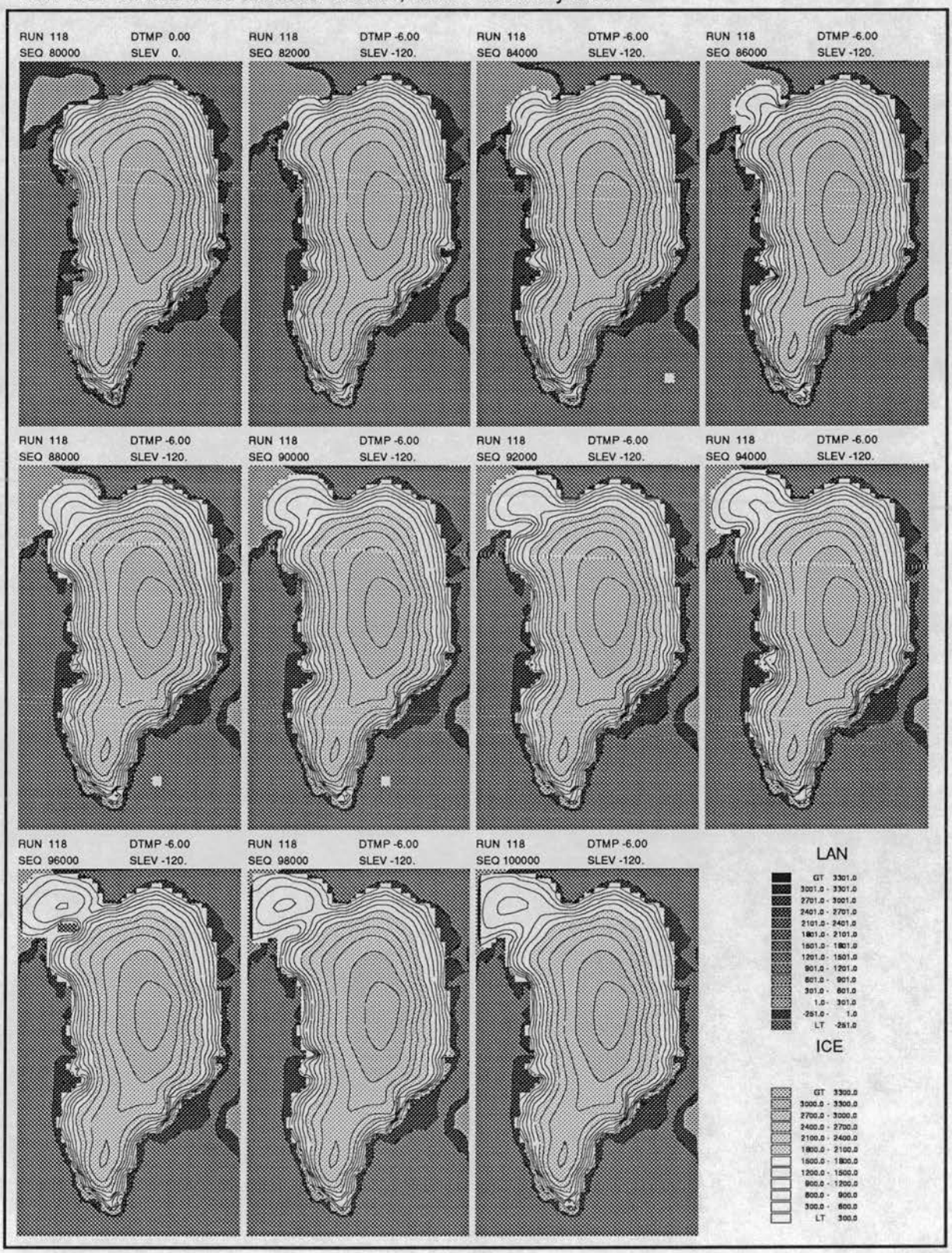

Figure 75: Modelled land and submarine surfaces with superimposed ice surfaces whilst moving the model between two different maximum state conditions.

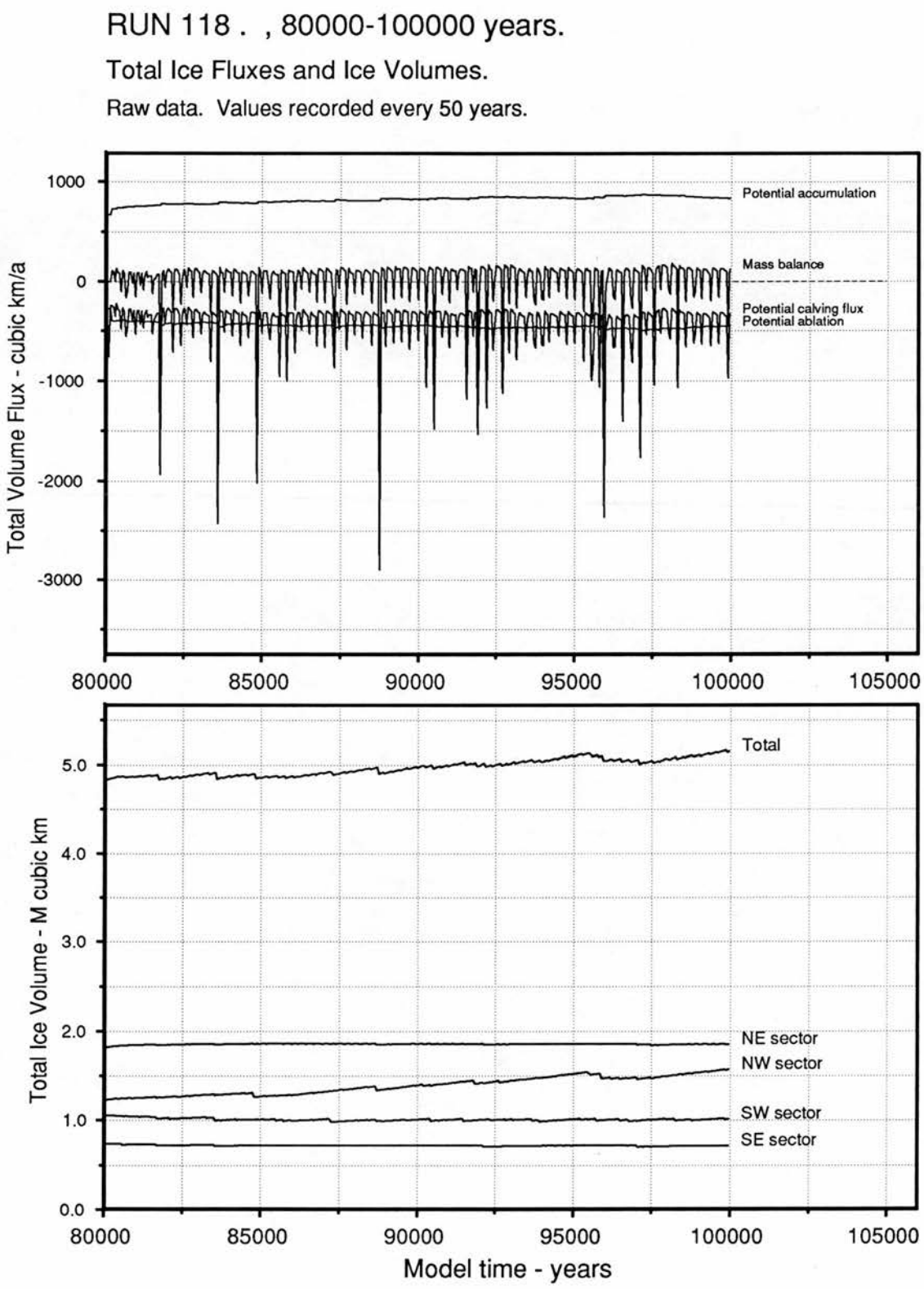

Figure 76: Total ice volumes and mass balance whilst moving the model between two different maximum state conditions.

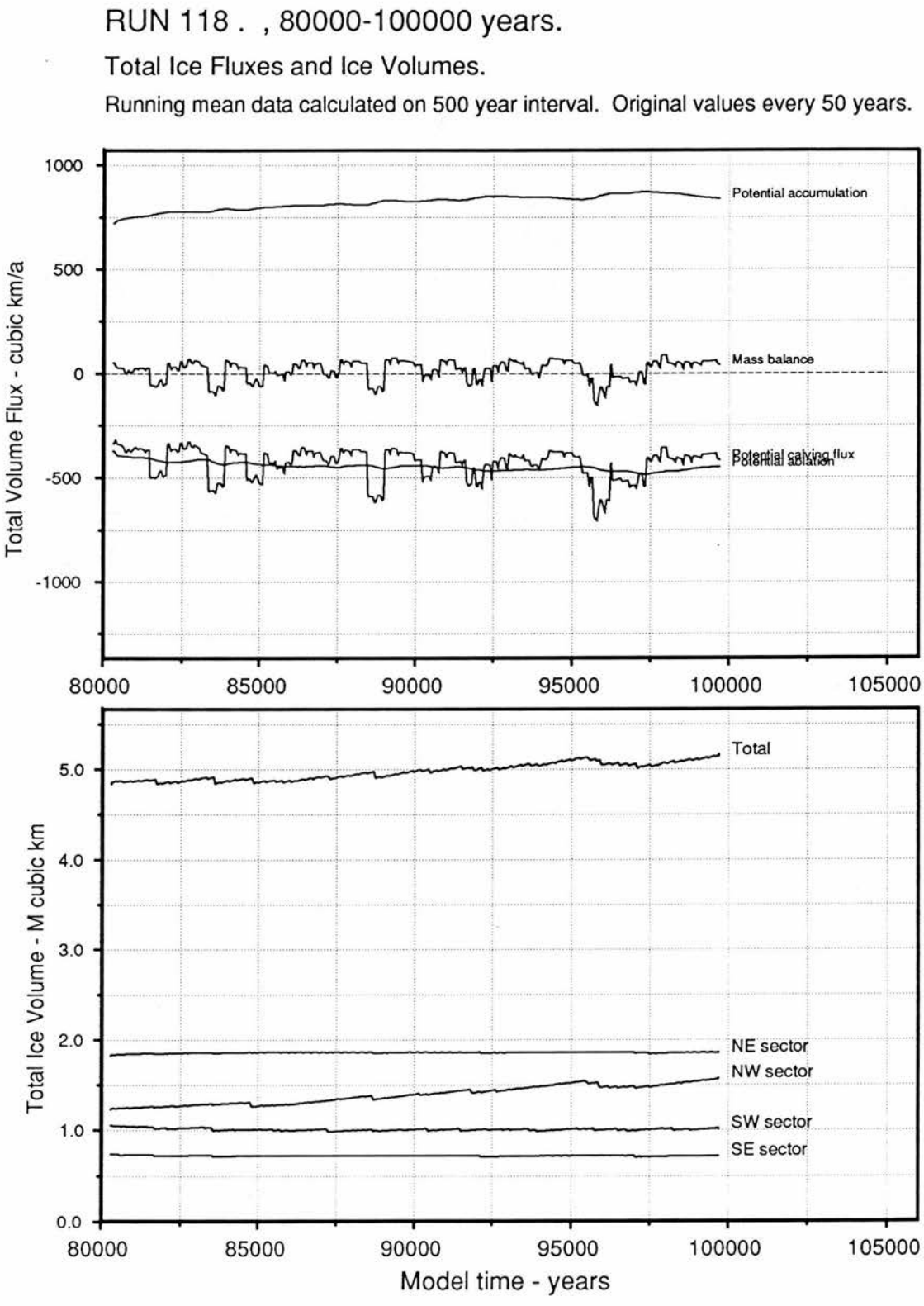

Figure 77: Total ice volumes and mass balance calculated as a 500 year running mean, whilst moving the model between two different maximum state conditions. There is a small change in total ice volume but the magnitude of the calving variability increases.

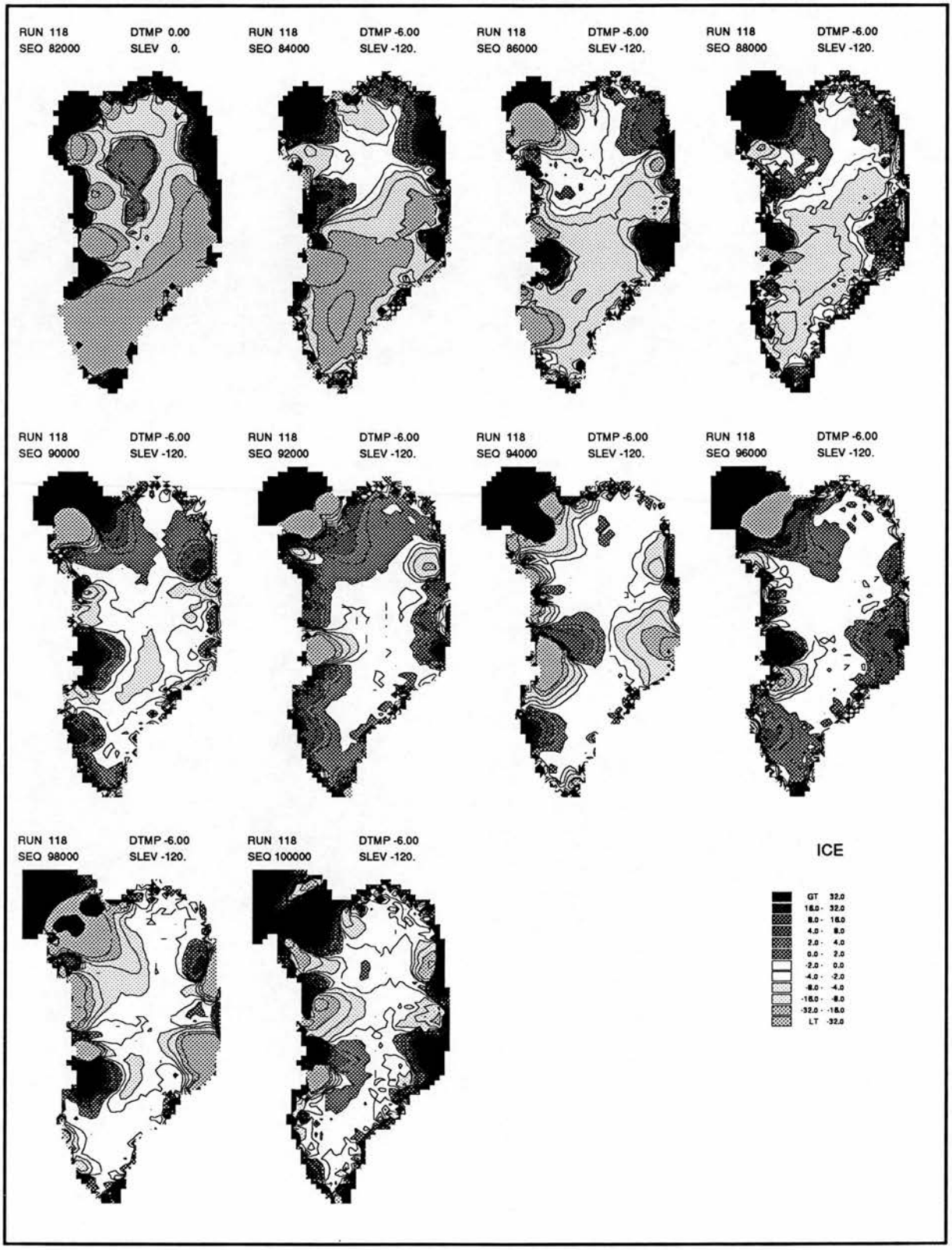

Figure 78: The figure shows changing ice thickness calculated for successive periods whilst moving the model between two different maximum state conditions. The modelled ice thins early on except at the margins and over Ellesmere Island.

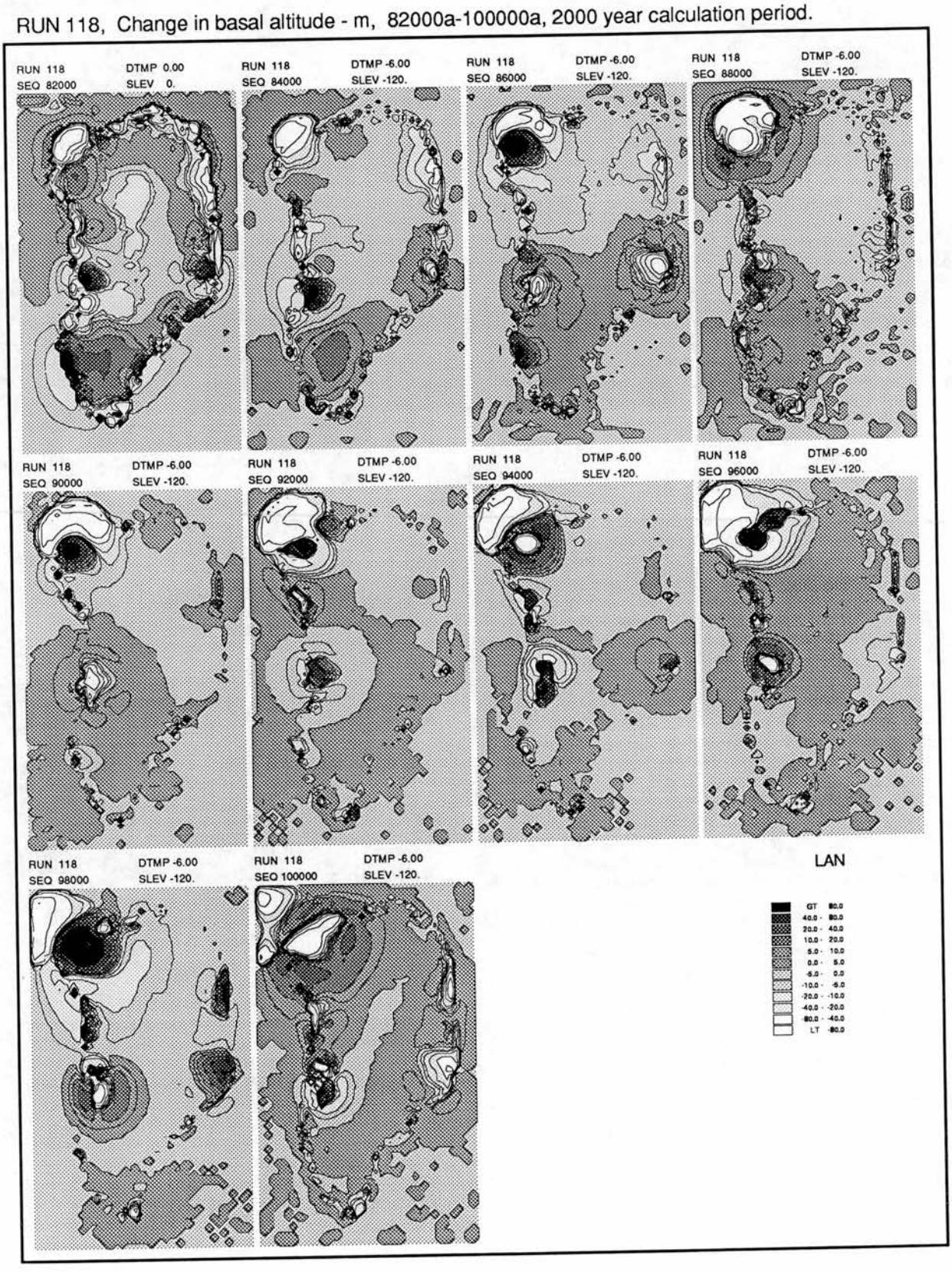

Figure 79: The figure shows changing basal elevations calculated for successive periods whilst the model moves between two different maximum state conditions.

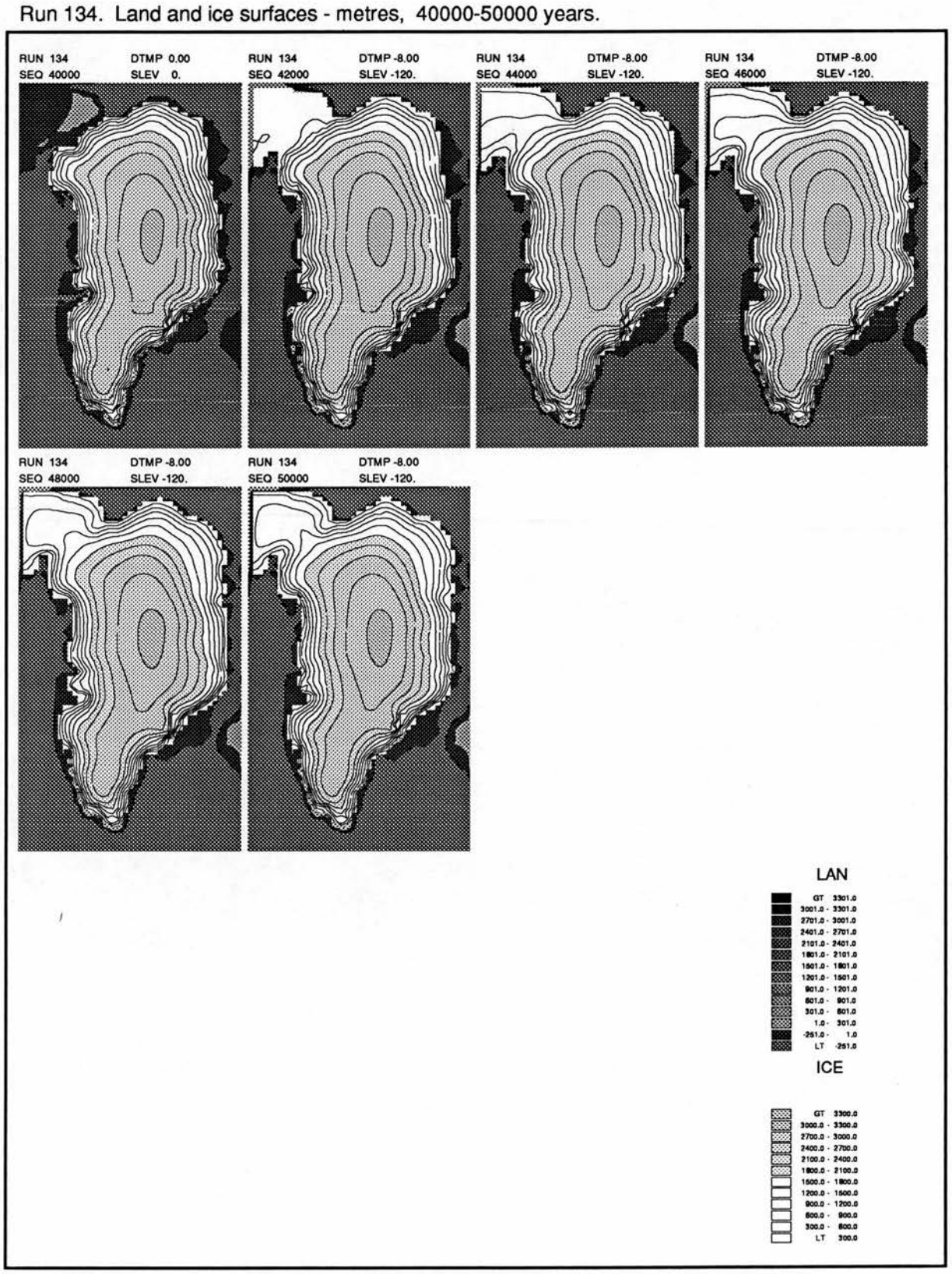

Figure 80: Modelled land and submarine surfaces with superimposed ice surfaces whilst moving the model to an equilibrium at $-8°C$ The ice expands to occupy a larger area over the continental shelf.

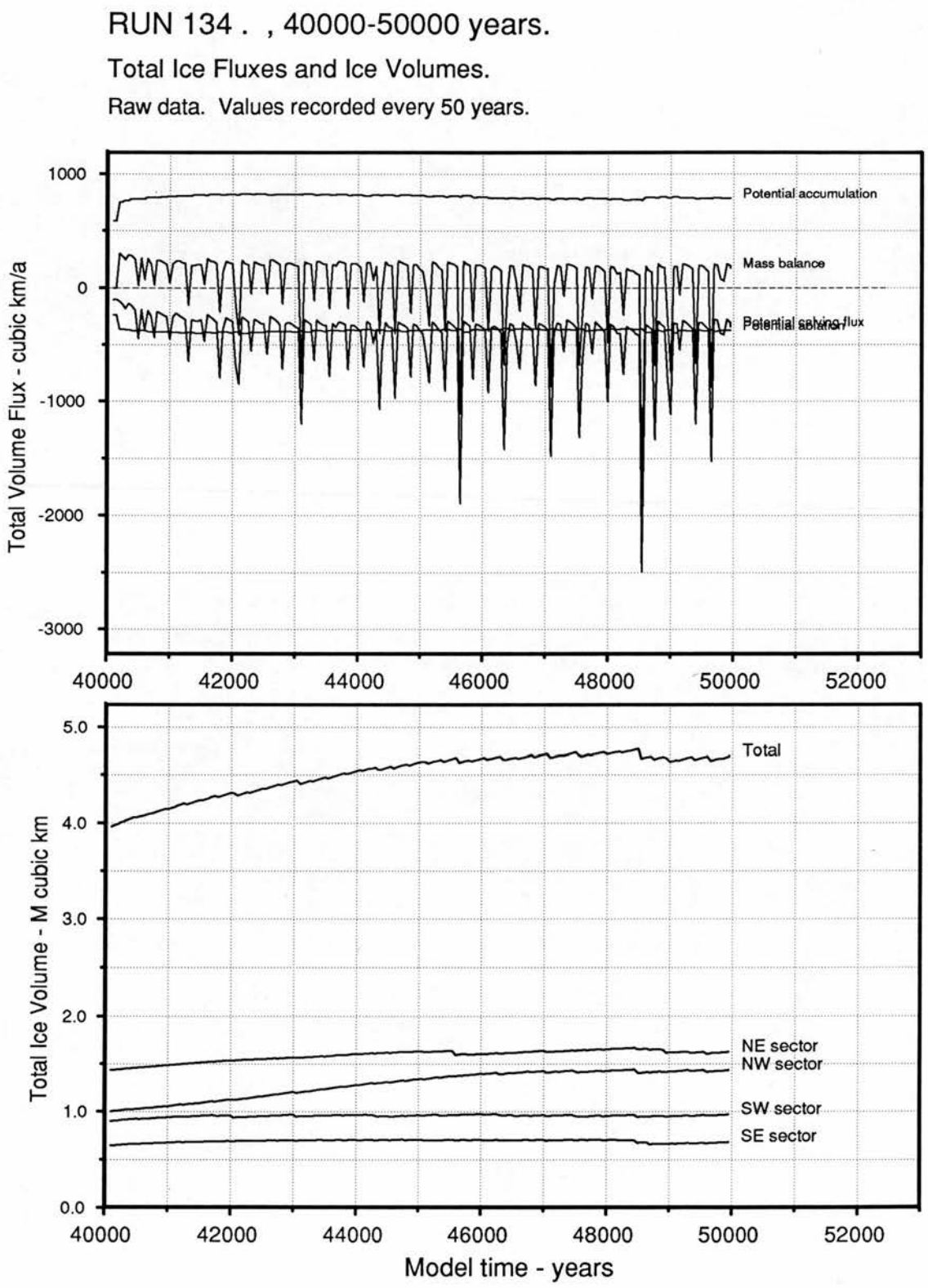

Figure 81: Total ice volumes and mass balance, whilst moving the model to an equilibrium at $-8°C$

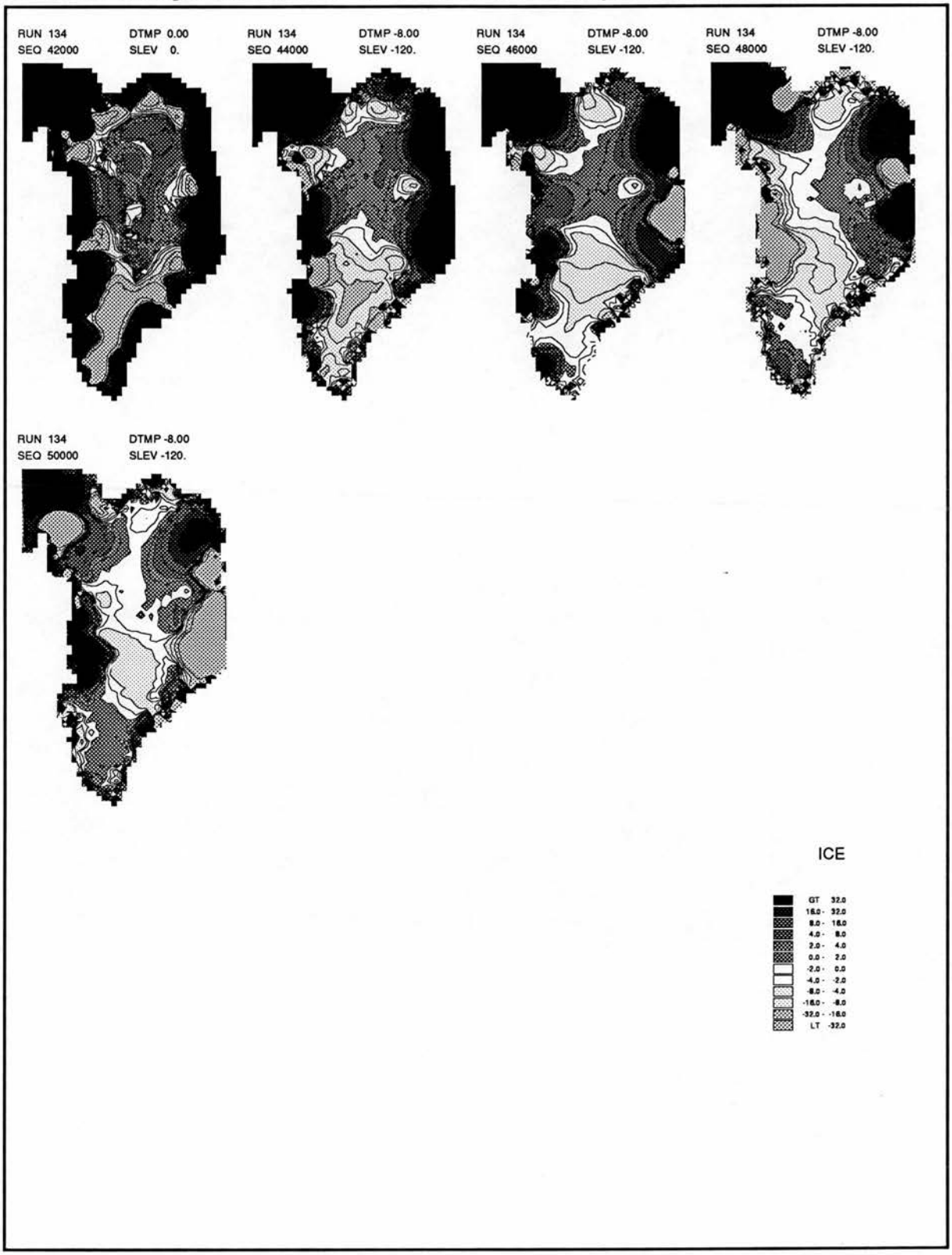

Figure 82: The figure shows successive changes in ice thickness between record steps whilst moving the model to an equilibrium at $-8°C$

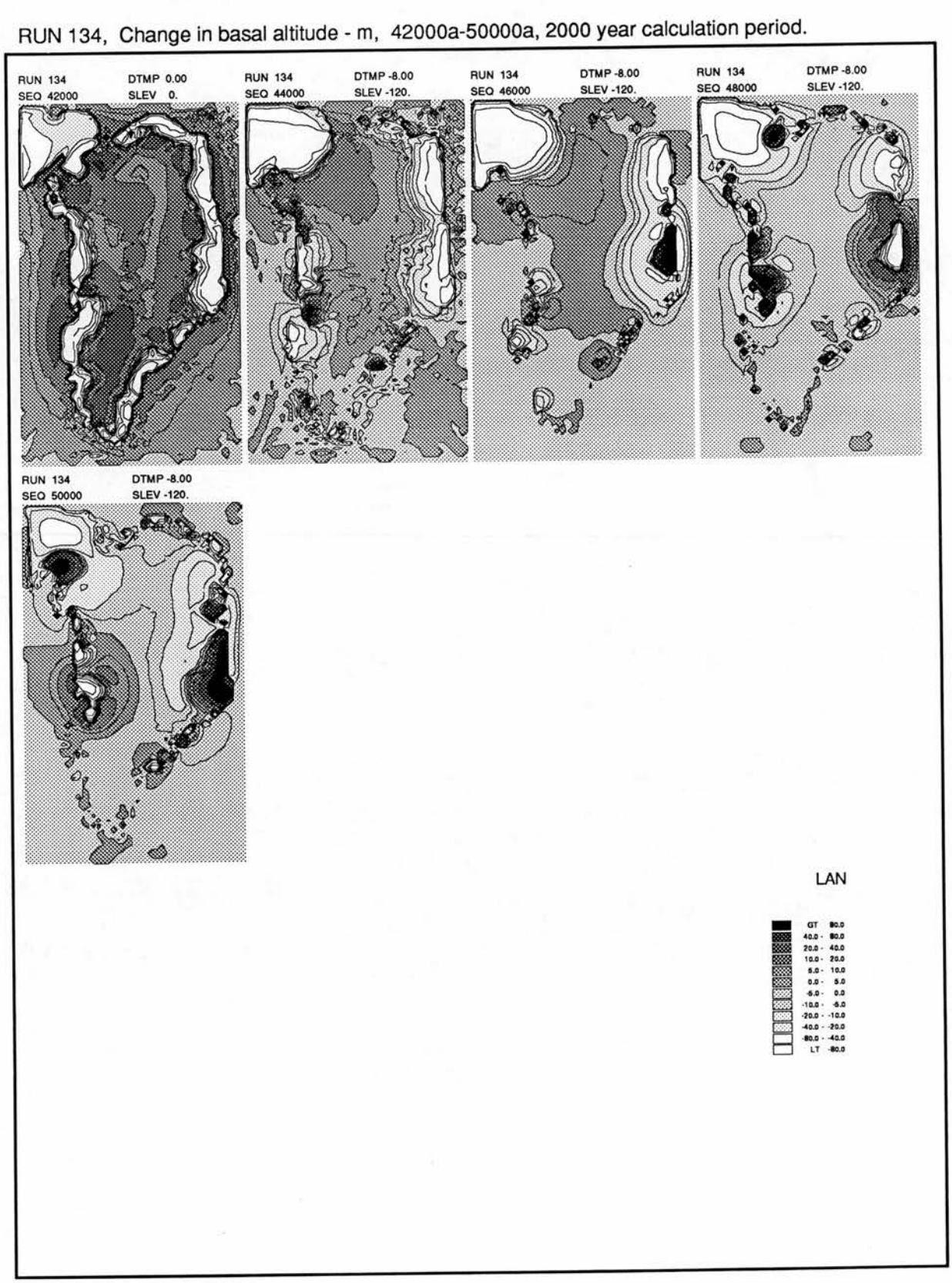

Figure 83: Successive changes in basal altitude whilst moving the model to an equilibrium at $-8°C$

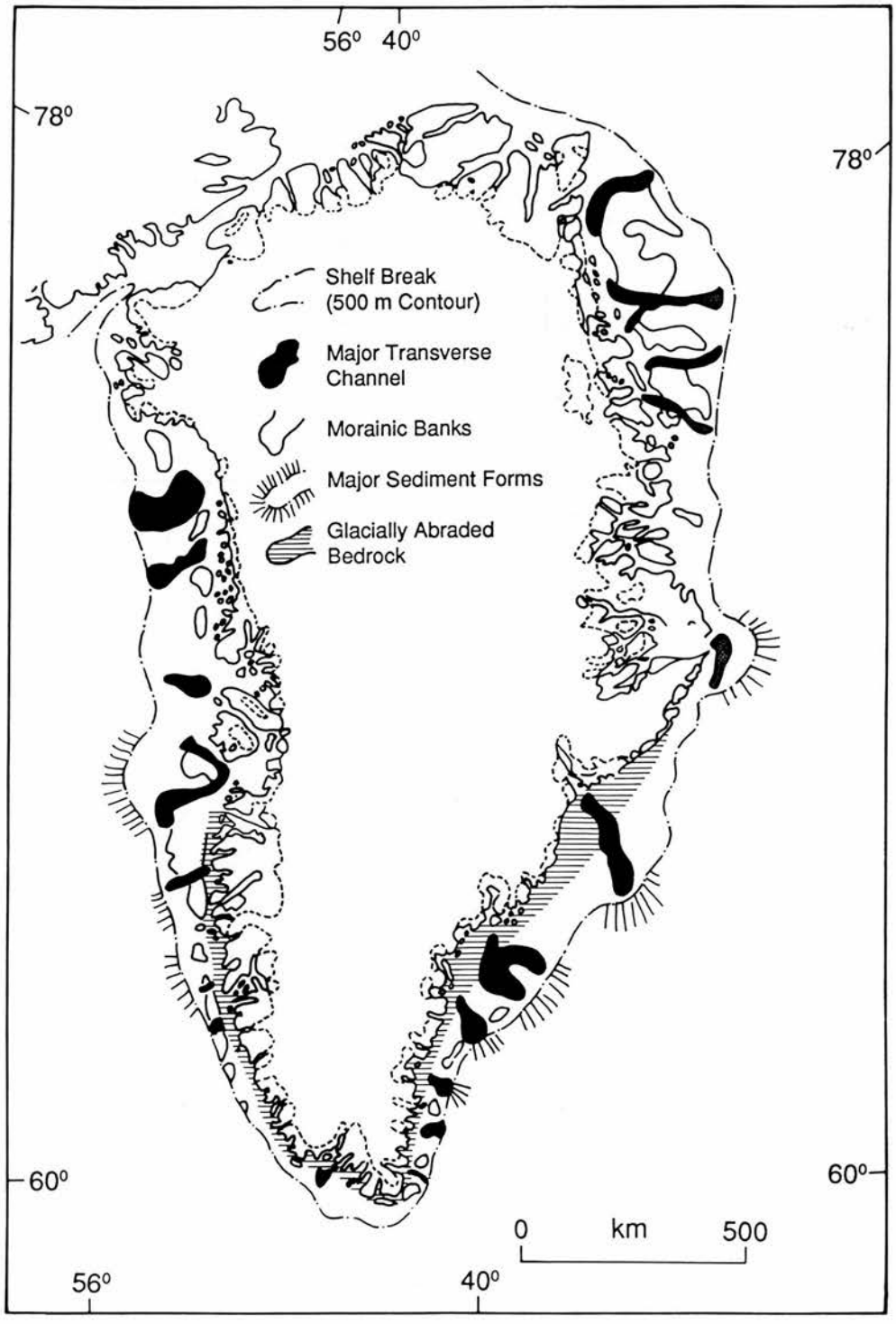

Figure 84: The delimitation of maximal glacial limits and the occurrence of glacially scoured bedrock. Redrawn from a synthesis by Funder (1989). Sources: Brett and Zarudzki(1979); Sommerhoff(1983); Larsen(1983); Nichols(1969); Kelly and Bennike(1985); Funder and Hjort(1980); Hjort(1979, 1981a, 1981b); Koch and Wegener(1911); Brooks(1979); Bogvad(1940); Kelly(1985).

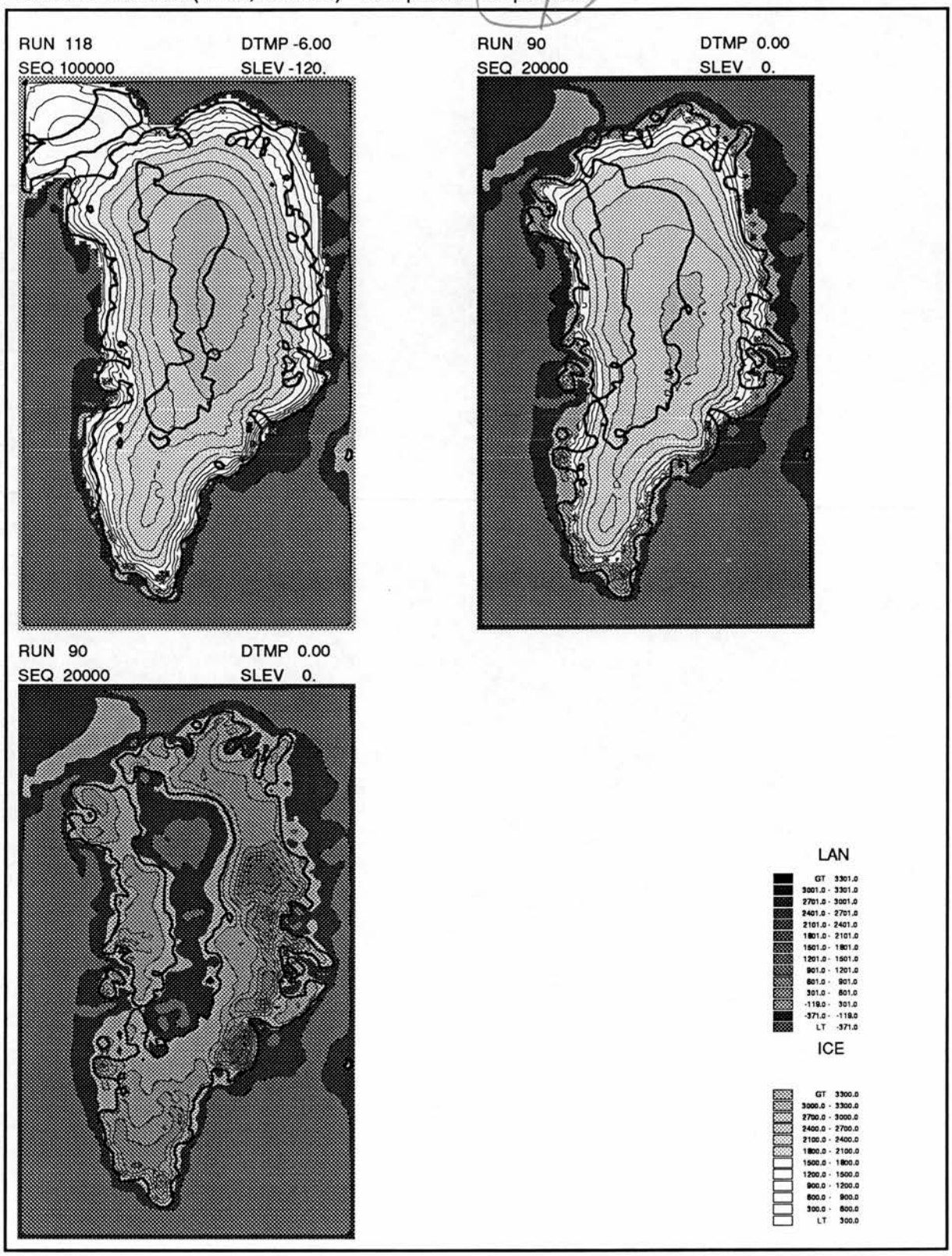

Figure 85: The position of the modelled maximum ice position in relation to present-day topography. Top left, maximum ice state with present day line superimposed, top right, present-day conditions with maximum superimposed. Lower is present subglacial surface with superimposed maximum shoreline.

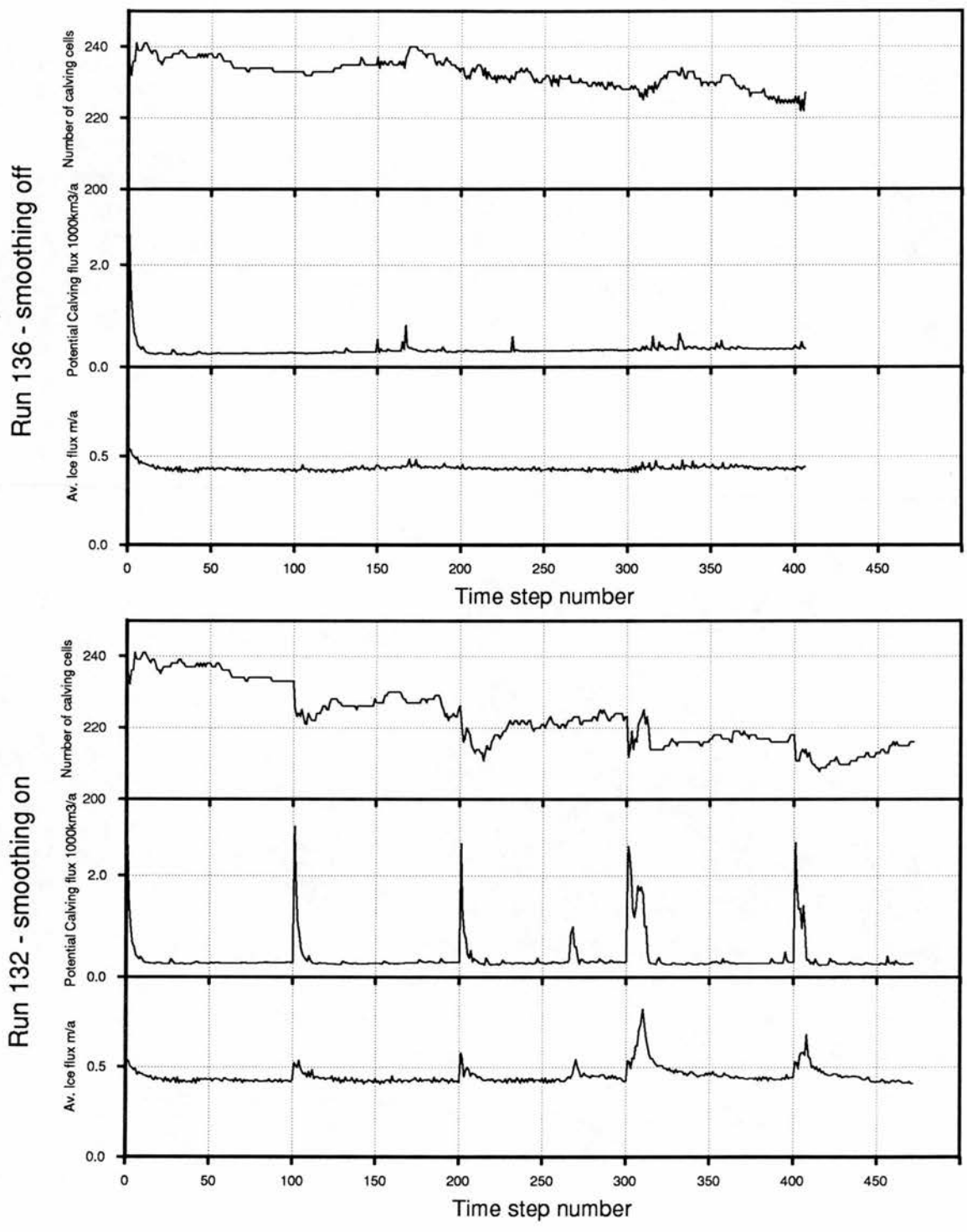

Figure 86: The figures shows the relationship between calving activity and imposed numerical smoothing. The smoothing routine forces the model into a temporarily unbalanced state which can stimulate calving activity.

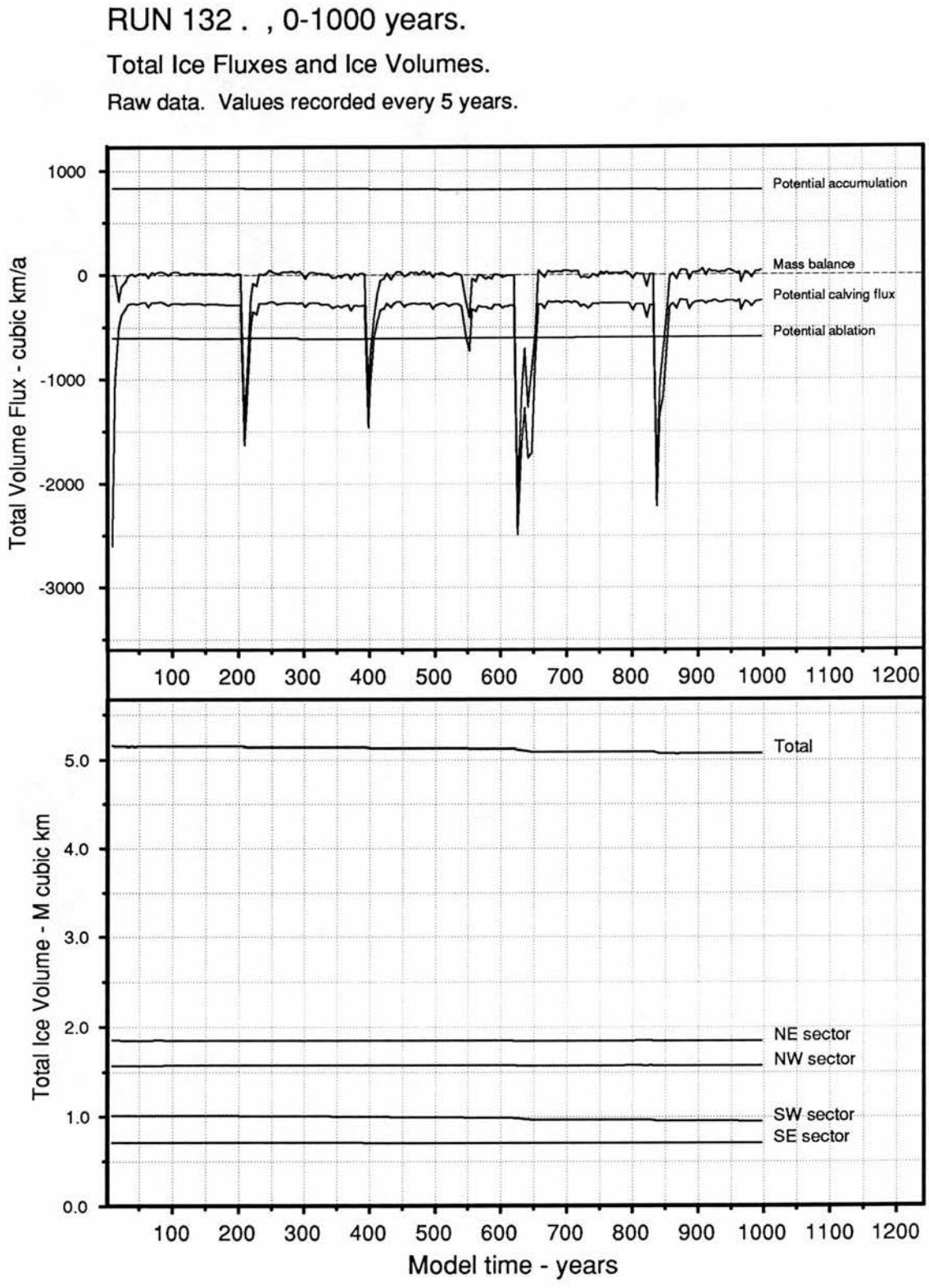

Figure 87: Short-term ice sheet fluctuation under maximum ice conditions (Run 132). The figure show total ice volumes and mass balance rates when the maximum state model is being smoothed. Regular smoothing acts as a trigger to catastrophic calving events giving an apparent cyclicity.

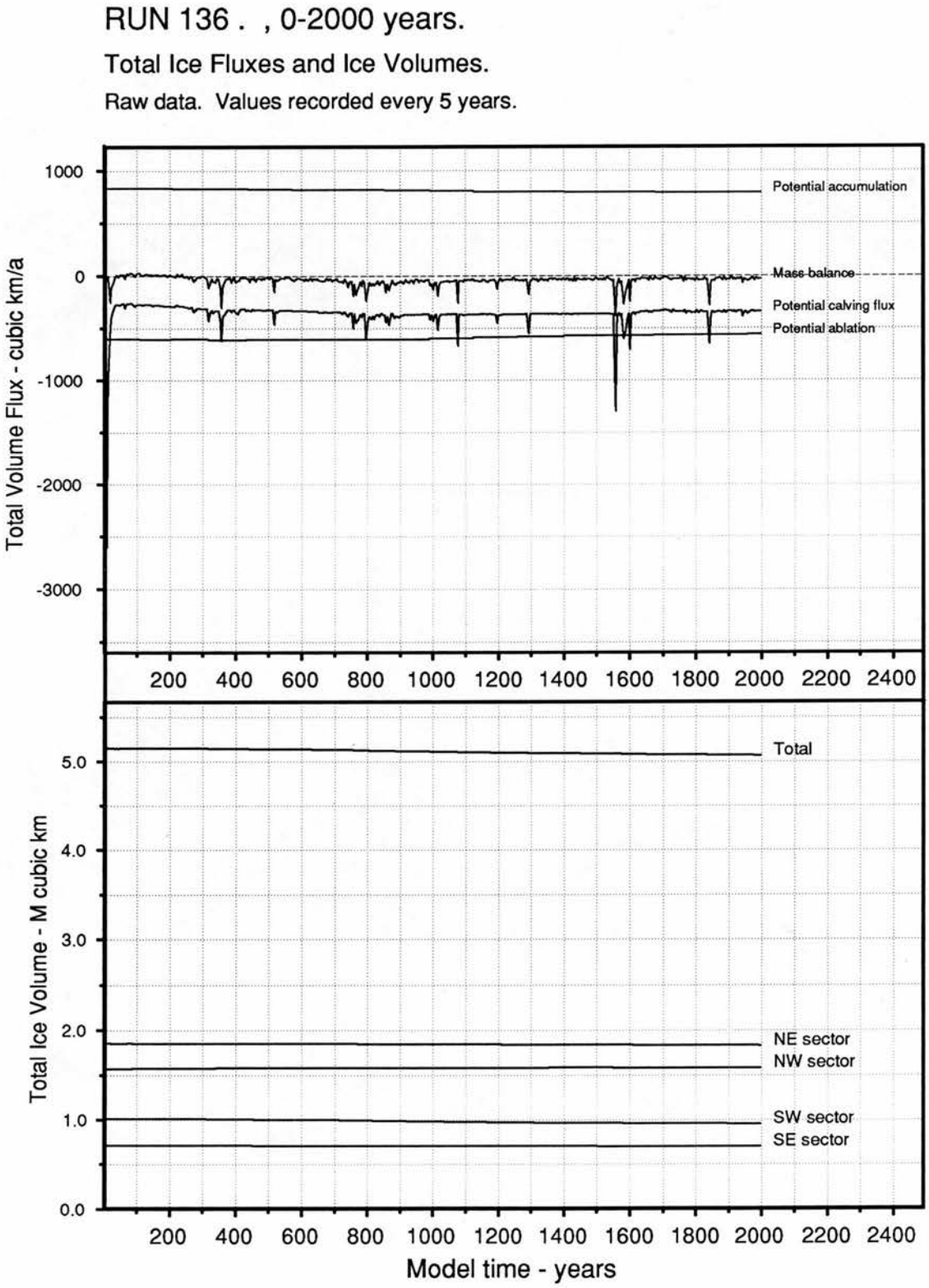

Figure 88: Short-term ice sheet fluctuation under maximum ice conditions (Run 136). The figure shows total ice volumes and mass balance rates when the maximum state model is not being smoothed. Calving is still irregular but at much less catastrophic magnitudes because the modelled calving outlets do not have a substantial enough trigger.

Run 132. Land and ice surfaces - metres, 650-875 years.

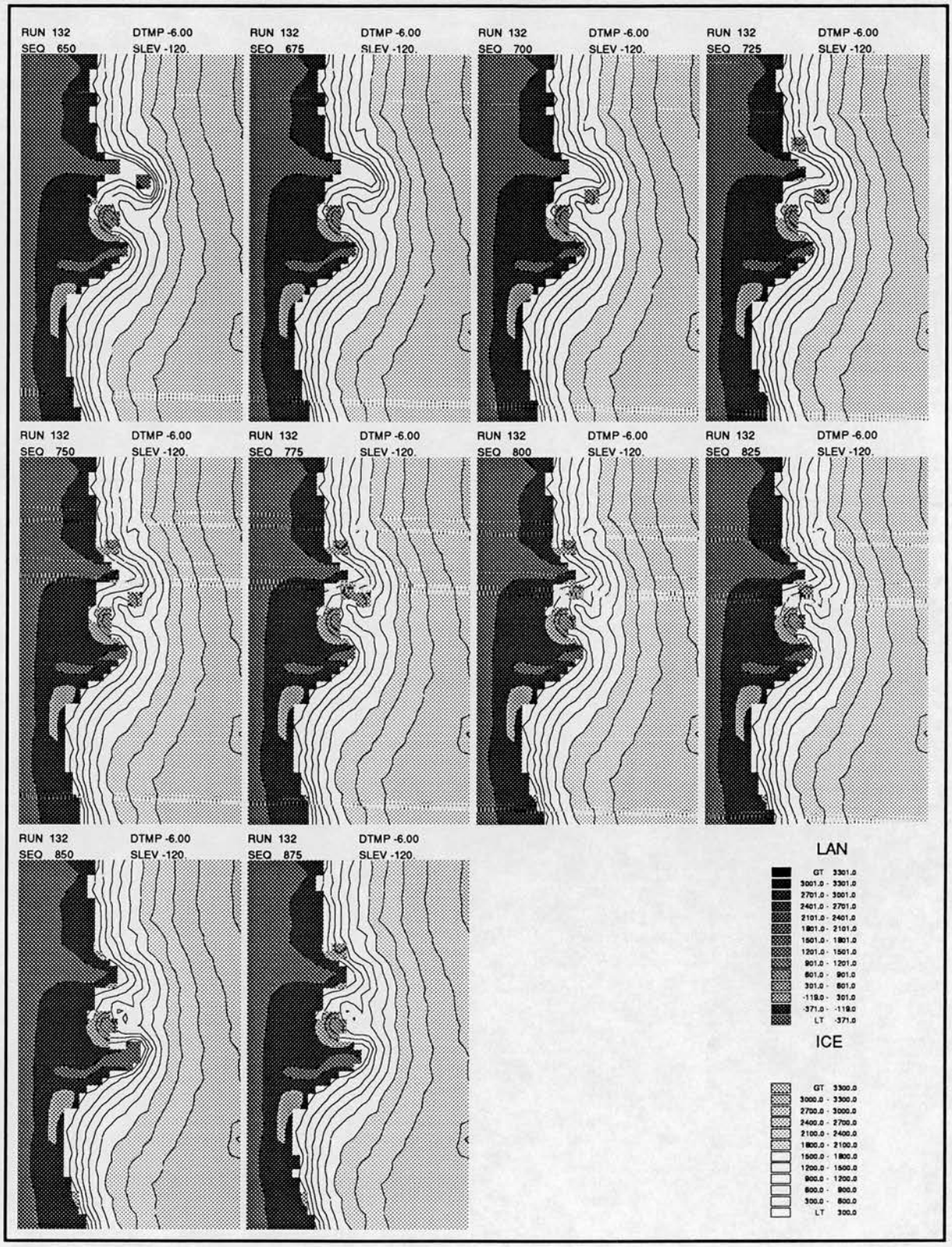

Figure 89: Short-term ice sheet fluctuation under maximum ice conditions (Run 132). The figure shows detail of calving activity on the west coast. Umanaq Bay and Disko Bugt calve rapidly in the run at maximum ice conditions. Similar conditions occur at other times in the run.

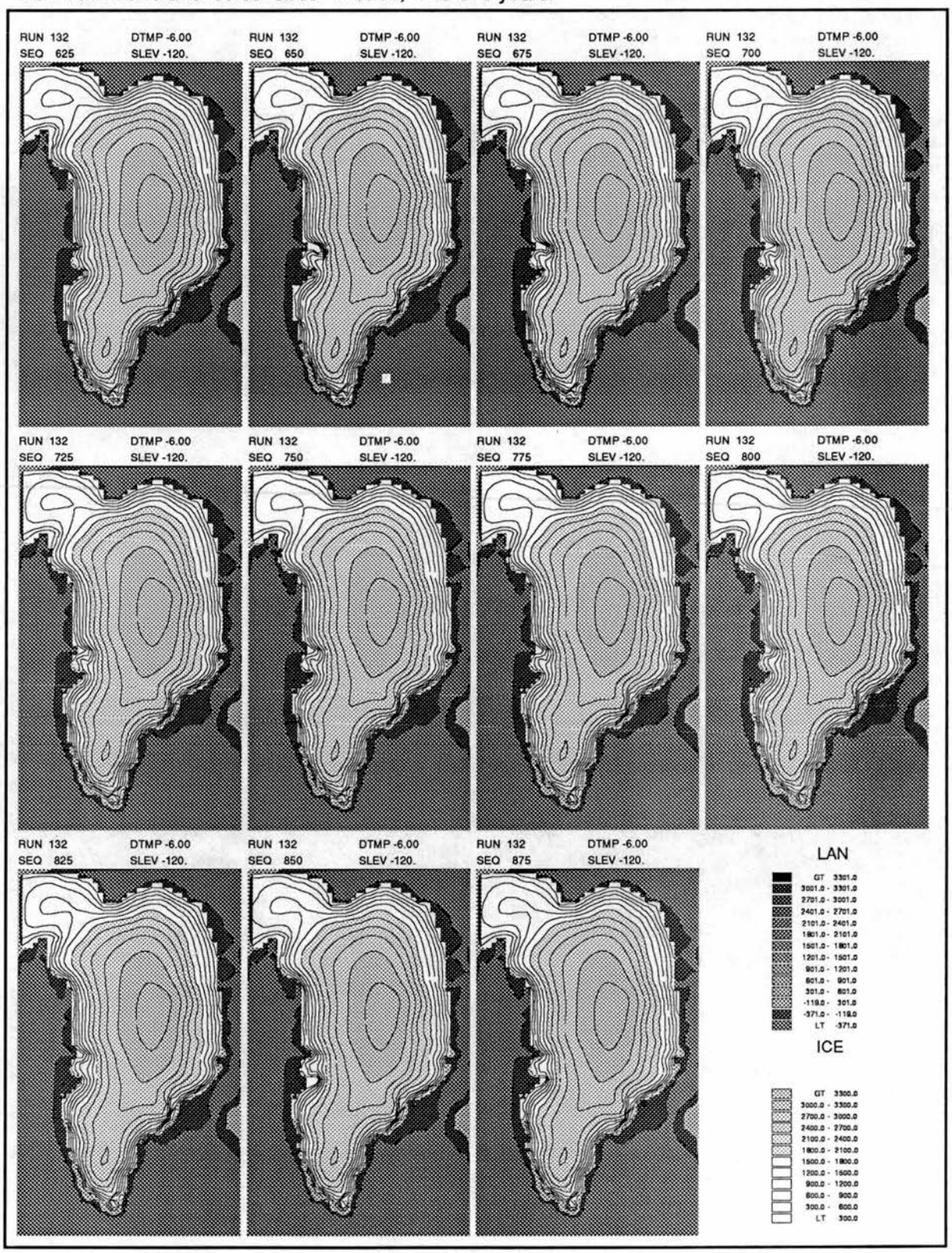

Figure 90: Ice sheet variability under maximum conditions (Run 132). Modelled land and submarine surfaces, with superimposed ice surface. Even with long-term equilibrium, the ice sheet varies in extent because of calving events which are differently located.

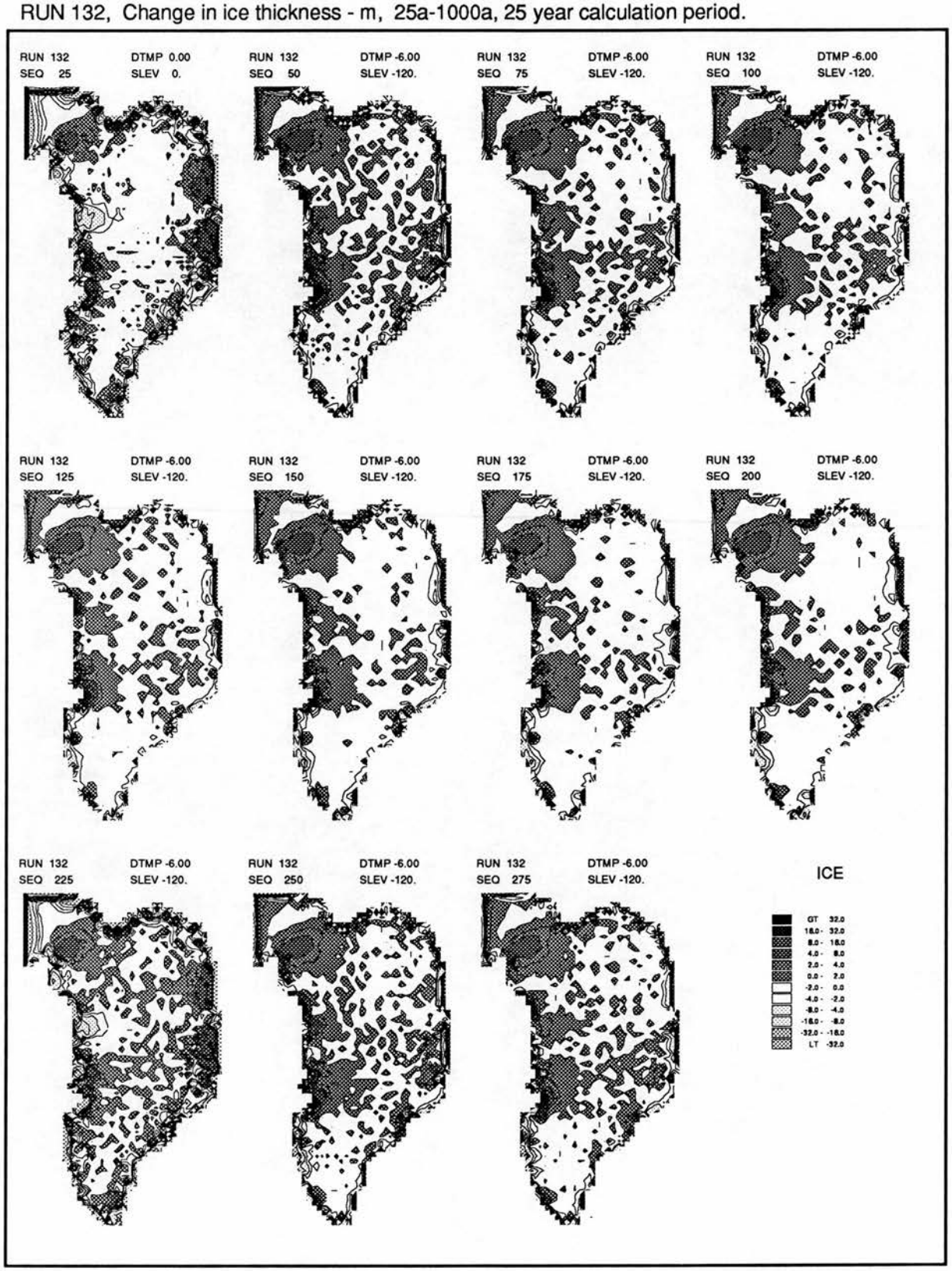

Figure 91: Ice sheet variability under maximum conditions (Run 132). Change in ice thickness over successive 25 year time periods (page 1). Throughout this period the ice continues to build up in the Disko Bay area. Most of the central area demonstrates very little change in ice thickness over 25 year periods.

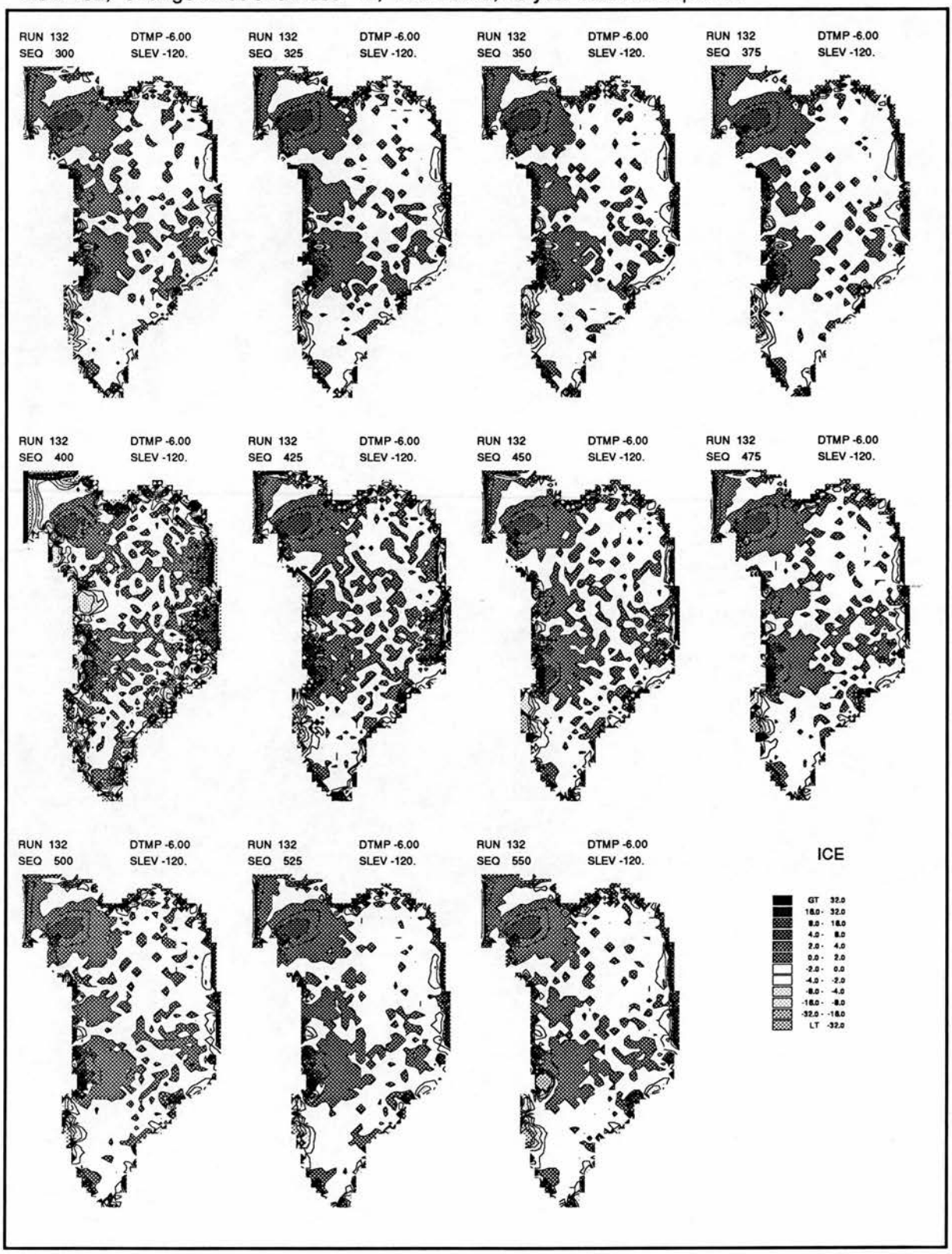

Figure 92: Ice sheet variability under maximum conditions (Run 132). Change in ice thickness over successive 25 year time periods (page 2). Two large calving events can be identified: One in the region of Melville Bay at 400a, the other at Disko Bay at 550a.

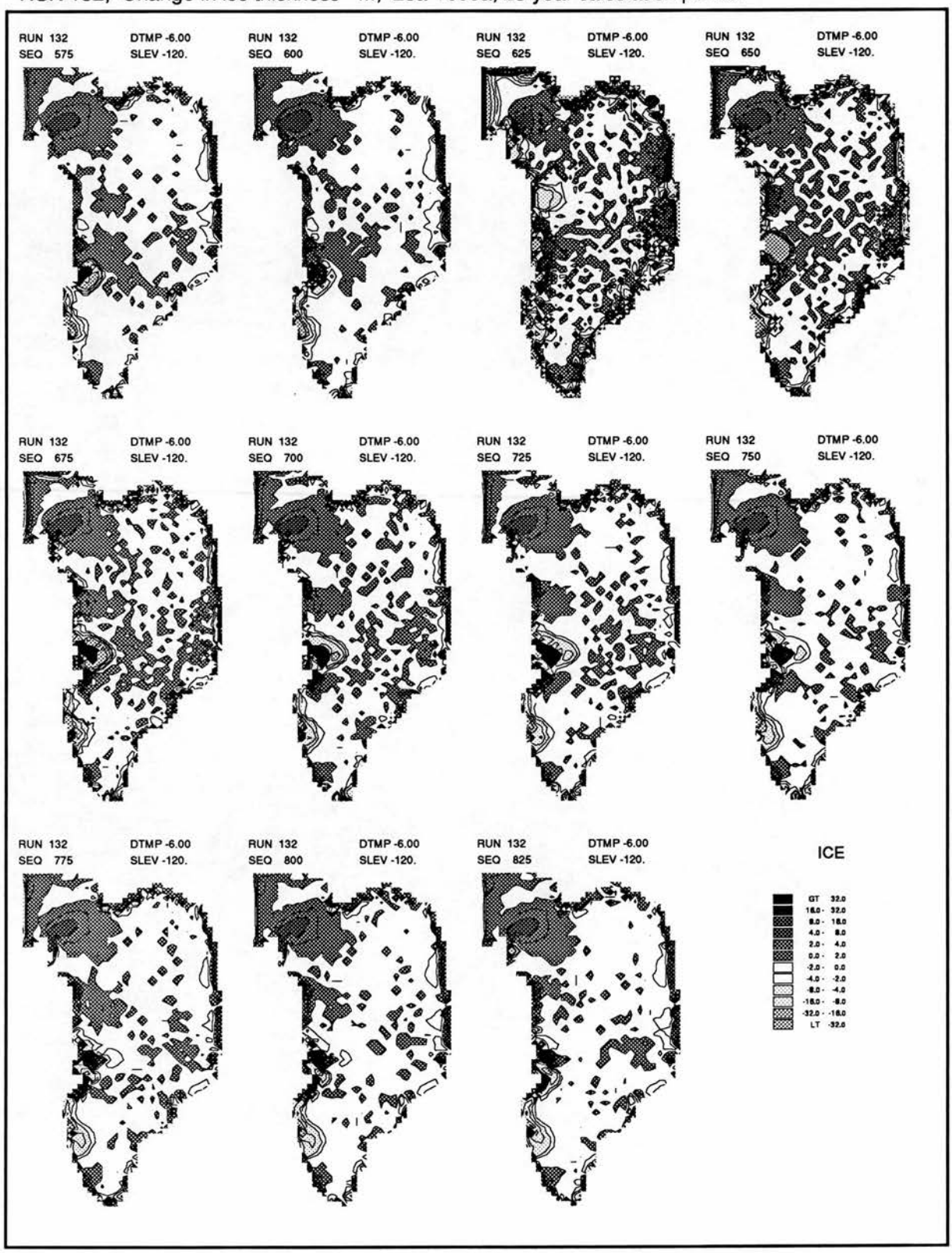

Figure 93: Ice sheet variability under maximum conditions (Run 132). Change in ice thickness over successive 25 year time periods (page 3). A very large calving event at 650a at Umanaq causes subsequent infilling from the surrounding basin, thus transmitting the calving signal back onto the main ice sheet.

Figure 94: Ice sheet variability under maximum conditions (Run 132). Change in ice thickness over successive 25 year time periods (page 4). Similar to the calving event at Umanaq (previous page) another calving event occurs at Disko Bay at 850a.

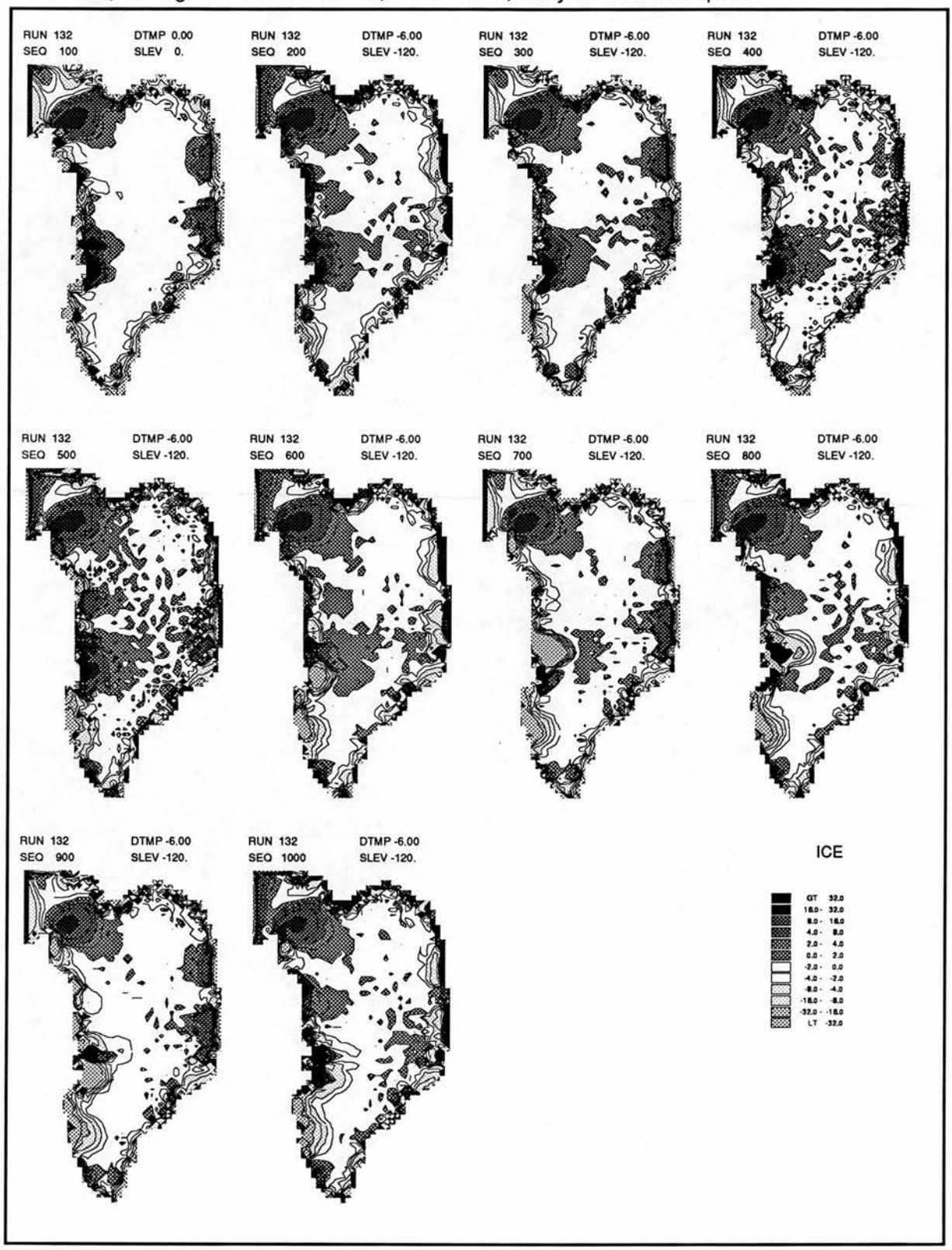

Figure 95: Ice sheet variability under maximum conditions (Run 132). Change in ice thickness over successive 100 year time periods. Some of the detail of the calving events seen over 25 year periods (previous pages) is lost. Some events, like the Umanaq event appear clearly (at 700a) Other trends, like the long-term infilling of the Nares Strait are more apparent than over 25 year periods.

Run 132, Change in ice thickness(upper) and basal elevation(lower) over 1000 year period.

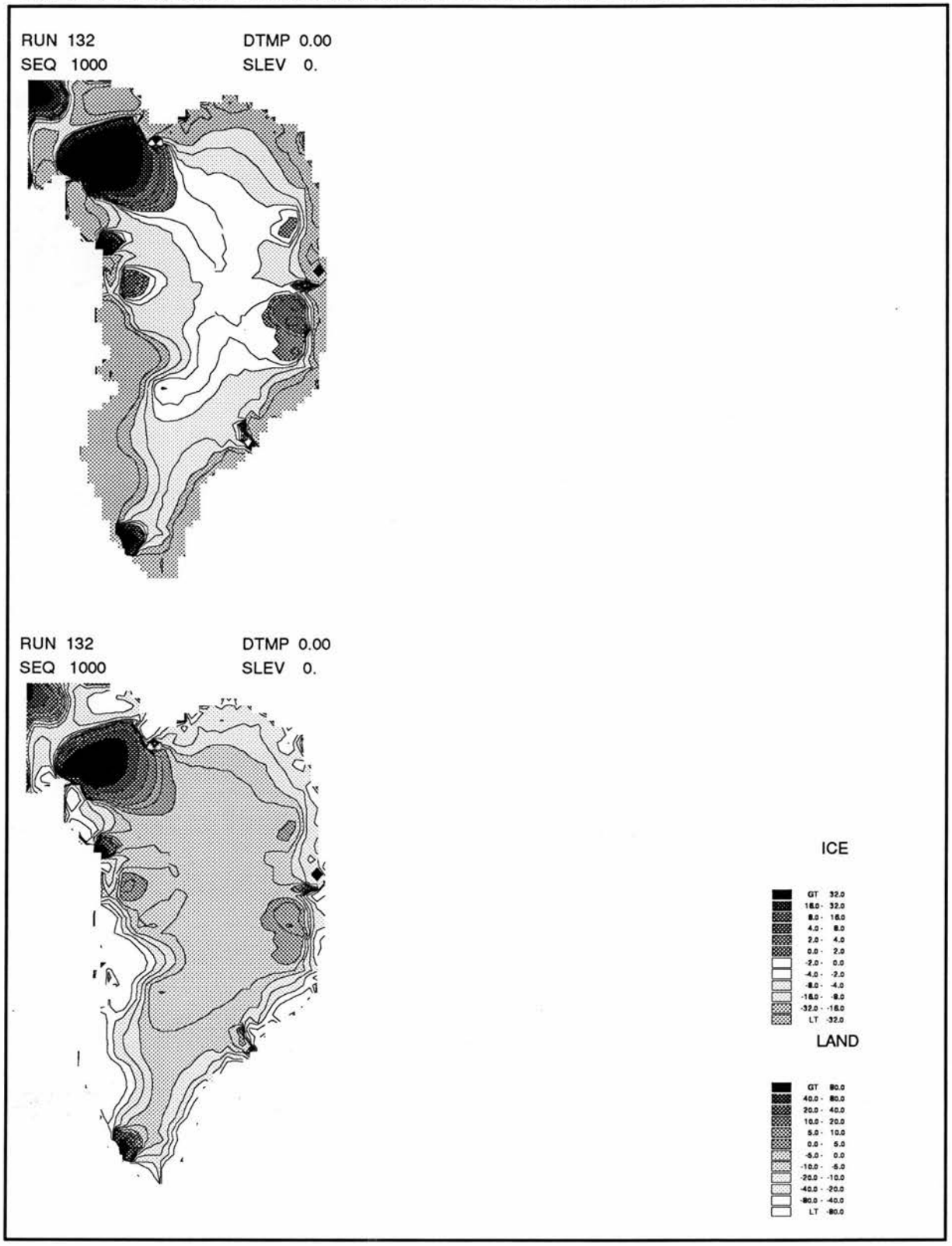

Figure 96: Ice sheet variability under maximum conditions (Run 132). Change in ice thickness and bed elevation over 1000 years. The figure shows how ice thickness and bedrock change calculated over 1000 year periods can only give partial information about short term variability (compare previous, subsequent pages). Only a few major trends are now apparent. The damped bedrock adjustment is a better indicator of the major fluctuating areas.

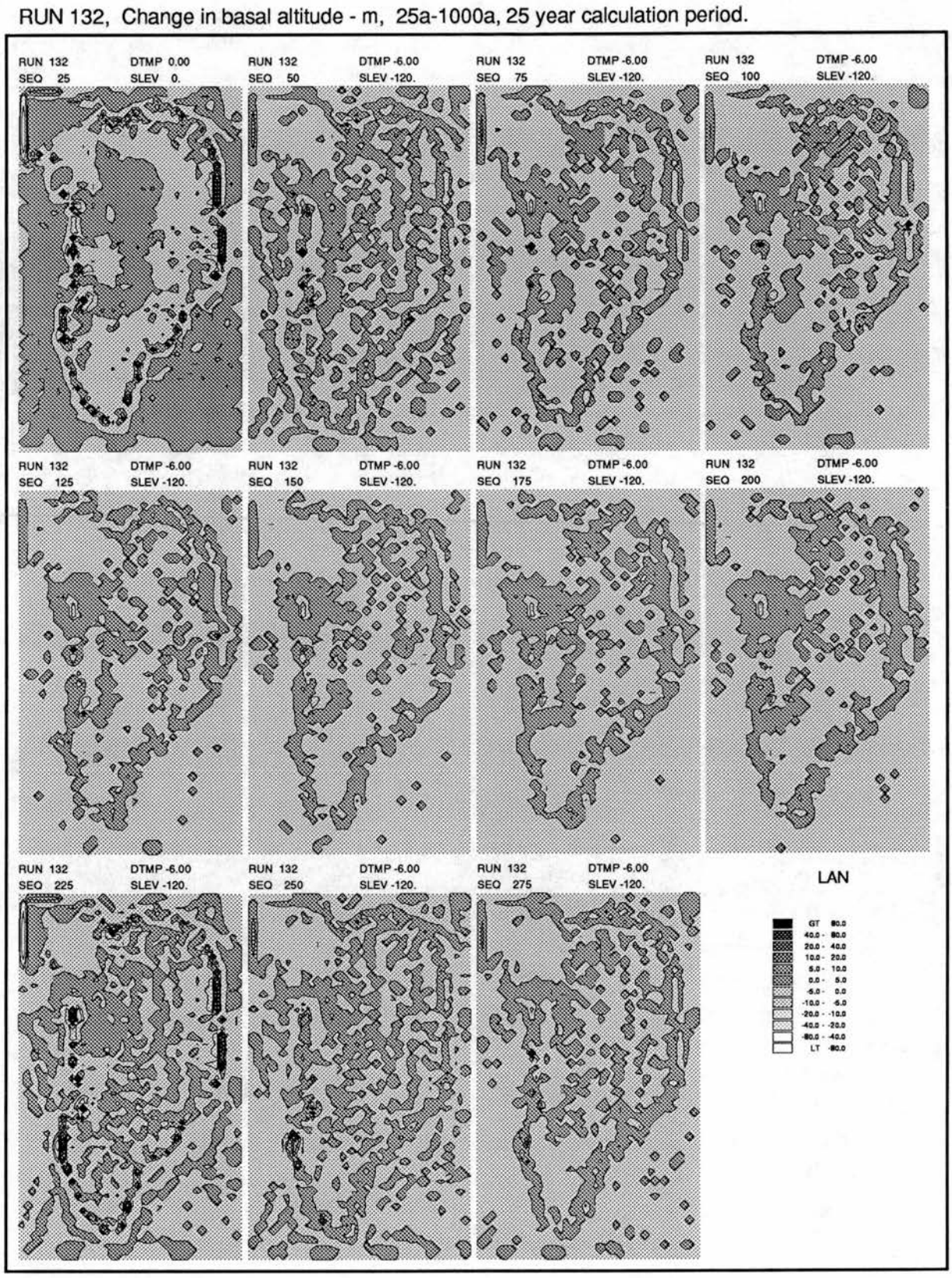

Figure 97: Ice sheet variability under maximum conditions (Run 132). Change in bed elevation over successive 25 year time periods (page 1).

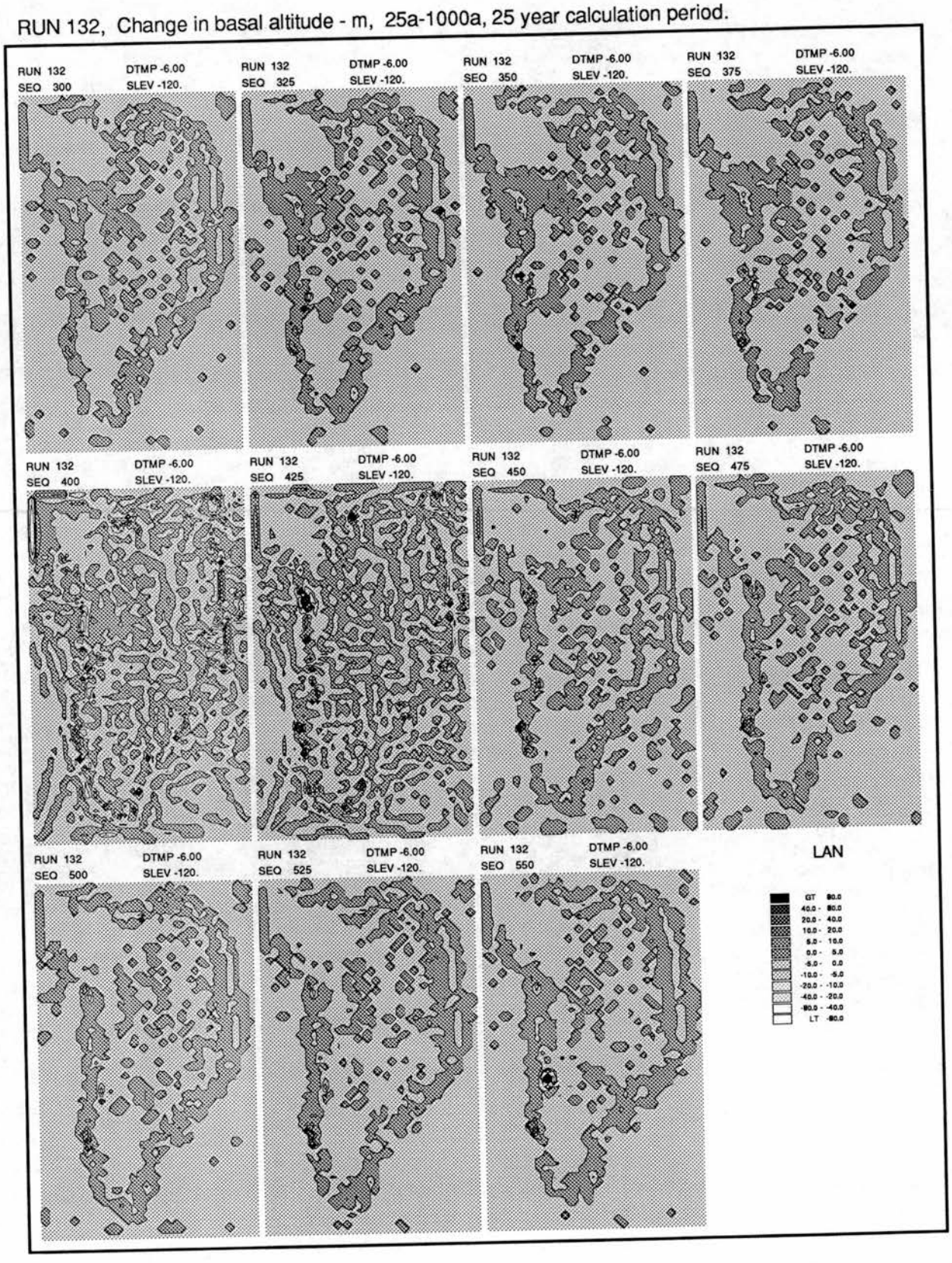

Figure 98: Ice sheet variability under maximum conditions (Run 132). Change in bed elevation over successive 25 year time periods (page 2). The effect of the calving at Melville Bay (425a) and Disko (550a) is just visible.

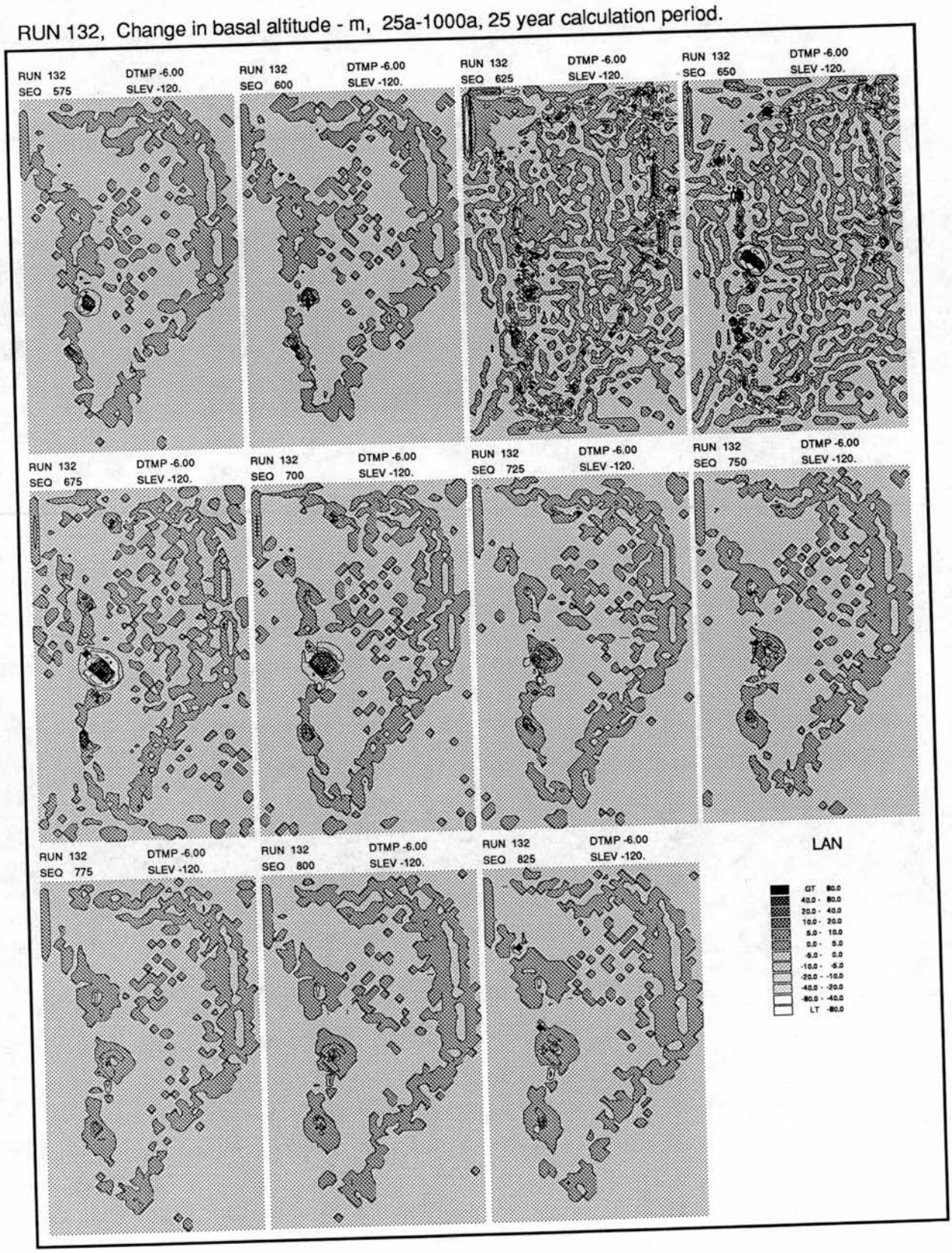

Figure 99: Ice sheet variability under maximum conditions (Run 132). Change in bed elevation over successive 25 year time periods (page 3). The large calving event which occurs at Umanaq (650a) has a significant localised response under the isostasy model used.

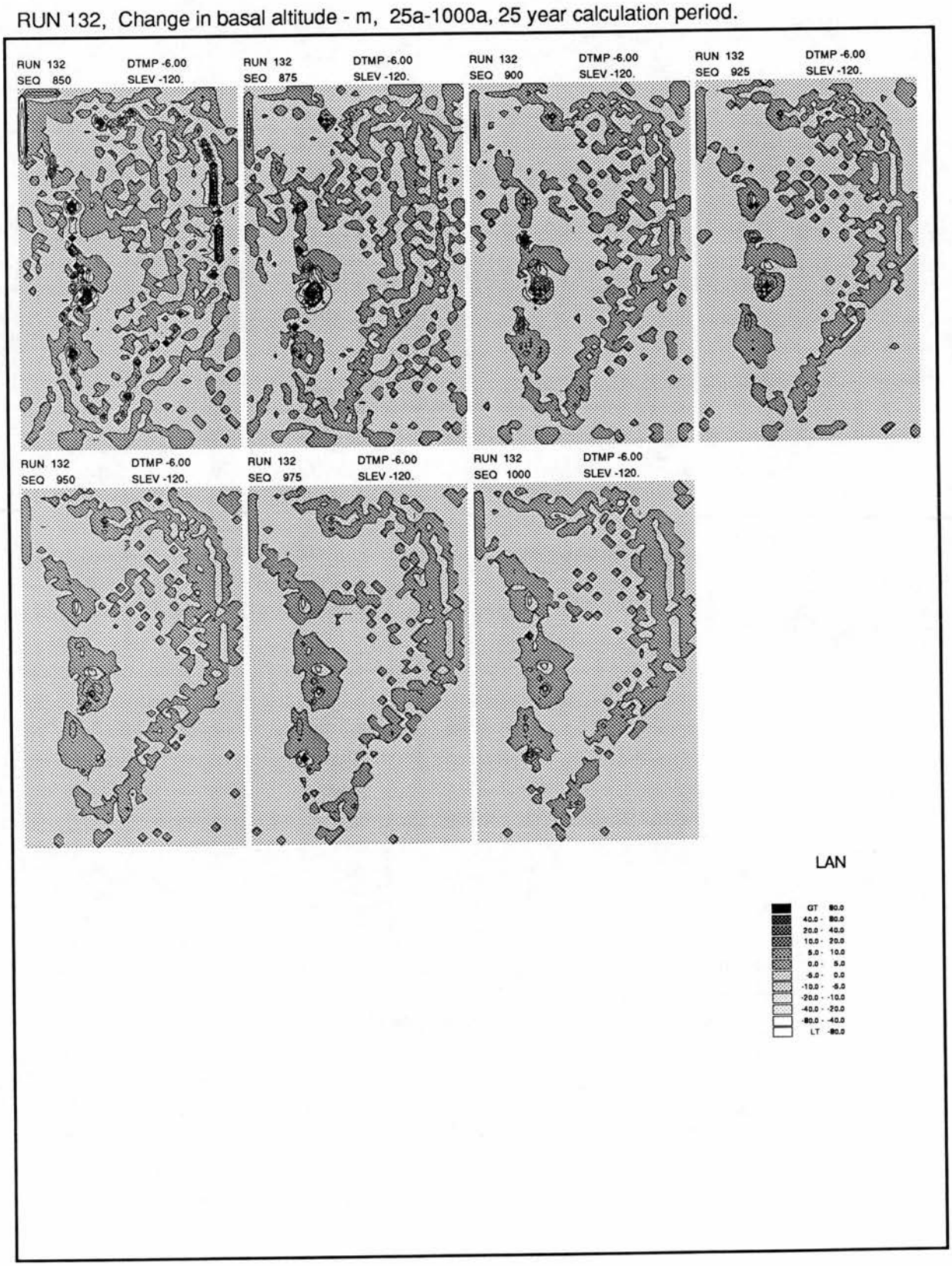

Figure 100: Ice sheet variability under maximum conditions (Run 132). Change in bed elevation over successive 25 year time periods (page 4). The isostatic response to modelled calving in Disko Bay is clear.

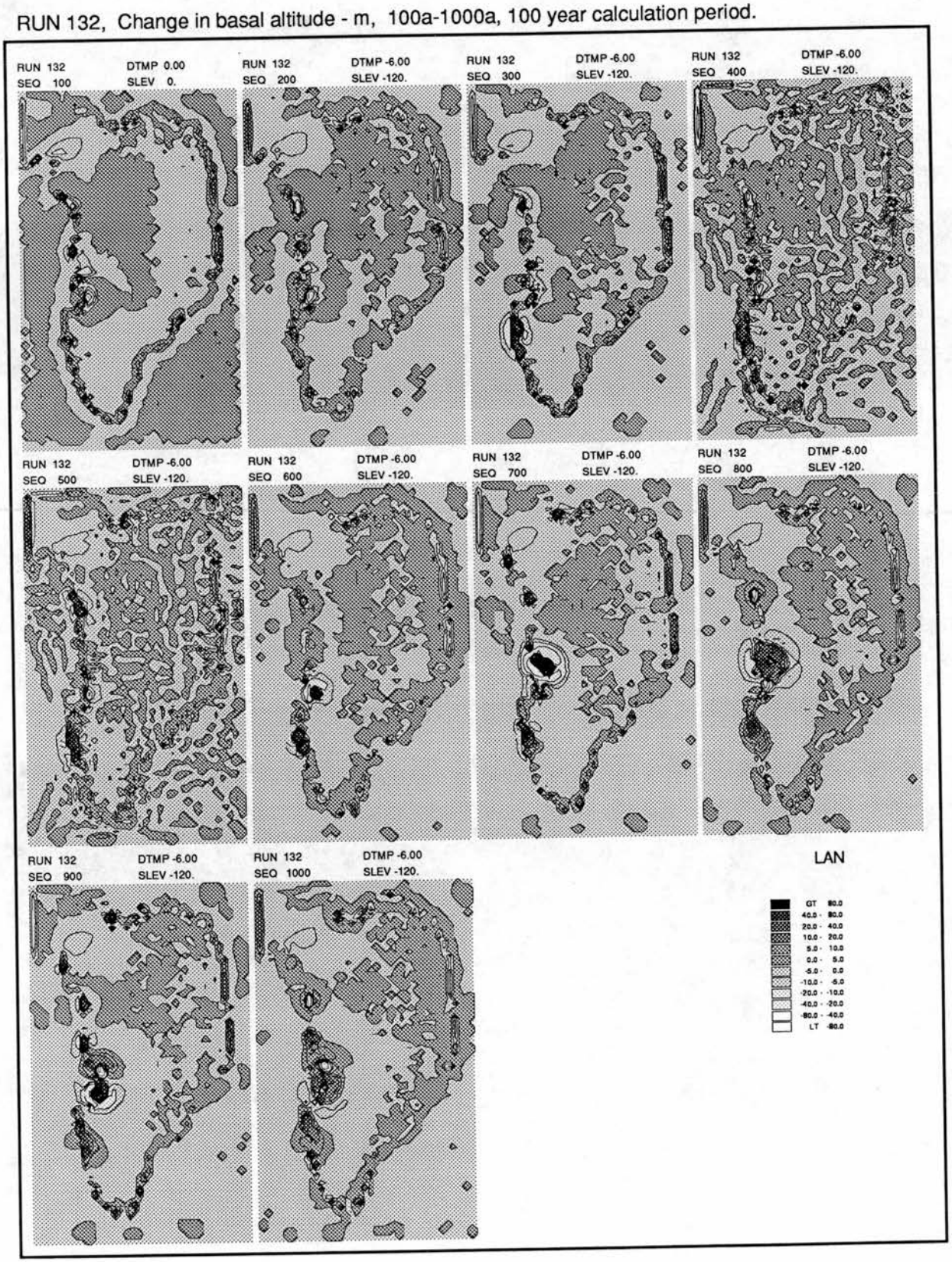

Figure 101: Ice sheet variability under maximum conditions (Run 132). Change in bed elevation over successive 100 year time periods. The figure shows how over longer averaging periods isostasy better represents ice sheet fluctuations than does change in ice thickness itself.

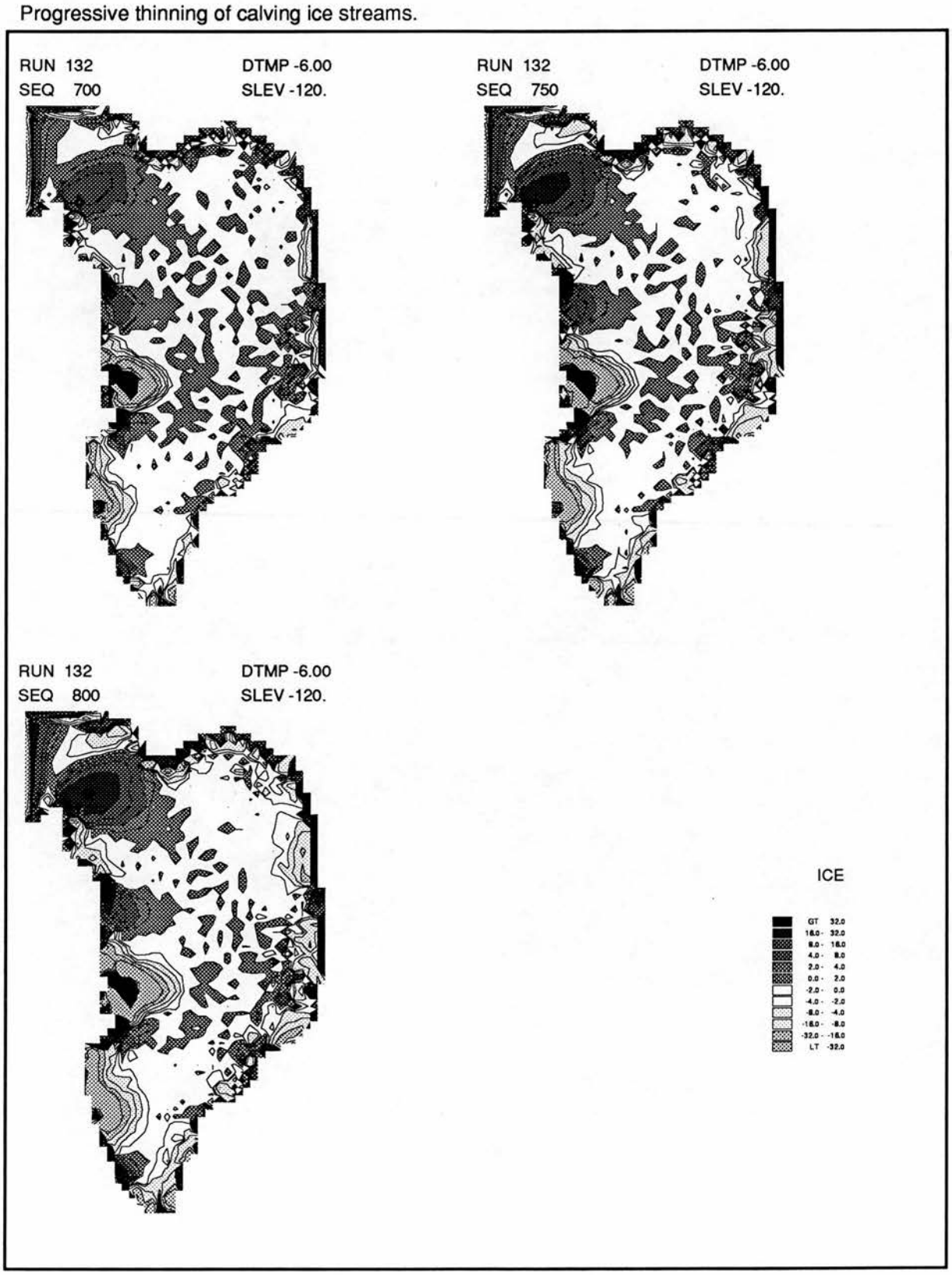

Figure 102: Ice sheet variability under maximum conditions (Run 132). The thickness change in the figure is calculated back to a fixed point (at 650a) and therefore measures cumulative change in ice thickness. This shows how thinning ice progressively lowers the gradient of calving basins after the calving event at Umanaq (650a).

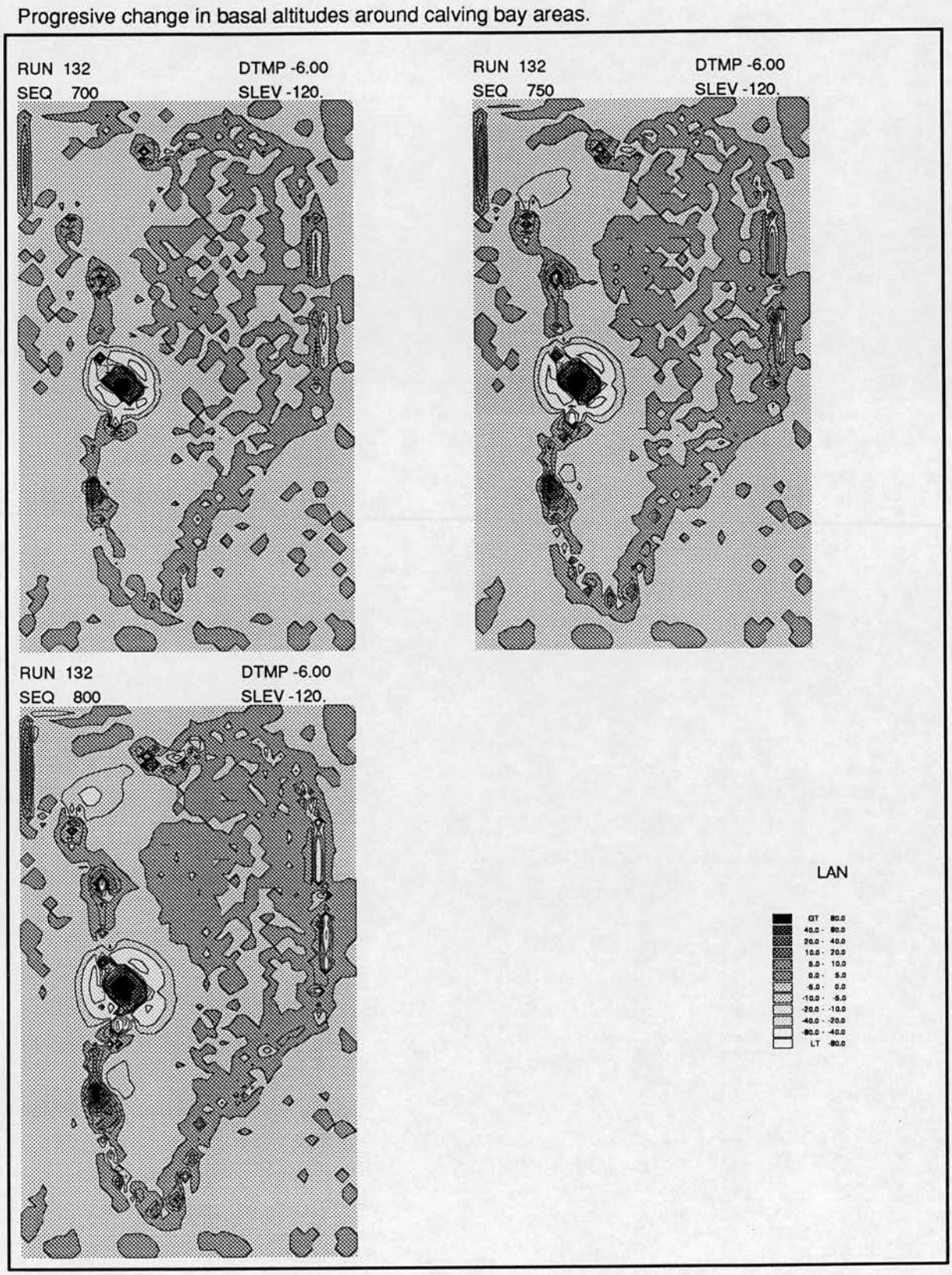

Figure 103: Ice sheet variability under maximum conditions (Run 132). The bed elevation change is calculated back from 650a measuring cumulative change (compare previous page). The figure shows how change in basal altitude propagates as a wave away from the source area of isostatic deflection.

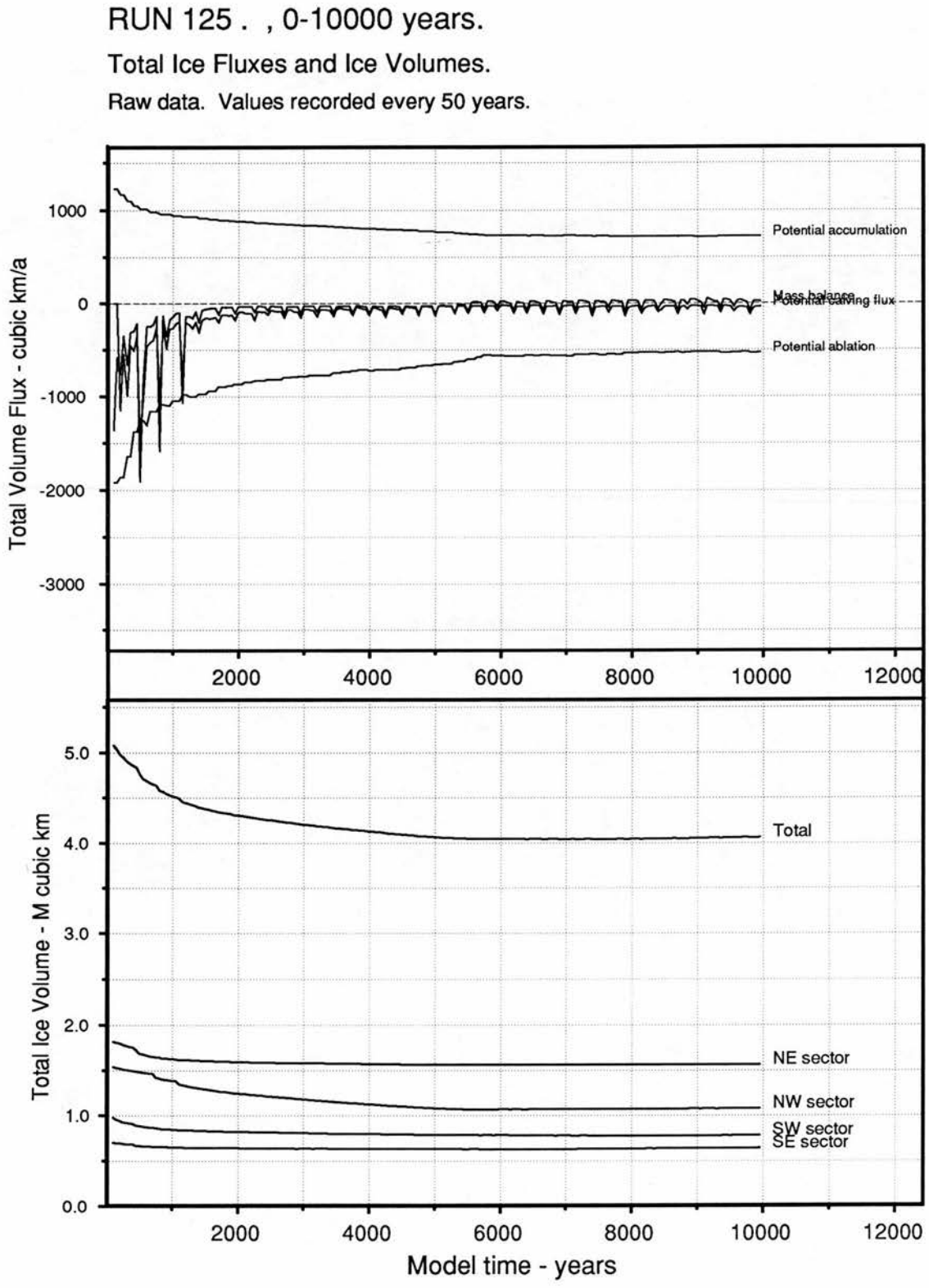

Figure 104: One step deglaciation forcing from $-6°C$ to $0°C$ (Run125). Total ice volumes and mass balance, with superimposed ice surfaces. Initial rapid change is followed by relaxation.

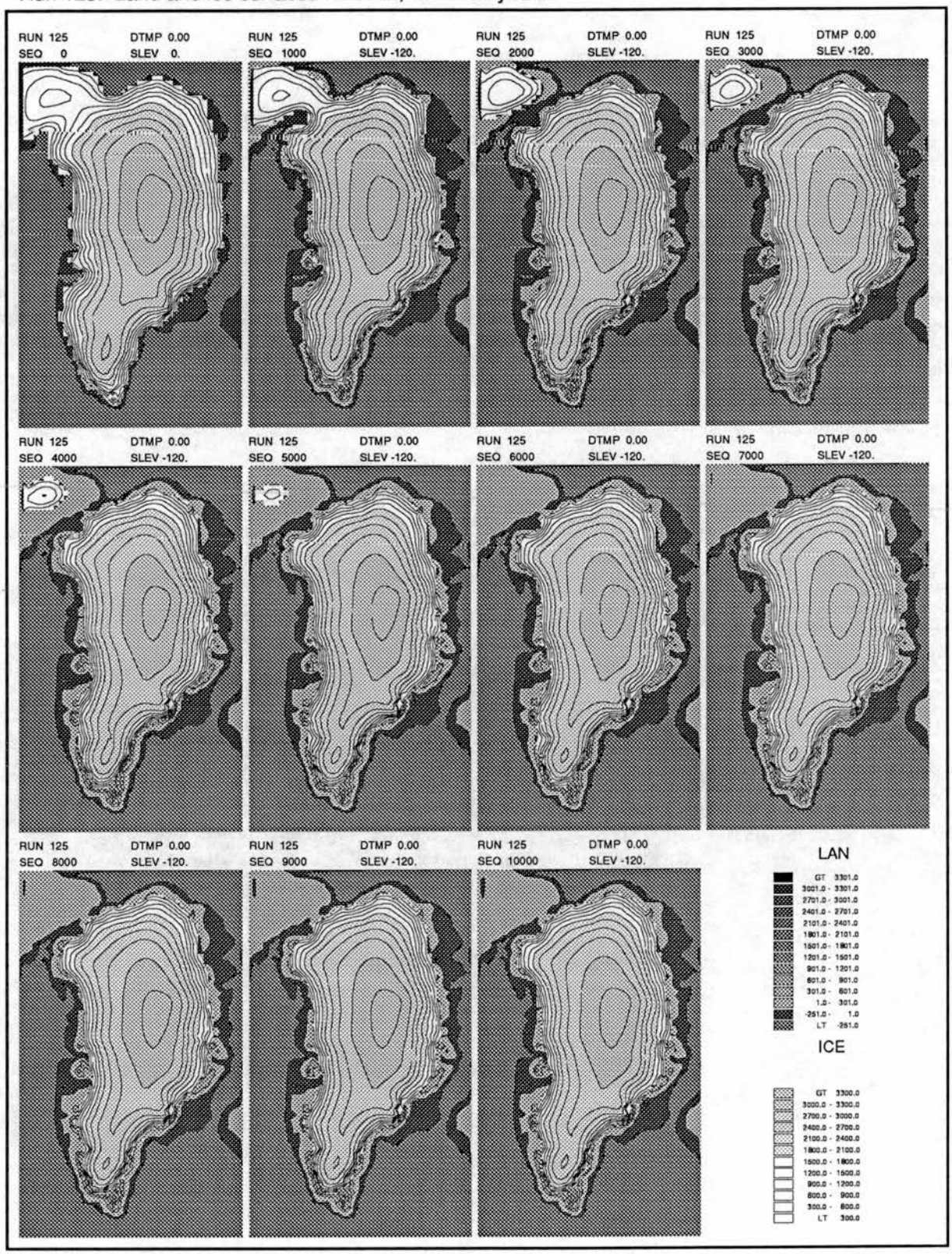

Figure 105: One step deglaciation forcing from $-6°C$ to $0°C$ (Run125). Modelled land and submarine surfaces with superimposed ice surfaces. The response to warming is initially rapid but decreases exponentially, allowing the ice sheet to reach a condition similar to the present within 10000 years.

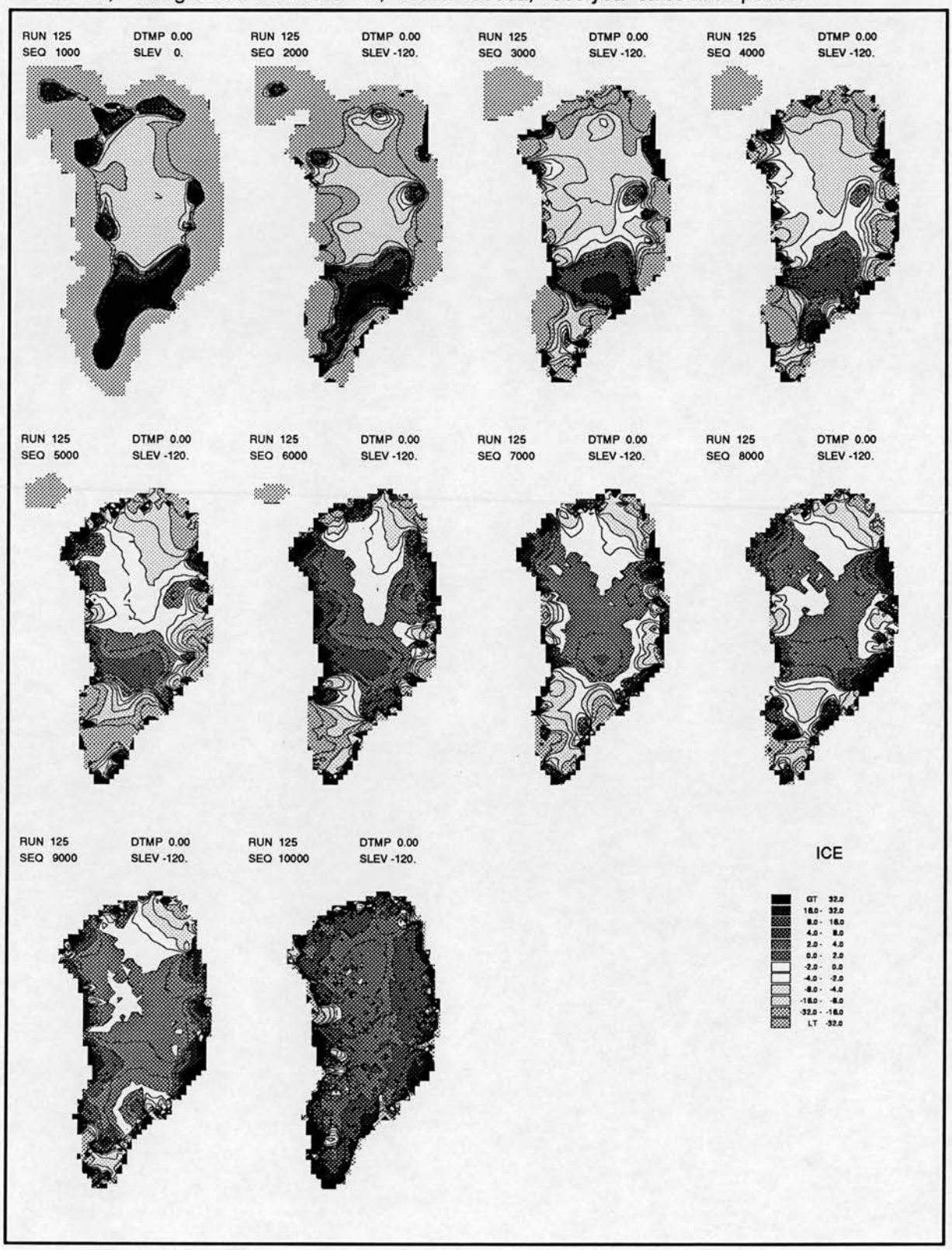

Figure 106: One step deglaciation forcing from $-6°C$ to $0°C$ (Run125). Successive changes in ice thickness. Initial rapid change is followed by relaxation with a variable pattern of thinning and thickening and then slight but consistent overall thickening at 10000a.

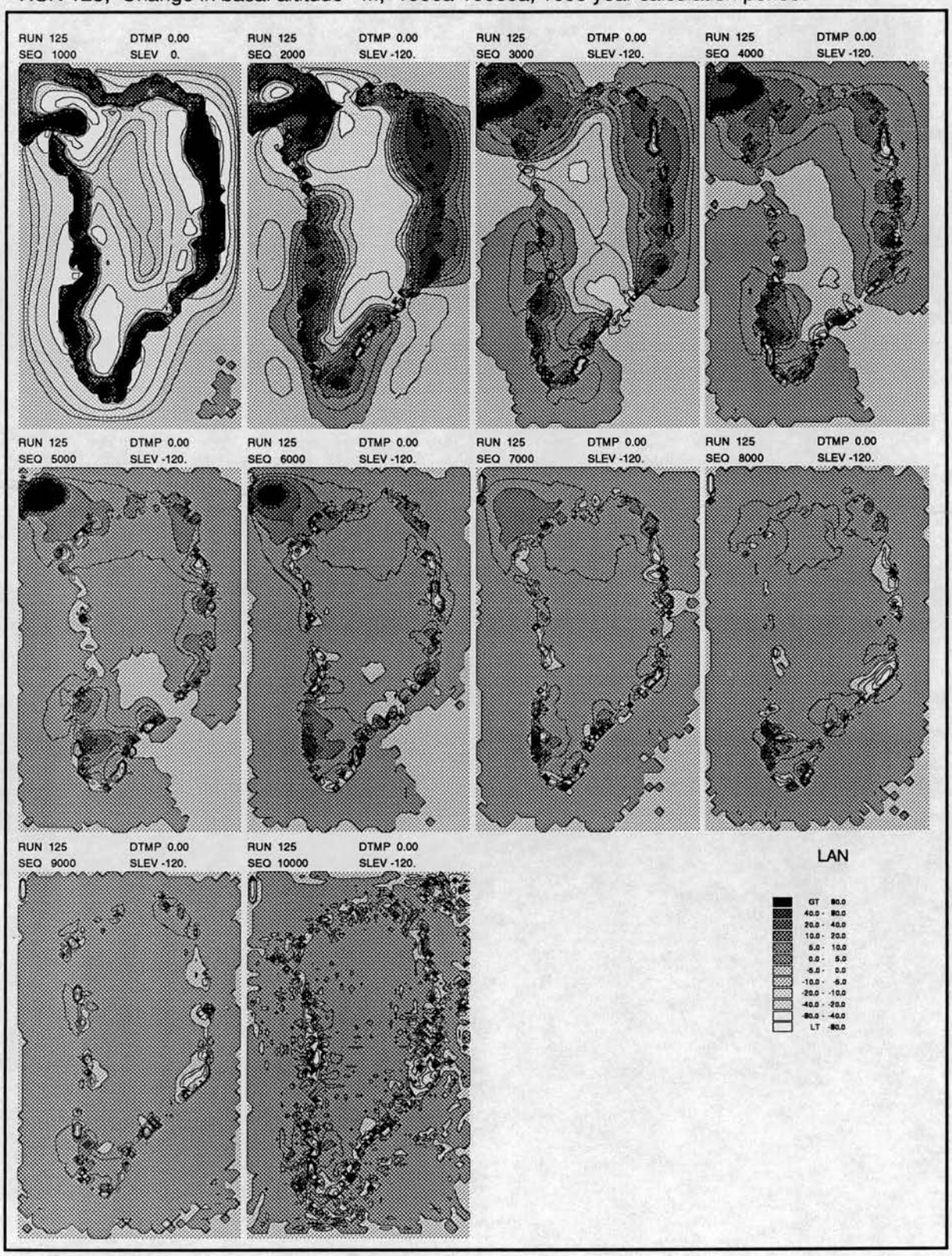

Figure 107: One step deglaciation forcing from $-6°C$ to $0°C$ (Run125). Basal altitude change. The initial rapid decay of the ice sheet has a more damped isostatic response on the underlying topography.

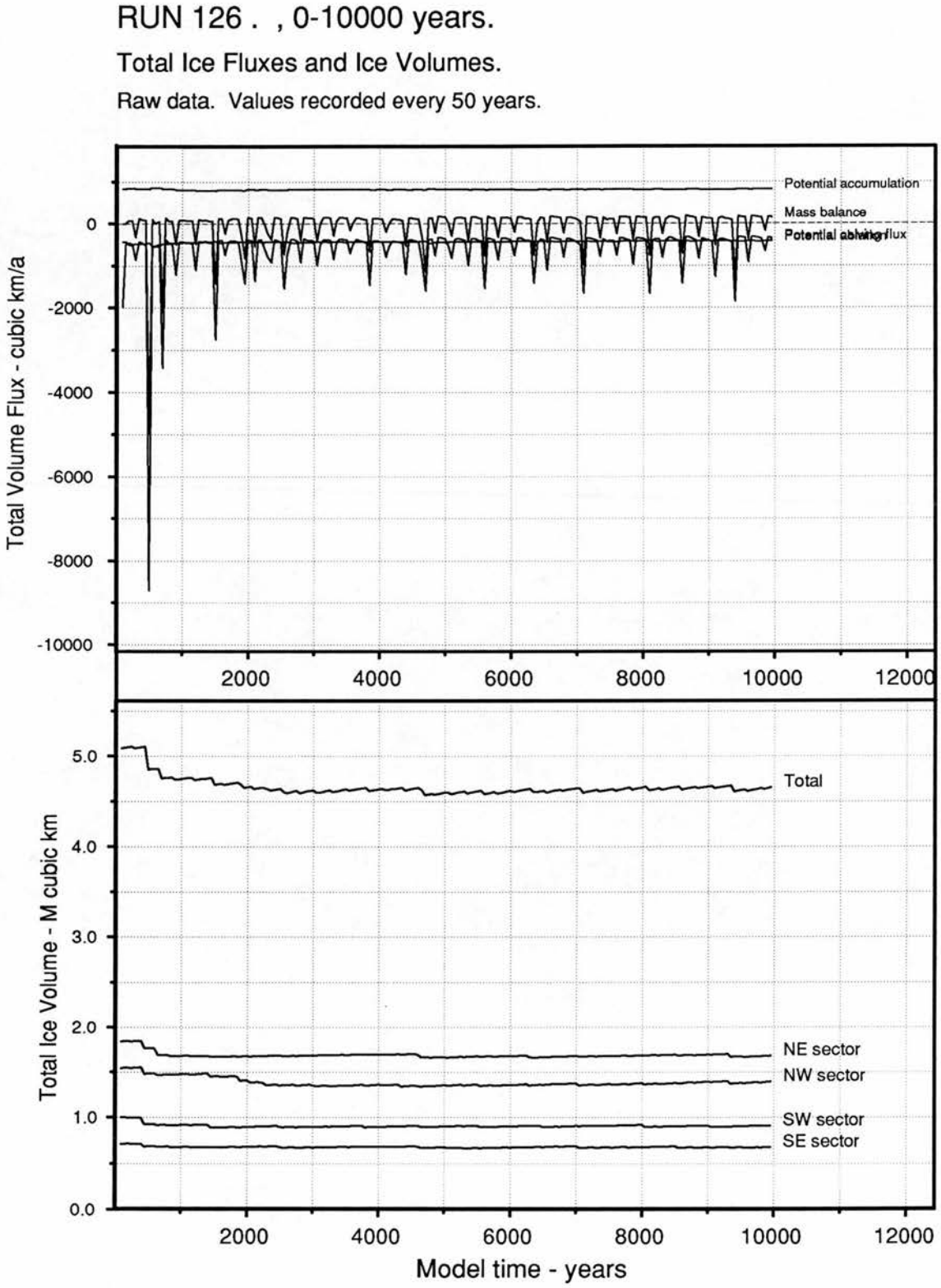

Figure 108: One step deglacial forcing of -120m to 0m sea level (Run 126). Total ice volumes and mass balance. With sea-level forcing calving rates are kept high throughout the run after initially increased rates. Overall volume loss is not as large as occurs with the $6°C$ warming.

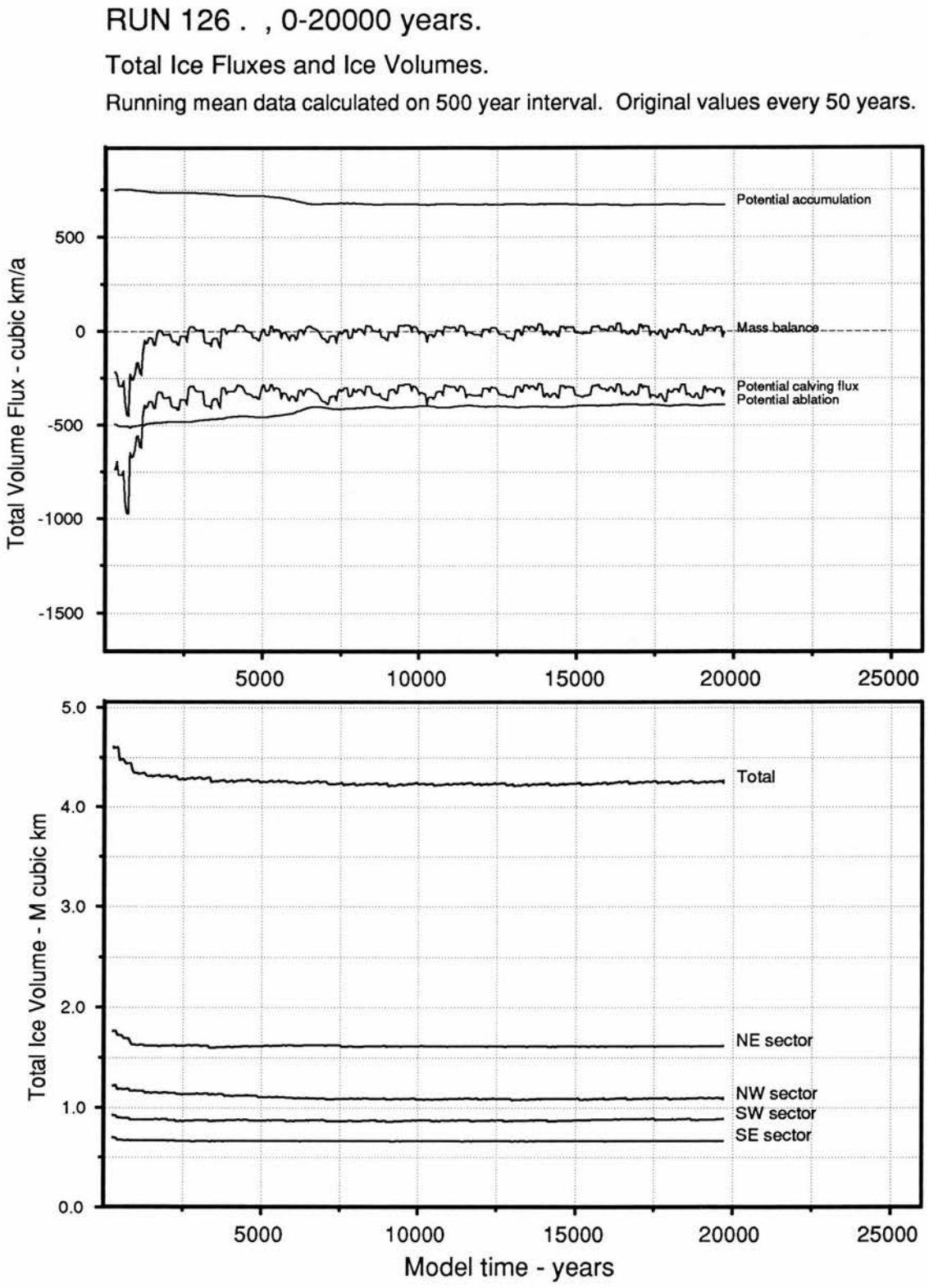

Figure 109: One step deglacial forcing of -120m to 0m sea level (Run 126). Total ice volumes and mass balance averaged over a 500 year running mean.

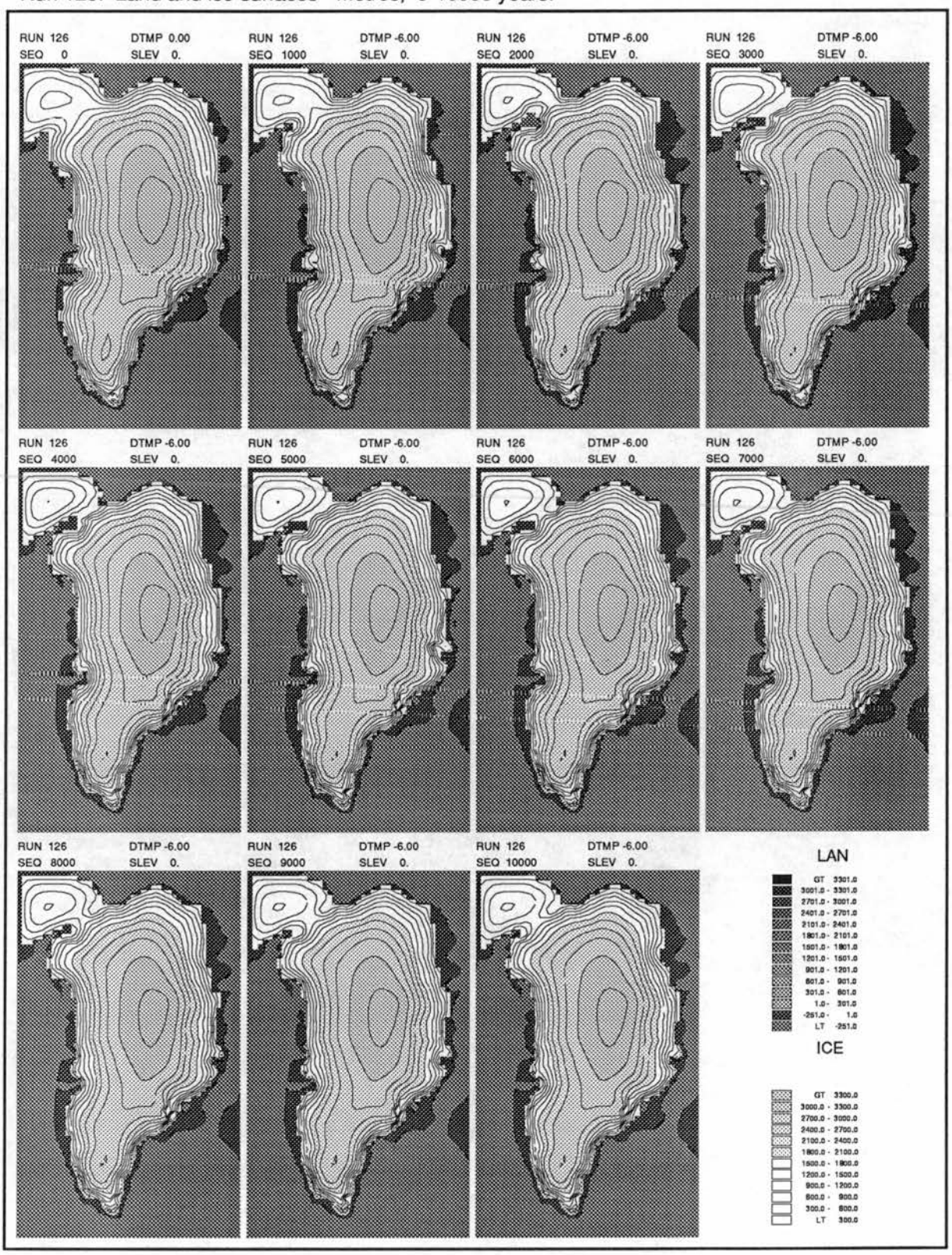

Figure 110: One step deglacial forcing of -120m to 0m sea level (Run 126). Modelled land and submarine surfaces with superimposed ice surfaces. The ice extent remains significant at cool temperatures and is held by the marine limit.

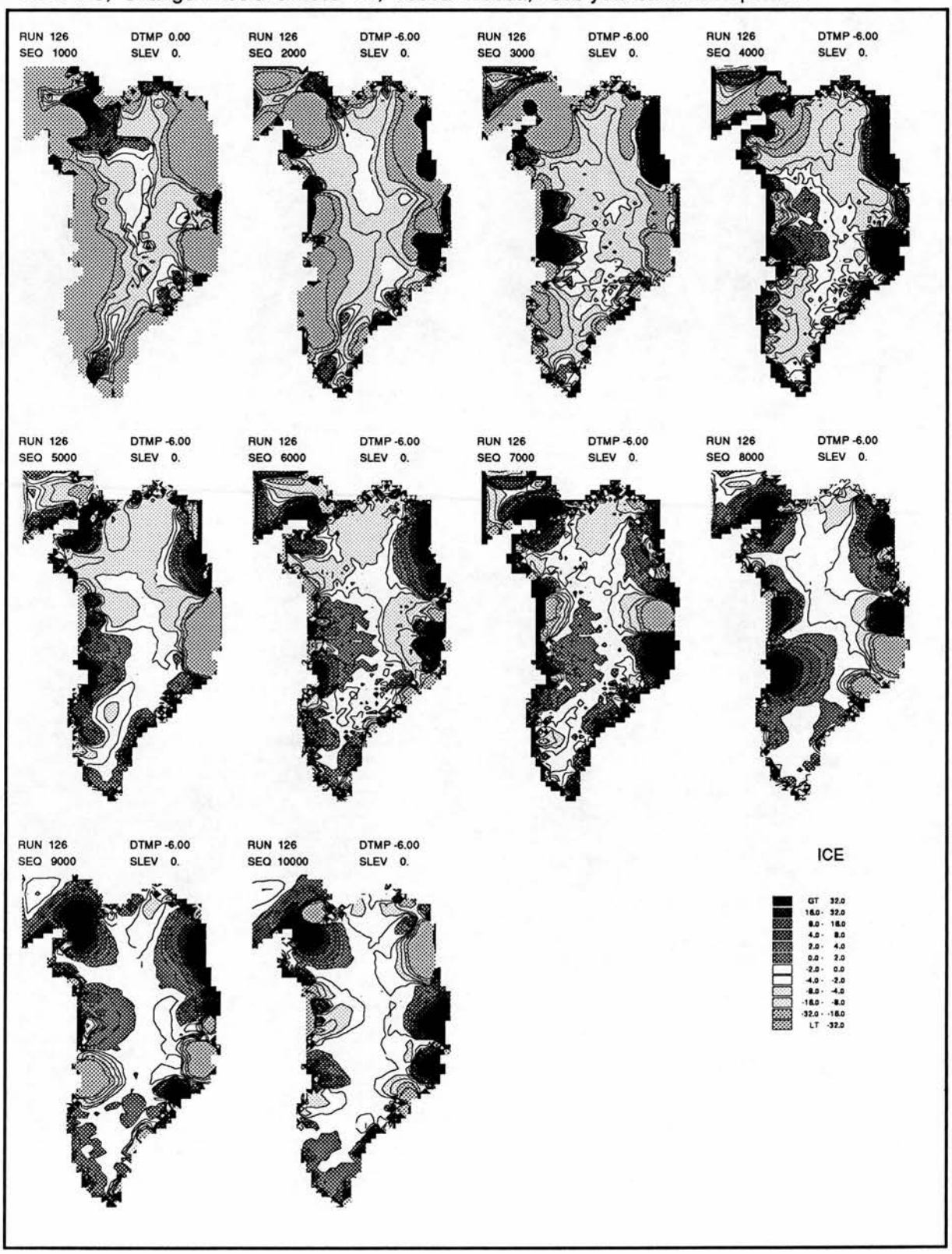

Figure 111: One step deglacial forcing of -120m to 0m sea level (Run 126). Successive changes in ice thickness between successive periods. Initial rapid thinning throughout is evident for the first 3-4000 years after which ice thickness change is high and flucuates in the basins draining into calving fronts.

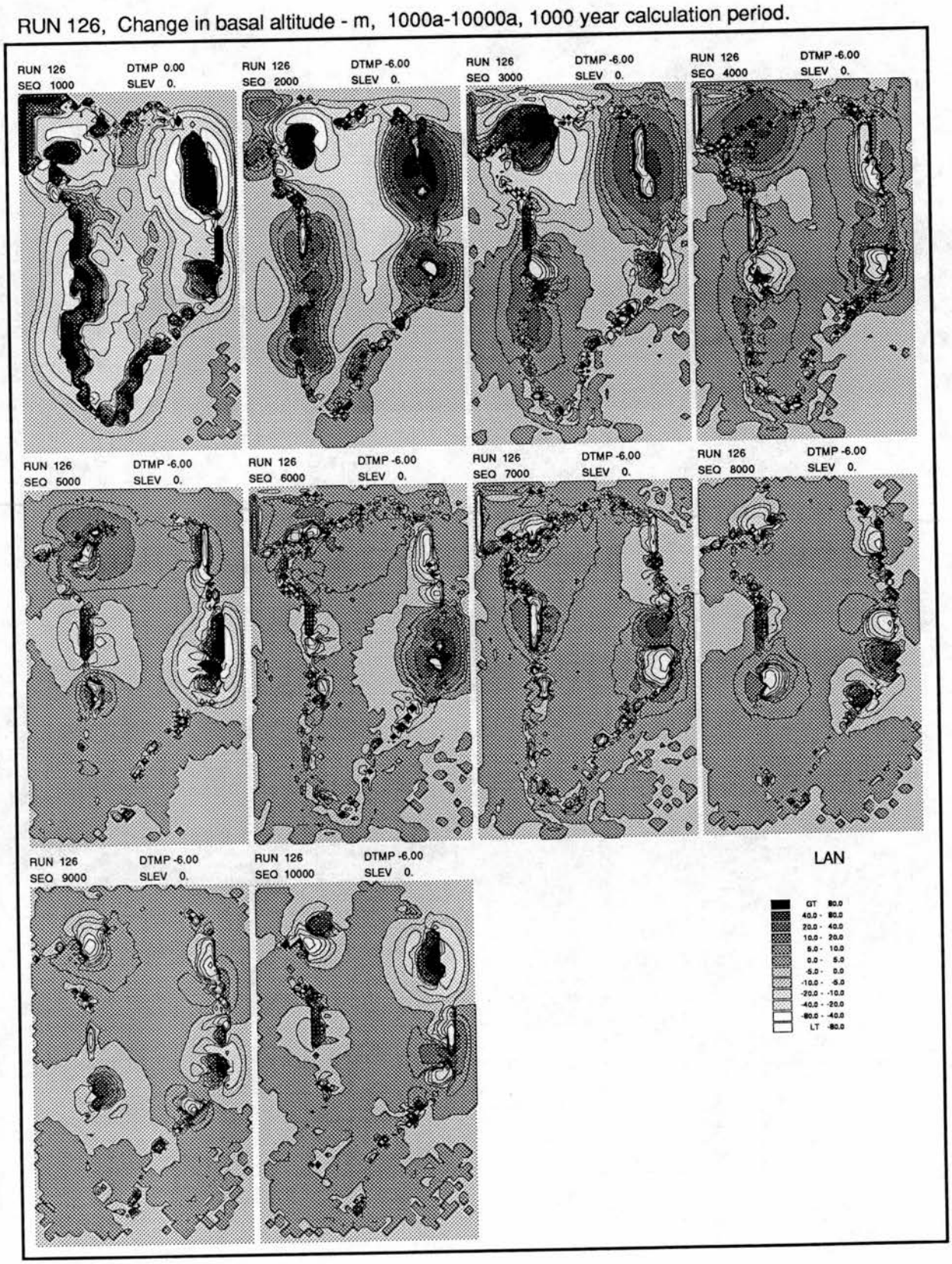

Figure 112: One step deglacial forcing of -120m to 0m sea level (Run 126). Change in basal elevations between successive time periods. Initially, the deglacial fringe rises rapidly whilst subsidence occurs in the adjacent margin areas. This is followed by relaxation and a general gradual rise in the bed under the thinner ice while marginal areas show fluctuation associated with calving.

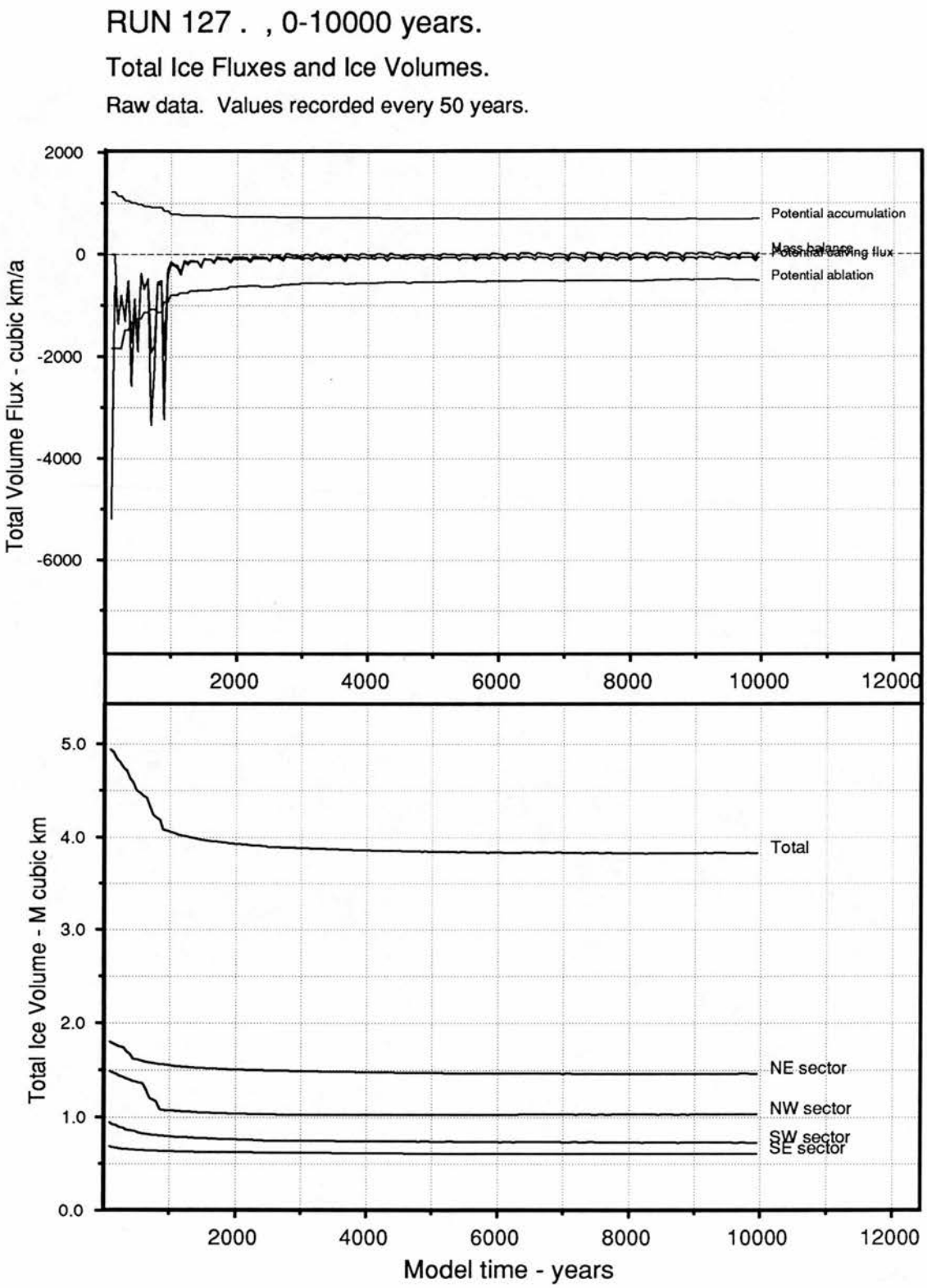

Figure 113: One step deglacial forcing of -120m to 0m sea level and 6°C Warming. Total ice volumes and mass balance. With sea-level forcing calving rates are kept high throughout the run after initially increased rates.

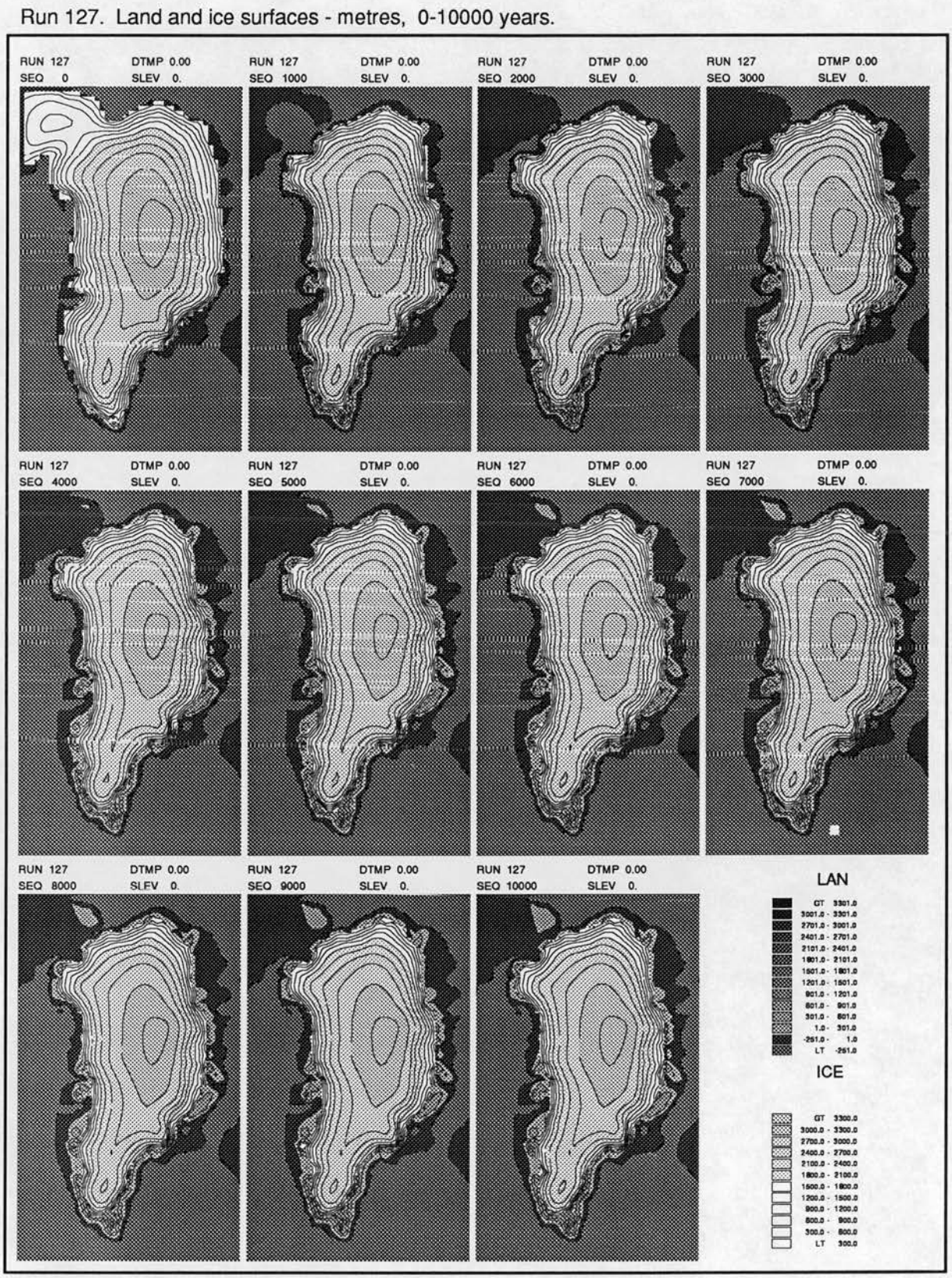

Figure 114: One step deglacial forcing of -120m to 0m sea level and 6°C warming. Modelled land and submarine surfaces with superimposed ice surfaces.

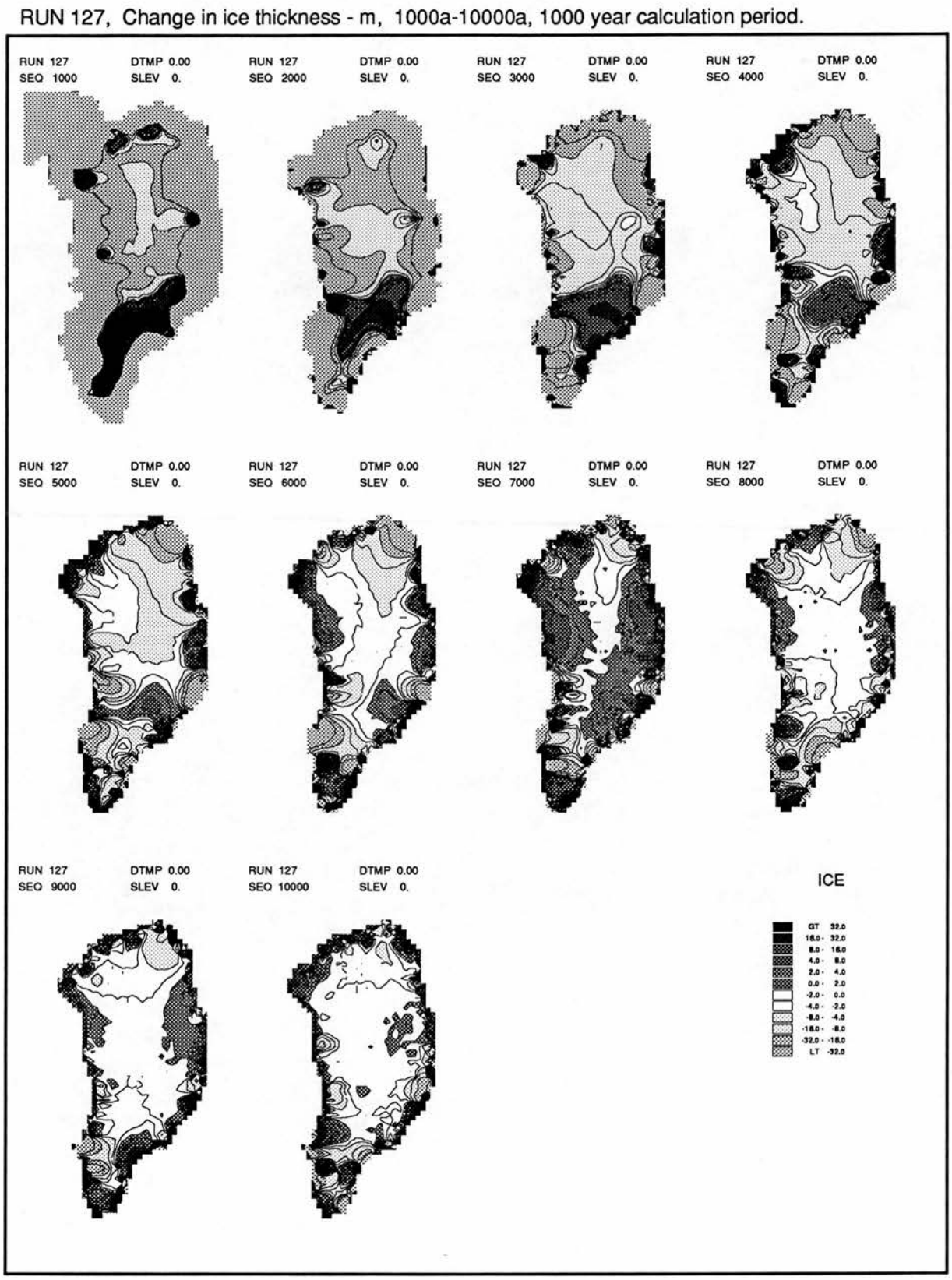

Figure 115: One step deglacial forcing of -120m to 0m sea level and 6°C warming. Successive changes in ice thickness between time periods.

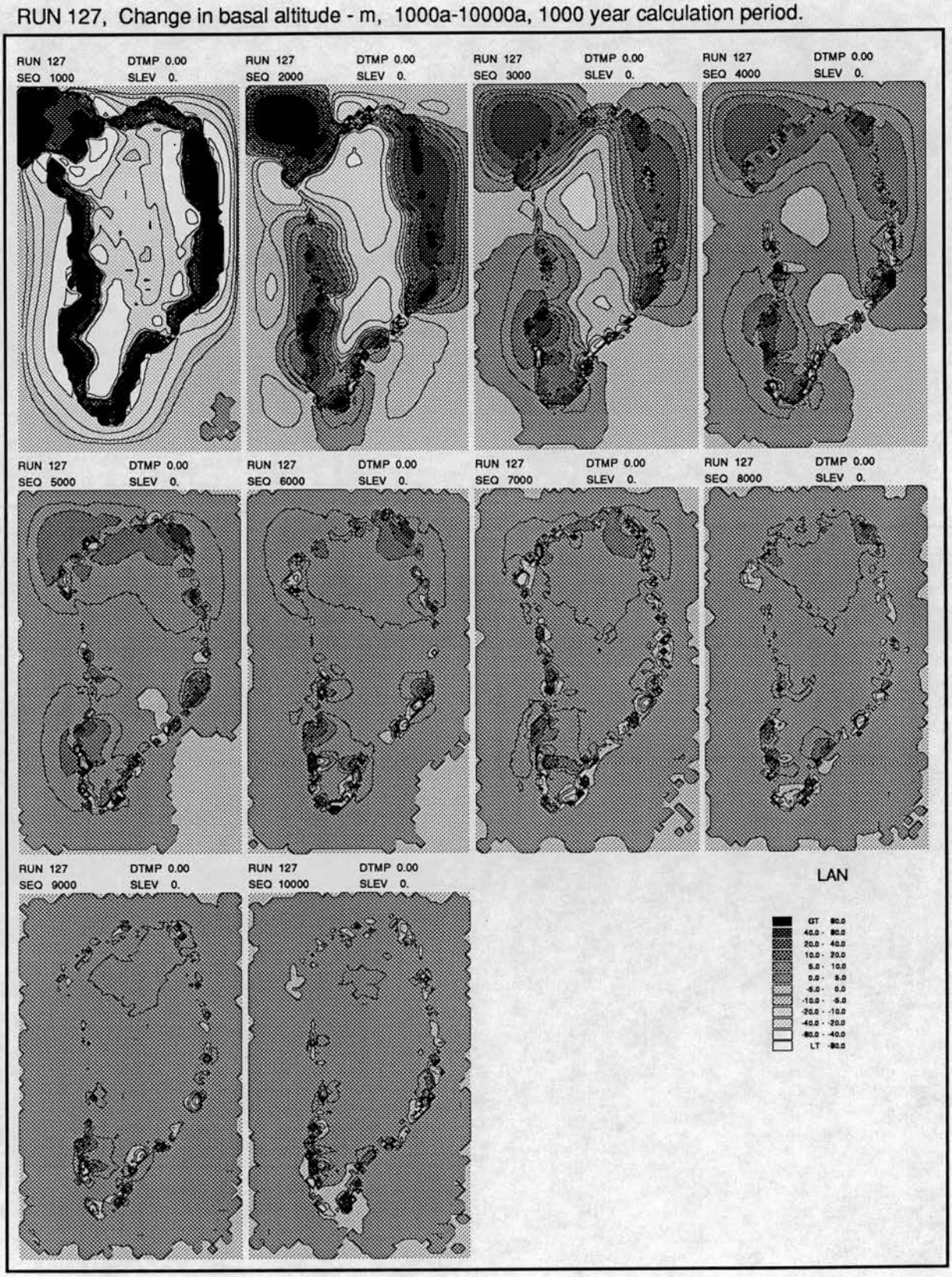

Figure 116: One step deglacial forcing of -120m to 0m sea level and 6°C warming. Successive changes in basal elevation between time periods.

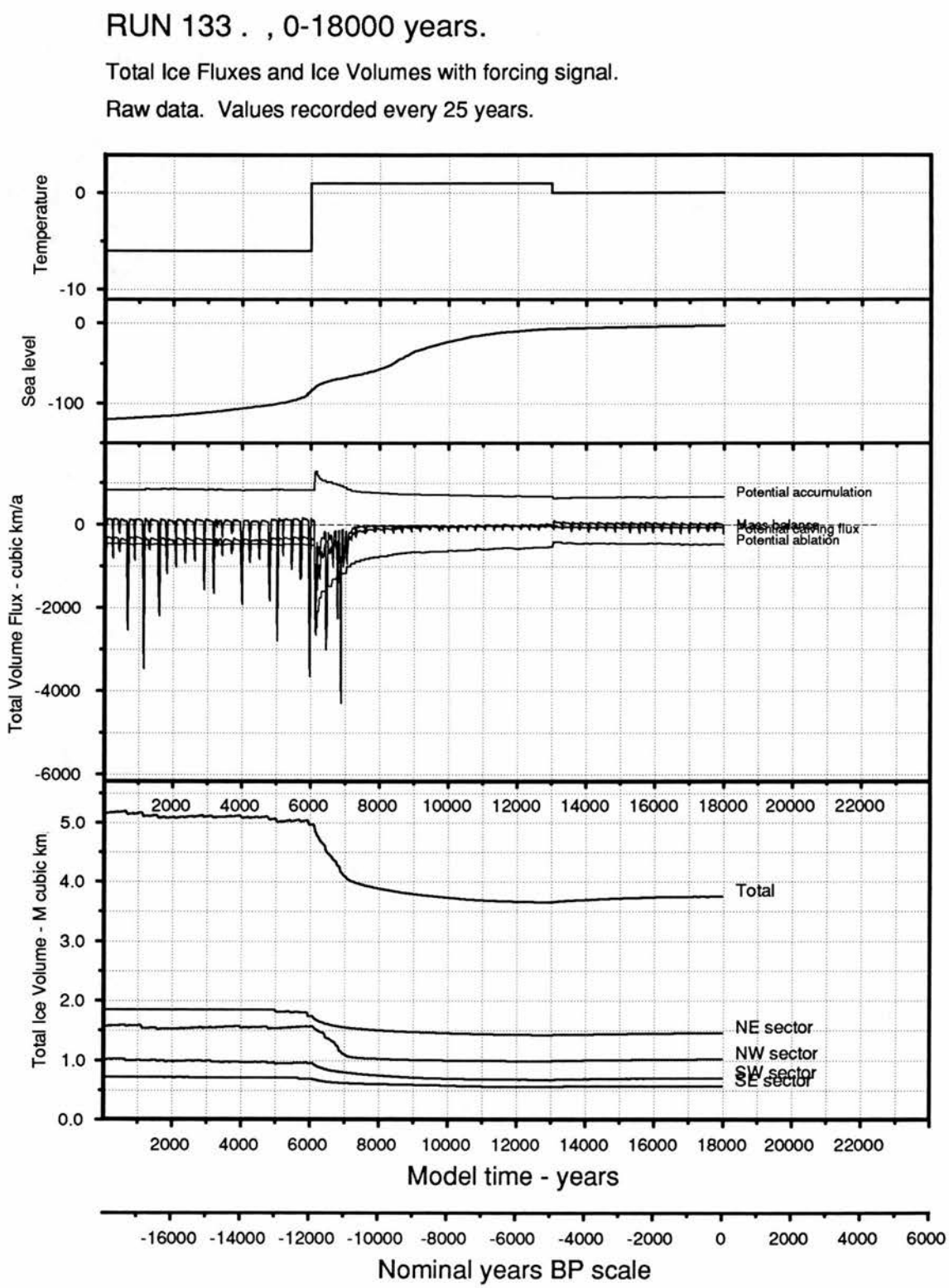

Figure 117: Total ice volumes and mass balance. Modelling of deglaciation with a two step temperature curve and continuous sea-level curve (Run 133). Changes in mass balance relate to the forcing signal. The temperature steps cause sudden, substantial disequilibrium and the model changes through subsequent readjustment.

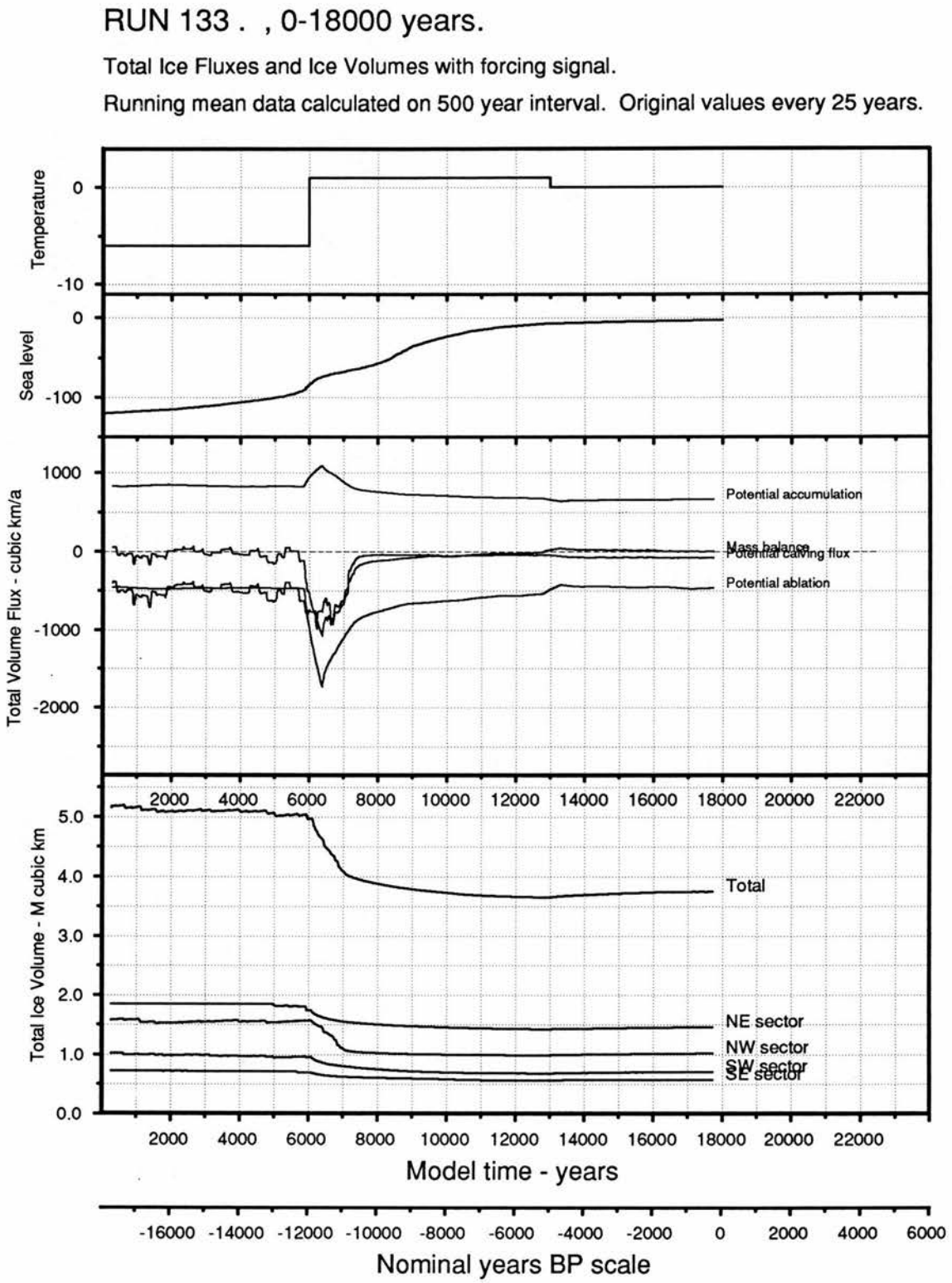

Figure 118: Total ice volumes and mass balance calculated over a 500 year running mean. The figure shows the average tendency of the calving signal.

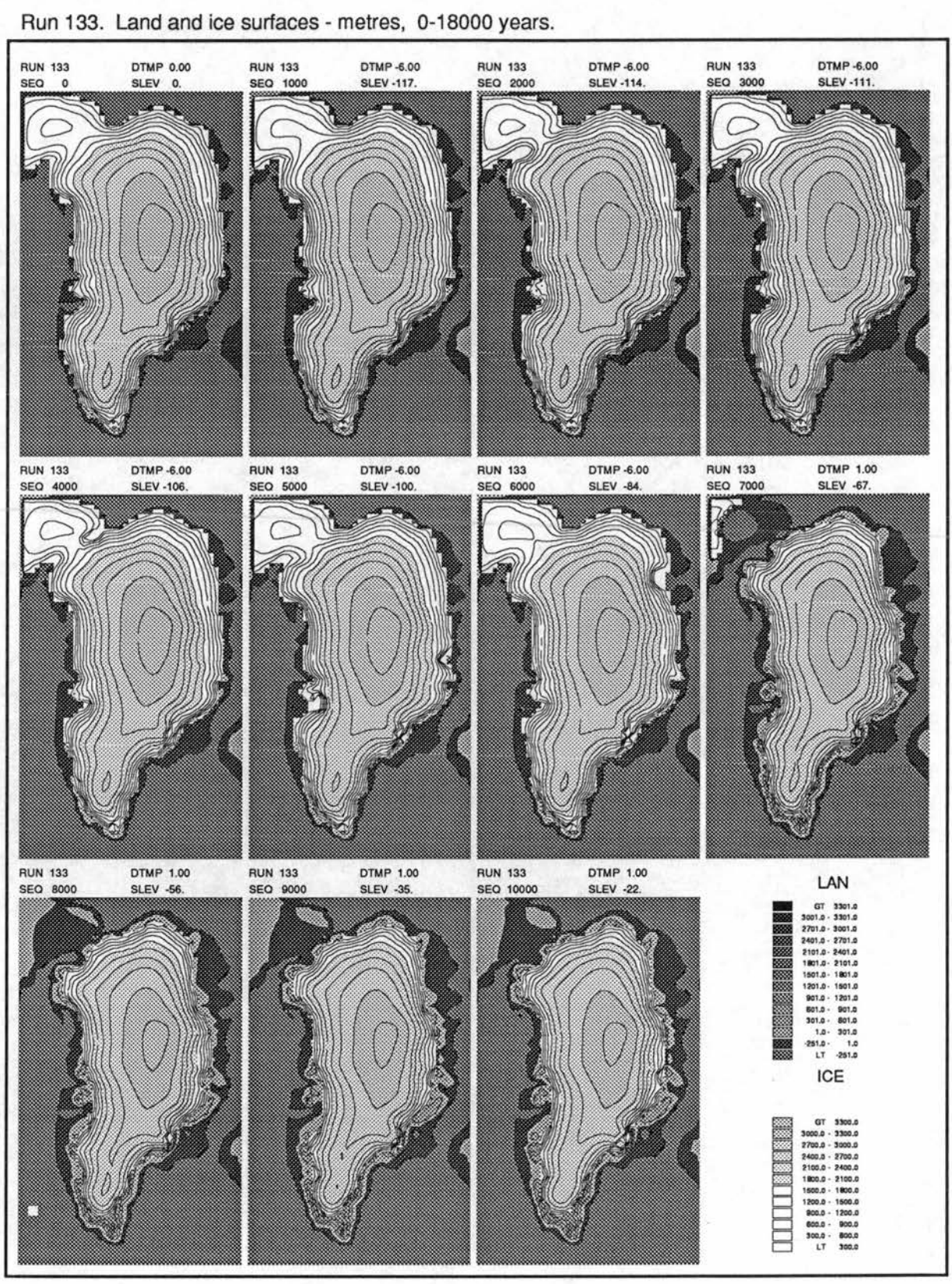

Figure 119: Modelling of deglaciation with a two step temperature curve and continuous sea-level curve (Run 133). Ice sheet surfaces (page 1). The effect of the temperature step at 6000a is substantial, although some shrinkage has occurred through sea-level forcing prior to this forcing signal.

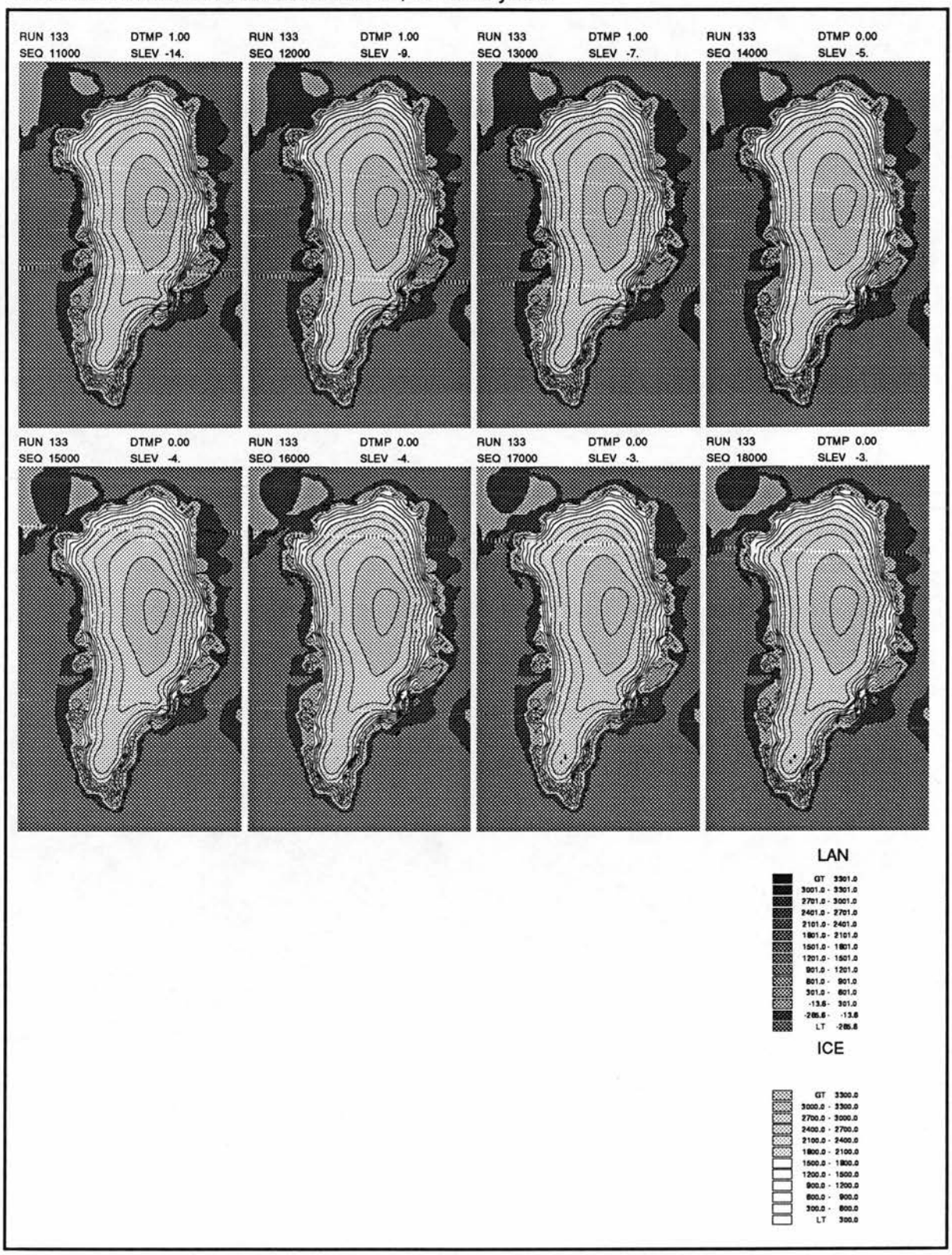

Figure 120: Modelling of deglaciation with a two step temperature curve and continuous sea-level curve (Run 133). Ice sheet surfaces (page 2). The ice sheet reaches a minimum condition at 14000a after which the minor cooling causes slight regeneration.

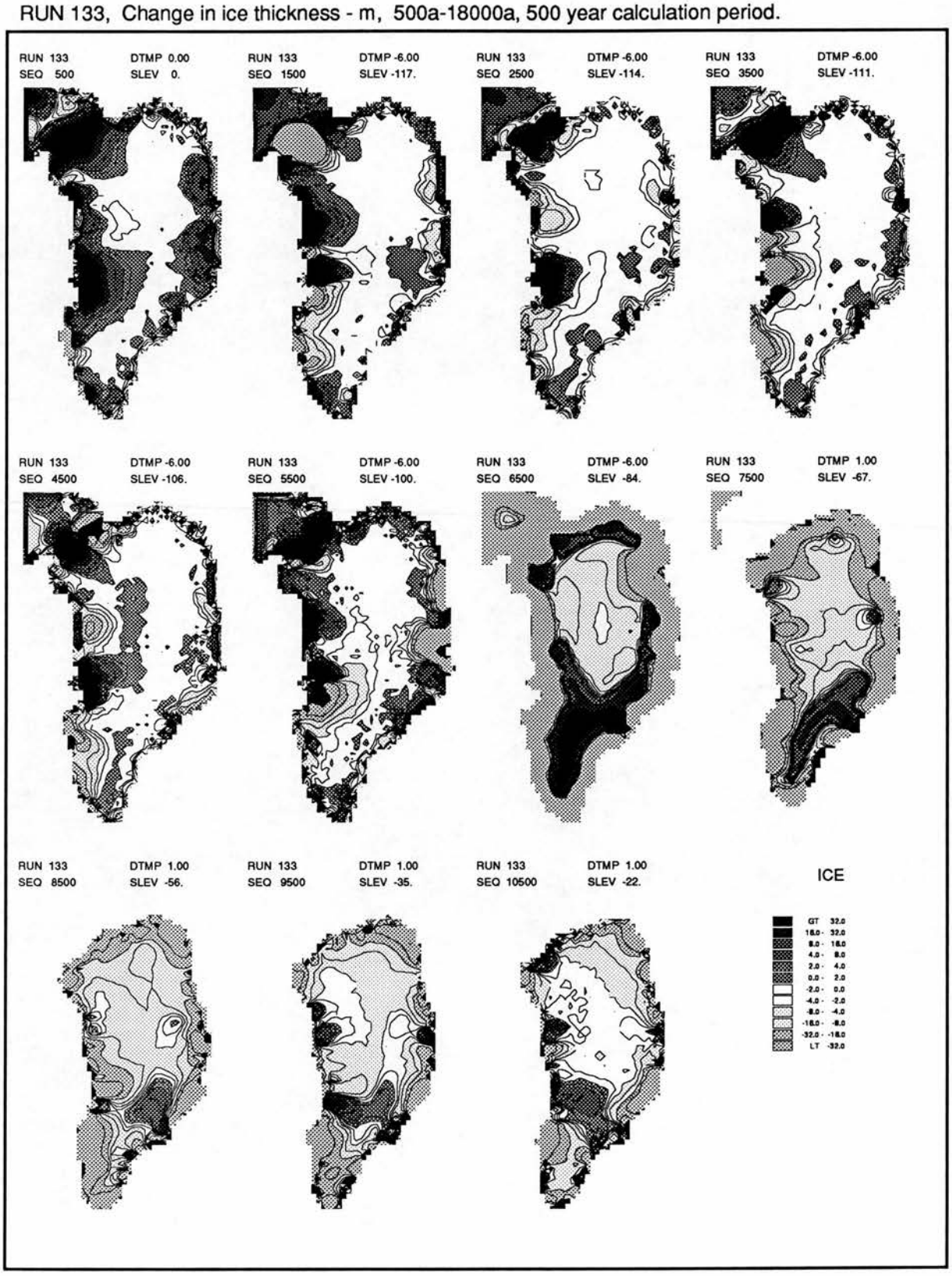

Figure 121: Modelling of deglaciation with a two step temperature curve and continuous sea-level curve (Run 133). Ice thickness change (page 1). Trends in ice sheet development become more obvious, especially the temperature change at 6000a. Prior to this there is change associated with calving activity in the major outlets under sea-level forcing.

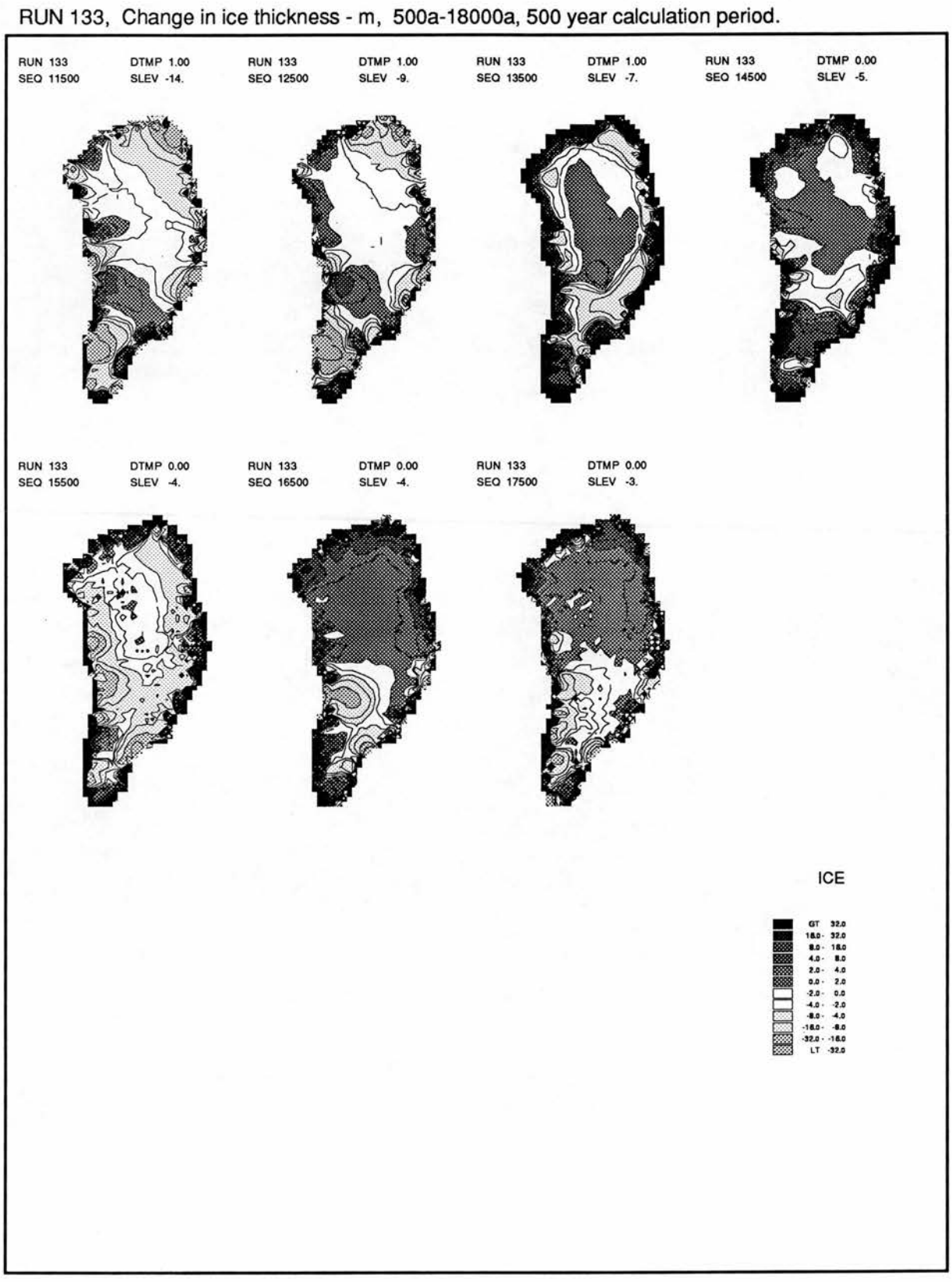

Figure 122: Modelling of deglaciation with a two step temperature curve and continuous sea-level curve (Run 133). Ice thickness change (page 2). As on the previous page, the temperature change at 13000a has the most marked effect on overall ice development. Under the rising sea-level, calving still effects substantial influence in some areas.

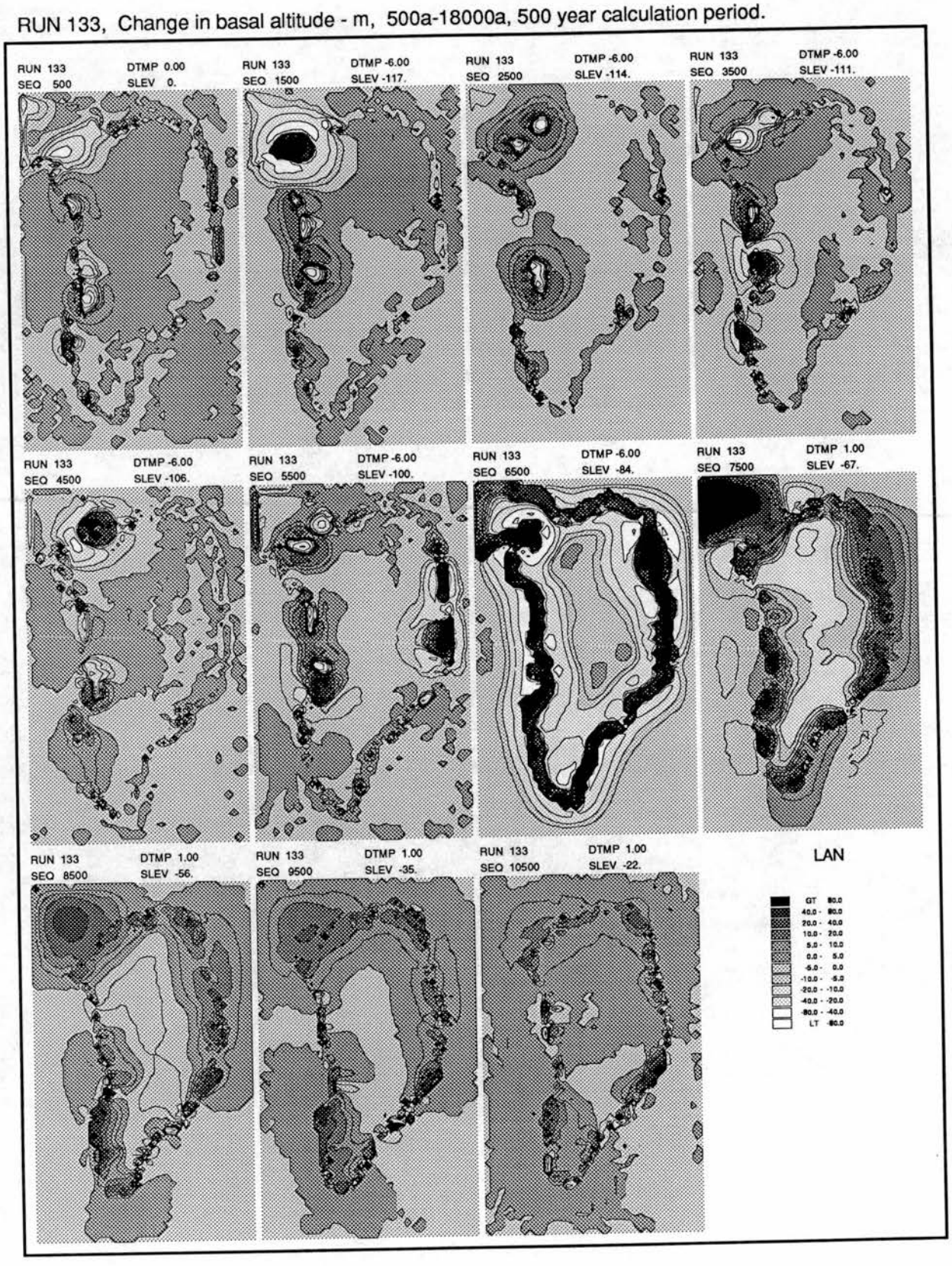

Figure 123: Modelling of deglaciation with a two step temperature curve and continuous sea-level curve (Run 133). Bed elevation change (page 1). This shows areas responding to calving prior to 6500a and then the large uplift of the exposed fringe at 6500a which is still recovering at 9500-10500a.

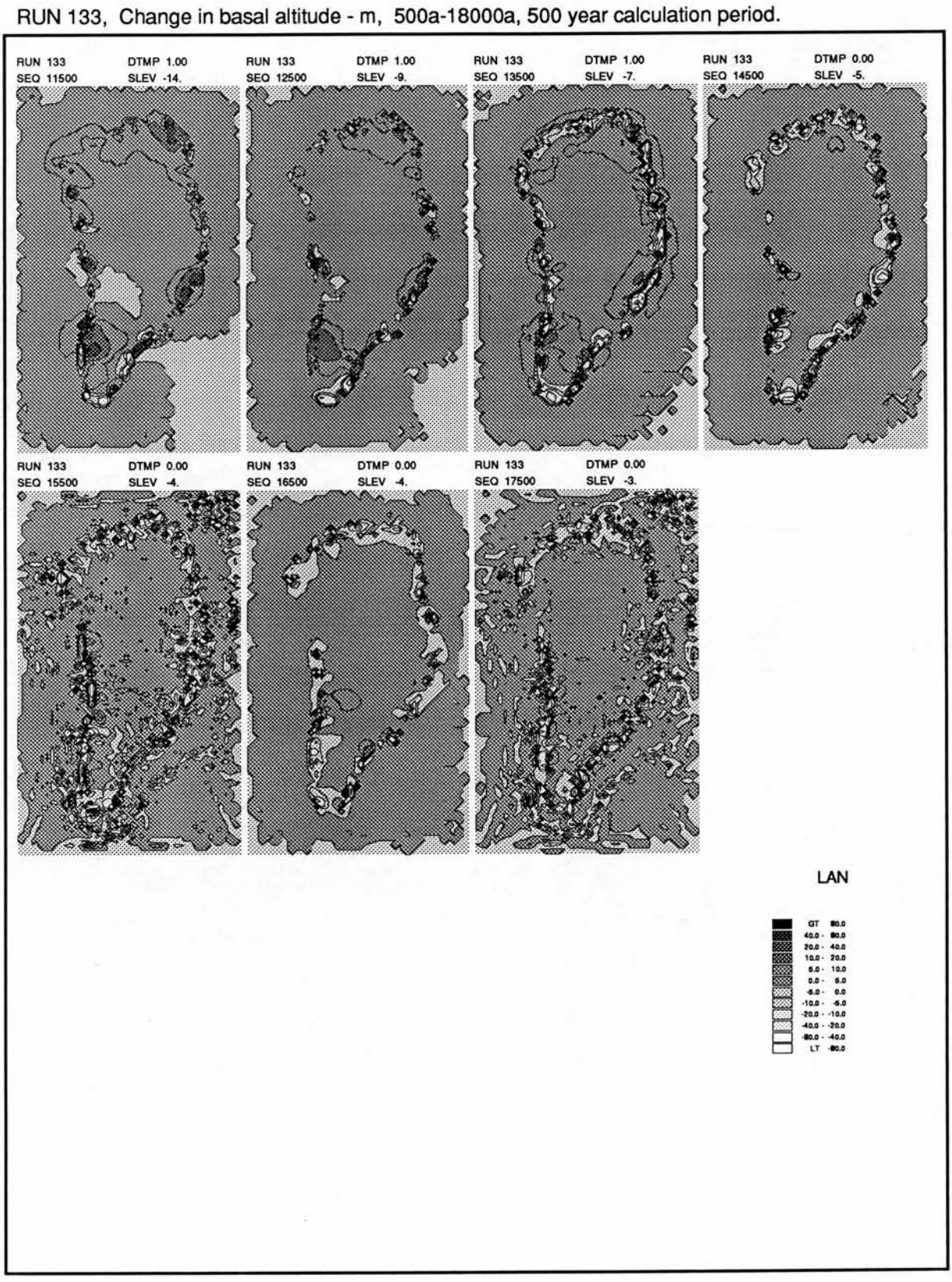

Figure 124: Modelling of deglaciation with a two step temperature curve and continuous sea-level curve (Run 133). Bed elevation change (page 2). Here the adjustment is mainly to minor calving events. The effect of minor ice expansion at 13500a is just discernable.

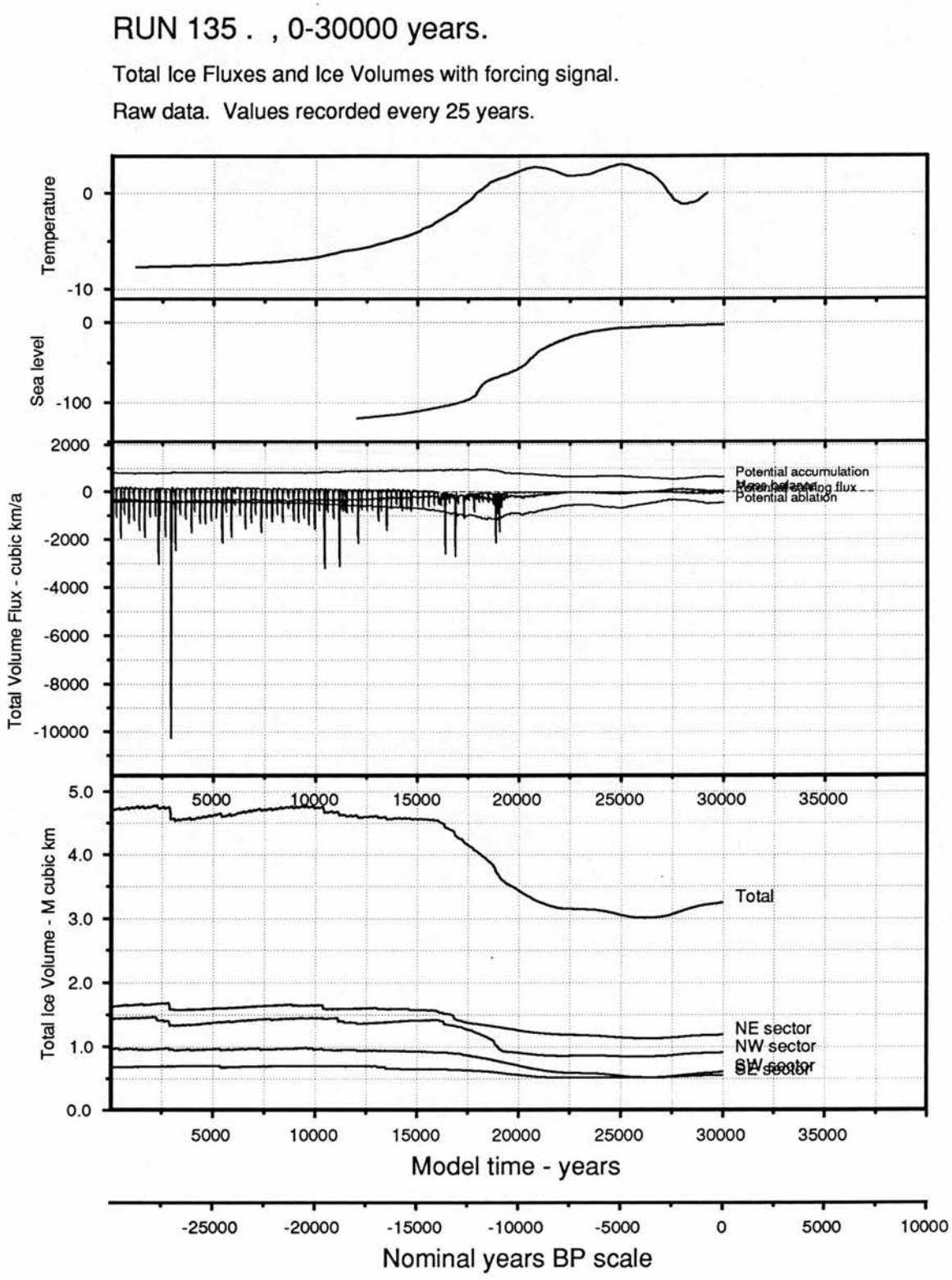

Figure 125: Simulated deglaciation using Camp Century temperature and Barbados sea-level curves (Run 135). Total ice volumes and mass balance. Rapid deglaciation only occurs once sea-levels start to rise. Earlier warming has only a small effect but more rapid warming at 15000-20000a coincides with the rising sea-level, to produce rapid ice removal.

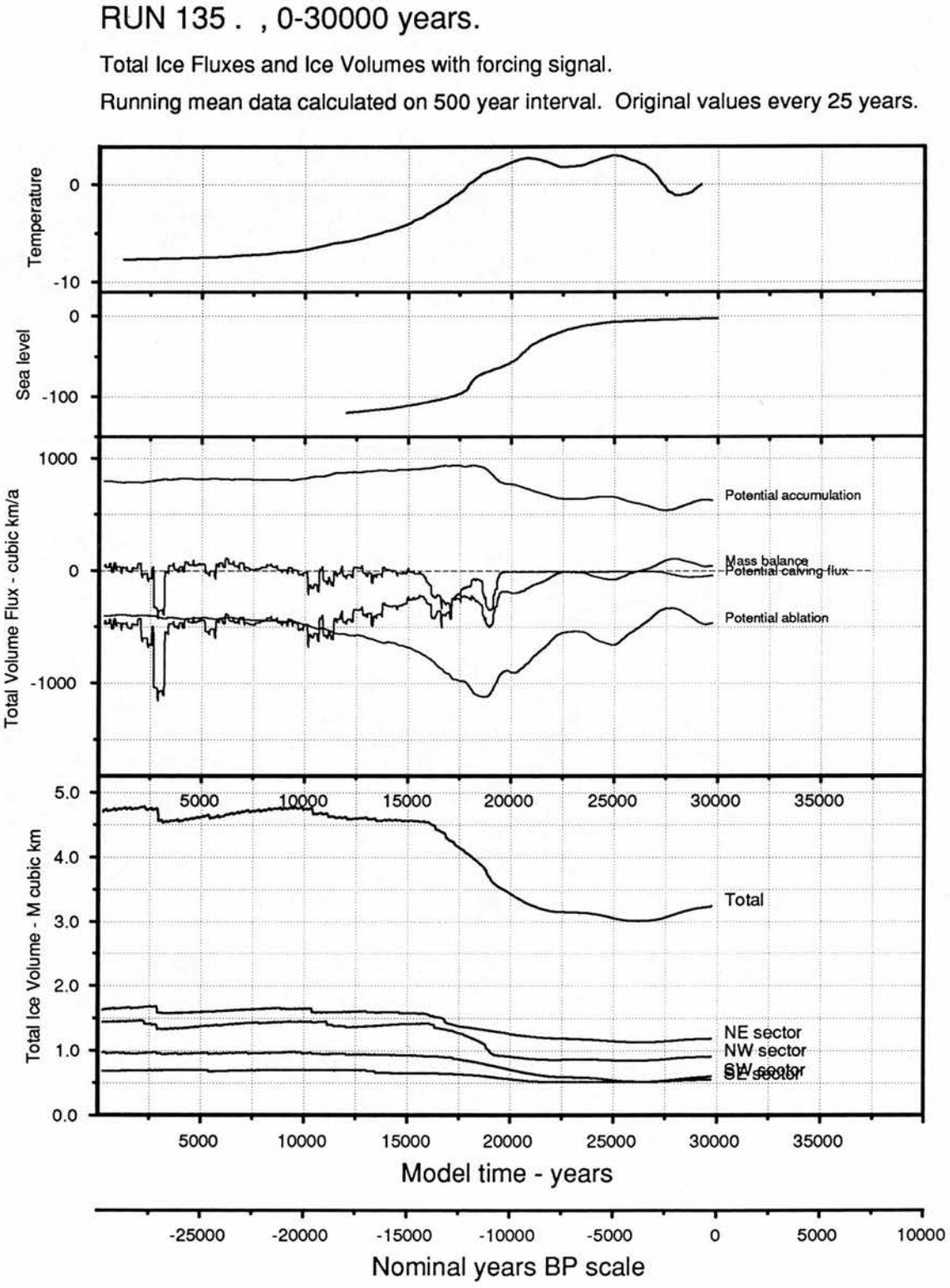

Figure 126: Simulated deglaciation using Camp Century temperature and Barbados sea-level curves (Run 135). Total ice volumes and mass balance calculated as a 500 year running mean. The smoothed version confirms how long-term balance is maintained until about 15000a. The second increase in calving flux coincides with the destabilisation of ice over the Ellesmere Island area.

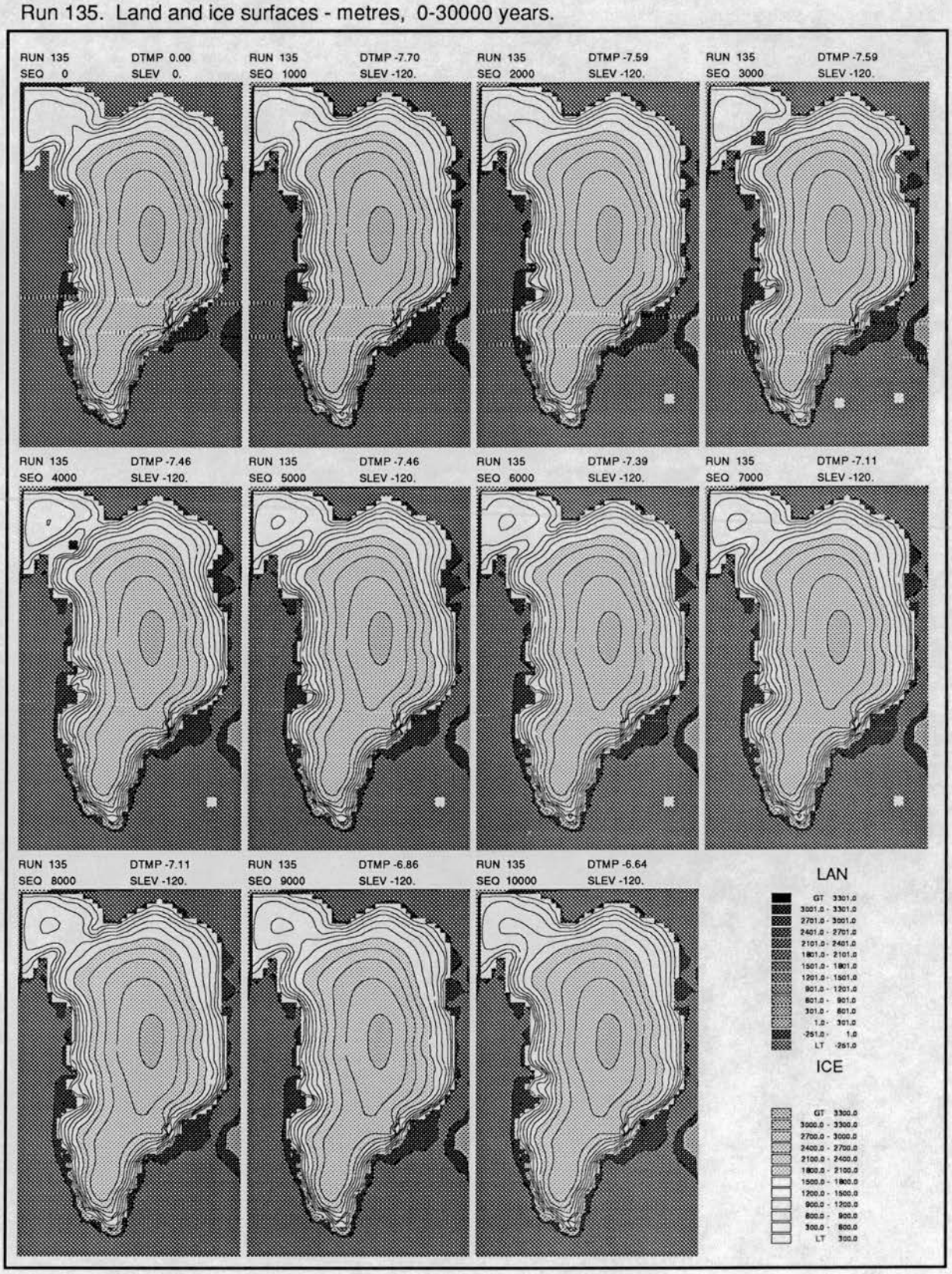

Figure 127: Simulated deglaciation using Camp Century temperature and Barbados sea-level curves (Run 135, page 1). The ice sheet stays relatively stable throughout this period, though movement of the margins associated with calving is evident.

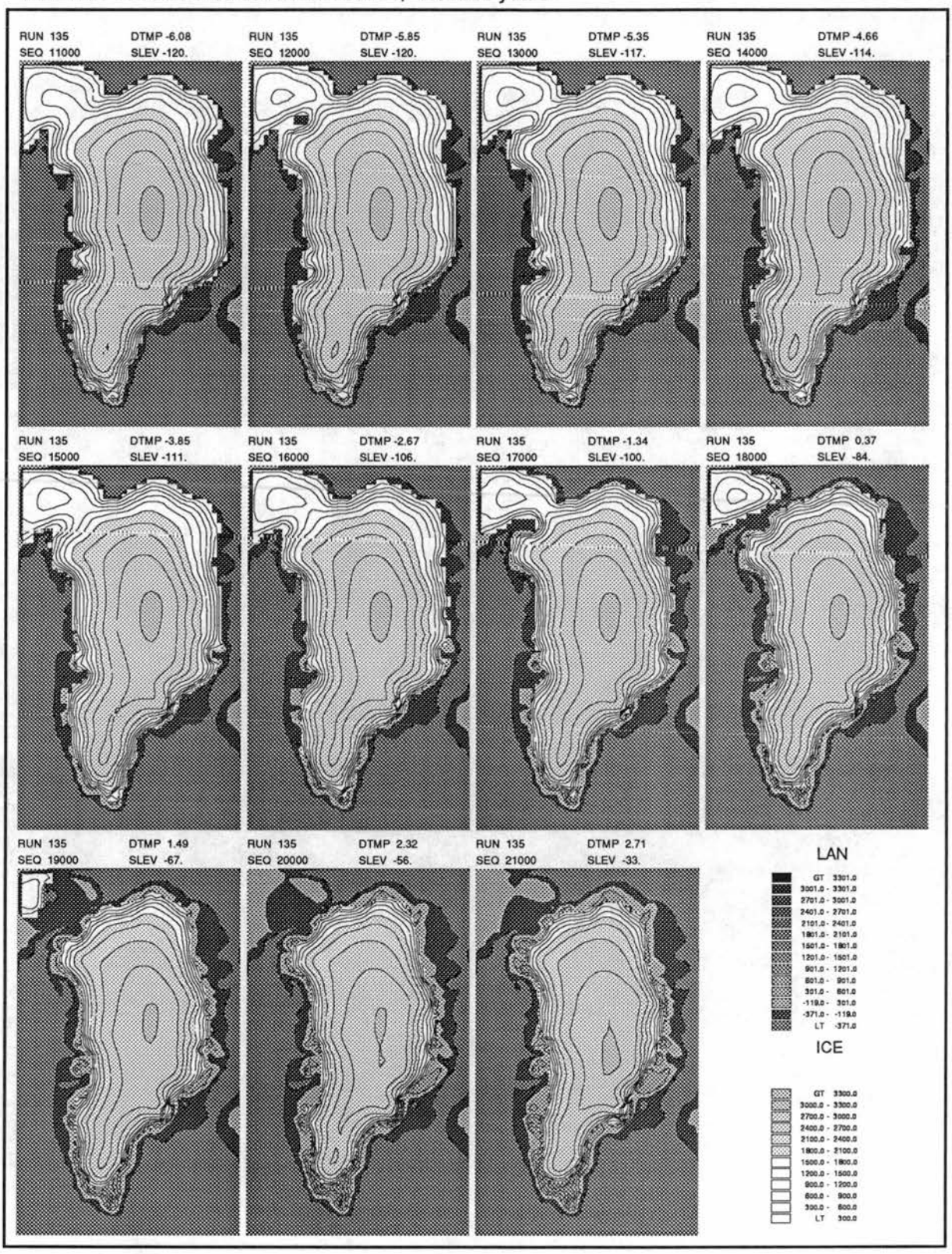

Figure 128: Simulated deglaciation using Camp Century temperature and Barbados sea-level curves (Run 135, page 2). Rapid deglaciation starts at about 15000a. By 19000a, the ice margins have largely drawn back beyond the shoreline (cf calving rates fig 125). Ice is evacuated quickly from Ellesmere island once separated from the main ice body (18-19000a).

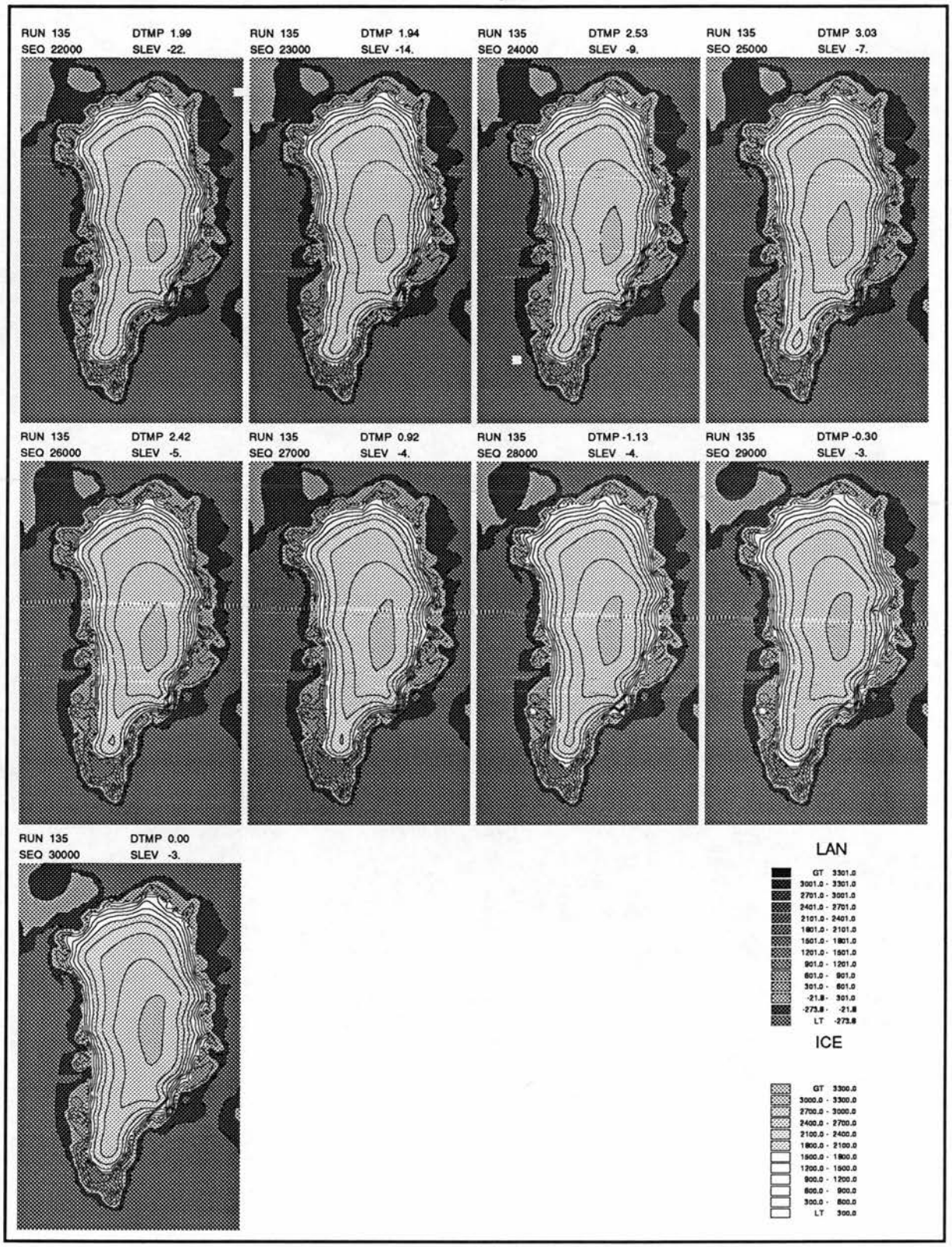

Figure 129: Simulated deglaciation using Camp Century temperature and Barbados sea-level curves (Run 135, page 3). Warm conditions at 25000a cause the ice margins to retreat beyond the present-day limit. Subsequently the ice expands to almost return to present proportions.

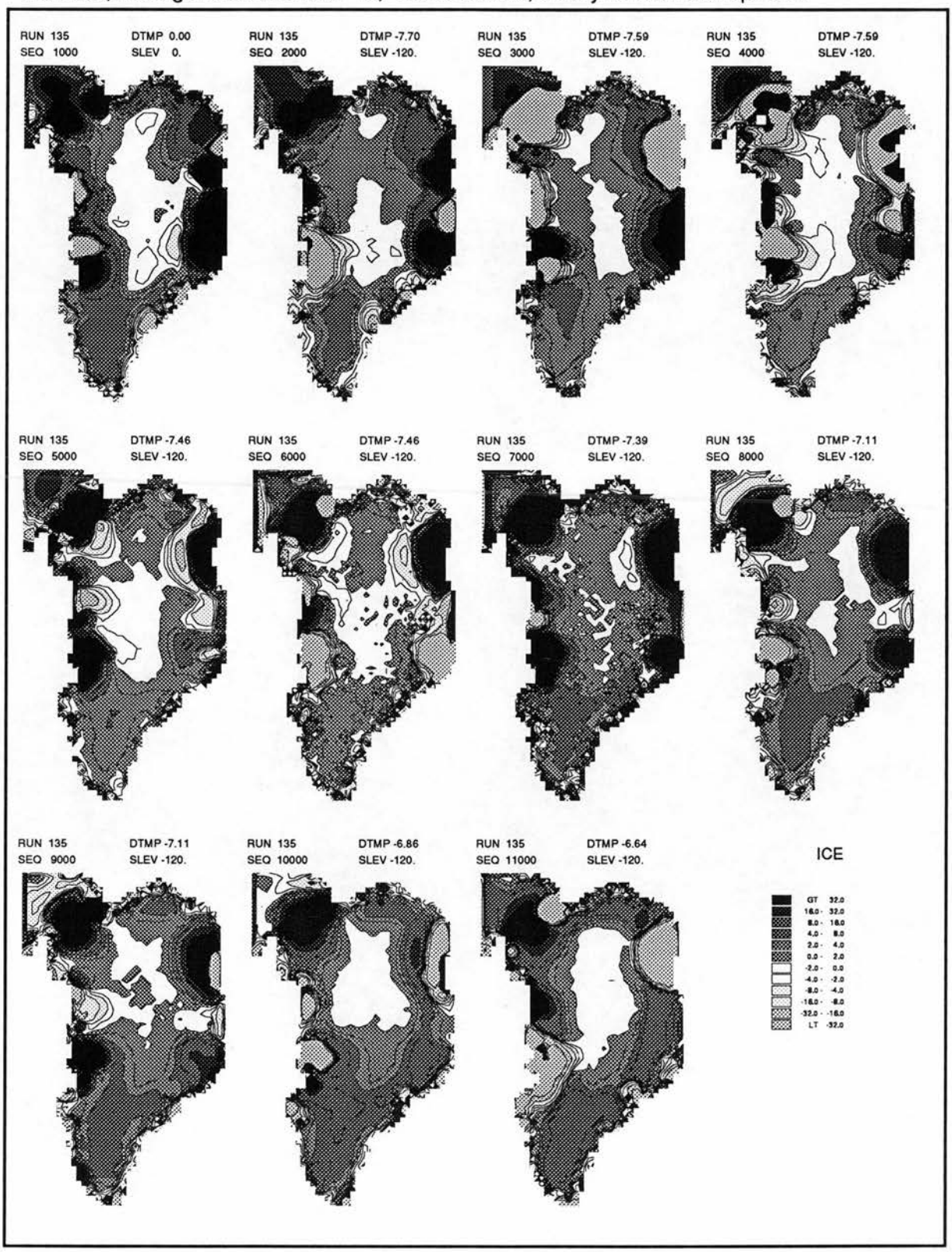

Figure 130: Simulated deglaciation using Camp Century temperature and Barbados sea-level curves (Run 135). Changes in ice thickness, page 1. Under the initial slight warming, much of the ice sheet actually thickens, steepening gradients, particularly the southern dome. The margins show evidence of considerable fluctuation associated with calving.

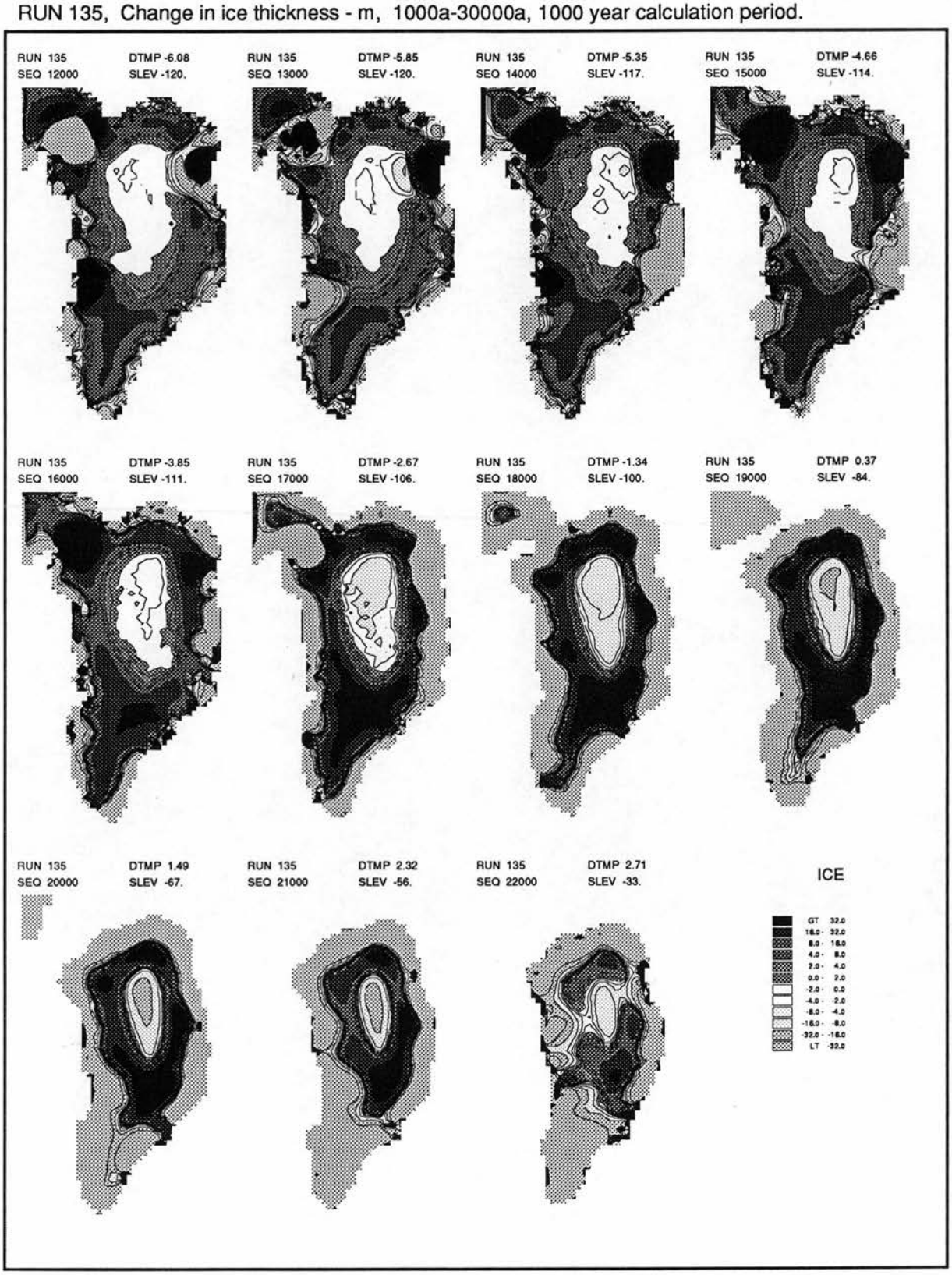

Figure 131: Simulated deglaciation using Camp Century temperature and Barbados sea-level curves (Run 135). Changes in ice thickness, page 2. From 12-16000 years the characteristic pattern is for the northern dome to be largely stable whilst the southern dome continues to stee pen and thicken. With stronger warming after 16000a this trend is characteristic of the whole ice sheet, with the zone of wasting ice moving back towards the ice centre.

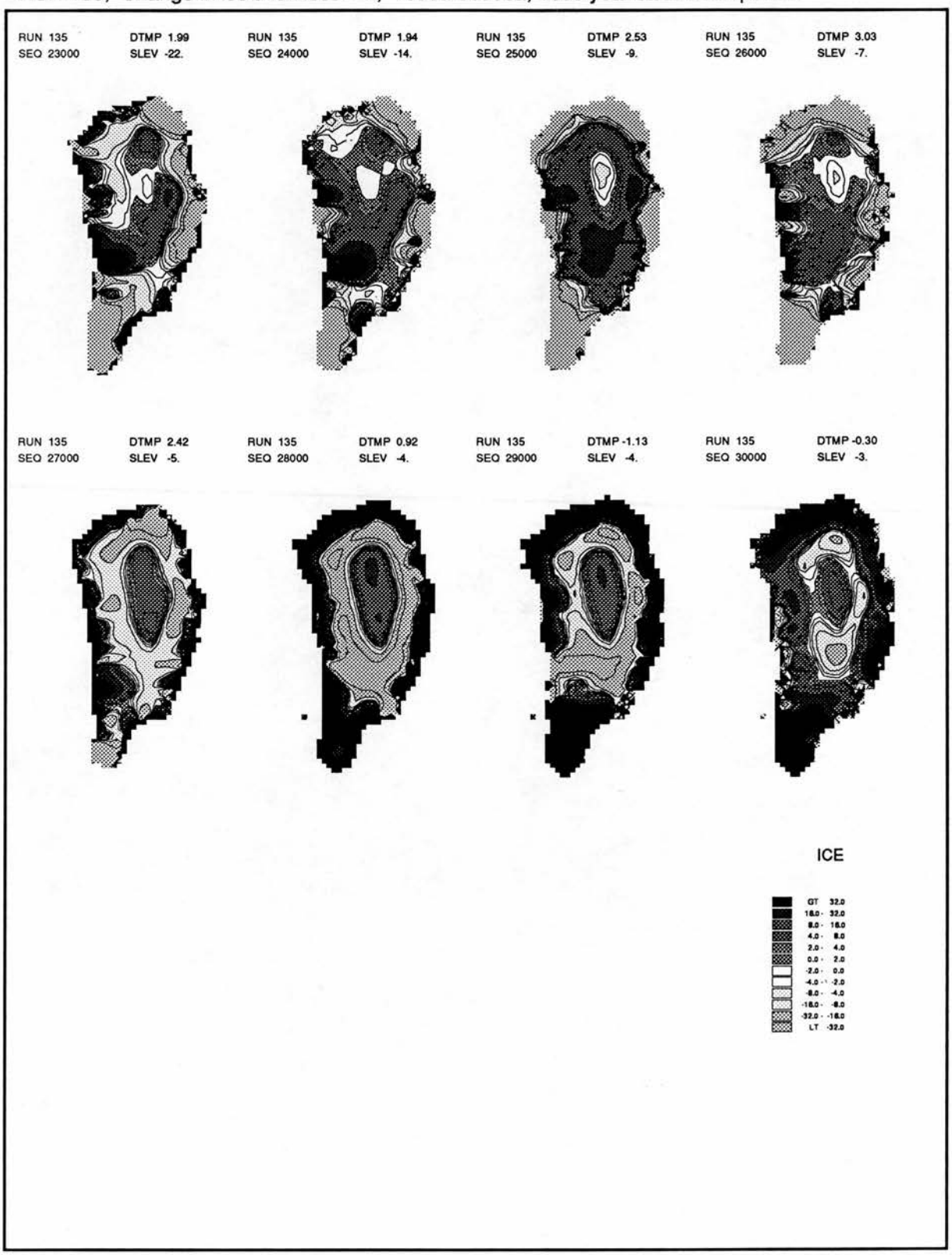

Figure 132: Simulated deglaciation using Camp Century temperature and Barbados sea-level curves (Run 135). Changes in ice thickness, page 3. The reversal in temperatures after 25000a allows the ice sheet to eventually expand, but there is a 2000 year lag before substantial thickening around the margin occurs.

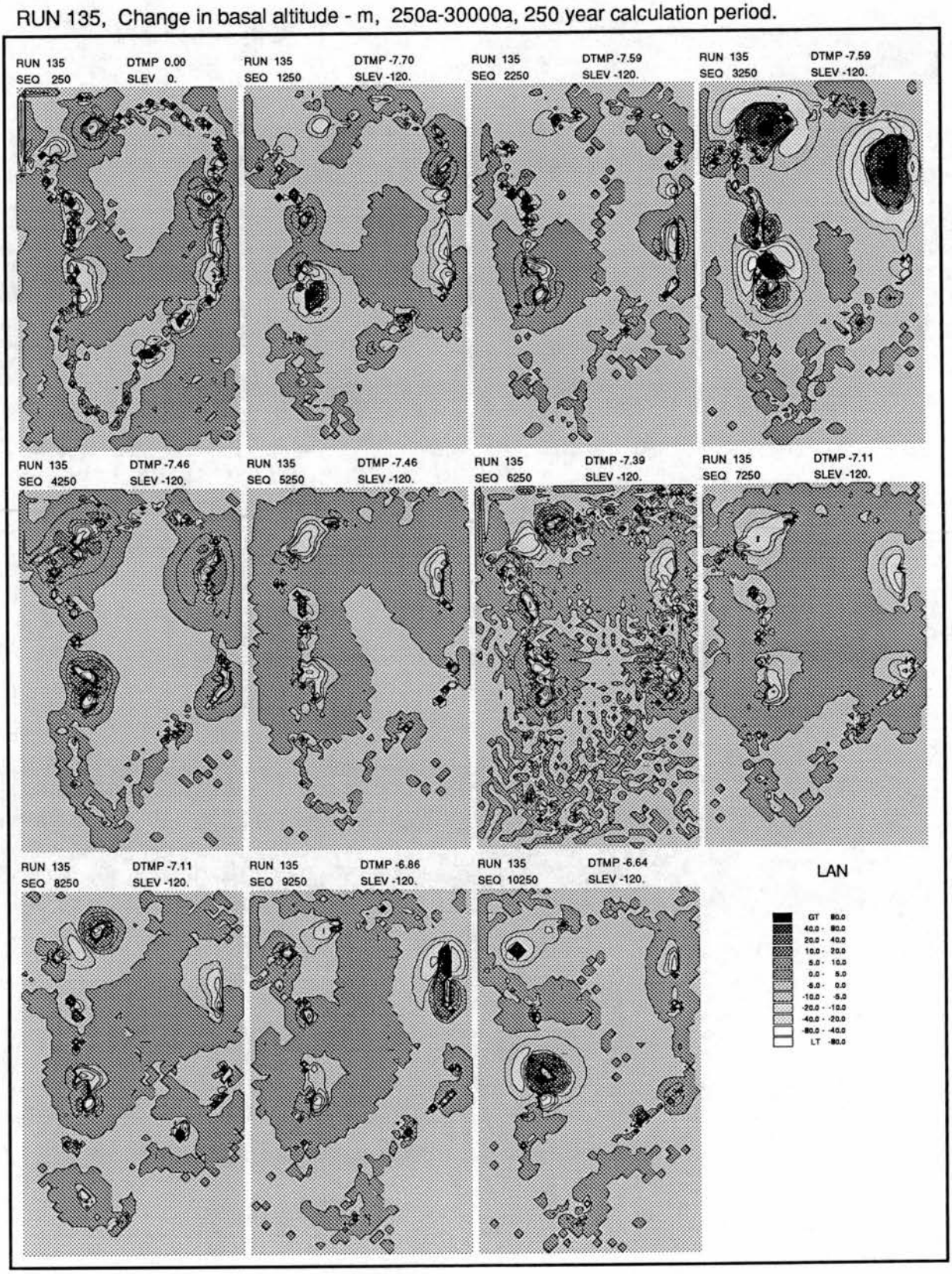

Figure 133: Simulated deglaciation using Camp Century temperature and Barbados sea-level curves (Run 135). Basal elevation change, page 1. The lack of overall change in the ice sheet is demonstrated by the low rates of isostatic adjustment up to 10250a. Calving areas show up strongly.

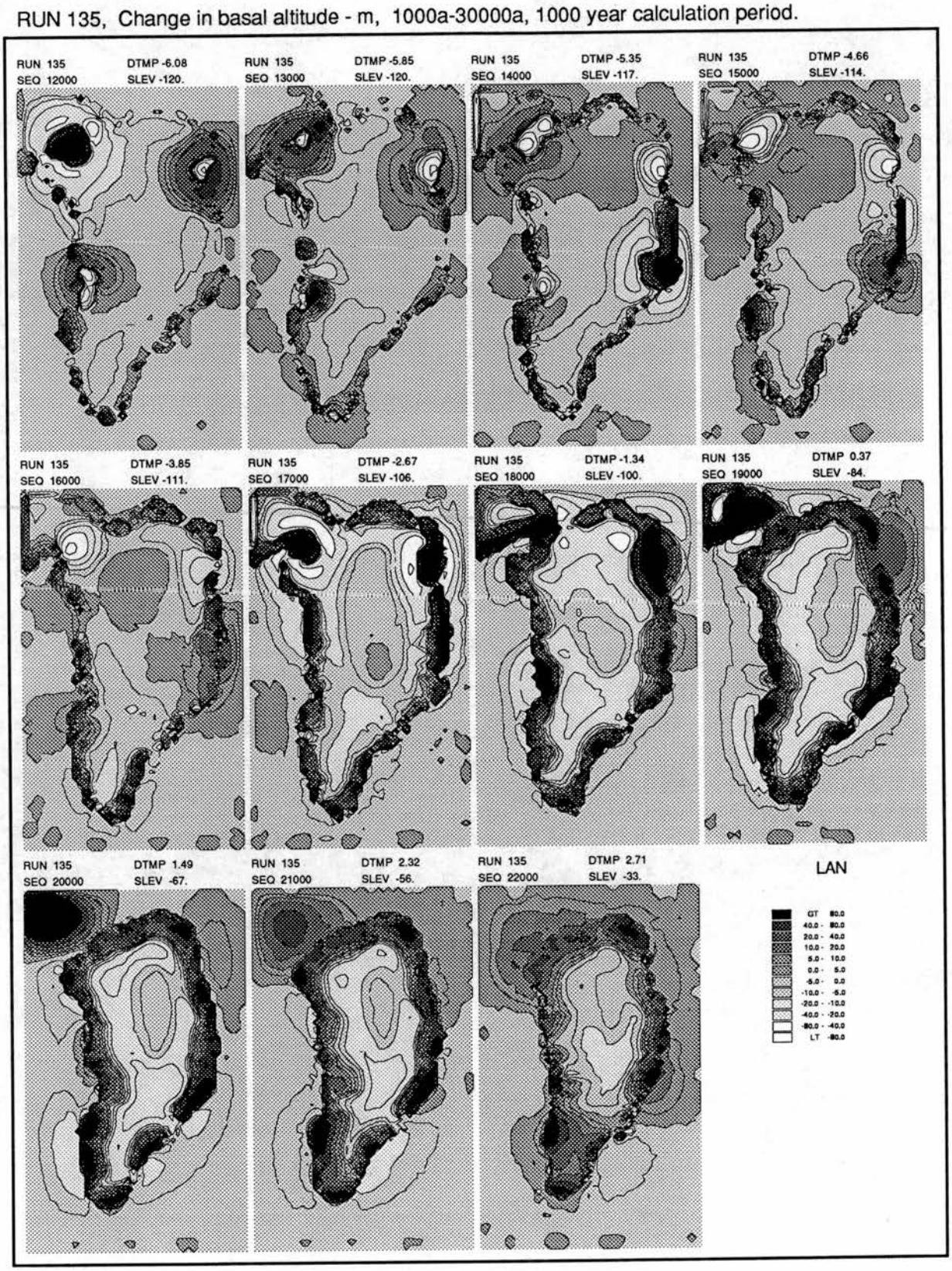

Figure 134: Simulated deglaciation using Camp Century temperature and Barbados sea-level curves (Run 135). Basal elevation change, page 2. After 12250 years, the uplift around a deglaciating fringe is evident. This intensifies after 16250a. The adjustment is largely not transmitted far into other areas because deglaciation is relatively constant rather than instantaneous.

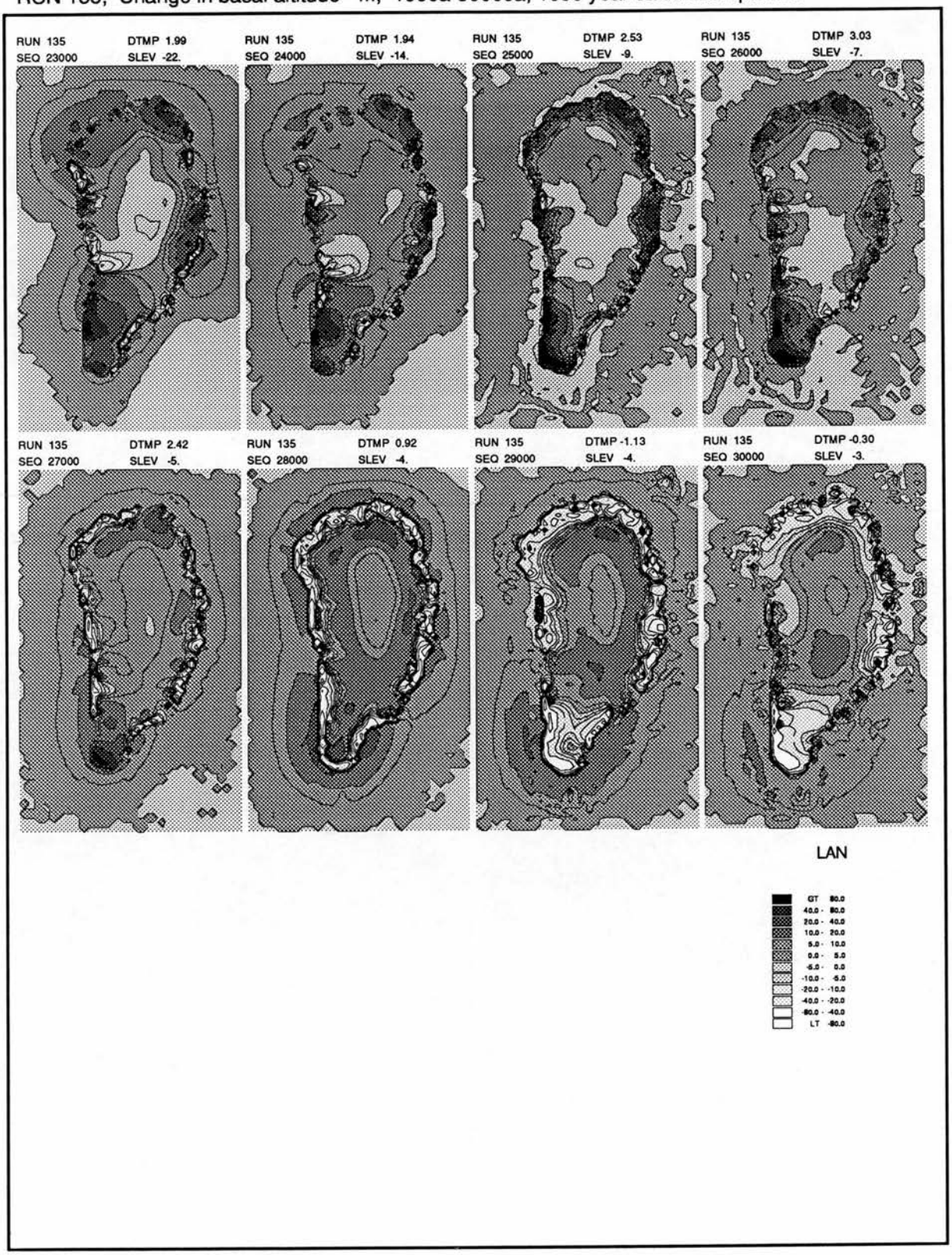

Figure 135: Simulated deglaciation using Camp Century temperature and Barbados sea-level curves (Run 135). Basal elevation change, page 3. After 26250a, the expanding margin reverses the isostatic response.

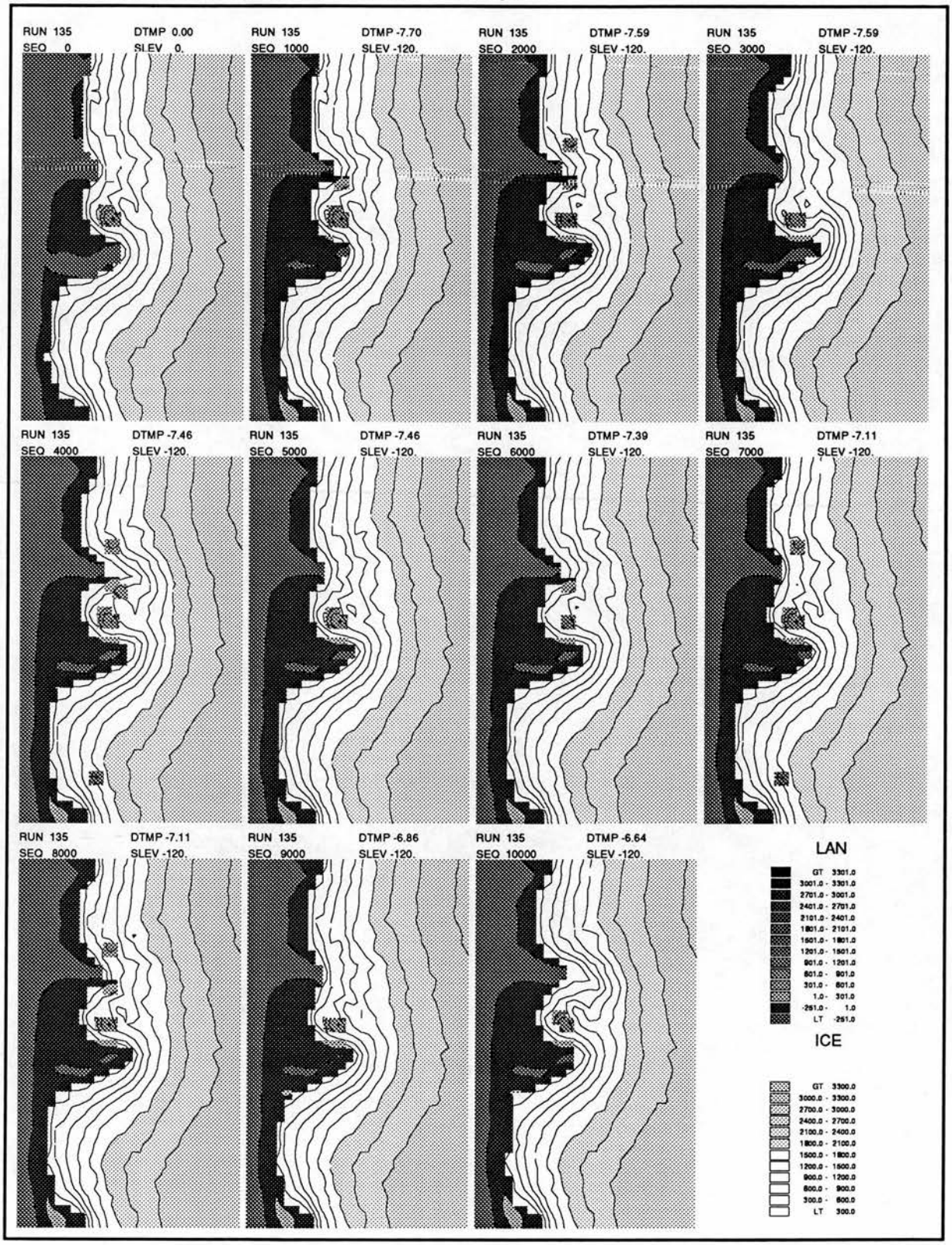

Figure 136: Simulated deglaciation using Camp Century temperature and Barbados sea-level curves (Run 135). West Coast detail, page 1. Up to 10000a, the margin is largely stable. Calving followed by advancement of the margin occurs at Disko (3000a) and Umanaq (10000a).

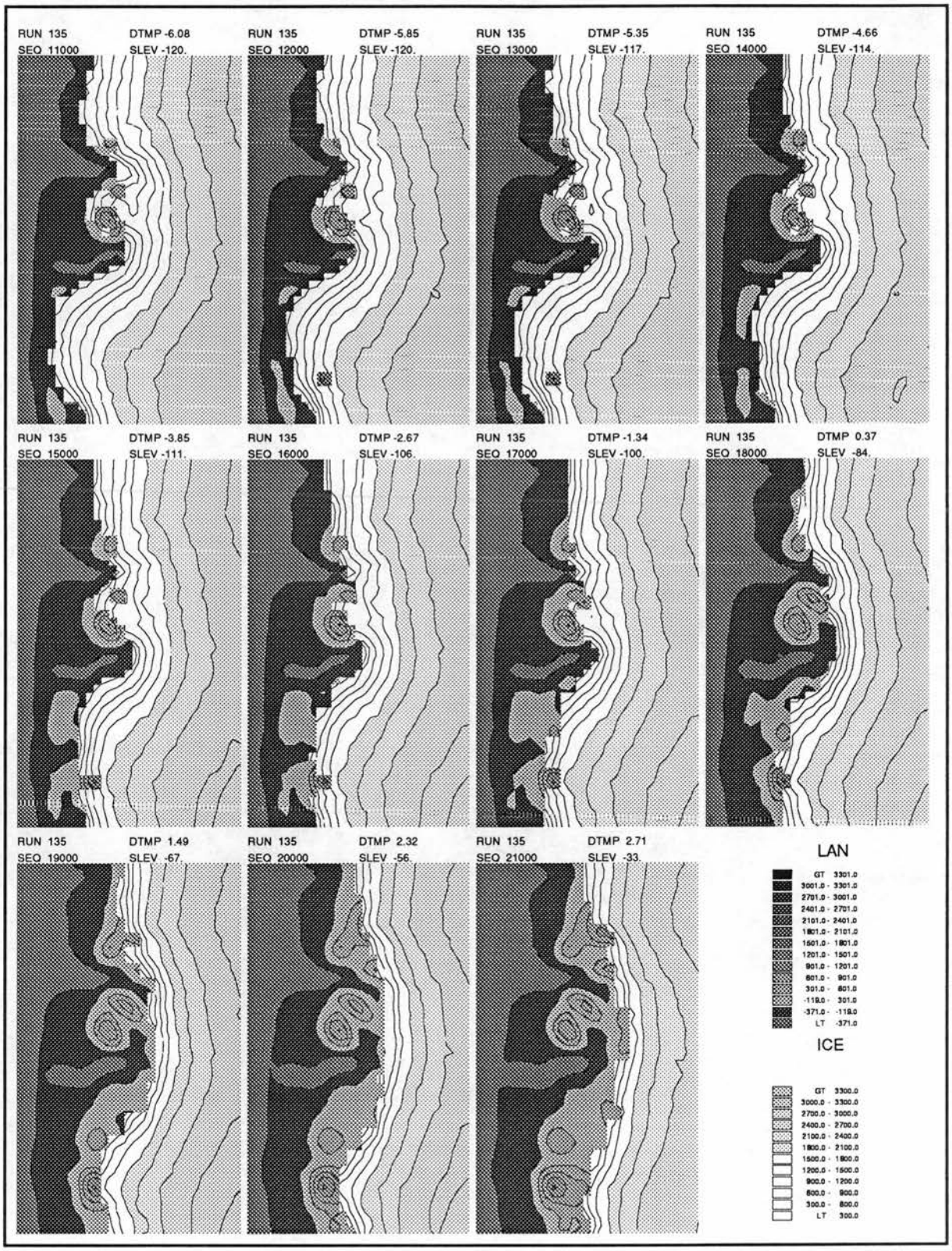

Figure 137: Simulated deglaciation using Camp Century temperature and Barbados sea-level curves (Run 135). West Coast detail, page 2. Deglaciation is precipitated by calving in the channels surrounding Disko Island. Concurrent isostatic adjustment with deglaciation along Lersletten keeps the deglaciating margin near the shoreline until 18000a. The high ground near Sukkertoppen holds ice well (20000a).

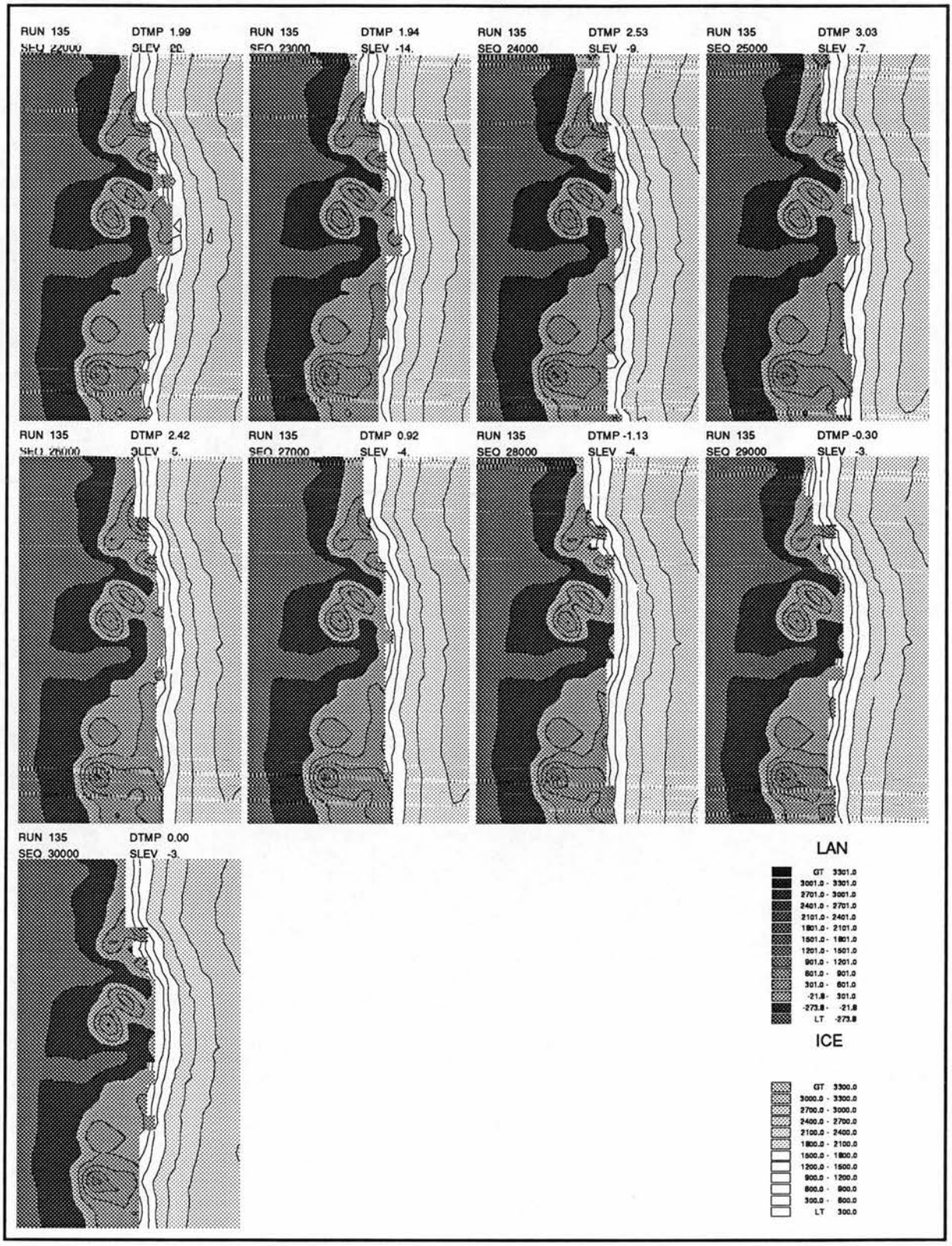

Figure 138: Simulated deglaciation using Camp Century temperature and Barbados sea-level curves (Run 135). West Coast detail, page 3. The ice margin retreats behind the present-day limit and advances again with renewed cooling but this is only obvious after 28000a

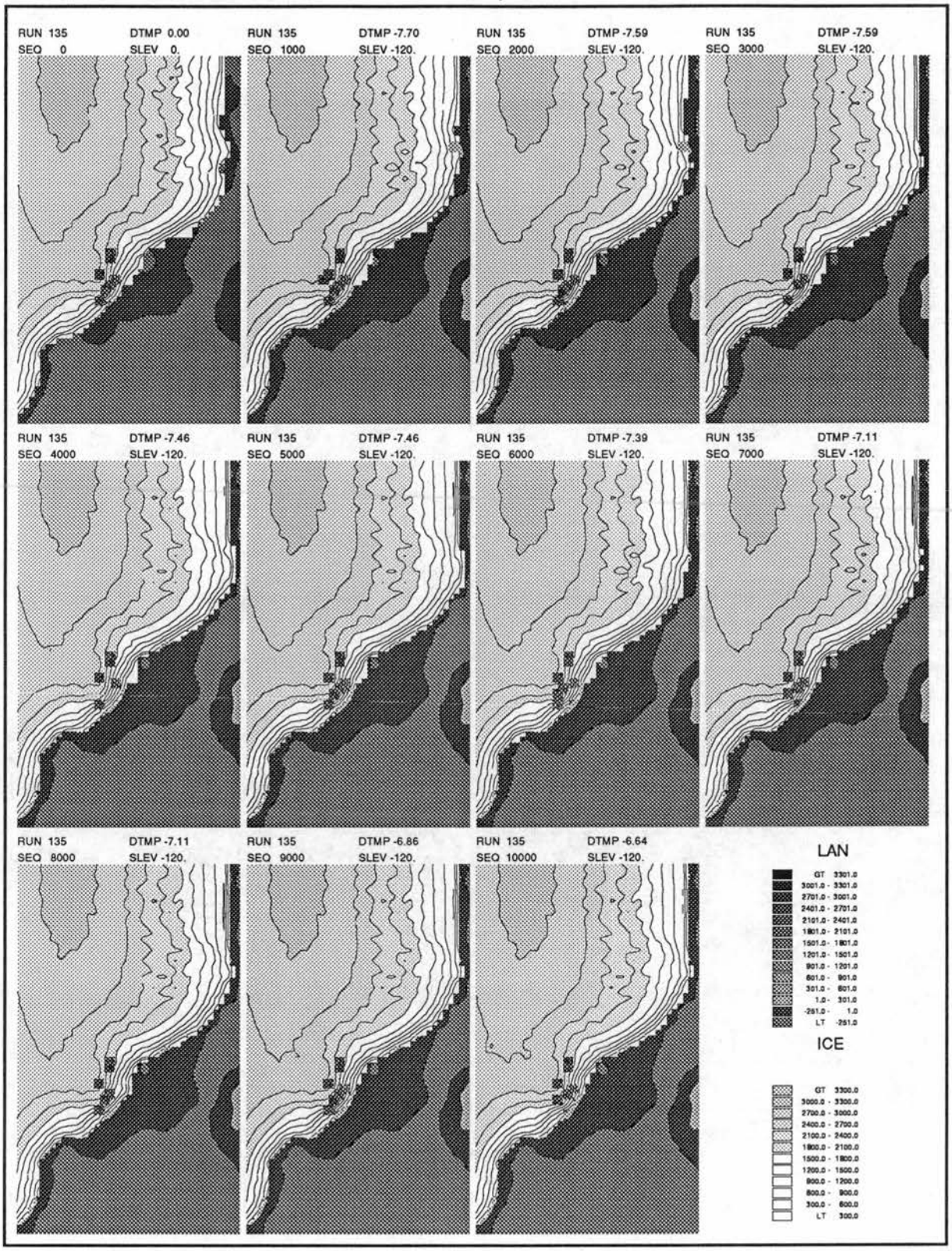

Figure 139: Simulated deglaciation using Camp Century temperature and Barbados sea-level curves (Run 135). East Coast detail, page 1. The ice margin is virtually static in this period (up to 10000a). High ice velocities and the complicated subglacial topography causes the ice to run into marked streams.

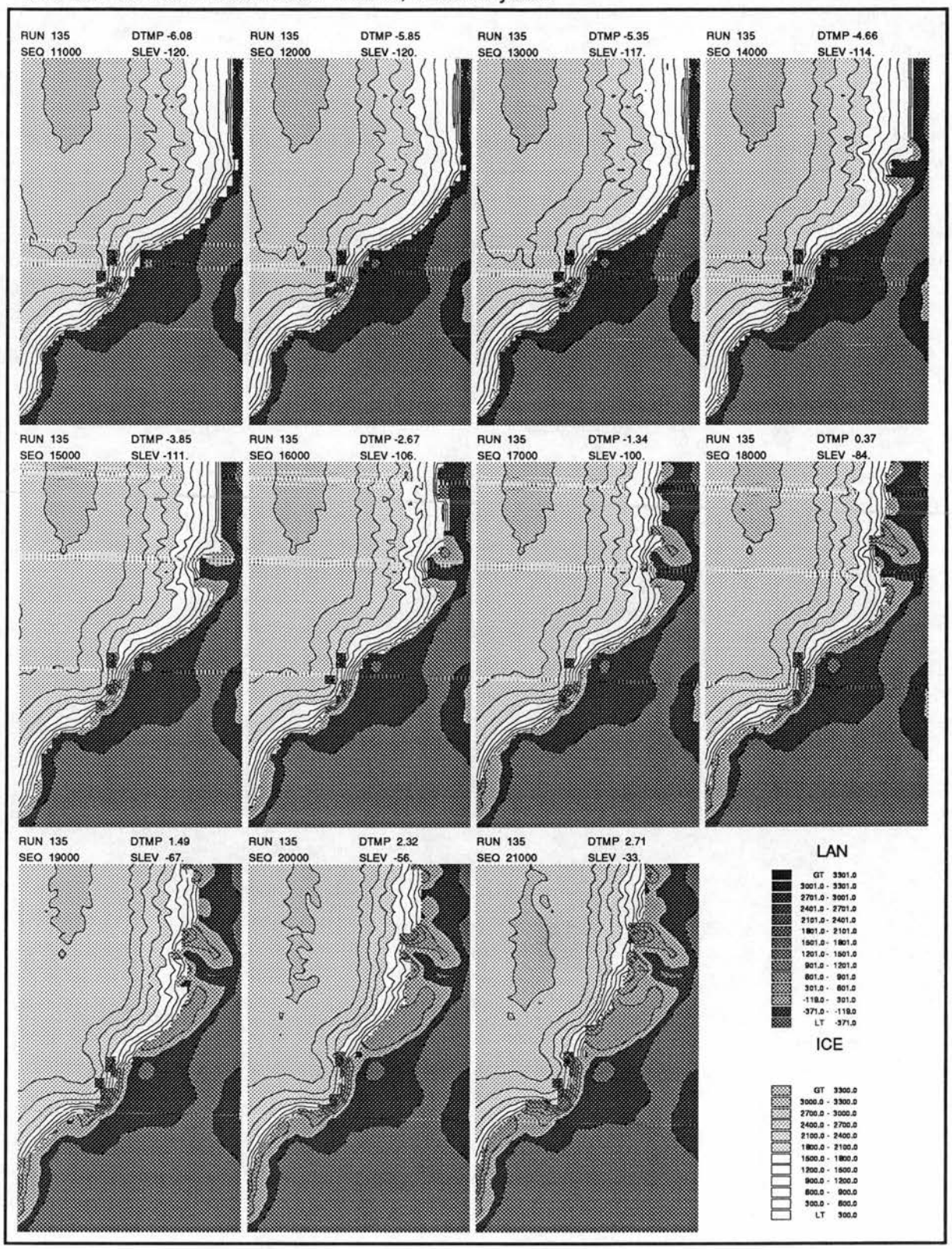

Figure 140: Simulated deglaciation using Camp Century temperature and Barbados sea-level curves (Run 135). East Coast detail, page 2. At 14000a, Scoresby Sund provides a large channel to effect margin retreat by calving in advance of the rest of the margin. This effect is pushed back up the fjord in the subsequent 2000 years.

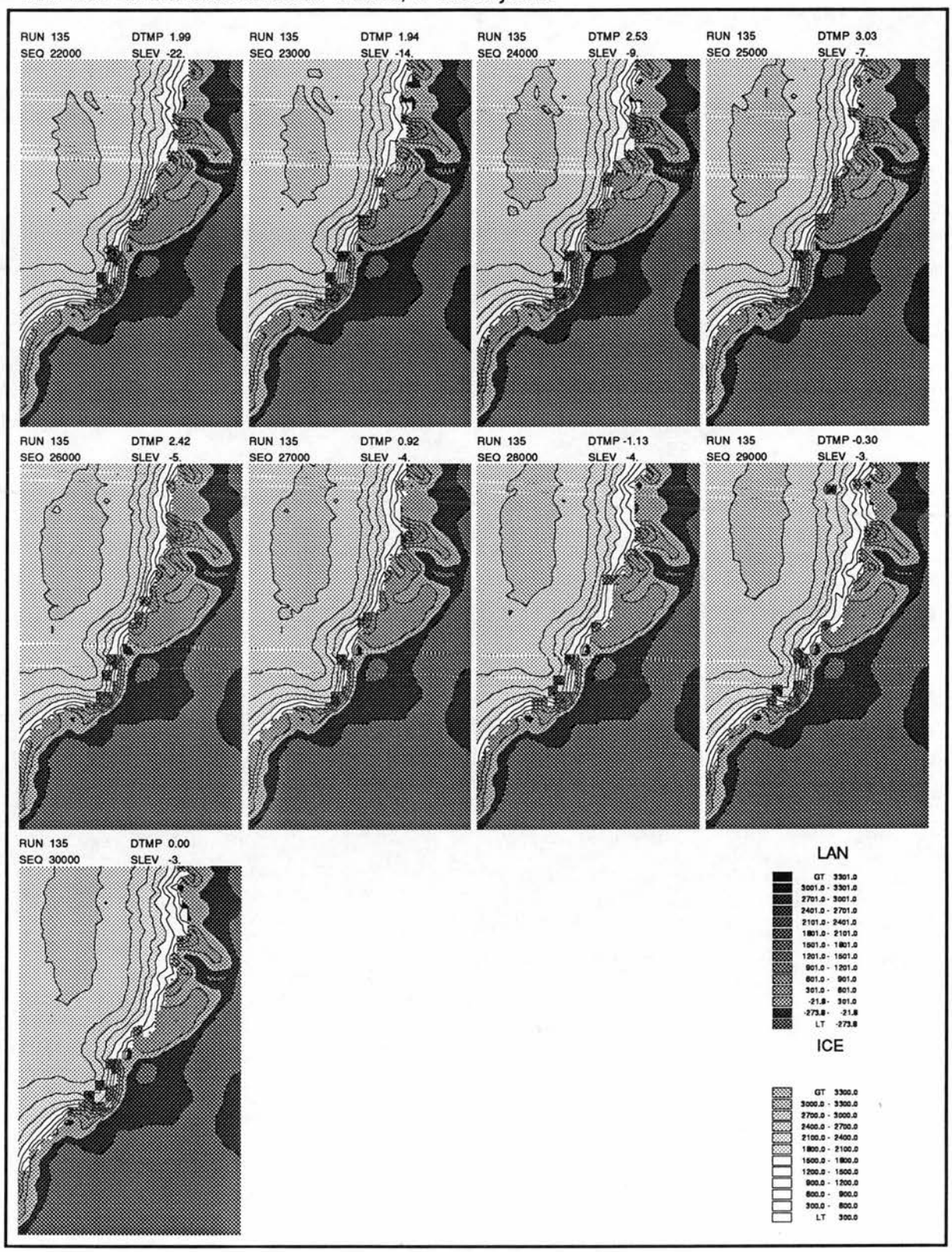

Figure 141: Simulated deglaciation using Camp Century temperature and Barbados sea-level curves (Run 135). East Coast detail, page 3. Once the mountains over Knud Rasmussens land have deglaciated, they do not become ice covered again. In reality, there is presently glaciation in this area.

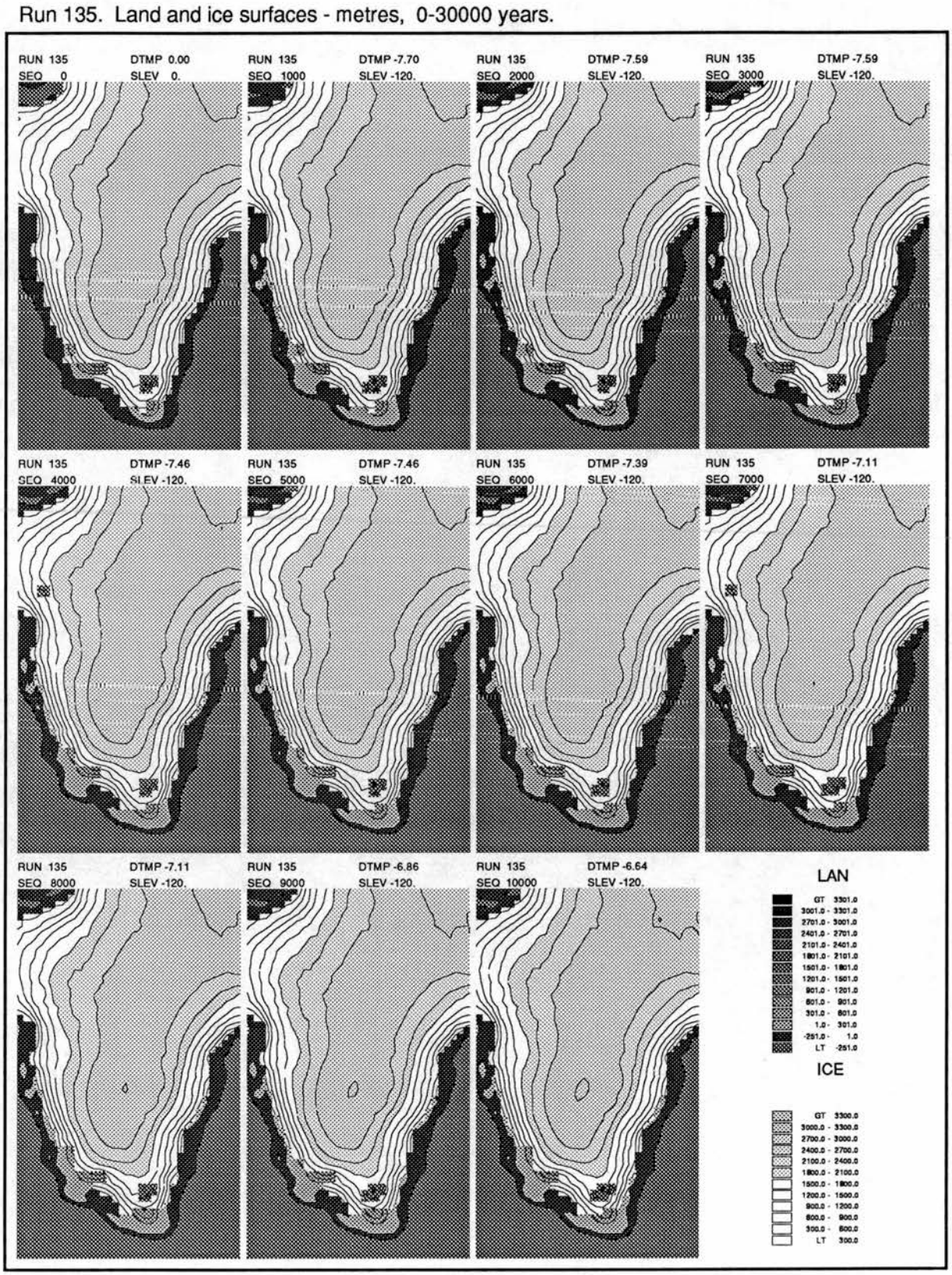

Figure 142: Simulated deglaciation using Camp Century temperature and Barbados sea-level curves (Run 135). South Coast detail, page 1.

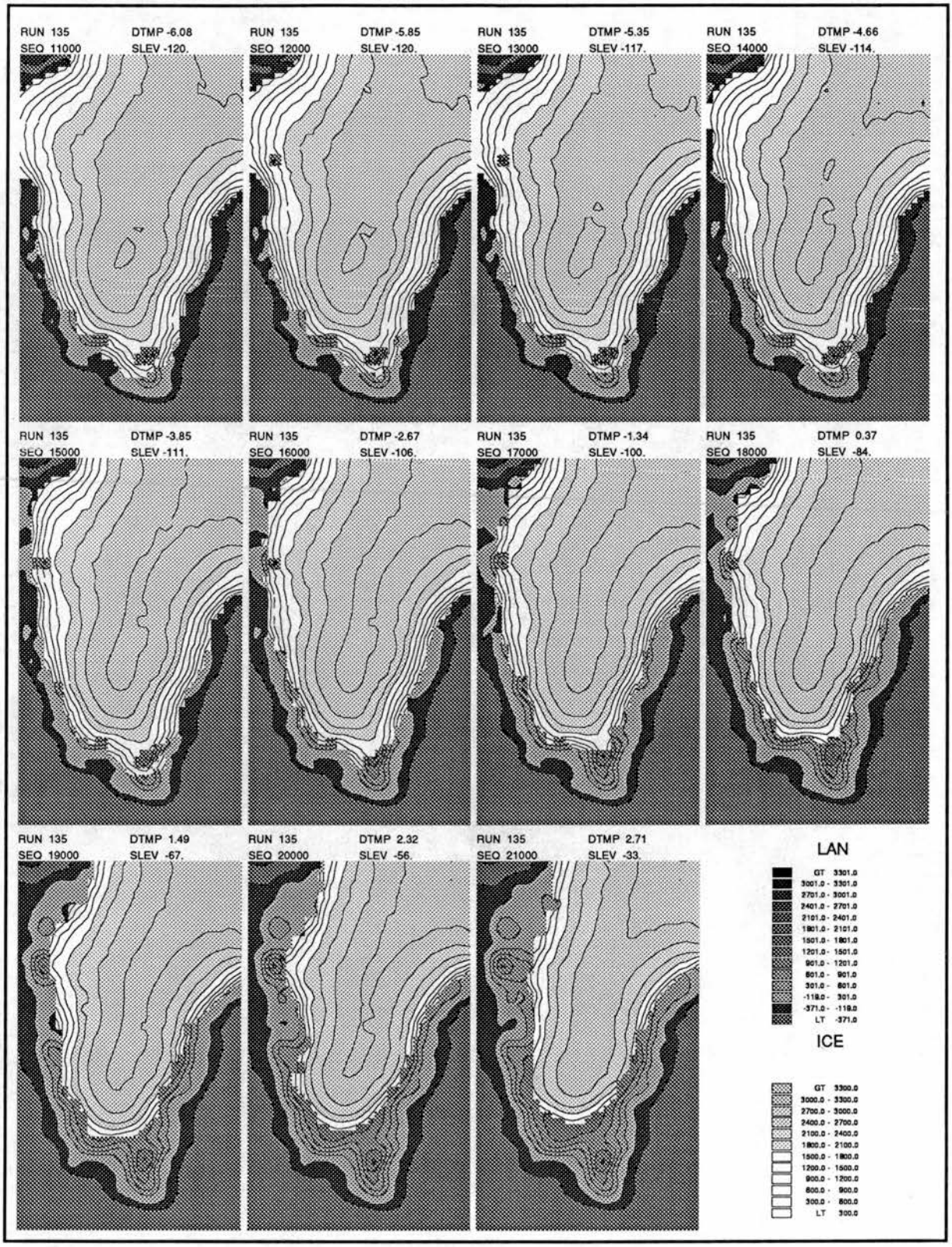

Figure 143: Simulated deglaciation using Camp Century temperature and Barbados sea-level curves (Run 135). South Coast detail, page 2. Ice moves off the marine fringe relatively early in this sector (c 13000a).

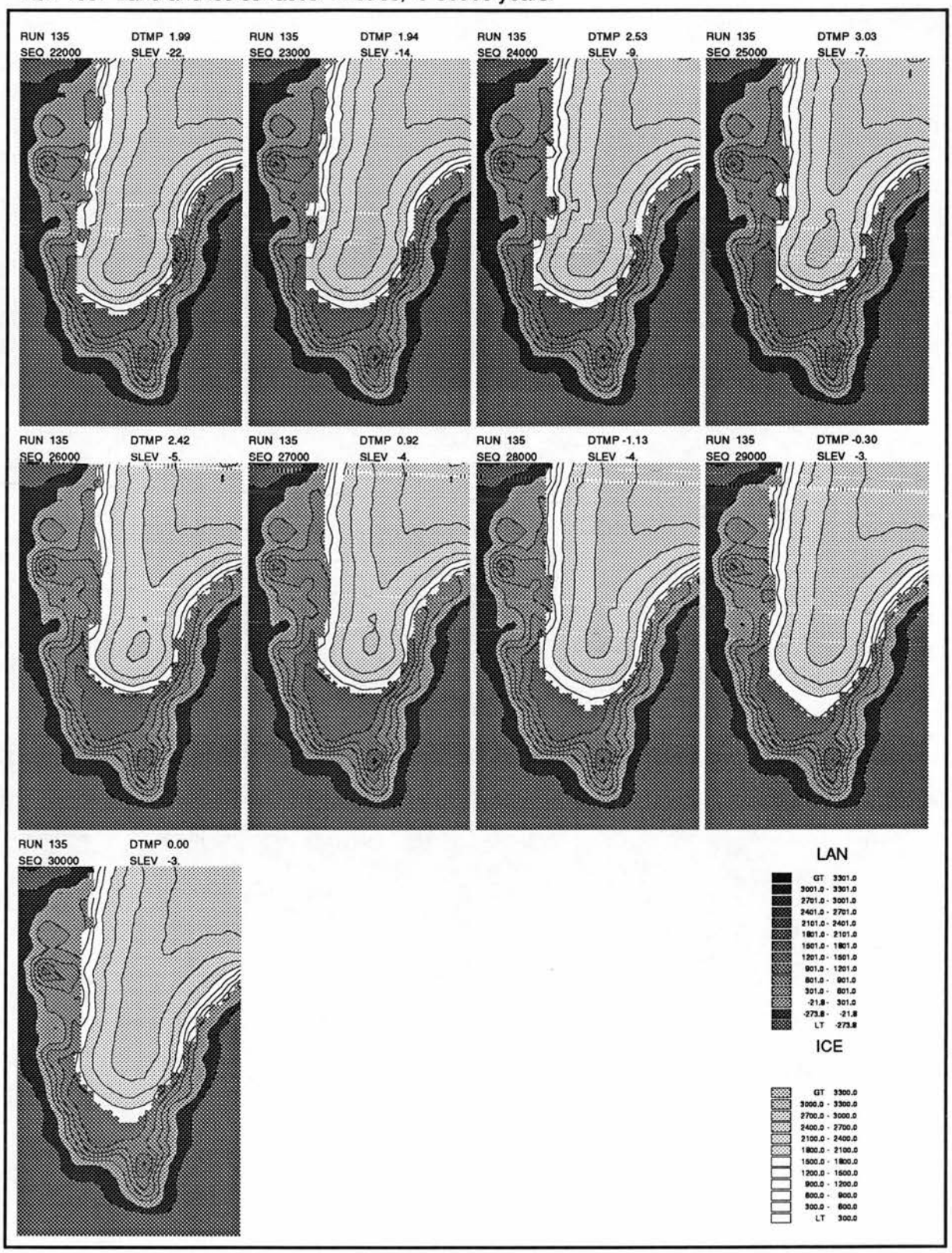

Figure 144: Simulated deglaciation using Camp Century temperature and Barbados sea-level curves (Run 135). South Coast detail, page 3. The model predicts that the southern ice dome comes near to collapse in the postglacial warm period. The quality of the model's simulation for the present-day is not as good here as it is in areas further north.

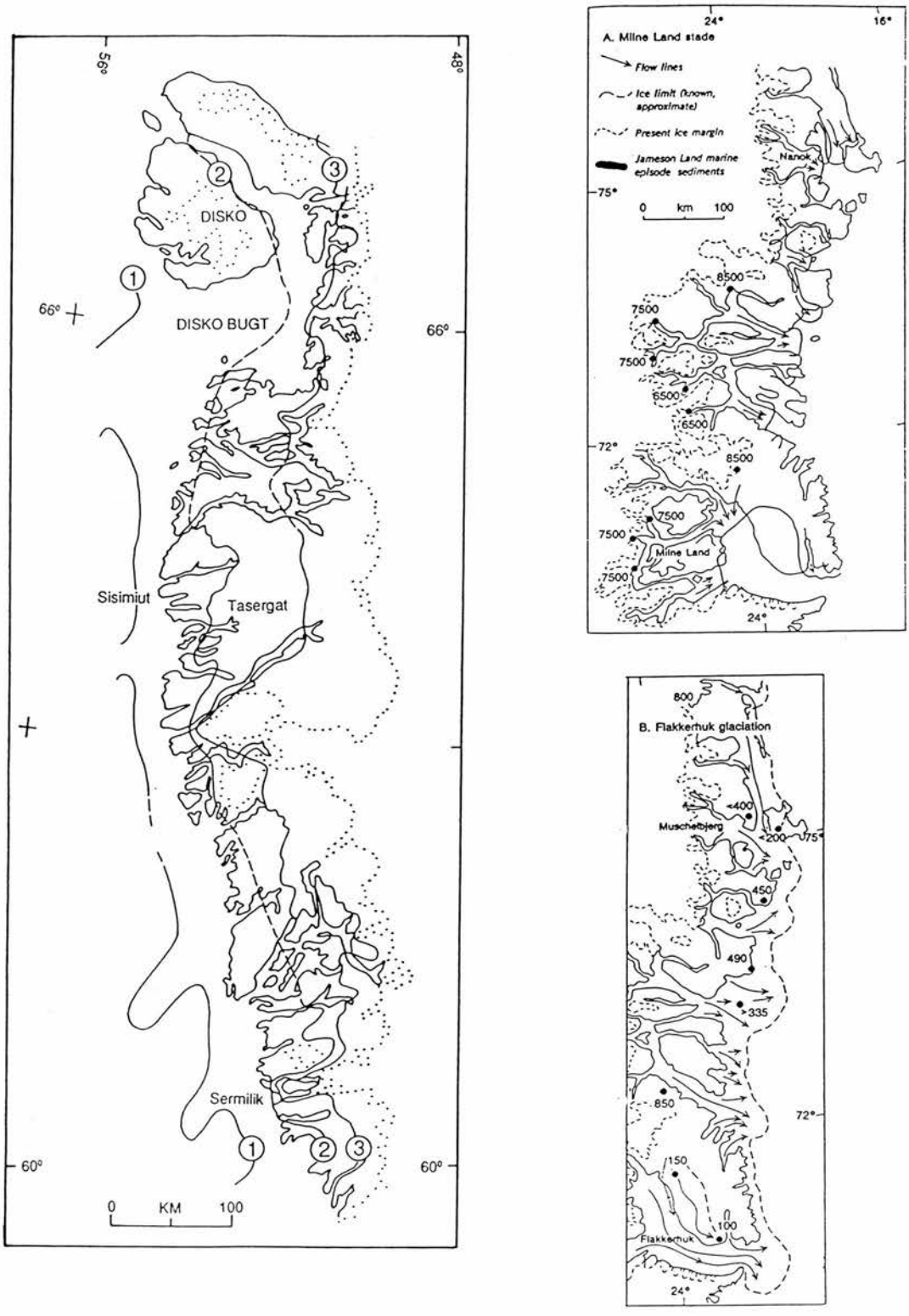

Figure 145: Major glacial retreat stage interpreted from geomorphology. (From a synthesis by Funder 1989). Left: West Greenland, 1 - Sisimiut maximum stage (c. 14ka BP), 2 - Taserqat stage (c. 10ka BP), Fjord stage (c. 8ka BP). Right: Milne Land stage (10ka BP)(upper) and the glacial maximum (lower)

Chapter 5

CONCLUSIONS

5.1 New Knowledge

In the broadest terms, this conclusion sets out to summarise and evaluate the knowledge that this research has provided. The first section gives a brief collation of what the model tells us about the behaviour of the Greenland Ice Sheet, and discusses how this compares with what is already known. The following section discusses the value of a modelling approach in the understanding of ice sheets and the ways in which modelling work simultaneously enhances and benefits from other kinds of research. Finally, some assessment needs to be made about what this model tells us about the Greenland Ice Sheet. Did the research achieve what it set out to do and how viable does the approach seem to be ? What limitations does the model have and what could be done to improve it ?

Ice sheet models form only a small specialised subset of environmental models. Ice sheet models are relatively numerous because of their relative physical simplicity but the breadth of environmental modelling continues to expand. This emergence of modelling throughout Geography and Environmental Science coincides presently with major growth in computer and digital data resources. Therefore, some time will be devoted to discussing some of the technical achievements of the model and what they imply for the role of environmental modelling within the emerging field of GIS. How do technical considerations both promote and limit the effectiveness of the environmental models ?

5.2 The Greenland Ice Sheet

It is important to establish the extent to which the model results have a bearing on real events. Are they true and how do they explain reality ? Some specific categories of results can be looked at with these considerations in mind.

5.2.1 The concurrence of modelled and real states

The model produces conditions which closely resemble reality. When driven with a mass balance model which simulates present day conditions, the ice dynamics model responds with a result which differs only in detail from the present day ice sheet. The model and real situations are overwhelmingly similar, both in margin boundary and in overall dimension. The differences in detail point to the deficiencies in the climatic model. These are mainly caused by the underprediction of accumulation rates and apply particularly to local glaciers. When forced by cooling and lowered sea-levels the model extends to positions which match those which the real ice sheet is believed to have reached under maximum conditions. This is established largely on the evidence of submarine erosional and depositional features. In addition, the model, in simulating deglaciation, configures the ice sheet into a series of characteristic states which have direct parallels in the geomorphological record. With given mass balance signals, the model appears to produce certain responses which have real-world counterparts.

The next thing to scrutinise is the mass balance. It could be possible that the model is producing close fits but that it is so robust that the results are spurious because it is being driven by an unrealistic mass balance. The mass balance model's ability to produce separate ablation and accumulation terms whose rates are close to the real-world observed values lends support to its validity. These real-world measurements differ widely themselves and are based on small amounts of data. The empirical parametrization used to model accumulation means that total values inevitably end up close to the real estimates (Table 1.1). The model ablation rates are relatively high for the present-day, and calving rates low compared to the real estimates, but the overall mass balance rates are similar. The paucity of the real data may account for the way it differs from the modelled results but it does not assist corroboration.

Some further confidence in the mass balance model can be gained from looking at ice sheet behaviour in the overall glacial-deglacial cycle. The forcing relationships in the two parts of the mass balance model are scaled in terms of present-day geographical variations in temperature and mass balance. The $-8°C$ glacial maximum

temperature signal from Camp Century and the -120m sea-level from the Barbados curve are derived independently of the mass balance model, but if these two values are applied to the ice sheet model, maximum ice conditions result. Present-day conditions return if temperatures and sea-levels are restored to present-day values. The mass balance model, the forcing signals, and the resultant ice configurations are established and tested independently of one another. The ability to produce independently testable ice configurations with an independently derived mass balance model and independent forcing values forms a triangle of corroboration.

The opposite view needs airing. It is possible, yet never completely testable, that both the mass balance and ice dynamics are wrong, whilst together they appear to give correct results. This seems unlikely, and such a conclusion is rejected in the absence of testable cases when corroborative evidence suggests otherwise. The assumption is made that the model's ice dynamics and mass balance parts are correctly described and dimensioned. If this is the case, then the model is saying some fairly important things.

In the case of the present-day, the model shows why the ice sheet is where it is. It indicates the mass balance rates that need to be maintained throughout the length of Greenland in order to allow the ice sheet to exist as a whole. In part, the positive surface balance over the higher, northern dome can feed the negative areas to the south. The evidence of deglaciations seems to suggest that the east coast mountains effectively anchor the ice sheet there. With one margin stabilised, the lower west coast margin is more easily sustained. If the east side were lower, the margin would need to be further back from the coast, and this would reduce the altitude of the central dome and as a result the area of positive mass balance feeding the more active west coast margin would be smaller. In addition, the southern part of Greenland progressively narrows. In the model, this leads to relatively high accumulation rates because the continentality term in the surface temperature equation is reduced. If the island were wider here, conditions would be drier and the chances of maintaining its highly energetic dome much reduced. Persistence of ice in South Greenland is favoured because many areas there are quite high.

This understanding of mass balance extends to other glacial scenarios in Greenland. It indicates how the surface mass balance divergence is associated with the temperature forcing needed to produce particular glacial conditions. The model shows that the response of the ice sheet to temperature forcing can be rapid and continues at a progressively slower rate until some equilibrium state is reached. The simulated

temperature of Run 135 sets the model into a phase of constant adjustment. The present-day morphology that occurs at the end of this deglacial sequence must be seen as only the end of a period of renewed glacial activity in the recent past. Against this background of overall change and response, the model also demonstrates the differing sensitivity of different locations. It shows a substantial difference between the highly changeable conditions of forcing and response in the south in comparison to more settled conditions in the north. Differences in bed relief produce further disparities in glacial sensitivity; high areas are more stable than low ones. The marginally glacierized areas have the largest response to the glacial-deglacial cycle.

Some indication of adjustment times can also be gained from the results as a whole. There is a higher potential for negative mass balance with warming, and so one can reasonably expect deglacial phases to be shorter than growth phases. In particular, the stepped deglacial models show the rapidity of the response to sudden deglacial forcing. Typically, half the ice loss occurs within 1000 years and the rest over the subsequent 4000 years. Nonetheless, the ice dynamics model still requires periods of 10000 to 20000 years to achieve complete equilibrium. As we have seen, under more continuous forcing signals, there is a corresponding response to new forcing, but nevertheless it is always slightly lagged. It is worth reiterating the conclusion that, in general, larger forcing produces more rapid responses which subsequently take longer to settle than smaller ones. Growth lag times show similar behaviour but take longer still. For instance, even after 10000 years of run 134 which forces the model from $-6°C$ to $-8°C$, sustained equilibrium is some way off. Even the slower ice growth which takes place in the Initial Standard Run could be said to have not completely settled after 20000 years.

These characteristic model lag times support the general view that, for ice sheets, ice sheet growth takes longer than decay. However, the interrelationship of ice extent, albedo and temperature, largely held to be responsible for some of the lags in global scale glaciation (eg. Oerlemans and Van der Veen 1984), cannot be replicated in this kind of model; there is no feedback between the external temperature input and ice extent over Greenland. The temperature signal itself is assumed to be driven by wider global climatic change. Also, a good picture of isostatic response times is difficult to ascertain. Overall, for a given disturbance, the response times vary from twice to an order of magnitude longer than those involved in the adjustment of the overlying ice. They are a step removed from the original forcing influence. Towards the end of isostatic adjustment to a perturbation, the effects may be too small to identify

easily, even if a constant trend remains. Isostatic responses are typically a wave form rather than consisting of simple uplift. This complicates interpretation and serves to illustrate the difficulties of working out the meaning of inferred isostatic change over regional scale areas. The results for Greenland are nonetheless consistent with what is known about the history of isostatic rebound, for example as elaborated by research on raised shorelines in the south-west (Weidick and Ten Brink 1974, Sugden 1972).

This analysis of response times allows us to say how the ice sheet might respond to global warming whether of natural or anthropogenic origins. There are three major conclusions. Even with fairly large ($+6°C$) warming, the total change is unlikely to be large within the next 200 years. The model predicts that the volumes of ice involved would cause centimetres rather than metres of sea-level rise. The second conclusion is that the initial change is likely to be characterised by a steepening of ice gradients. In particular, accelerated mass loss by ablation could result in rapid shrinkage of the margins but over the interior the ice sheet is likely to thicken. Any ice thickness change, observed remotely over large areas of the centre of the ice sheet, needs to be interpreted in this light. With substantial warming, margin retreat could be more significant, easier to observe, and more conclusive. There are some putative warming effects that the model cannot predict, for example the extension of individual ice lobes caused by warmer and faster sliding conditions. The final conclusion is that even the changes introduced by slight warming are unlikely to have been resolved into equilibria within 200 years.

The model gives further pointers to the effects of longer term warming, even though this was not one of the main purposes of research. Assuming constant sea levels, the model predicts that with a $+6°C$ climatic warming the present ice sheet over Greenland will all but disappear within 20000 years (Fig.71). Whilst such conjecture may be interesting in itself, it hardly impinges on present concerns. Perhaps more significant are the pointers that warming experiments provide for how the ice sheet may have existed in previous interglacials. A recent article by Koerner (1989), which considers evidence from the base of the Camp Century and Dye-3 ice cores, suggests that 'the Greenland ice sheet melted extensively or completely during the last interglacial period' (p964). Ice texture and gas content indicate the presence of small ice caps during the last interglacial and so the inference is made that the the ice must have melted substantially in the early part of the last interglacial, at temperatures some $+3°C$ warmer than present. Koerner suggests that this retreat must have

been at least as far as the locations of the two drill sites. This implies collapse of the southern dome and substantial retreat of the northern margins. The results of Run 120 which simulates such conditions suggest just this. If this is a good simulation, then the positioning of the two drill sites outside the reduced margin perhaps creates something of a false impression of the overall scale of retreat in North Greenland.

If the totality of the model's input and corresponding output is assumed to be correct then the ice flow is also probably modelled reasonably correctly. The way in which different areas of Greenland evolve different flow regimes with changes in form is observable. Characteristic ice dynamics patterns are associated with certain topographies. As the model changes it is possible to single out the separate topographic and climatic effects that lead to the variation in ice dynamics. But the two are interrelated. From surface balance considerations alone, the topographic configuration of Greenland influences the size and morphology of an ice sheet at any given glacial stage. Surface mass balance conditions determine the energy status of the ice sheet and hence the ice gradients that can be supported. It is possible, therefore, to associate changes in form directly with climatic change. But the climate model interrelates with topography to explain relative stability and instability both in the speed of ice sheet development and in ice sheet permanency. The role of topography becomes yet more important as calving activity increases. Calving activity becomes the major constraint on further ice growth under maximum ice conditions. The sharp change in water depth at the continental shelf determines the ice sheet's maximum extent. Moreover, the model predicts that under maximum ice conditions calving is likely to be characterised by periods of relative activity and quiescence. Major acceleration and deceleration of calving rates occurs in suitable 'calving bay' locations. During retreat, these areas quickly collapse. With present-day conditions, the role of calving diminishes but sea-level is still important in influencing overall ice sheet size. The status of calving and its relationship to topography evolves during the change from glacial to interglacial conditions.

The model has a number of advantages when compared to previous models of the Greenland ice sheet. First, the relationship with climate and the reason for ice sheet evolution are explained. The models by Reeh (1982) and Radok and others (1982) do not link climate with ice sheet change explicitly. Reeh's model focuses on the balance profiles that might be associated with static equilibria. The set of models developed by Radok and others are only really concerned with present-day climate. The second primary advantage of this research is that the model is dynamic over

time. This allows transient change to be modelled and the processes associated with the transition explored. Time variability and response lags can only be examined with models which develop continuously through time. The identification of key processes in this research was only possible with this capability. In this respect the model is similar to the model of Grigoryan and others (1985) but their model is limited in the simple representation of climate. The model used in this thesis perhaps takes a more critical approach than previous studies on Greenland. Reeh's model predefines the limit of particular states and the models by Radok and others work out physical parameters from pre-existing conditions. The opportunities for independently testing the conclusions are limited in each case. In contrast the model developed here takes derived topography, climate and ice dynamics independently and therefore the comparison of results with real situations can be assessed more critically. In this respect the Grigoryan model is similar but at a lower resolution.

5.3 Implications for Ice Sheet Modelling : The importance of climate

The ice dynamics part of the model is relatively robust. Even with substantial changes in ice velocity, the overall configuration of the ice sheet, in particular the total area covered, is barely affected. The research did not investigate whether such changes speed up or slow down the response time of the model but, over long periods, similar equilibrium positions are likely to evolve within the wide bands of modelled velocity. This very robustness introduces a problem, in that modelled ice flows could be relatively too slow or too fast and yet apparently correct. Unfortunately this problem is difficult to avoid since there is little direct evidence of past ice velocities to test modelled values against. Even for present-day ice caps suitable measurements are sparse. On the other hand, small relative changes in total mass balance have dramatic consequences. This highlights the importance of having correctly scaled climatic input into dynamic ice sheet models which replicate long term evolution. Ideally mass balance models need to be based on physical understanding and to treat input and output elements separately. In Greenland, the existence of the present ice sheet is the key to parametrizing the magnitude of the mass balance elements. Modern ice sheets can serve as useful analogues for other climatic conditions and other glacially affected areas. The mass balance part of this model was weakest in not having an explicit

relationship between energy balance changes and the temperature forcing of ablation, even though the implicit relationship used could be justified and seemed appropriate for inducing realistic change.

5.3.1 Simplicity vs. Complexity

The basic equations and assumptions of the model are fundamentally rather simple. The overall degree of complexity and non-linearity derives more from the subsequent interlinkages between these basic equations. The model can nevertheless produce good results despite the simplifying assumptions. The benefit of this is that it is relatively easy to interpret the processes that the model embodies and evaluate them against their real equivalents. In this instance, further complexity in the equations might not give a better result and their introduction would make it harder to understand what is going on. The relative significance of relationships involved in glaciological change would be harder to ascertain. Moreover, the model seems to suggest that major trends in natural processes can be explained from simple physical principles. These trends can be modelled provided that the requisite flows and feedbacks between different parts of the system are adequately replicated. The complexity of ice configurations in the model and reality stems more from the topography than from complex physical relationships embodied in the model. In explaining real change, we need to devote as much attention to the complexity of real geographies as we do to the complexities of physical process. Improvements in modelling could undoubtedly come with better derived mass balance and ice flow relationships and improved spatial resolution. Such enhancements, however, need to be balanced against the possibility that they will be more difficult to interpret. The sophistication needs to be appropriate to the problem tackled. If there is an emphasis on short-term ice flow, better flow laws are obviously needed. If emphasis is directed toward long-term evolution and climatic change, ice flow relationships become less critical. In the first case, climate and in the second case ice flow can be justifiably simplified. Spatial resolution needs to be similarly appropriate for the problem tackled and matched to the scales which the process models demand. For instance, finer resolution models for Greenland would require further sophistication of how strain rates vary with local topography. Complexity does not necessarily imply quality; it needs to be targeted to the job in hand.

5.4 The value of sensitivity tests and hypothetical situations

Even though the model was primarily directed toward understanding real events, the role of sensitivity tests in evaluating and developing the model was substantial. It allowed conclusions to be made about the relationships between individual parameters and the robustness of the model to their alteration. Altering one parameter under otherwise constant conditions, and then allowing the model to find its own equilibrium, highlighted the role of that one parameter. Individual theoretical relationships were examined in isolation. The relative influence of counterpoised variables is harder to work out but is more likely to be done with simple experiments like these. When the model is forced into continuous response, the effect of particular parameters is more easily lost in the complexity of the result. For this reason, the sensitivity tests proved particularly useful in establishing characteristic response times and patterns for given magnitudes of forcing.

5.4.1 The need for realistic models

Ultimately, to understand reality, models have to be addressed to real situations. There is therefore value in producing geographically realistic models. The benefits are that the models produce geographically realistic simulations which can be tested against real evidence. The influence of actual topographic circumstances and actual climate can be played out in the model and related to the behaviour of the modelled ice during the run. This provides an improved understanding of the role of specific topographies and specific climates. Large scale and long term processes can be identified and the relative importance of particular effects can be demonstrated.

5.4.2 This model and other work

It is worth considering the contribution of this work both to the modelling of the Greenland ice sheet and to the development of dynamic ice sheet-climate models as a genre. The first part is easier to establish. Previously, no detailed modelling work relating the dynamic stability the ice sheet in Greenland to its own self-influencing climate has been undertaken. This has been done both for the present-day(interglacial) situation and for a variety of different glacial and transitional forms. At each point, the ability of the model to relate a given regional climate to a distributed mass-balance

pattern and an evolving ice mass has been shown. Some of the work has been almost purely theoretical; it does not try to relate to any known situation. It tries to establish the tendency of the system to evolve a particular form given long-term invariance in the input parameters. This gives a good indication of the main controlling relationships within the overall system, so that when the model is dynamically forced, system lags are more easily understood. The model shows the importance of correctly modelling climate for realistic simulations. For instance, in the present-day simulation, small deflections in mass balance terms easily disturb the model.

Compared to workers developing models for other areas and situations this model is perhaps more in line with work of Payne(1988) than Budd and co-workers. The main differences are the resolution at which the models operate and the representation of climate. Budd's models work at relatively low resolutions (50-100km grids) and tend to prescribe climate somewhat simply, either as a single altitude-net balance relationship or by taking accumulation patterns as fixed and only varying ablation. Oerlemans and Van der Veen(1984) develop more sophisticated climate models but still work at relatively low resolutions. The approach in this research has been to try and integrate the more sophisticated aspects of some of these models such as isostasy and dynamic climate modelling to examine the interplay of localised and wider ranging processes over a variety of time periods. Given the assumptions about the behaviour of the natural system embodied within the model this work tried to identify characteristic features of the Greenland situation in terms of its unique topography, location and history that makes it respond in the way it does. One of the important aspects has been to look at how a regional climatic signal is played out through the mass balance and how the response of the ice sheet to this is amplified or attenuated because of certain topographic situations.

5.4.3 Modelling vs. field work

There are major benefits in the insight provided by numerical models. They can pull together parts of different theories to produce new information about the real world. Given certain assumptions about how the ice sheet works, the results describe how various parts of the ice sheet system interact. What is more, the magnitude of those relationships can be specified. The model allows an holistic approach to understanding whilst at the same time permitting the consideration of detail and reality. However, the value of the model can only be assessed with reference to real

data sources. Knowledge gained from the model does not exist in theoretical isolation. It applies to reality because the partial knowledge we already have about the behaviour of the ice sheet has been tested against it. The model is therefore a sophisticated exploration of what is already known in order to produce new knowledge. By interweaving theory, the model seeks to suggest multiple possibilities for why real phenomena occur in the way they do. Modelling therefore aims to maximise the values of hard-won field evidence by advancing theoretical constructs, but it can only produce meaning because of its relationship to the real world. For instance, if Weidick (1968) and Ten Brink had not already worked out what the likely pattern of retreat was in West Greenland, all the modelled retreat stages would be untestable. Moreover, it would be hard, on the basis of the field alone, to suggest exactly what the causal climatic fluctuations and ice dynamics were. If we accept that there is a degree of sustainable commonality between the geomorphic evidence and the modelled results, then there is reason to suppose that aspects of the modelled behaviour reflect processes causing retreat in the real world. It is then possible to suggest what the primary influences in the deglaciation pattern have been and how they relate to wider trends.

5.5 Environmental Models, GIS and Geography

The practical links between the computer model and its input and output data were relatively cumbersome. It would be useful if the raw data, the processed inputs and different kinds of output could be stored in a common database. It would then be beneficial to produce model algorithms as separate features that could, at the same time, take input from and return output to the common data set. Separate programs could be written to access the same physical data in order to produce graphical and tabular output. Presently, there is no software available that has the necessary capabilities to integrate into one package the storage, modelling and graphical requirements needed for this kind of excerise. In the course of this research the capture and storage of raw data was done using ARC-INFO because it offered the best means to capture and store vector data and to incorporate other digital data sources. The main program was written in Fortran for numerical computing efficiency. A raster graphics package, UNIRAS, was used to produce maps and plots because it could do the necessary interpolation much faster than vector systems. In addition, UNIRAS exists as a set of Fortran subroutines which can access the data files directly without the need for

intervening meta-data. As a result, it can be specifically tailored to the data and is relatively quick. This speed is important if the the computer software is considered as a tool for investigating the model results. For compactness, the model data itself was stored in Fortran binary files. The VMS operating system was used to link the data from each element together. The whole therefore involved a somewhat ad hoc, hand crafted architecture with the specific task in mind. More time was spent on controlling data and developing graphical and analysis tools than was actually spent in modelling. This side of the research is important because the interpretation and usefulness of the results is directly proportional to the ease with which the numerical output can be turned into meaningful charts and graphs. A single figure of the ice sheet morphology represents about 0.5 mega-bytes of raw data but requires 1.5 megabytes of plotting information.

From a practical point of view, the model could have been made easier and more portable if there was a GIS which had both raster and vector processing capabilities and into which user-specified modelling routines could be introduced. The data models in such a GIS would need to be conceived from the outset with modelling in mind. The capability to pass information between the geographical units of the data model has to be inherent in the data structuring. Modelling can then be introduced as a set of rules which define the way in which information is transferred and used to redefine the values of the attributes associated with geographical elements.

Ice sheet models are fairly specialised, but in other areas of environmental study, for instance, hydrology or hillslope evolution, there are benefits to be gained from having common data which can be accessed by more than one set or subset of models. This highlights the need for modularity. Where possible, the programs for this research were written in such a way that they could apply to any ice sheet. Sufficient locational information is passed to the model for it not to need to be explicitly specified within the program. The mass balance model exists as a series of separate subroutines. If the model were run for a different ice sheet, the only thing that would need redefining would be the mass balance subroutines. The ice sheet model itself could remain unchanged. Modularity introduces the further possibility of parallel processing. In reality, ice sheets develop simultaneously at all points, and therefore the concept of representing each ice block not only as a separate data item but also as a separate process in communication with adjacent ice blocks is intuitively attractive. At a larger scale, parallelism brings in the possibility of running a separate moisture and energy balance model for both climate and ice sheet. These two models could

be independent but allowed to communicate with each other in order to update their boundary conditions continually. The possibilities for future development remain exciting.

LIST OF REFERENCES

Atkinson B. W. (ed.) 1981.
Dynamic meteorology - an introductory selection. Methuen and Co. Ltd., London.

Balise M. J. and C. F. Raymond, 1985.
Transfer of Basal Sliding relations to the surface of linearly viscous glaciers. *Journal of Glaciology* 109, p308-318.

Bader H., 1961.
The Greenland Ice Sheet. CRREL Monograph, Hanover New Hampshire I-B2.

Bauer A., 1955.
The balance of the Greenland ice sheet. *Journal of Glaciology* 2, 17, p456-462.

Bauer A., 1967.
Nouvelle estimation du balance de masse de l'Inlandis de Groenland. *Deep Sea Research* 14, p13-17.

Bauer A., A. Ambach, and O. Schimpp, 1968.
Movement et variation d'altitude de la zone d'ablation ouest de L'Indlandsis du Groenland entre 1948 et 1959. *Meddelelser om Grønland* 174, 1.

Battle W.R.B., 1951.
Glacier movement in N.E. Greenland 1949. *Journal of Glaciology*, 1, 10, p559-563.

Benson C. S., 1962.
Stratigraphic studies in the Snow and Firn of the Greenland Ice Sheet. US Army Cold Regions Research and Engineering Laboratory, Hanover,New Hampshire. CRREL Reaserch report No.70

Bøgvad, R. 1940.

Quaternary geological observations etc. in south-east and south Greenland; *Meddelelser om Grønland*, v107, no. 3, 42p.

Braithwaite R. J. and O. B. Olesen, 1989.
Calculation of glacier ablation from air temperature, West Greenland. in, J. Oerlemans(ed), *Glacier fluctuations and climatic change.* Kluwer Academic Publications. p219-233.

Brett C. P. and Zarudzki E. F. K., 1979.
Project Westmar. A shallow marine geophysical survey on the West continental shelf. *Rapport Grønlands Geologiske Undersøgelse* 87, 27p.
Brooks C. K. 1979.
Geomorphological observations at Kangerdlugssuaq, East Greenland; *Meddelelser om Grønland*, Geoscience no.1, 21p.

Brown C. S., M. F. Meier and A. Post, 1982.
Calving speed of Alaska tidewater glaciers. With application to Columbia Glacier. Geological Survey Professional Paper 1258 - C.

Budd W. F. and D. Jenssen, 1975.
Numerical modelling of glacier systems in: *Snow and Ice (Proceedings of the Moscow Symposium)* IASH publication Number 104, 257-291.

Budd W. F. and I. N. Smith, 1981.
The growth and retreat of ice sheets in response to orbital radiation changes. *Sea Level, Ice and Climatic Change.* International Association of Hydrological Sciences, Publication number 131, p369-410.

Budd W. F., and I. N. Smith, 1982.
Large-scale numerical modelling of the Antarctic ice sheet. *Annals of Glaciology* 3, p42-49.

Budd W. F., D. Jenssen and I. N. Smith, 1984.
A Three Dimensional Time-Dependent Model of The West Antarctic Ice Sheet. *Annals of Glaciology* 5, p29-36.

Chadwick P., 1976.
Continuum Mechanics, Concise Theory and Problems. George Allen and Unwin.

Colbeck S. C. (ed.), 1980.
Dynamics of Snow and Ice masses. New York, Academic Press.

Dahl-Jensen D., 1985.
Determination of flow properties at Dye-3, South Greenland by borehole tilting and perturbation modelling. *Journal of Glaciology* 31, 108, p92-98.

Dansgaard W. and S. J. Johnsen., 1969.
A flow model and a time scale for the ice core from Camp Century, Greenland. *Journal of Glaciology*, Vol. 8, No. 53, p215-224.

Dansgaard W., S. J. Johnson, H. B. Clausen and C. C. Langway Jr, 1971.
Climatic record revealed by the Camp Century ice core. In Turekian K. K. (ed), *The Late Cenozoic Glacial ages.* London and New Haven: Yale University Press, p37-56.

Dansgaard W., H. B. Clausen , N. Gunderstrup, C U. Hammer, S. F. Johnsen, P. M. Kristinsdottir and N. Reeh. 1982.
A New Greenland Deep Ice Core. *Science.*, 218, 4579, p1273-1277.

Dansgaard W., S. J. Johnsen, H. B. Clausen, D. Dahl-Jensen, N. Gunderstrup, C. U. Hammer and H. Oeschger, 1984.
North Atlantic Climatic oscillations revealed by Deep Greenland Ice Cores.
Proceedings of the Ewing Symposium, Oct 1982. Columbia Univ, Lamont-Doherty Geol Observatory. New York, American Geophysical Union special volume.

Donner J., 1978.
Holocene history of the West Coast of Disko, Central West Greenland. *Geografiska Annaler* 60A, p63-72.

Fairbanks R. G. 1989.
A 17,000-year glacio-eustatic sea level record: influence of glacial melting rates on the Younger Dryas vent and deep-ocean circulation. *Nature*, vol 342, p637-642.

Fastook J. L., 1985.
Ice shelves and ice streams: three modelling experiments. in, *Glaciers, icesheets and sea level: effect of a CO2-induced climatic change.* Report of a workshop held in Seattle, Washington 13-15 September 1984, p279-300.

Fastook J. L. and W. F. Smith, 1982.

Finite element analysis of calving from ice fronts. *Annals of Glaciology* 3, p103-106

Friese-Greene T. W. and Pert G. J., 1965.
Velocity fluctuations of the Bersakerbrae, East Greenland. *Journal of Glaciology* 5, 41, p739-747.

Funder S., 1978.
Holocene stratigraphy and vegetational history in the Scoresby Sund area,East Greenland. *Bulletin Grønlands Geologiske Undersøgelse* 129, 66p.

Funder S., 1979.
The Quaternary Geology of the Nassaq area , South Greenland, *Rapport Grønlands Geologiske Undersøgelse* 86, p24.

Funder S., 1989.
Quaternary geology of the ice free areas and adjacent shelves of Greenland, In:Fulton R. J. (ed.); *Quaternary Geology of Canada and Greenland,* Geological Survey of Canada, Geology of Canada, no. 1.

Funder S., and C. Hjort 1980.
A reconnaissance of the Quaternary geology of North Greenland; *Rapport Grønlands Geologiske Undersøgelse* 99, p99-105.

Geophysical Monograph Series, 1985.
Vol. 33. Greenland Ice Core , *Geophysics, Geochemistry and the Enviroment* No. 19.

Glen J. W., 1955.
The creep of polycrystalline ice. *Proceedings of the Royal Society of London,* series A., 226, p519- 538.

Grigoryan S. S., S. A. Buyanov, M. S. Krass and P. A. Shumsky, 1985.
The mathematical model of ice sheets and the calculation of the evolution of the Greenland Ice Sheet. *Journal of Glaciology*, 31, 109, p281-292.

Harris J., 1977.
Rheology and non-Newtonian flow. Longman.

Hjort C., 1979.

Glaciation in Northern East Greenland during the Late Weichselian and early Flandrian. *Boreas,* 8 , p281-296.

Hjort C., 1981.(a)
Studies of the Quaternary in Northeast Greenland. Thesis 9, University of Lund, Depatment of Quaternary Geology, p29.

Hjort C., 1981.(b)
Quaternary Geology in Northeasternmost Greenland; in *Geoscience During the Ymer-80 Expedition to the Arctic,* V. Schytt, K Boström, and C. Hjort(eds); Geologiska Föreningens i Stockholm Förhandlingar, v.105 p234-243.

Hodge S. M., 1985.
Two-dimensional, time dependent modelling of an arbitrarily shaped ice mass with the finite element technique. *Journal of Glaciology* 31,109,p351-359.

Holtzscherer J. and A. Bauer 1954.
Contribution á la connaissance de l'Inlandsis du Groenland. Resultats Scientifiques NIII, 2, NII, 3., Paris. Expeditions Polaires Francaises.

Hooke R. L., C. F. Raymond, R. L. Hotchkiss, and R. J. Gustafson. 1978
Calculations of velocity and temperature in a polar glacier using the finite-element method. *Journal of Glaciology* 24, 90, p131-146.

Hughes T. J., 1987.
Deluge II and the continent of doom: rising sea-level and the collapsing Antarctic ice sheet. *Boreas* 16, p89-100.

Hughes T.J., 1987.
Ice dynamics and deglaciation models when ice sheets collapsed. In: Ruddiman W. F. and H. E. Wright (ed.), *North America and adjacent oceans during the last glaciation.* Boulder, CO, Geological Society of America, p183-220.

Hutter K., 1983.
Theoretical Glaciology; material science of ice and the mechanics of glaciers and ice sheets. Dordrecht, D Riedel Publishing Company.

Hutter K., and T. Alts, 1985.

Ice and snow mechanics; a challenge to theoretical and applied mechanics. In Niordson F.I. and Olhoff N. (eds.), *Theoretical and applied mechanics.* Amsterdam, Else vier, p163-217.

Jenssen D., 1983.
Elevation and climatic changes from total gas content and stable isotopic measurements. In: Robin G. de Q. (ed.), *The climatic record in polar ice sheets.* Cambridge University Press.

Kamb B., 1970.
Sliding motion of glaciers: theory and observation. *Reviews of Geophysics and Space Physics* 8, 4, p673-728.

Keen R. A., 1984.
Statistical- Dynamical Model of Accumulation on the Greenland Ice Sheet. *Annals of Glaciology* 5, p69-74.

Kelly M., 1973.
Radiocarbon dated shell samples fom Nodre Stromfjord, West Greenland, with comments on models of glacio-isostatic uplift. *Rapport Grønlands, Geologiske Undersøgelse* 59, p20.

Kelly M., 1980a.
Preliminary investigations of the Quaternary of Melville Bugt and Dundas, North-west Greenland. *Rapport Grønlands Geologiske Undersøgelse* 100, p33-38.

Kelly M., 1980b.
The Status of the Neoglacial in western Greenland. *Rapport Grønlands Geologiske Undersøgelse* 96, p24.

Kelly M. 1985.
A review of the Quaternary geology of Western Greenland; in *Quaternary Environments of Eastern Canadian Arctic, Baffin Bay and Western Greenland,* J. T. Andrews (ed); Allen and Unwin, Boston p461-501.

Kelly M. and Bennike, O. 1985
Quaternary geology of parts of central western North Greenland. *Rapport Grønlands Geologiske Undersøgelse*, 126 p111-116.

Koch J. P. and Wegner A., 1911.
Die glaziologsichen Beobachtungen der Danmark-Expedition; *Meddelelser om Grønland*, v.46, p1-76.

Koerner R. M., 1989.
Ice core evidence for extensive melting of the Greenland Ice Sheet in the last Interglacial. *Science*, Vol. 244, p964-968.
Kuhn M., 1987. Micro-meteorological conditions for snow melt. *Journal of Glaciology* 33, 113, p24-26.

Larsen B., 1983.
Geology of the Greenland-Iceland Ridge in the Denmark Strait; In:Bott M. H. P., S. Saxov, M. Talwani and J. Theide (ed), *Structure and Development of the Greenland-Scotland Ridge.* Plenum Press, New York, p425-444.

La Chapelle E., 1955.
Ablation studies in the Minit Julep area, southwest Greenland. In: *Project Minit Julep, Part 2,* Maxwell Air Force Base. AC Arctic, Desert, Tropic information center, Research Studies Institute Aiv University, p51-72. Special Scientific Reports ADTIC Publication A-104B.

Lliboutry L., 1968.
General theory of subglacial cavitation and sliding of temperate glaciers. *Journal of Glaciology* 7, p21-58.

Loewe F., 1936.
Hohenverhaltnisse und Massenhaushalt des grönlandischen Inlandeises. *Gerlands Beitrage zur Geophysik,* 46, p317-330, 48, 86-89.

Loewe F., 1964.
Das Grönlandische Inlandeis nach neuen Feststellungen. *Erdkunde* 18, 3, p189-202.

MacAyeal D. R. and R. H. Thomas, 1982.
Numerical modelling of ice-shelf motion. *Annals of Glaciology* 3, p189-194.

Mahaffy M. A. W., 1976.
A numerical three-dimensional ice flow model. *Journal of Geophysical Research* 81, p. 1059-1066.

Mercer J. H., 1961.
The response of fjord glaciers to changes in the firn limit. *Journal of Glaciology*, 3, 29, p850-858.

Mock S. J. 1967.
Calculated patterns of accumulation of the Greenland ice sheet. *Journal of Glaciology*, 6, 48, 795-803

Mock S. J. and W. F. Weeks, 1966.
The distribution of ten-metre snow temperatures on the Greenland ice sheet. *Journal of Glaciology*, 6, 43, p23-42.

Morland L. W. 1984.
Thermo-mechanical balances of ice sheet flows. *Journal of Geophysical and Astrophysical Fluid dynamics*, Vol 29, p237-66.

Morland L. W., and G. D. Smith, 1984.
Influence of non-uniform temperature distribution on the steady motion of ice-sheets. *Journal of Fluid Mechanics* 140, p113-133.

Morland L. W., G. D. Smith and G. S. Boulton, 1984.
Basal sliding relations deduced from ice-sheet data. *Journal of Glaciology* 30 (105), p131-139.

Muszynski I., and G. E. Birchfield: 1987.
A coupled marine ice-stream-ice-shelf model. *Journal of Glaciology* 33, 113, p3-15.

Nichols R. L., 1969
Geomorphology of Inglefield Land, Northern Greenland; *Meddelelser om Grønland*, v153, no. 3, 127p.

Nye J. F., 1951.
The flow of glaciers and ice sheets as a problem in plasticity. *Proceedings of the Royal Society of London,* Series A, 207, p554- 572.

Nye J. F., 1952[a].
A method of calculating the thickness of the Ice-sheets. *Nature*, Vol. 169, No 4300, p529-530.

Nye J.F., 1952[b].
The mechanics of glacier flow. *Journal of Glaciology* 2, p82-93.

Nye J. F., 1957.
The distribution of stress and velocity in glaciers and ice sheets. *Proceeding of the Royal Society of London,* Series A 239, p113-33.

Nye J. F., 1959.
The motion of ice sheets and glaciers. *Journal of Glaciology* 3, p493-507.

Oerlemans J., 1981.
Modelling of the Pleistocene European Ice Sheet. Some experiments with simple mass balance parametrizations. *Quaternary research 15,* p77-85.

Oerlemans J., 1982.
A model of the Antarctic Ice Sheet. *Nature* 297, p550-553.

Oerlemans J., and C.J. Van der Veen, 1984.
Ice Sheets and Climate. D. Reidel Publishing Company, Dordrecht, Holland.

Paterson W. S. B., 1980.
Ice sheets and ice shelves. In: Colbeck S. C. (ed.), *Dynamics of snow and ice masses.* New York etc Academic Press, p1-79.
Paterson W. S. B. ,1981. *The Physics of Glaciers,* (2nd Edition) Pergamon Press, Oxford etc, New York.

Payne A. J., 1988.
Modelling Former Ice Sheets. Unpublished PhD. Thesis, University of Edinburgh.

Putins P., 1970.
The Climate of Greenland. In: Orvig S. (ed.), *Climates of the Polar Regions. World Survey of Climatology 14*, p3-128.

Radok V., R. G. Barry, D. Jenssen, R. A. Keen, G. N. Kiladis
and B. McInnes, 1982. *Climatic and physical characteristics of the Greenland ice-sheet, Parts I and II.* Cooperative Institute for Re search in Enviromental Sciences (CIRES), University of Colorado, Boulder.

Reeh N., 1968.

On the Calving of Ice from Floating Glaciers and Ice Shelves. *Journal of Glaciology*, Vol. 7, No. 50, p215-232.

Reeh N., 1982.
A plasticity theory approach to the steady-state shape of a three-dimensional ice sheet. *Journal of Glaciology*, 28, 100 p431-455.

Robin G. de Q., 1983.
The climatic record from ice cores. In: Robin G. de Q. (ed.), 1983, The Climatic Record in Polar Ice Sheets. Cambridge University Press.

Roksandic M. M., 1979.
Geology of the continental shelf off West Greenland between 61N15 and 64N00: an interpretation of sparker seismic and echosounder data. *Rapport Grønlands Geologiske Undersøgelse* 92, p15.

Smith G. D., 1985.
Numerical Solution of Partial Differential Equations: Finite Difference Methods (Third Edition). Clarendon Press, Oxford.

Sommerhoff G., 1983.
Untersuchungen zur Geomorphologie des Meeresbodens in der Labrador-und Irmingersee; *Münchener geographische Abhandlungen,* Vol. 28, 86p.

Sugden D. E., 1972.
Deglaciation and isostasy in the Sukkertoppen Ice Cap area, West Greenland. *Arctic and Alpine Research,* Vol. 4, p177-195.

Ten Brink N. W., 1971[a].
Continued investigations of Quaternary deposits between Søndre Strømfjord, the Inland Ice, and the Sukkertoppen Ice Cap. Geological Survey of Greenland, Report 35, p13-17.

Ten Brink N. W., 1971[b].
Holocene Delevelling and Glacial History between Søndre Strømfjord and the Greenland Ice Sheet, West Greenland. PhD. dissertation, University of Washington, Seattle, 191p.

Ten Brink N. W., 1974.

Glacio-isostasy; New data from West Greenland and geophysical implications. *Bulletin of the Geological Society of America,* 85, p219-228.

Ten Brink N. W., 1975.
Holocene History of the Greenland Ice Sheet based on radio-carbon dated moraines in West Greenland. *Meddelelser om Grønland* 201, 4, 44p.

Walcott R. I., 1973.
Structure of the earth from glacio-isostatic rebound. *Annual review of Earth and Planetary Science* 1, p15-37.

Warren C. R. and N. R. J. Hulton, 1990.
Topographic and Glaciological Controls on Holocene Ice Sheet Margin Dynamics, Central West Greenland. *Annals of Glaciology* 14, 1990.

Weidick A., 1963.
Ice Margin Features in the Julienhaab District, South Greenland. *Bulletin Grønlands Geologiske Undersøgelse*, 35.

Weidick A., 1968.
Observations on some Holocene glacier fluctuations in West Greenland. *Meddelelser om Grønland.* v165, no. 6, 202p.

Weidick A., 1972[a].
Holocene shorelines and glacial stages in Greenland- an attempt at correlation. *Rapport Grønlands Geologiske Undersøgelse*, 41, p39.

Weidick A., 1972[b].
Notes on Holocene glacial events in Greenland. In: Vasari Y., H. Hyarinen and S. Hicks, (eds,), *Climatic changes in arctic areas during the last ten thousand years.* Acta Universitatis Oulensis Series A3 , (geological 1), p177- 204.

Weidick A., 1975[a].
A review of Quaternary investigations in Greenland. Ohio State University Institute of Polar Studies, Report 55, 161p.

Weidick A., 1975[b].
Quaternary geology of the area between Frederikshavn, Isblink and Ameralik. *Rapport Grønlands Geologiske Undersøgelse*, 70, 22p.

Weidick A., 1976[a].
Glaciation and the Quaternary of Greenland. In: Escher A. and W. S. Watt (eds.), *Geology of Greenland.* Copenhagen. Geological Survey of Greenland, p430-460.

Weidick A., 1976.[b]
Glacio-Isostatic uplift ended 4000-5000 years ago. in, *Geology of Greenland.* A. Escher and W. S. Watt (eds.), The Geological Survey of Greenland Denmark.

Weertman J., 1957.
Deformation of floating ice shelves. *Journal of Glaciology* 3, p38-42.

Weertman J., 1964.
The theory of glacier sliding. *Journal of Glaciology* 5, p287-303.

Weertman J., 1973.
Creep of ice. In: Whalley E., S. J. Jones and L. W. Gold (eds), *Physics and Chemistry of Ice.* p320-337. Royal Society of Canada, Ottawa, Canada.

Zarudzki E. F. K., 1980.
Interpretation of shallow seismic profiles over the continental shelf in West Greenland between latitudes 64N and 69N30. *Rapport Grønlands Geologiske Undersøgelse*, 100, p58-61.

Zwally H. J., 1989.
Growth of the Greenland Ice Sheet: Interpretation. *Science* Vol 246, p1589-1590.

Zwally H. J., A. C. Brenner, J. A. Major, R. A. Bindschandler,
and J. G. Marsh, 1989. Growth of the Greenland Ice Sheet: Measurement. *Science* Vol 246, p1590-1591.

Appendix 1: Symbols used in thesis

$\cdot$ Dot product

∇ The vector grid operator

A Arrhenius constant

b External mass-balance rate

B Bed elevation

B' Relaxed bed elevation

B_0 Sea level

C Continentality factor

D Diffusivity constant

E Surface elevation

E_0 1m/year ablation altitude

F Ablation forcing constant.

g Gravitational constant

h altitude

HC Conducted heat

HL Latent heat

HS Sensible heat

i Iteration subscript

L Load

L_i Ice load

L_w Water load

n Ice flow law power constant

NB Overall radiation energy sum

p Accumulation

P Precipitation

q Ice flux rate

t Time

T Absolute temperature

T_s Surface temperature

T_0 Sea-level temperature

U Ice velocity

$\overline{U}$ Vertical averaged velocity

$\overline{U}_d$ Deformation velocity

V Mass-balance rate

V_a Ablation flux

V_c Calving flux

V_p Accumulation flux

x Directional subscript

y Directional subscript

Z Ice thickness

Z_* Effective thickness

α Surface slope

$|\alpha|$ Average surface slope

η Energy

γ_b Basal shear stress

$\dot{\varepsilon}$ Ice strain rate

ρ_i Ice density

ρ_w Water density

ρ_m Mantle density

σ Stephan Boltzman constant

τ Effective shear stress

Θ Latitude North

Appendix 2: Equations used in thesis

$$\frac{\delta Z}{\delta t} = b - \nabla\left(\overline{U} \cdot Z\right) \tag{1}$$

$$\frac{\partial Z}{\partial t} = b - \frac{\partial q_x}{\partial x} - \frac{\partial q_y}{\partial y} \tag{2}$$

$$Z_{(t+1)} = Z_t + \Delta t\left(b - \frac{\partial q_x}{\partial x} - \frac{\partial q_y}{\partial y}\right) \tag{3}$$

$$\frac{\partial q_x}{\partial x} \simeq \frac{q_{x_{i+\frac{1}{2}}} - q_{x_{i-\frac{1}{2}}}}{\delta x} \tag{4}$$

$$q_{i+\frac{1}{2}} = \left(\frac{u_{i+1} + u_i}{2}\right) \times \left(\frac{Z_{i+1} + Z_i}{2}\right) \tag{5}$$

$$\dot{\varepsilon}_{xz} = A\tau^{n-1}\tau_{xZ} \tag{6}$$

$$\dot{\varepsilon}_x Z = \frac{1}{2}\left(\frac{\partial U_y}{\partial Z} + \frac{\partial U_\varepsilon}{\partial y}\right) \tag{7}$$

$$U_{dx} = 2A\left(n+2\right)^{-1}\left(\rho g\right)^n Z^{n+1}|\alpha|^{n-1}\alpha_x \tag{8}$$

$$\alpha_x \simeq \left(\frac{E_{i+1} - E_{i-1}}{2\delta x}\right) \tag{9}$$

$$|\alpha| = \sqrt{\left(\alpha_x^2 + \alpha_y^2\right)} \tag{10}$$

$$U_s = \frac{k\gamma_b}{Z_*^2} \tag{11}$$

$$\gamma_b = \rho g Z \alpha \tag{12}$$

$$Z_* = Z - \frac{\rho_w B}{\rho_I} \tag{13}$$

$$\frac{\rho_w}{\rho_i} B = 0 \tag{14}$$

$$\overline{U}_x = \overline{U}_{x0} + \Delta x \varepsilon_s \tag{15}$$

$$\frac{\partial B}{\partial t} = D_a \nabla^2 \cdot (B' - B + L) \tag{16}$$

$$L = L_i + L_w \tag{17}$$

$$L_i = Z \frac{\rho_i}{\rho_w} \tag{18}$$

$$L_i = Z_* \frac{\rho_i}{\rho_w} \tag{19}$$

$$L_i = 0 \tag{20}$$

$$L_w = \frac{\rho_w}{\rho_m} (B_0 - B) \tag{21}$$

$$L_w = 0 \tag{22}$$

$$\frac{\partial^2 (B' - B + L)}{\partial x^2} + \frac{\partial^2 (B' - B + L)}{\partial y^2} \tag{23}$$

$$\frac{\partial^2 (B' - B + L)}{\partial x^2} \simeq \frac{\left[(B' - B + L)_{i+1} - 2(B' - B + L)_i + (B' - B + L)_{i-1}\right]}{\delta x^2} \tag{24}$$

$$L = z \frac{\rho_i}{\rho_m} \tag{25}$$

$$b = V_p + V_a + V_c \tag{26}$$

$$\log_{10} V_a = \frac{1}{2000} (E_0 - E) \tag{27}$$

$$E_0 = a + b\Theta + c\Theta^2 \tag{28}$$

$$\Theta'_0 = \Theta_0 + F\delta T \tag{29}$$

$$F = dL/dT \tag{30}$$

$$F = (dL/dE)(dE/dT) \tag{31}$$

$$NB + HS + HL + HC + HM = 0 \tag{32}$$

$$\eta = \sigma T^4 \tag{33}$$

$$T_s = T_0 + \frac{dT}{dE}(E - E_0) \tag{34}$$

$$T_0 = -83.4 + \left(3.53\Theta \times 10^{-2}\right) - \left(0.3104\Theta \times 10^{-2}\right)^2 - 9.787C \tag{35}$$

$$T = T_0 - 7.46 \times 10^{-3}E \tag{36}$$

$$T = T_0 - 3.67 \times 10^{-3}E - 8.32 \times 10^{-7}E^2 \tag{37}$$

$$\frac{dT}{dE} = -7.468 \times 10^{-3}E°C/m \tag{38}$$

$$\frac{dT}{dE} = -3.67 \times 10^{-3} - 1.67 \times 10^{-6}\ E°C/m \tag{39}$$

$$r_m^2 = \frac{\sum(Res^2)}{\sum\left(\overline{T} - T\right)^2} \tag{40}$$

$$Res = T_{model} - T_{real} \tag{41}$$

$$V_a = -2.721 - 9.24 \times 10^{-3}T_s + 8.84 \times 10^{-5}T_s^2 \tag{42}$$

$$P = max\left(0.05; \left(0.3 + 14s - 4 \times 10^{-5} h\right)/C\right) \tag{43}$$

$$V_a = (a + bS + cT_s)/C \tag{44}$$

$$V_c = -28.75B \tag{45}$$

$$\Delta t_{max} = \frac{(\Delta x)_2 |\alpha'|}{2U'Z'n} \tag{46}$$

$$E^+_{i,j} = \frac{1}{16}\left(E_{i+2,j} + E_{i-2,j} + 10E_{i,j} - 4\left(E_{i+1,j} + E_{i-1,j}\right)\right) \tag{47}$$

Appendix 3 : A note on the model diagrams

The graphical output from the model was produced using UNIRAS subroutines embedded into a number of Fortran routines. Most often model states were only recorded at the beginning of the run and at 1000 or 2000 year intervals in order to reduced computer storage. Some later runs recorded the information more densely. The graphical output therefore reflects the amount of information originally recorded. Although in many of the models, little variation occurs in the ice sheet state after the first few recorded states, most often all the states are shown. Partly this is for completeness and to demonstrate the invariance of the model conditions as they approach equilibrium. In part it was quicker to standardise the output format. In general, the smaller sized plots have been averaged to a 40km square resolution for plotting purposes only. This gave vastly increased plotting speeds and reduced storage requirements. In general, there is little loss of visual impression at these sizes. Additional plots which are not thought to be crucial to the main thrust of the discussion, but which remain of interest are included in Appendix 4.

In the titles to the plots and the accompanying text,the abbreviation 'a' for years is used interchangeably with 'years' to describe calculation time periods and is also attached to the year times of specific records. In some of the land and ice surface plots, holes appear in the bedrock surface. This is because these areas are by chance the same as the UNIRAS null value to indicate no plotting. Whilst they detract from the pictures they are of no real significance.

Appendix 4. Additional plots in run order

Run 48. Sliding velocities - metres/a, 0-10000 years.

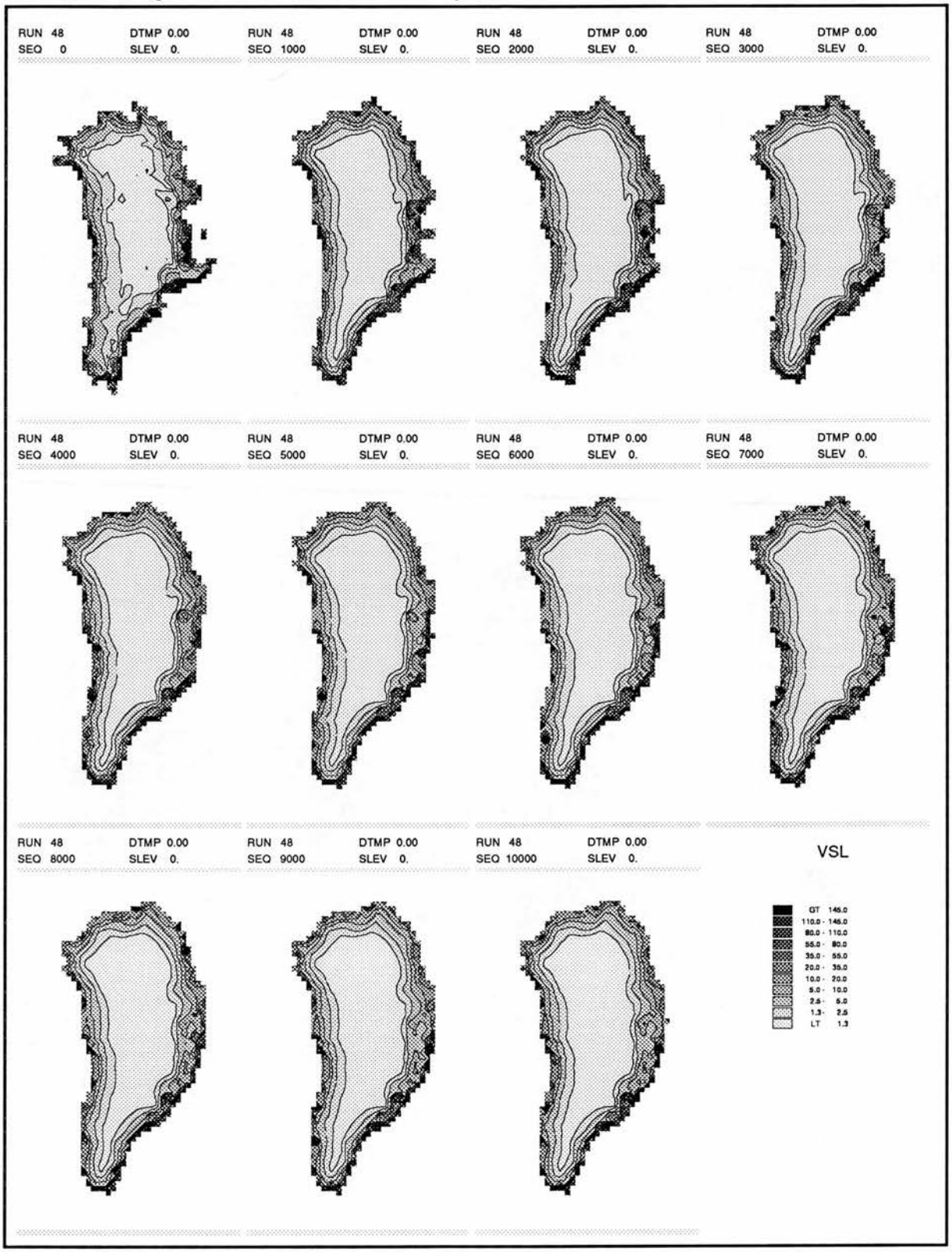

Run 58. Sliding velocities - metres/a, 0-10000 years.

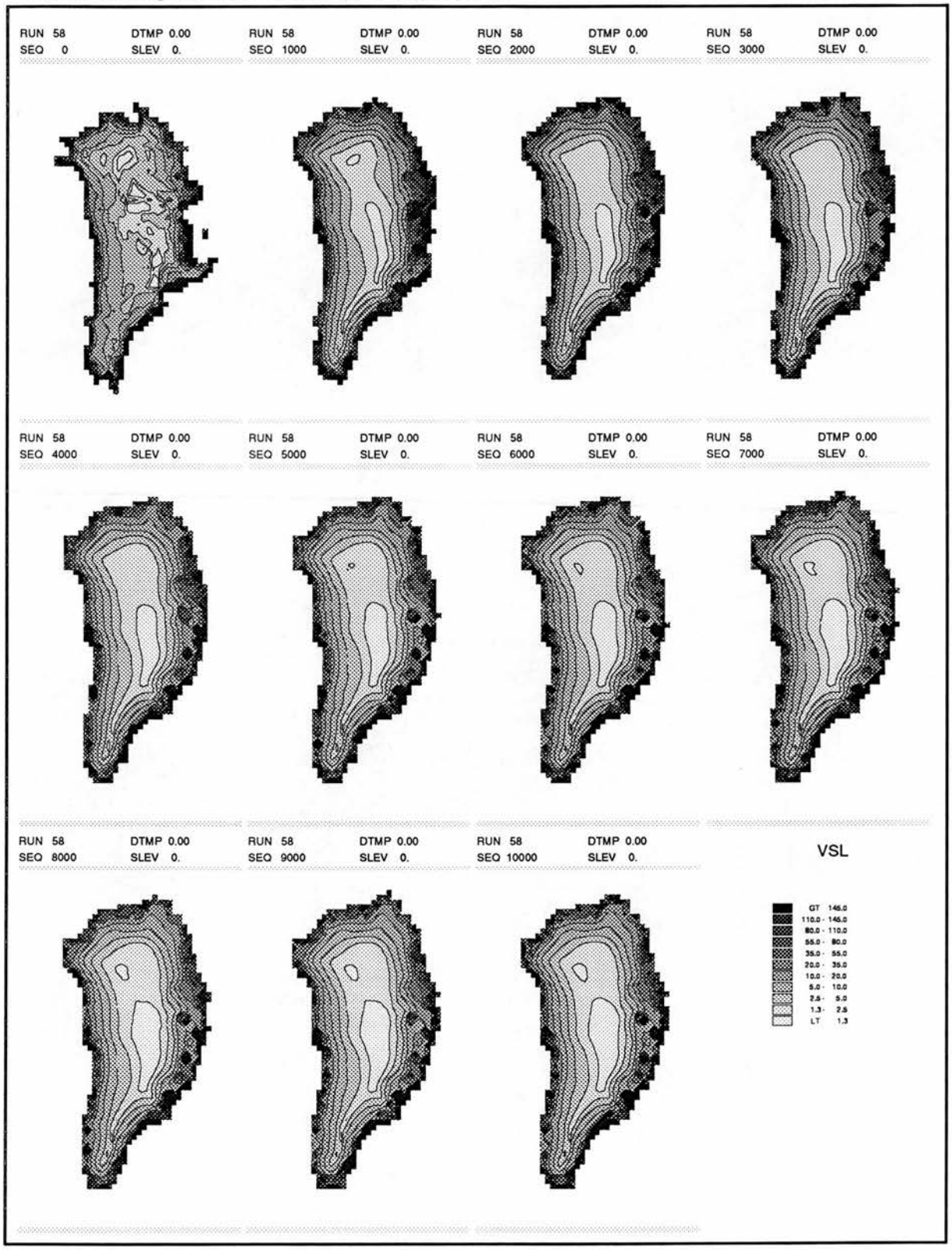

RUN 74 . , 0-10000 years.

Total Ice Fluxes and Ice Volumes.

Raw data. Values recorded every 50 years.

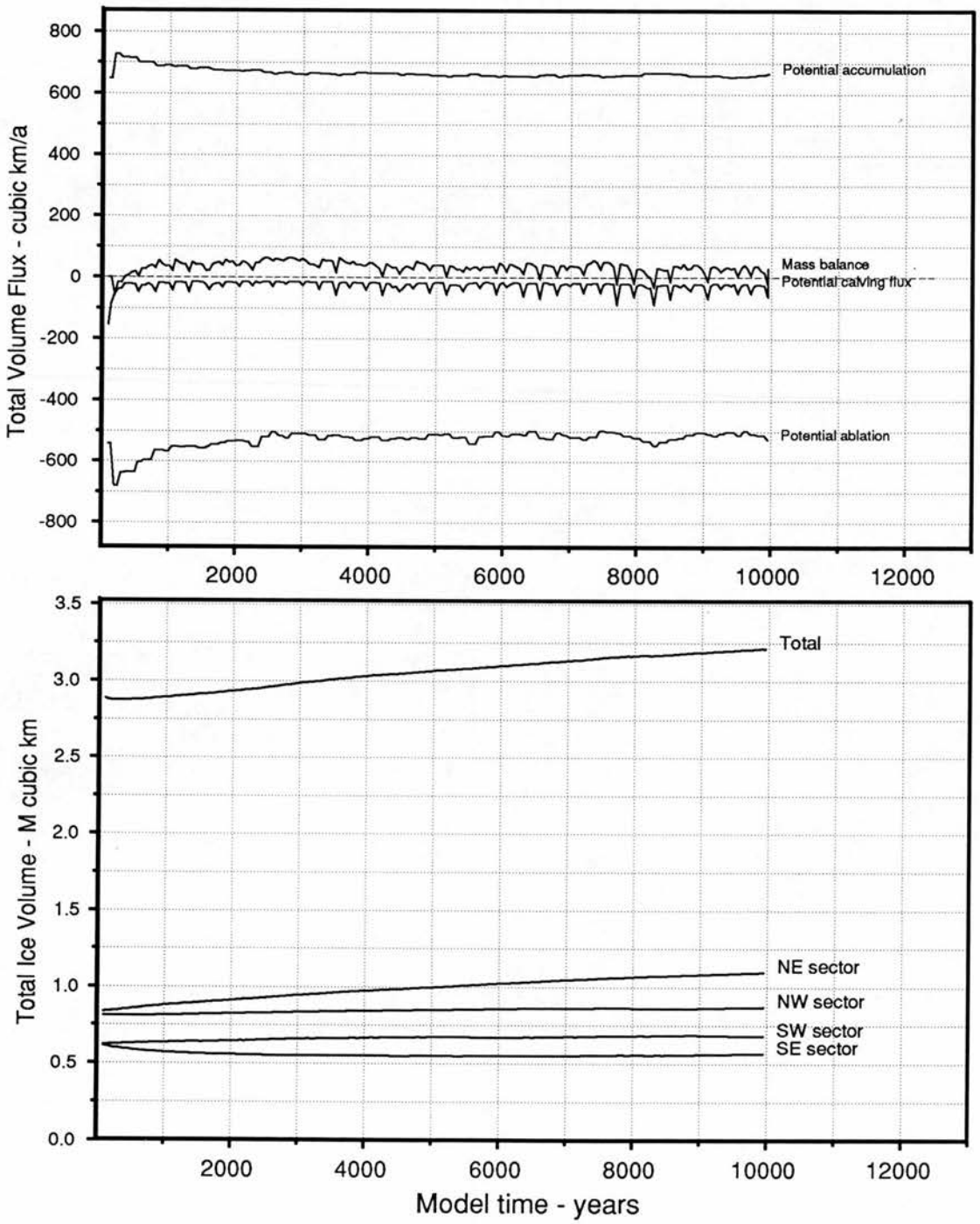

RUN 75 . , 0-10000 years.

Total Ice Fluxes and Ice Volumes.

Raw data. Values recorded every 50 years.

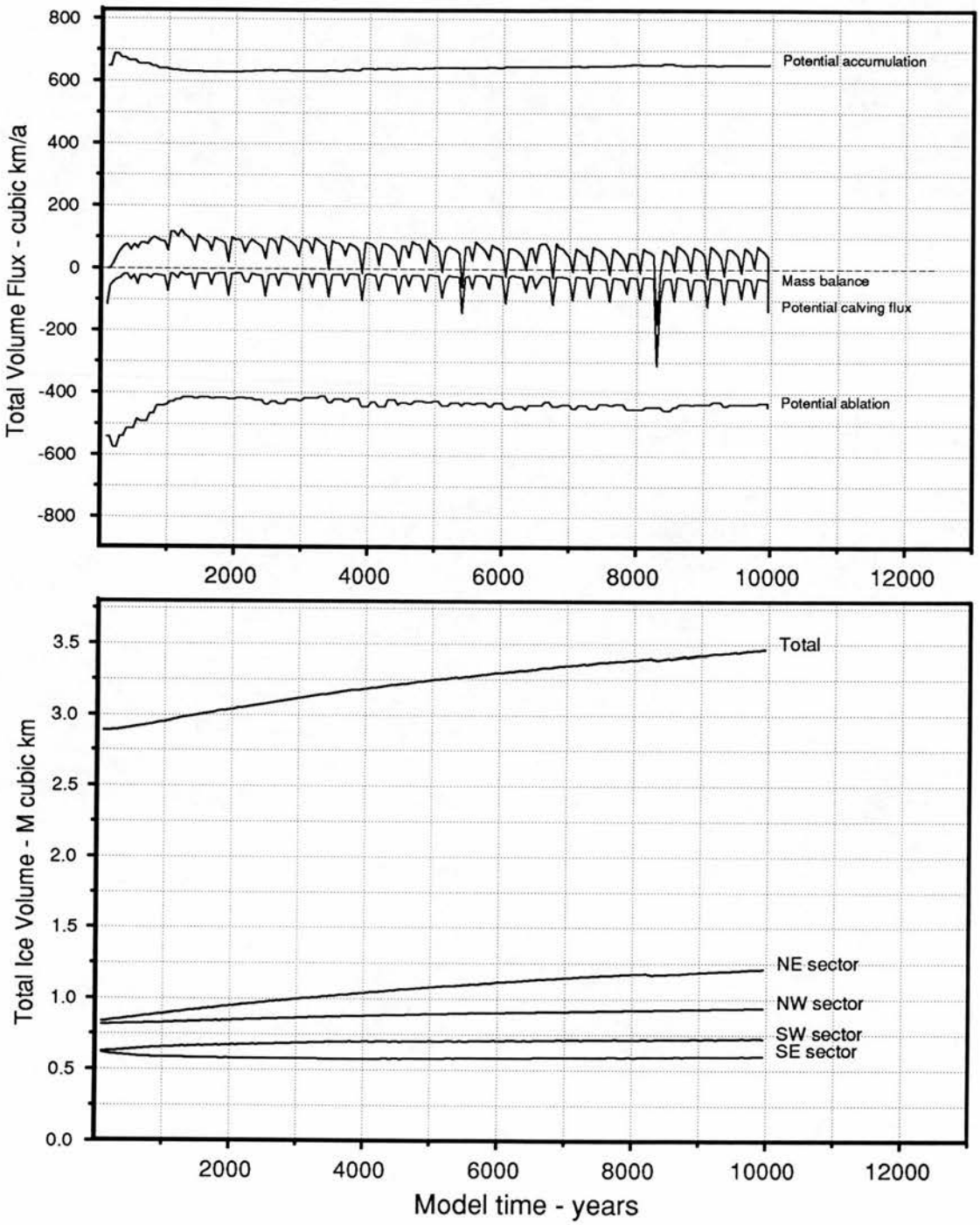

Run 76. Accumulation - centimetres/year, 0-10000 years.

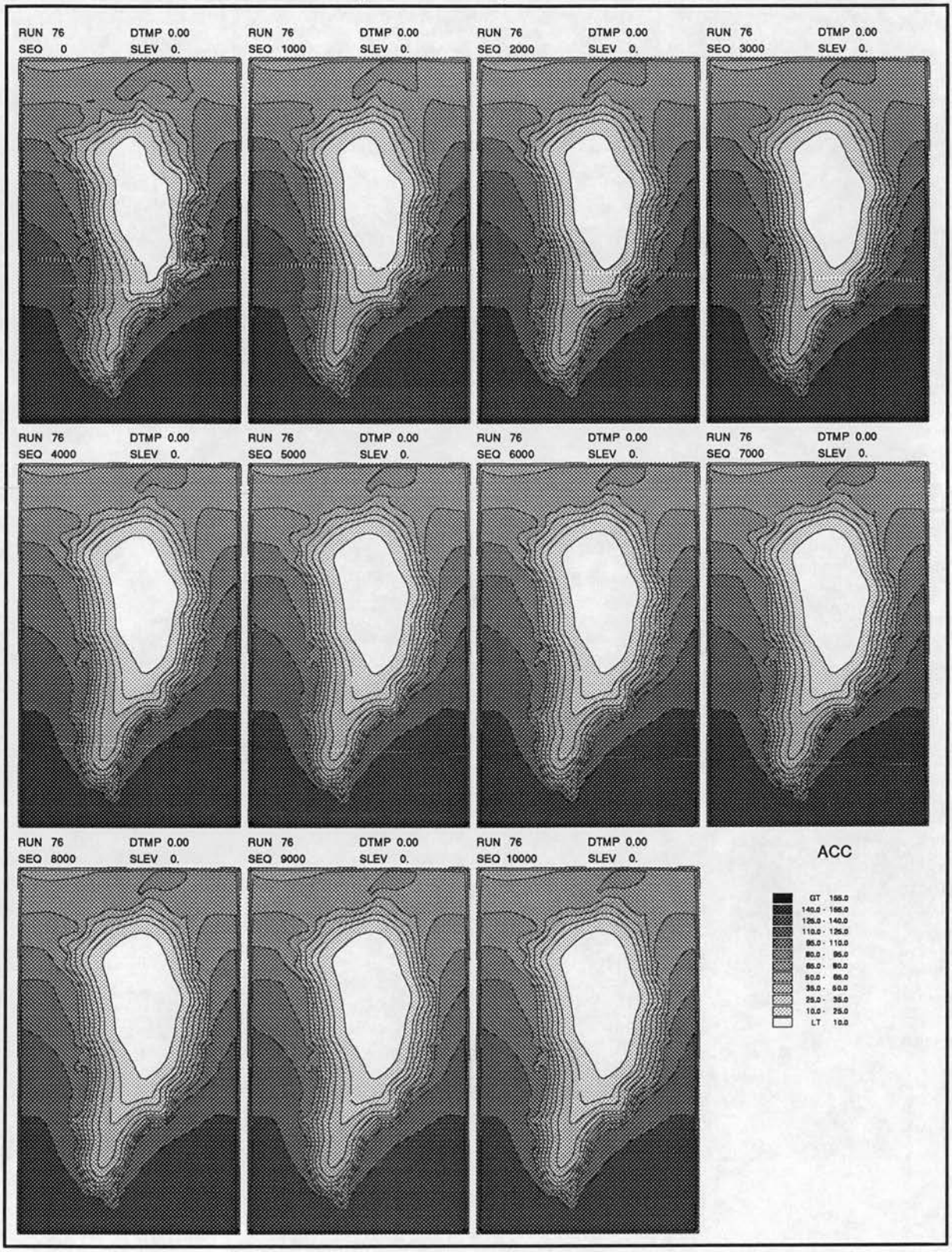

RUN 78 . , 0-10000 years.

Total Ice Fluxes and Ice Volumes.

Raw data. Values recorded every 50 years.

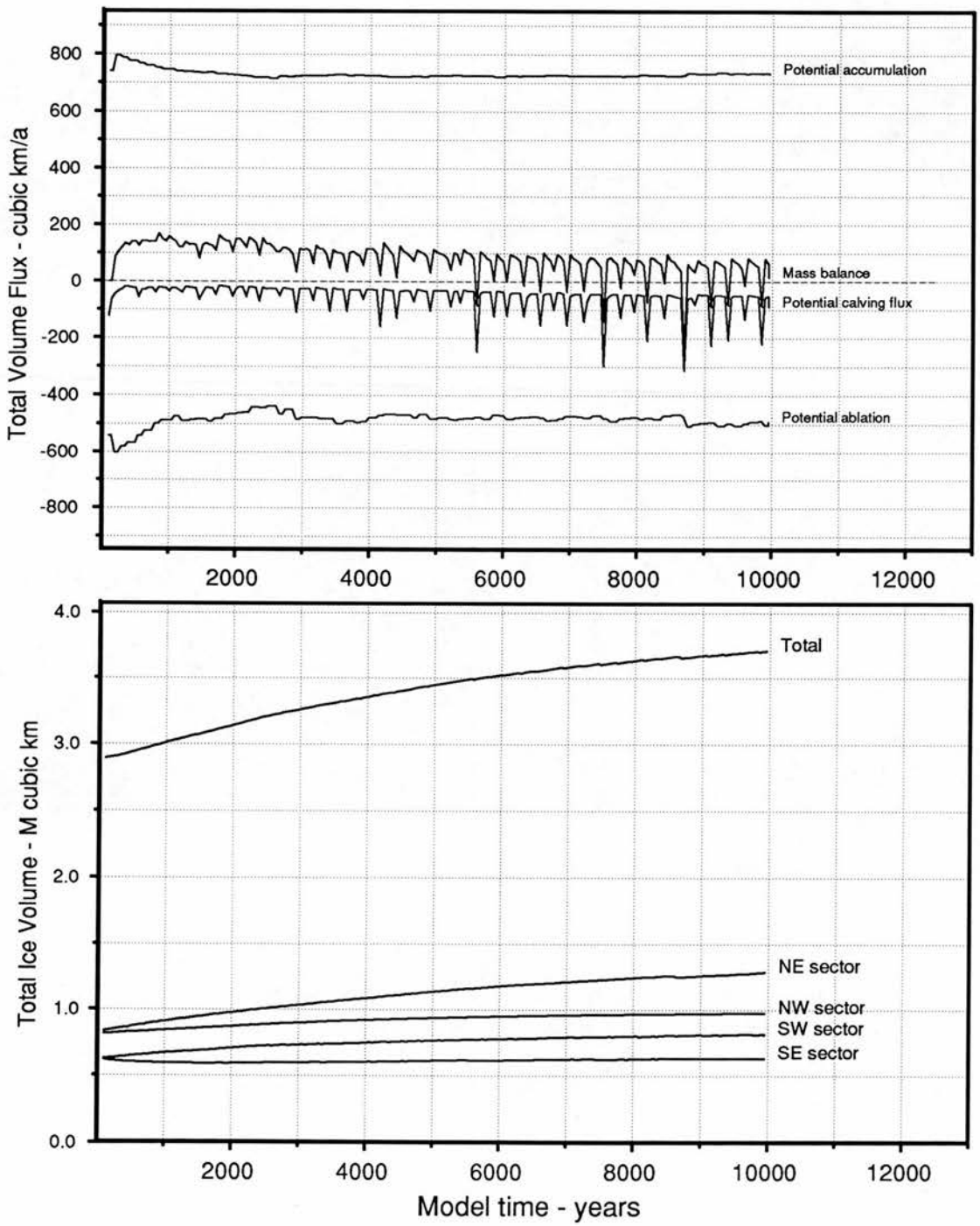

RUN 119, Change in basal altitude - m, 22000a-40000a, 2000 year calculation period.

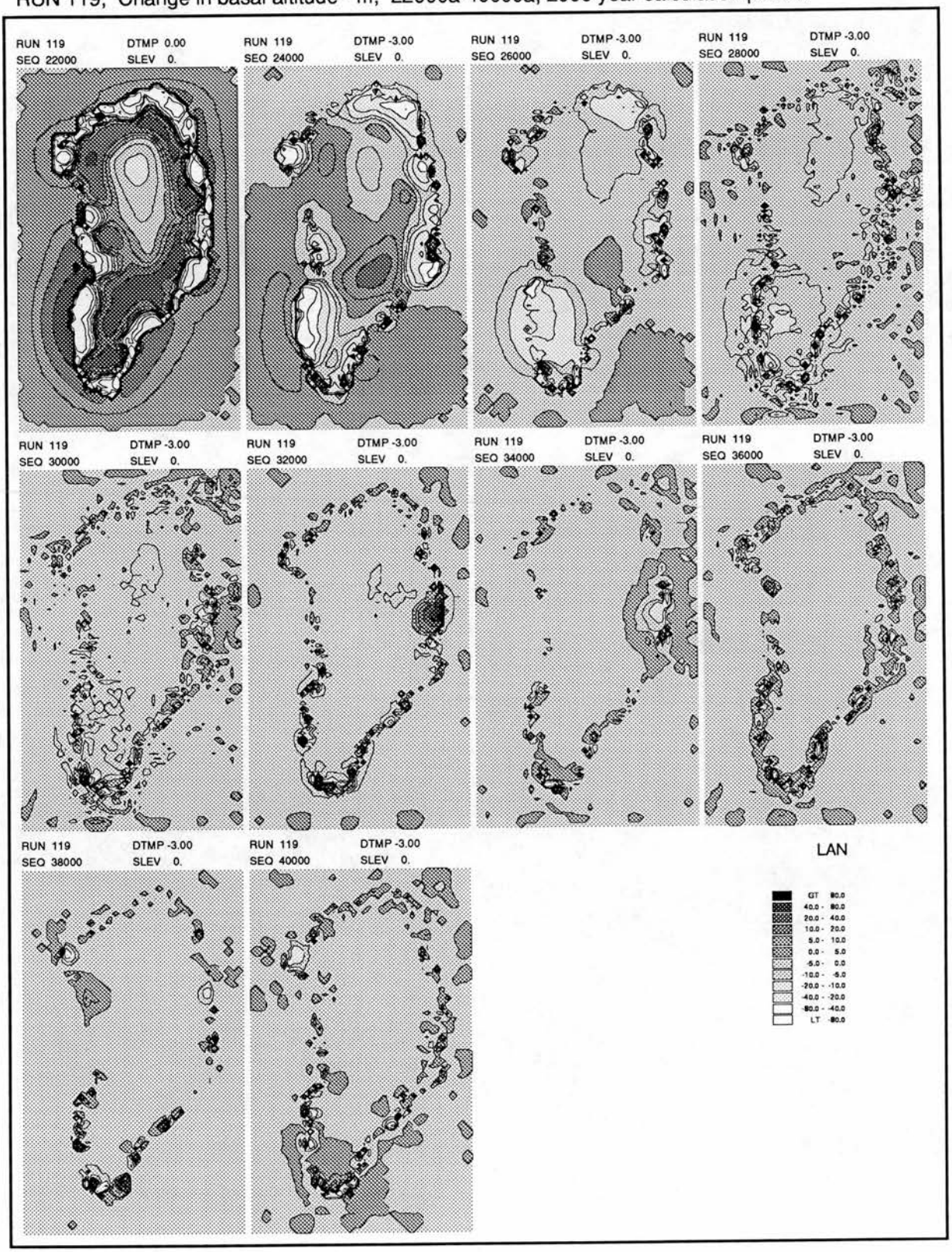

RUN 120, Change in ice thickness - m, 22000a-40000a, 2000 year calculation period.

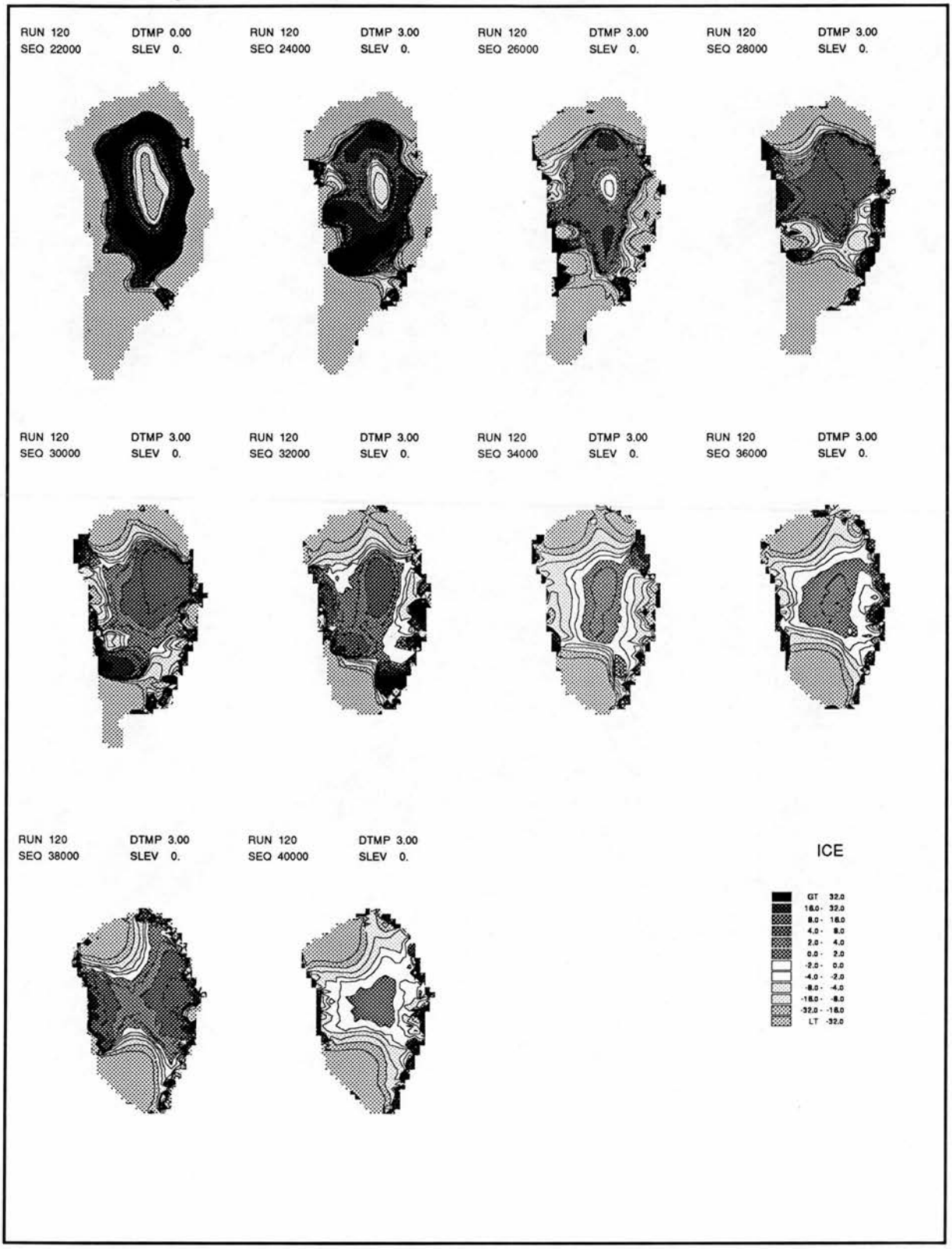

RUN 121, Change in basal altitude - m, 22000a-40000a, 2000 year calculation period.